A CRUSTAL SEISMIC SURVEY IN THE RED LAKE-EAR FALLS AREA OF NORTHWESTERN ONTARIO USING QUARRY BLASTS AS THE SOURCE

by

BRIAN A. MAXWELL

A thesis
presented to the University of Manitoba
in partial fulfillment of the
requirements for the degree of
M.SC.
in
DEPARTMENT OF EARTH SCIENCES

Winnipeg, Manitoba

ISBN 0-315-33926-8

A CRUSTAL SEISMIC SURVEY IN THE RED LAKE- EAR FALLS AREA OF NORTHWESTERN ONTARIO USING QUARRY BLASTS AS THE SOURCE

BY

BRIAN A. MAXWELL

A thesis submitted to the Faculty of Graduate Studies of the University of Manitoba in partial fulfillment of the requirements of the degree of

MASTER OF SCIENCE

I hereby declare that I am the sole author of this thesis.

I authorize the University of Manitoba to lend this thesis to other institutions or individuals for the purpose of scholarly research.

BRIAN A. MAXWELL

I further authorize the University of Manitoba to reproduce this thesis by photocopying or by other means, in total or in part, at the request of other institutions or individuals for the purpose of scholarly research.

BRIAN A. MAXWELL

The University of Manitoba requires the signatures of all persons using or photocopying this thesis. Please sign below, and give address and date.

ABSTRACT

In the summer of 1980, a portable crustal seismic survey was carried out in the Red Lake-Ear Falls area of northwestern Ontario by the University of Manitoba. Open pit mine blasts from Griffith mine were used as the seismic source for the survey. Griffith mine is located 25 Km north of Ear Falls on Highway 105. Two profiles along Highway 105 were recorded, one to the south (17 Km) of the mine entrance and the other to the north (40 Km). Portable recorders were placed at a 1 Km spacing on both profiles except for the last 4 recording sites on the North profile which were at a 5 Km spacing. Because of the nature of the mine's production needs, the blasts were several seconds in duration resulting in a source signal several seconds long.

Due to the complex nature of the source signal and poor timing information, the quality of the data was generally marginal. For this reason, much effort was made in studying possible methods of processing and interpreting the data. Also, because of the nature of the source signal a detailed study of the source was carried out.

The source study involved an attempt to synthetically model the source signal by convolving a series of spikes representing individual shots in the shot patterns with either a Ricker or cylindrical source wavelet. The results showed that there are many types of arrivals recorded at the source recorder other than just a direct p-

wave. The source study also helped to sort out p and s-wave arrivals and make the processing of the data simpler.

After filtering the data two techniques of processing the data were tried. The first technique attempted was a vertical stack. All common receiver records were stacked in order to try to increase the S/N of the first breaks. All records with a source-receiver distance between 3 and 5 Km were also stacked in order to recover deep near vertical reflections such as the Riel and Moho discontinuities. Both of these stacks were not successful due to the poor timing information.

Because of the complex nature of the source signal, cross-correlation was also tried. This technique was not successful because the source signal was not random in nature.

Two techniques were attempted in the interpretation of the data. Ray tracing (Whittal and Clowes, 1979) was used in order to try and model the shallow structure using first break information. Shallow crustal models were derived for each of the two proflies. The models showed large scale features such as a shear zone probably associated with the East Lake Fault on the North profile and structures associated with the Bruce Lake fault zone on the South profile. WKBJ modelling (Chapman, 1978) of various crustal models was also tried in order to locate deep reflections such as the Riel and Moho discontinuities in the data. The crustal models of Hall and Hajnal (1973) were used because the data from this model was recorded in the same general area. The results showed only minor evidence of

these deep reflections due to the marginal quality of the data and the complex source signal.

The results of the project showed that this type of survey can be viable with proper planning of shot patterns and survey parameters although more study of the source conditions is necessary.

ACKNOWLEDGEMENTS

The author would first like to thank Griffith Mine and the Ontario Geological Survey (especially Dr. V.G. Gupta and Dr. R.B. Barlow) for their co-operation and assistance in this survey. Thanks also to John Wenham for keeping the portable recording units in operating order during the data collection and those who assisted in the collection of the data (Wanda DeLandro, Sandy Jenkins and Sheraz Khan). Thanks to Tom Millar for his assistance in the processing of the data and Gordon Maxwell for his assistance with the geologic portion of the work. I also thank Ian Noble, Al Carswell, Roger Tang and Chris Dillistone who assisted me while I was not present at the University. I especially thank Dr. D.H. Hall and Dr. W. Moon for their guidance and supervision and Texaco Canada Resources Limited for their patience. Most of all, I thank my family for their continued support throughout my school years.

CONTENTS

LIST OF FIGURES

LIST OF TABLES

Chapter I

INTRODUCTION

In the summer of 1980 a crustal seismic survey was carried out in northwestern Ontario along highway 105 between Red Lake and Ear Falls (figures 1.1 and 1.2). This experiment was carried out by the University of Manitoba with the co-operation of Griffith mine and the Ontario Geological Survey.

Griffith mine is an open pit iron mine located 25 Km north of Ear Falls. The mine consists of two pits; the larger one 1 Km north of the other. Figure 1.3 illustrates the locations of the two pits. Twice a week the mine blasts from one of these pits.

Ten self contained two-channel portable analogue recording units were used in the survey. Each unit recorded seismic data on one channel and timing information on the other. One portable unit was placed at the edge of the pit in order to record the form of the seismic signal as well as the absolute time of the shot. The remaining recorders were placed approximately 1 Km apart along highway 105 starting from the entrance to the mine. After seventeen blasts throughout the summer, data was collected for two profiles; one north of the mine entrance and the other to the south.

The mine is located in metasedimentary terrain about 5 Km north of the Red Lake-English River subprovince boundary. The southern

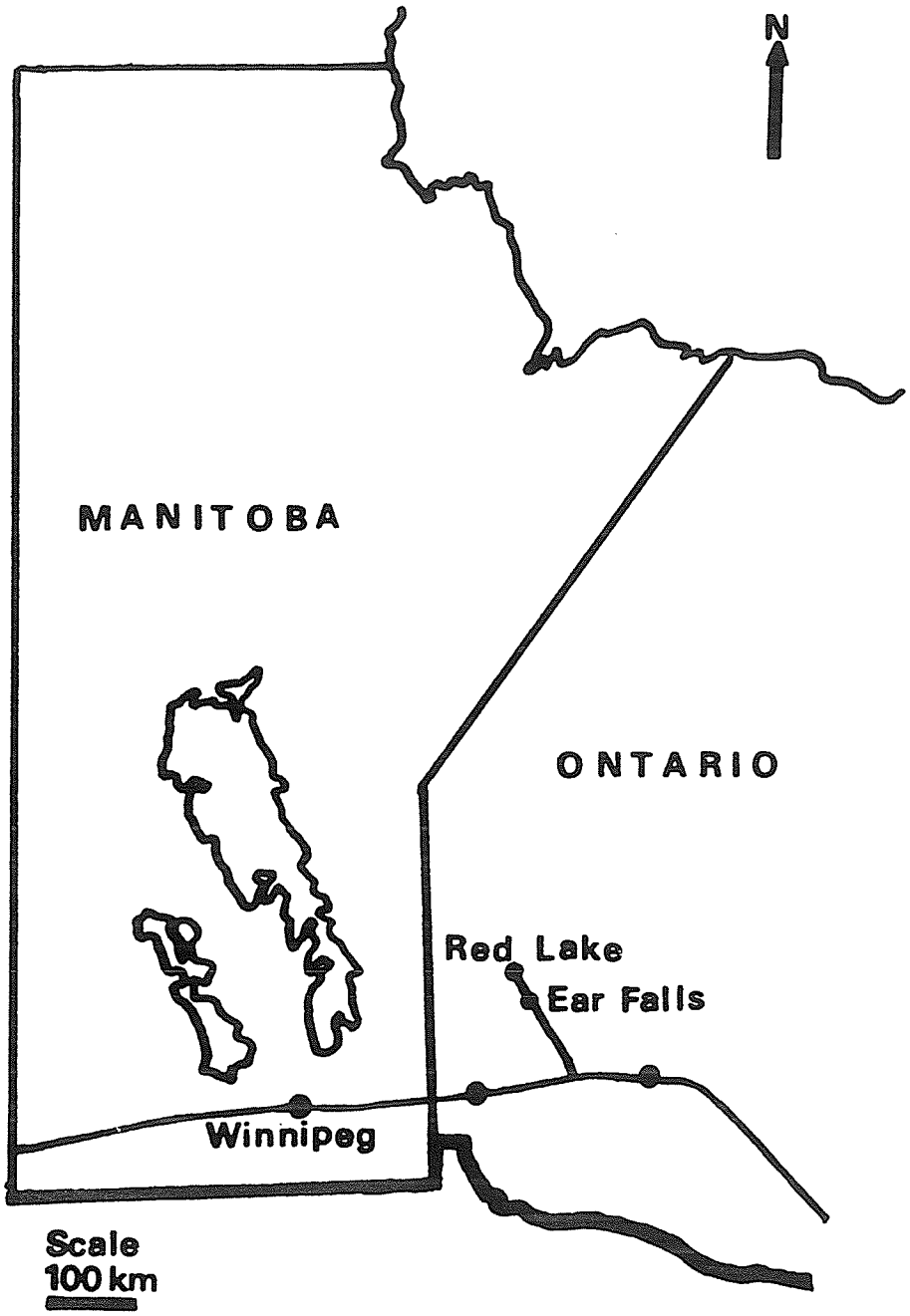

Figure 1.1: Location of survey area.

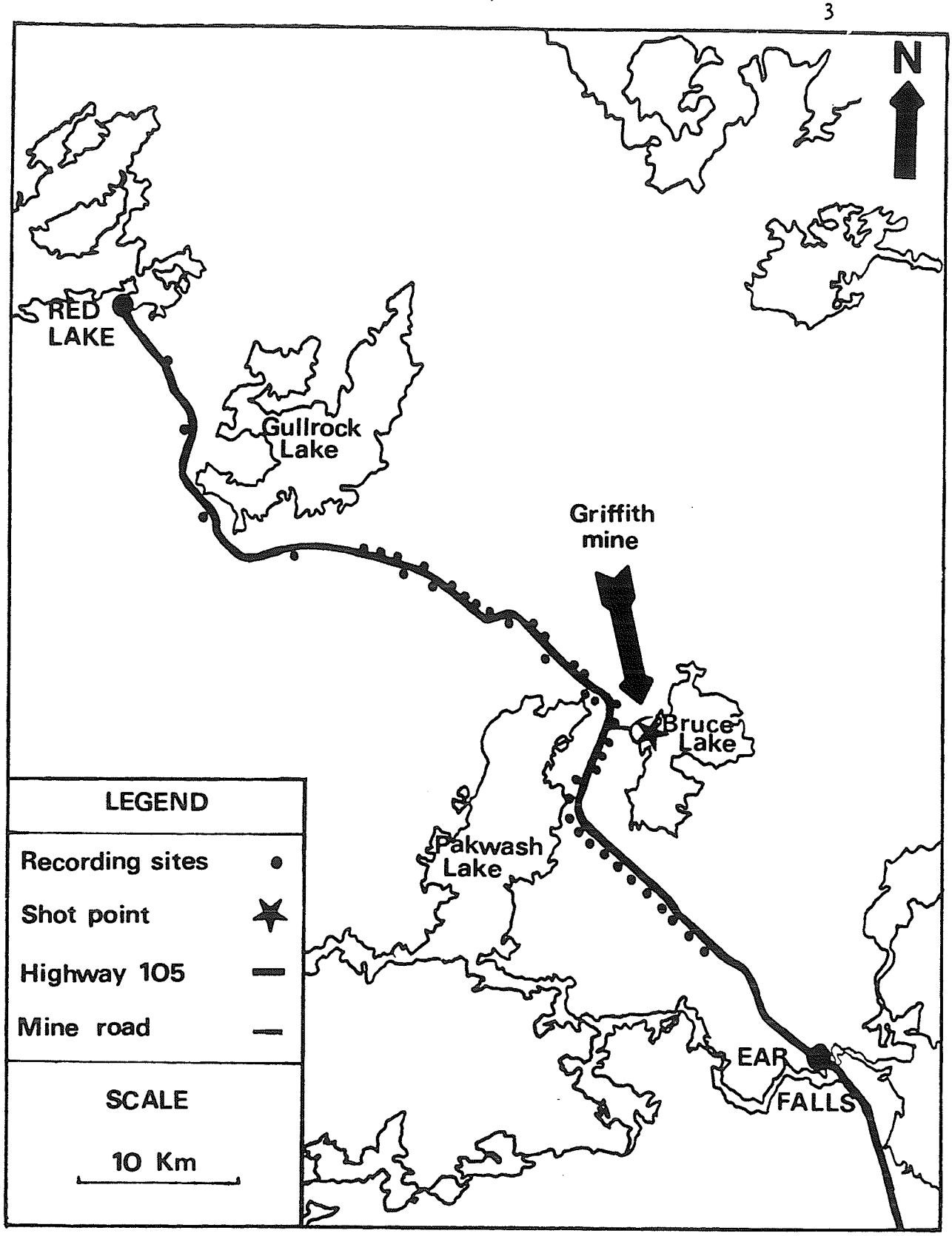

Figure 1.2: Location of Griffith mine.

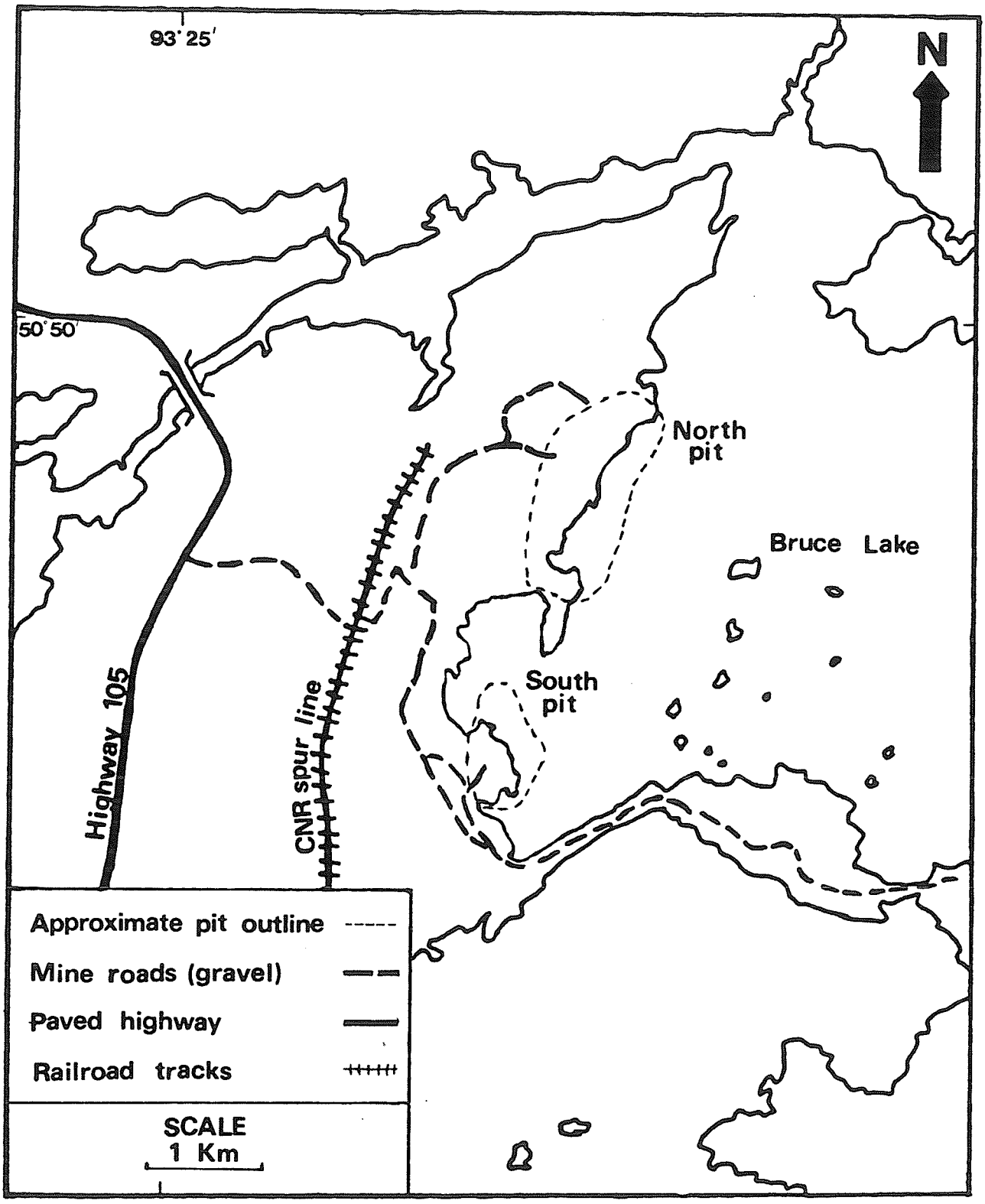

Figure 1.3: Location of North and South pits.

seismic profile extends across this boundary from the metasedimentary terrain of the Red Lake Subprovince to a metasedimentary gneissic terrain in the English River Subprovince. An important objective of this survey was to study the nature of this boundary.

A metavolcanic terrain is located north of the metasedimentary rocks. A granitoid mass is located north of these metavolcanic rocks. Studying this metavolcanic-granite boundary was another objective of the survey. Some other objectives of the survey were:

1. to determine velocities of constituent rocks in the area,
2. to delineate near surface discontinuities such as large scale faults and if possible determine dips and
3. to map any horizontal reflectors down to the Mohorovicic discontinuity.

Mine or quarry blasts are not ideal for this type of survey as the blasts are designed to break rock rather than create ideal seismic waves. The shots recorded in this survey were very complex and consequently one of the most important results from this work may be the production of interpretable seismic data.

Although some of the above objectives may not be attainable due to the complex nature of the source signal, the procedures involved in this thesis project to attain these objectives are:

1. to process the raw data,
2. to study the complex source by attempting to synthetically reproduce the source signal,

3. to try different techniques to process the the data and
4. to interpret the data using WKBJ (Chapman 1978) and ray tracing techniques (Whittal and Clowes 1979).

Since this is a new type of experiment, more emphasis is made on the processing of the data rather than the interpretation. Also, since the quality of the data is suspect due to inadequate timing and the lack of a reverse profile, the important results of this work will result from the studies of the source signal and the possible methods of interpreting the data.

Chapter II

FIELD PROCEDURE AND INSTRUMENTATION

2.1 INSTRUMENTATION

Ten two channel self contained portable analogue cassette recorders were used in the experiment. A complete description of the prototype of the recorders is given by Dorn (1974). The frequency response of the prototype is shown in figure 2.1.

Each portable unit records seismic data on channel 1 and timing information on channel 2. In order to achieve absolute timing of the traces the WWVB radio signal was recorded on channel 2. A Hall-Sears HS-10 geophone (peak frequency 1 Hz) was used with each recorder to detect the seismic signal.

2.2 FIELD PROCEDURE

2.2.1 Shot Point Recording

Twice a week Griffith mine blasts from one of two pits. Each shot consisted of one or more shot patterns from different locations in the pit. A recording unit was set up on bedrock at the edge of the pit in order to record the form of the signal and the absolute time of the shot. Since it was never important for the mine blast to occur at any specific time, the blast was often delayed by 5 minutes to an hour. For this reason the recorder was set to start re-

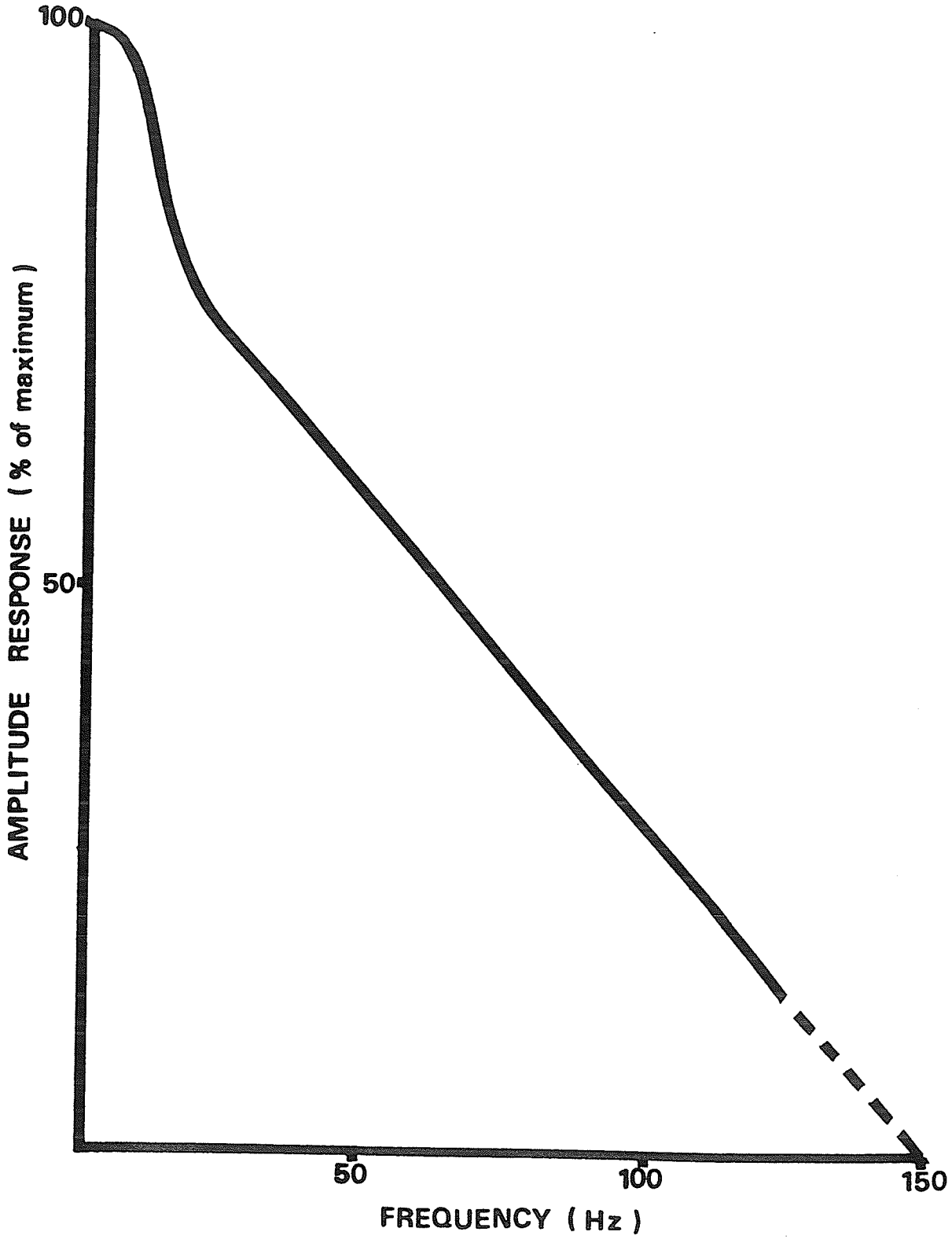

Figure 2.1: Frequency response of the recorder prototype. After Dorn, 1974.

cording 5 minutes before the scheduled blast time and the recorder was then allowed to record the entire length of the tape (45 minutes). Since the blasting engineers tried to ensure that the blast occurred within 45 minutes of the scheduled time only one shot was missed during the entire summer. The shot point recorder sites are shown in figure 2.2.

2.2.2 Field Recording

For each blast, recorders were set up at approximately 1.0 Km spacing along highway 105. Geophones were placed on bedrock or were buried for better coupling with the earth. The first recorder was set up at the mine entrance and data for profiles to the north and to the south of this point was collected throughout the summer. The location of each recording site was located using aerial photographs and major landmarks. These locations were then marked on a 1:50,000 scale map.

The records were played back each week to inspect the quality of the data. Poor records were repeated at a later shot. Records with a low S/N ratio were also repeated at a later shot in order to be stacked.

Often the shot point record was not recorded properly due to equipment failure. In this case a good record from that shot was repeated in a later shot. The remaining records of the initial shot could then be tied in with the later shot. Figure 2.3 illustrates the recorder locations as well as the locations of the shot patterns

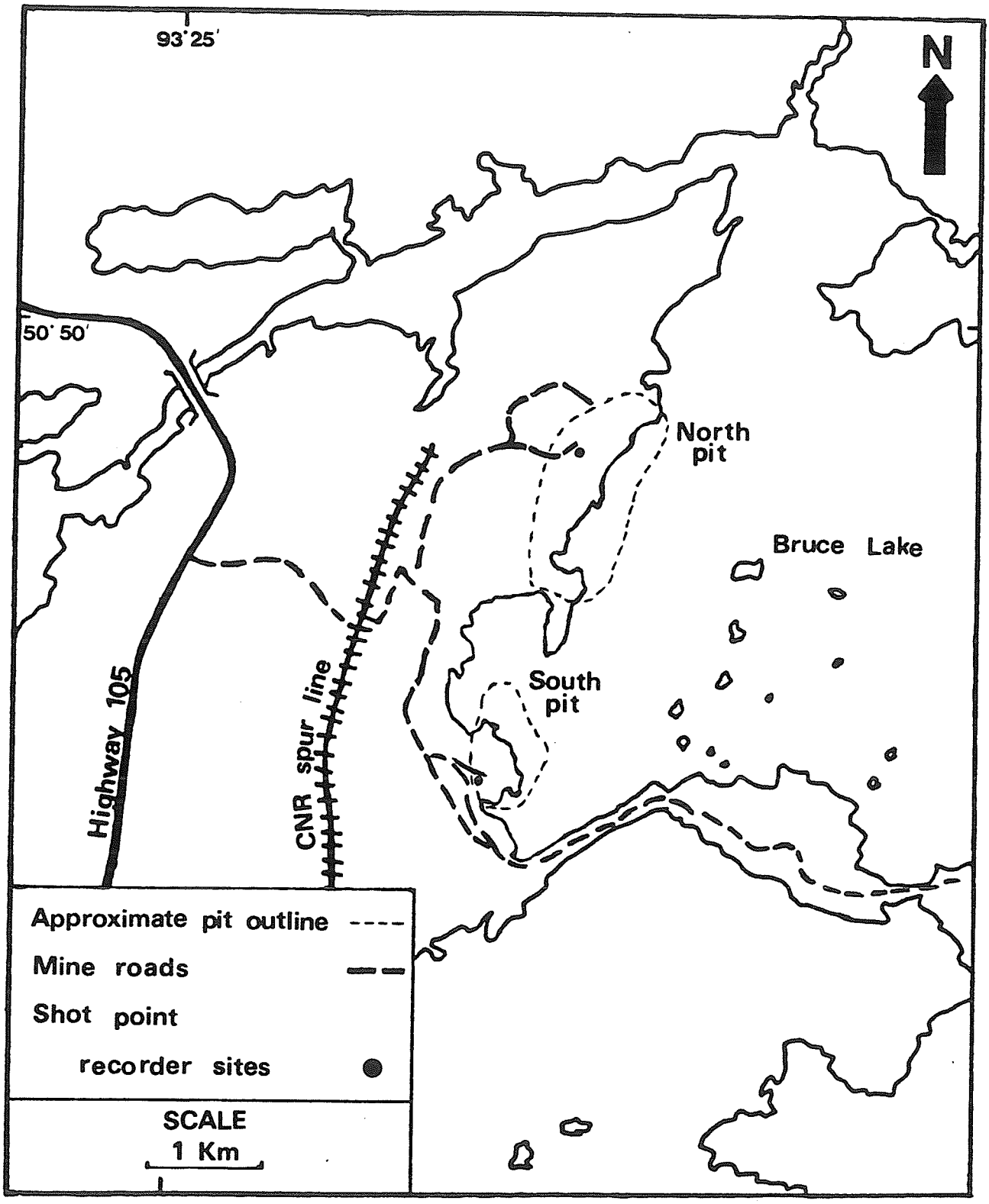

Figure 2.2: Location of the shot point recorders.

of shot #1. The recorder locations of the remaining shots are shown in Appendix A. The lost records indicated in figure 2.3 and Appendix A were due to either to equipment failure or human error. Note that since shot #15 was more than 45 minutes late, only the shot point record was recorded, consequently this shot will not be considered in further processing but will be used in the source modelling in Chapter 5.

The North profile is approximately 35 Km long. Records were taken at a spacing of 1 Km with the exception of the last 4 records which were recorded at a spacing of 5 Km. This was done in order to increase the coverage as well as to test two of the portable recorders which were modified to produce a higher gain. It was necessary to increase the gain on these units because some of the records farther away from the shot point showed a low S/N ratio. It was hoped that this would improve the recording capabilities of the recorders.

The South profile is approximately 12 Km in length with a 1 Km spacing throughout. Figure 2.4 shows the locations of both the North and South profiles.

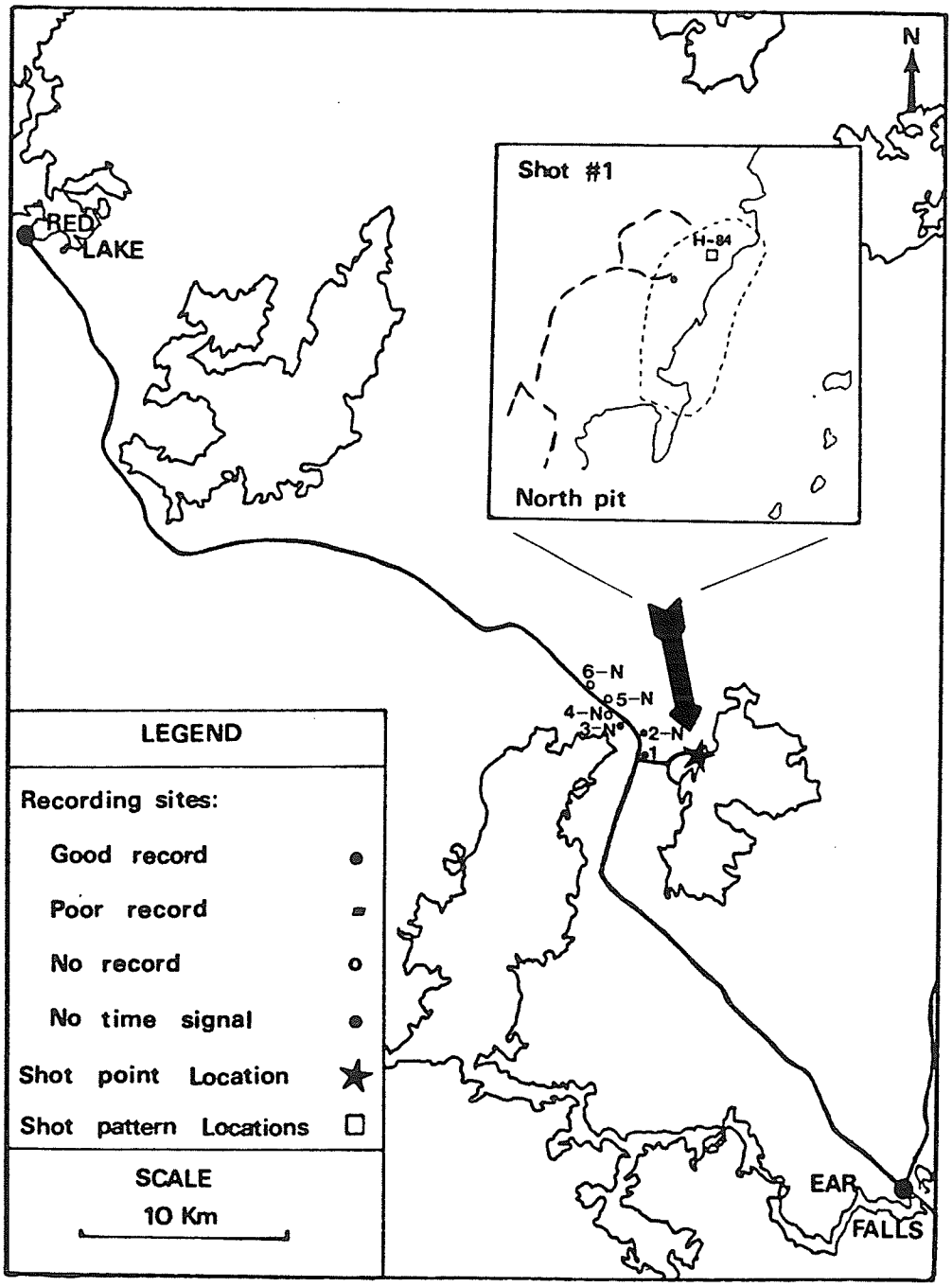

Figure 2.3: Recorder and shot pattern locations of shot #1.

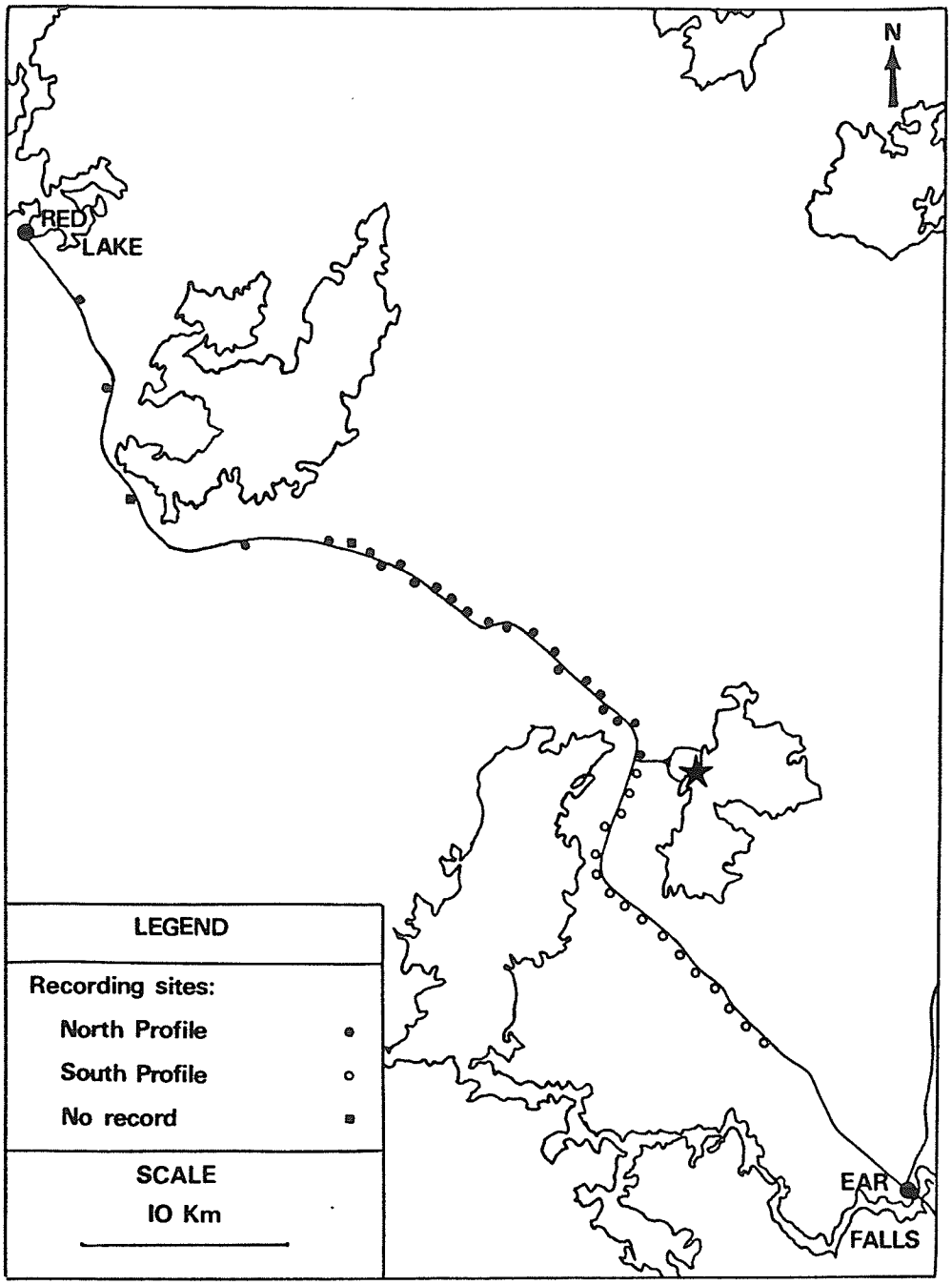

Figure 2.4: Recorder locations of the North and South Profiles.

Chapter III

GEOLOGY

The crustal seismic survey was carried out over two different geologic subprovinces. The North profile is situated entirely within the Uchi or Red Lake Subprovince while the South profile extends from the Red Lake Subprovince into the English River Subprovince located to the south (figure 3.1).

3.1 ENGLISH RIVER SUBPROVINCE

The English River Subprovince has been studied extensively by various authors. Good accounts of the area are given by Breaks et al (1978), Beakhouse (1977) and Wilson (1971). This area has also been studied in detail by Jones (1973) and Dwibedi (1966).

The English River Subprovince is an east-west trending belt of early Pre-cambrian felsic to intermediate amphibolite to granulite facies (Dwibedi 1966) gneisic rocks. The gneisses have been intruded by several felsic to intermediate plutons. The subprovince extends from southeastern Manitoba into northwestern Ontario and consists of two major components; the Winnipeg River batholithic belt in which felsic plutonic rocks predominate and the Ear Falls-Manitogan gneiss belt in which sedimentary gneiss predominates (Beakhouse 1977) (figure 3.1). Since the survey only extends into the Ear Falls-Manitogan gneiss belt, only this component will be discussed.

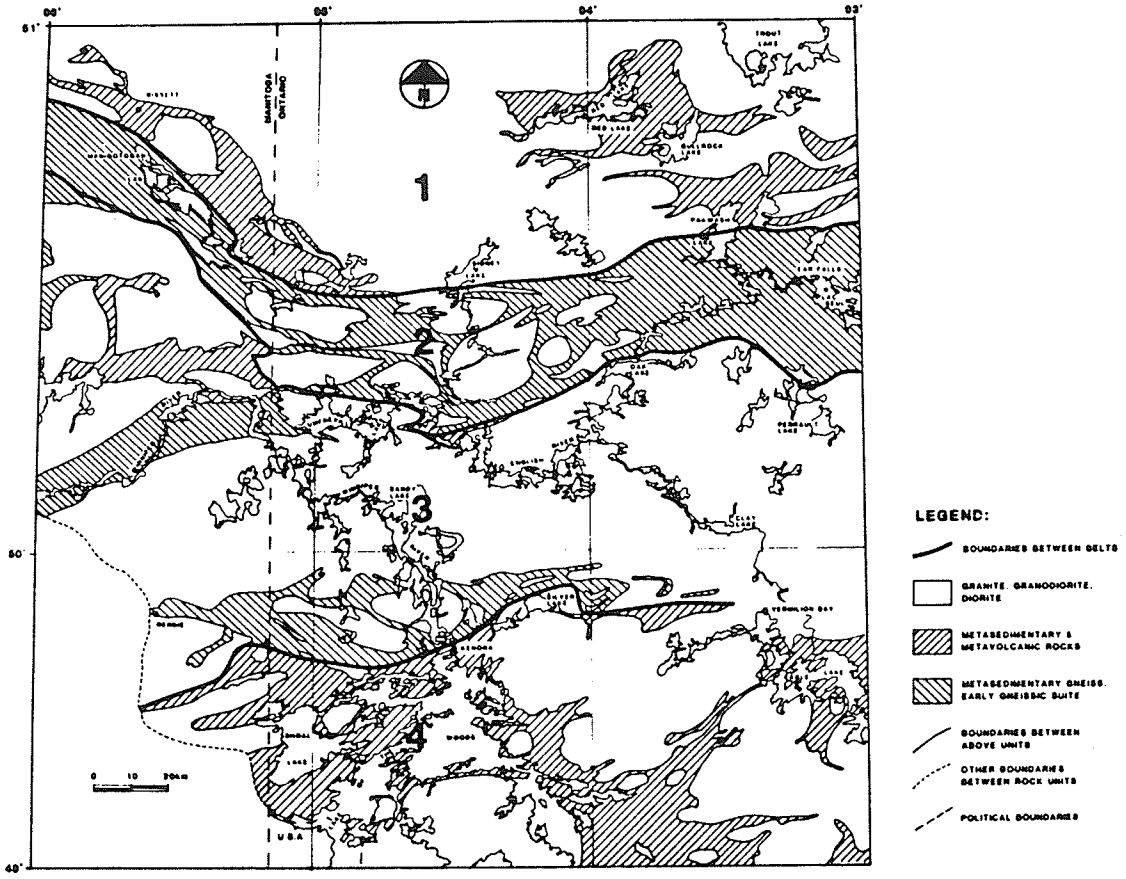

Figure 3.1: Geology of the Red Lake-English River Subprovinces. 1-Red Lake Subprovince. 2-Northern supracrustal belt of the English River Subprovince. 3-Southern supracrustal belt of the English River Subprovince (from Beakhouse, 1977).

The Ear Falls-Manitogan gneiss belt is composed of migmatized clastic sedimentary material characterized by a middle to upper amphibolite facies, metagreywacke-metasiltstone sequence intruded by subordinate felsic plutons (Beakhouse 1977).

A localized study of metasedimentary rocks proposed to be metamorphosed sandstone and shales (Jones 1973) was conducted by Van de Kamp and Beakhouse (1979) in the Pakwash Lake area. Since this study describes the actual terrain of the southern portion of the South profile, a brief description of the gneisses from this study is given.

The metasedimentary gneisses are compositionally layered which probably represents original layering (Van de Kamp and Beakhouse 1979). Layers range from 1 cm to 2 m thick while the grain size in the gneisses range from 0.25 mm to 1.0 mm in which the fine grained gneisses are mica poor and the coarse grained gneisses are mica rich. Within individual layers a gradation from biotite poor, quartz and feldspar rich portions to a biotite rich portion is common. Van de Kamp and Beakhouse (1979) propose that these probably represent original graded beds with the biotite representing an original shaley upper portion and the biotite poor portion representing a sandy bottom.

The gneisses are composed primarily of quartz (25-30%), plagioclase (40-60%) and biotite. Minor K-feldspar, muskovite, sillimenite, garnet and pyrite also occur.

The structure of the gneissic belt is mostly unresolved due to the extensive metamorphism. Foliation is generally parallel to sedimentary bedding while both foliation and bedding are concordant with the margins of larger plutons. The boundary between the gneissic belt and the Red Lake Subprovince consists of a mylonite zone (Beakhouse 1977) or fault zone. The location of the proposed Bruce Lake Fault at the subprovince boundary is indicated by lineaments and sheared rocks in the Bruce Lake area (Shklanka 1970). It was hoped that this boundary could be located in the survey (figure 3.2).

The Bruce Lake fault is thought to be a part of the Sydney Lake fault system which designates the boundary between the Red Lake and the English River subprovinces. The Sydney Lake fault has a minimum right lateral displacement of 6 Km (Breaks et al, 1978), as well as a vertical thrust component of 4.0 Km (Thurston and Breaks, 1978). An overthrust component to the north is also estimated to be 2.7 Km (Beakhouse, 1977). This large scale displacement is expected to be visible in the data collected in this experiment.

3.2 RED LAKE SUBPROVINCE

The Red Lake Subprovince has also been studied extensively by various authors although much of the survey area has not been recently studied in detail. Since Dowling (1894), Bruce (1924,1934) and Horwood (1940) studied the area, localized detailed studies have been undertaken by various authors. The area around the southern portion of the North profile has been studied by Shklanka (1970)

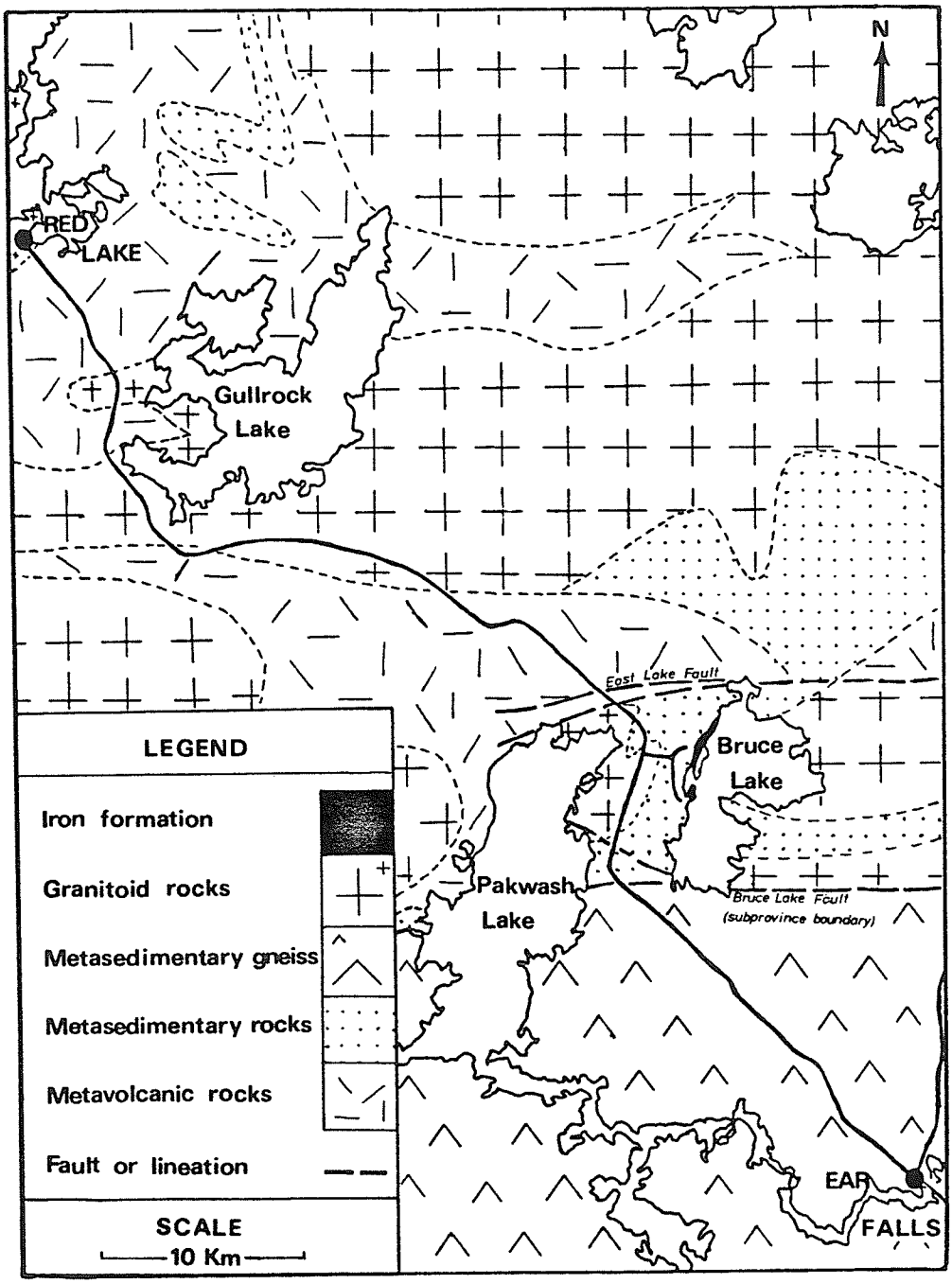

Figure 3.2: Geology of the survey area. The geology was compiled from various sources. These sources include Ferguson et al (1970), Beakhouse (1977) and Shklanka (1970).

while the northern portion has been studied by Ferguson (1968), Pirie (1978a,1979a) and Thurston (1981).

The Red Lake Subprovince is generally an east-west trending belt of metavolcanic-metasedimentary and granitic rocks extending from Paleozoic contact west of Hudson Bay to Lake Winnipeg (Thurston and Breaks, 1978). The grade of metamorphism is lower than that in the English River Subprovince and is characterized by subgreenschist to greenschist facies metamorphism (Thurston and Breaks, 1978). The metavolcanic-metasedimentary sequences form greenstone belts that are intruded by composite batholiths, ranging in composition from diorite to granite (Ayres, 1978).

A detailed study of the Bruce Lake area was carried out by Shklanka (1970). The following discussion of the terrain around Bruce Lake and the area immediately to the north is based on this study.

Immediately to the north of the Red Lake-English River subprovince boundary is a metasedimentary terrain of which the main rock type is metagreywacke. The rocks range from light to dark grey in colour, fine to medium grain in texture and from poorly foliated to schistose, depending on the mafic contact (Shklanka, 1970). The rocks are normally well bedded although rocks near granitic intrusions are coarser grained and the bedding is destroyed.

Shklanka (1970) classes the metagreywackes into three types, although gradations between these rock types occur interbedded with each other. The three types include biotite bearing, staurolite

bearing and amphibole bearing greywackes. The most common; biotite bearing greywacke is composed of quartz and plagioclase while some muscovite, garnet and microcline may be present. The staurolite bearing greywacke consists mainly of quartz and feldspar with staurolite forming up to 25% of the rock. Biotite and muscovite may also be present. The minor type of the three is the hornblende bearing greywacke which is composed mainly of amphibole, biotite, quartz and feldspar while some garnet may be present.

The shot point is located within an iron formation which is located at the west side of Bruce Lake on the east edge of the metasedimentary terrain. According to Shklanka (1970), the iron formation consists of magnetite-quartz interlayered with recrystallized chert or jasper. Locally magnetite-rich biotite schist occurs as well as hematite with magnetite. Interbedded metasediments also occur with fine grained greywackes the main constituent. Semi-calcareous greywackes also occur within the interbedded sediments. The metasediments are mainly composed of quartz and feldspar while biotite, amphibole, garnet and andalusite are present.

The iron formation is complexly folded while feldspar porphyry, lamprophyr and gabbro dikes intrude the formation (Shklanka 1970).

Located to the east of the iron formation underlying Bruce Lake is the Bruce Lake pluton.

A large quartz diorite to diorite pluton intrudes the metasediments along the north eastern part of Pakwash Lake. The Pakwash Lake pluton is mainly composed of plagioclase, microcline, perthite,

hornblende, biotite and quartz (Shklanka 1970). The contacts of the pluton with the surrounding metasediments are generally sharp in nature.

A metavolcanic belt mapped by Shklanka (1970) is located to the north of the metasediments. This belt is continuous with the Dixie Lake metavolcanic-metasedimentary belt to the west which is dominantly composed of a thick sequence of pillowed to massive, mafic to intermediate metavolcanic flows ranging from 2-9 metres thick (Breaks et al, 1974). The Dixie Lake belt is similar in composition to the northern part of the belt mapped by Shklanka (1970). In the southern part of the belt the majority of the volcanics are water-lain pyroclastics while minor rhyolite and mafic volcanics also occur (Shklanka, 1970). Lineaments which mark the boundary between the metasediments and the metavolcanics are generally regarded as faults. The rocks around the East Lake Fault (figure 3.2) are well bedded and interlayered with biotite bearing and hornblende bearing metagreywackes. Also, the rocks in the fault zone are sheared or mylonitized (Shklanka, 1970).

The pyroclastics in the metavolcanic terrain consists mainly of fine grained tuff with some rhyodacite and coarse grain tuff, although all gradations between these types are present (Shklanka, 1970). The volcanics are commonly interbedded with metasediments.

According to Shklanka (1970), the fine grained dacitic tuff is basically grey in colour and is composed of mainly quartz and sodic plagioclase. Biotite is also found while muscovite, amphibole,

chlorite, epidote or carbonate may also be present. The grain size is about 0.05 mm. The coarse grained tuff is found in minor amounts and consists of sodic plagioclase embedded in a fine grain matrix made up of biotite, quartz and sodic plagioclase. The sodic plagioclase crystals fragments are up to 4 mm in diameter while the grain size of the matrix is approximately 0.05 mm. The rocks are bedded and interlayered (some beds are graded) with other varieties of tuffs and metasediments. Beds range from a few inches to tens of feet in thickness.

Rhyodacite is another rock type found in minor amounts in the area. The rocks are light grey in colour and are composed of quartz, sodic plagioclase and muscovite while biotite, epidote or chlorite also may be present (Shklanka, 1970). The rhyodacite occurs as beds interlayered with mainly dacitic tuff or metagabbro.

Mafic volcanics also occur in minor amounts in the area and are dark green in colour and fine grained in texture (Shklanka, 1970). They are composed mainly of amphibole and are generally foliated.

The Gull Rock Lake Batholith is located north of the metavolcanic terrain and extends to the Red Lake Greenstone Belt. This area has not been studied in detail consequently only a brief generalized discussion of the batholith and its effects on the immediate terrain is given.

The Gullrock Lake Batholith is a massive body composed of medium grained biotite granodiorite to quartz monzonite (Breaks et al, 1976). The most dominant granitoid phase of migmatite near the Red

Lake greenstone belt is a medium grained leucocratic quartz to granite (Pirie, 1978a). Smaller medium to coarse grained leucocratic quartz monzanite intrusive bodies also cut the southern boundary of the greenstone belt (Pirie, 1979a).

Regional geological mapping of the Red Lake greenstone belt was carried out by Horwood (1940) while more detailed mapping has been done by Ferguson (1965,1966,1968). More recent studies in this area were carried out by Pirie (1978a,1978b,1979a,1979b), Wallace (1980,1981,1982) and Thurston (1981). Since the seismic survey was carried out over the southern region of the greenstone belt, only this portion will be discussed.

Much of the southern region of the greenstone belt is underlain by a sequence of Pre-cambrian mafic to felsic metavolcanics largely calc-alkaline in composition (Pirie, 1979a). The dominant component of the southern region of the greenstone belt is a felsic sequence composed of flows, tuff, lapilli-tuff and minor lapillistone (Pirie, 1978a). At the southern limits of the greenstone belt, these felsic rocks are intermixed with two types of intermediate metavolcanic flows. One is a fine grain amygdular flow while the other consists of a similar matrix containing numerous plagioclase phenocrysts. These flows are also found to be locally pillowed or breciated (Pirie, 1978a,1979a). Granitoid sheets and dikes also commonly intrude this metavolcanic complex. Further to the north a similar mixture of felsic and intermediate to mafic metavolcanics occurs with greater amounts of bedded clastic meteasediments derived from felsic volcanic rocks (Pirie, 1979a).

A large body of biotite hornblende trondjemite to quartz diorite intrudes this sequence just east of a narrow channel in Gullrock Lake. Dikes and sheets of medium grained gabbro and diabase also intrude the calc-alkaline metavolcanic sequence throughout the area (Pirie, 1979a). At the northern limits of the North profile an intermediate intrusion locally known as the 'Howey Diorite' occurs near the junction of highways 105 and 125 (Pirie, 1978a,1979a).

Structurally the greenstone belt is interpreted to be a synformal recumbent anticline forming the nose of a nappe which is embedded into the surrounding granitic rocks and basement (Thurston and Breaks, 1978). It is not likely that this structure can be resolved as only two recording sites were located within this region.

3.3 DEEP CRUSTAL STRUCTURE

An important objective of this study is to delineate deep horizontal reflectors, therefore it is important to discuss the deep crustal structure. Deep crustal studies have been carried out by Hall (1971), Hall and Hajnal (1969,1973) and Gupta and Barlow (1984) in the area of interest.

Studies by Hall and Hajnal (1969,1973) have shown that there are two distinct deep crustal layers in the area (the Riel and the Mohorovicic discontinuities). They used average compressional velocities of 6.05 Km/sec, 6.85 Km/sec and 7.92 Km/sec to calculate average depths of 18.3 Km for the Riel (or Conrad) discontinuity and 34.3 Km/sec for the Mohorovicic discontinuity.

A gravity study by Gupta and Barlow (1984) shows the depth of the Riel to be 14 Km at the Wabigoon/English River subprovince boundary 23.5 km at the English River/Red Lake subprovince boundary and 16 Km north of the English River/Red Lake boundary. They also found that the corresponding depths of the Moho were 37.5 Km, 31 Km and 37 Km at these points. The geometry of these deep interfaces calculated by Gupta and Barlow (1984) are in agreement (within 2 Km) with the seismic depths calculated by Hall and Hajnal (1969,1973) over the same region. These results show the crust is thinnest under the Sydney Lake fault system, while the thickest section of the Riel (23.5 Km) occurs over this point (figure 3.3). It is hoped that these depths can be further verified with the information acquired from this experiment. This will be further discussed in Chapter 7.

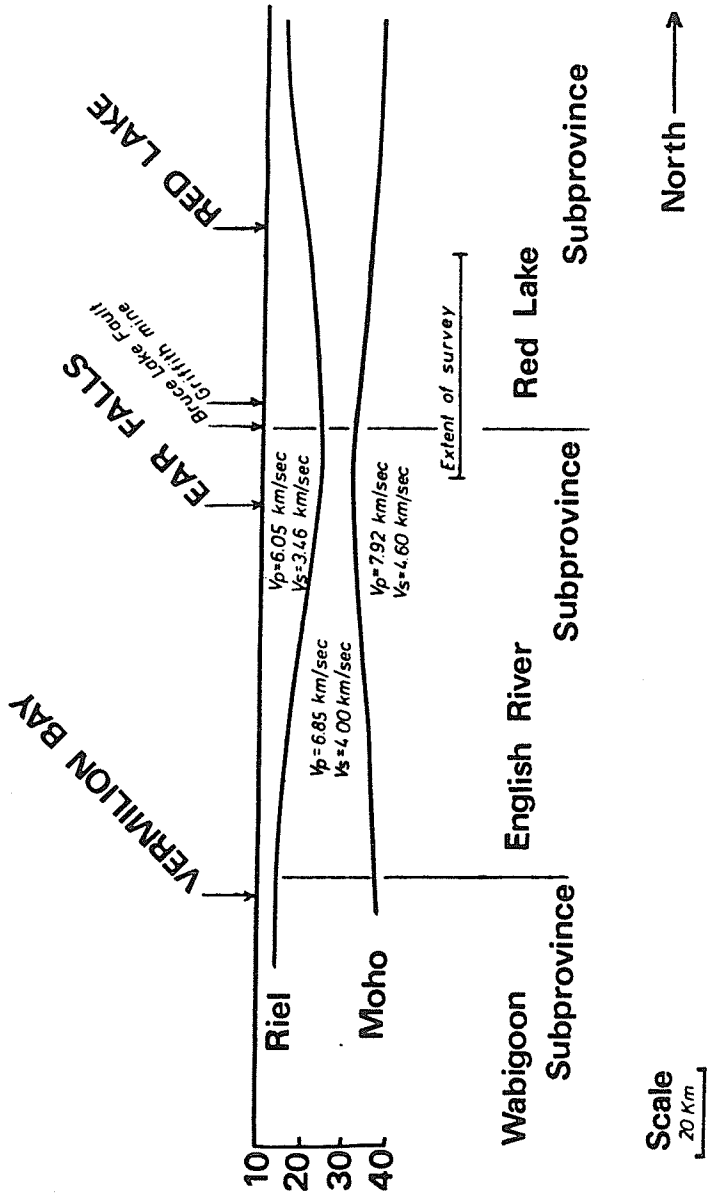

Figure 3.3: Deep Crustal Structure. The above information was derived from the studies of Hall and Hajnal (1973) and Gupta and Barlow (1984).

Chapter IV

PROCESSING OF RAW DATA

4.1 A/D CONVERSION AND DEMULTIPLEXING

The objectives of the processing sequence were both to enhance the signal to noise ratio and to obtain a technique to interpret the complex signal. The sequence is outlined in table 4.1.

Analogue to digital conversion was carried out using a Geo Space DAS-209 digital seismic field recorder. A remote playback unit read the cassette tapes, demodulated the information and fed it into the amplifiers of the Geo Space system. The signal was amplified by some pre-determined fixed gain (depending on the amplitude of the signal), then fed into the A/D converter which sampled at an interval of 1 msec. The digital signal then was recorded on 9 track 800 BPI tape.

Channel 1 contained seismic data and channel 3 contained timing information (WWVB time code). Channel 2 was not used as some internal problems were encountered with the system. Channels 4-30 also were not required.

The next series of steps were part of a processing package for data recorded by the Geo Space recording unit arranged by Owen Stephenson who was the seismic party chief at the Centre for Pre-camb-

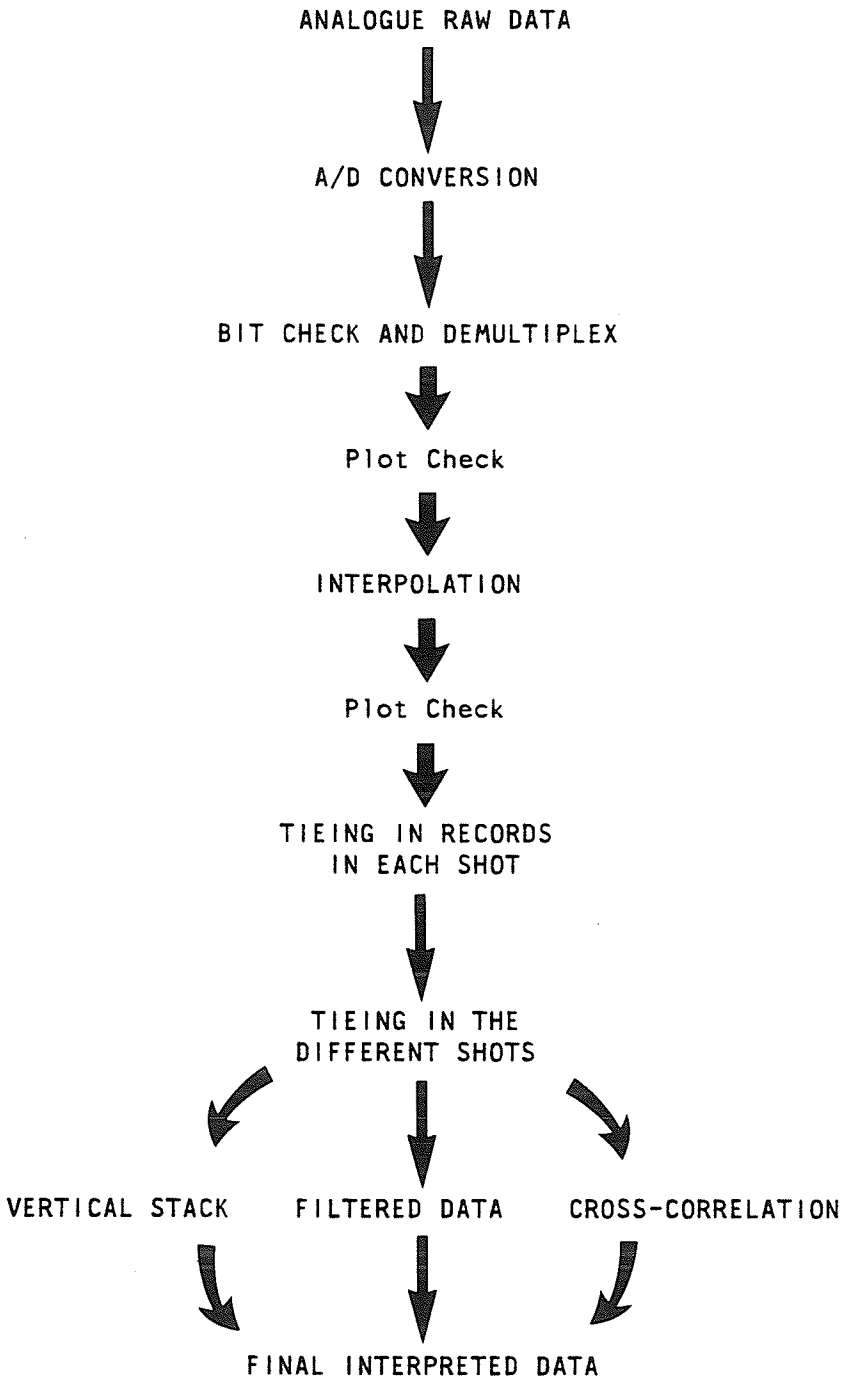

TABLE 4.1

Processing sequence.

rian Studies at the University of Manitoba. The package was further modified by Tom Millar who now holds that position.

All 30 channels were then transferred to 6250 BPI tape using a blocksize of 20008 bytes. The next stage involved a file finding program used to check the data for any error files which may have occurred in the preceding steps. The following step involved checking the data for missing bits and replacing them. The data was also demultiplexed during this stage.

The data was then plotted in order to check its quality. Records with poor quality due to the previous processing stages were re-digitized.

4.2 INTERPOLATION

The rate of digitization on each record was found to be different as the tape speeds of the recording units were not the same. These tape speeds were found to vary by as much as 10% from unit to unit. Figure 4.1 illustrates examples of this variation. Record 21-N and shot #5 are shown in this example. The seismic signal of the records is shown as well as the WWVB time signal. The number of digital intervals per second is also shown. Anderson (1979) found that the number of digital intervals per second varied by less than 1% along each trace (using the same recording units). The data collected in this experiment varied by as much as 5% (figure 4.2), consequently in order to make each record consistent with all of the others it was necessary to interpolate each record in sections. A

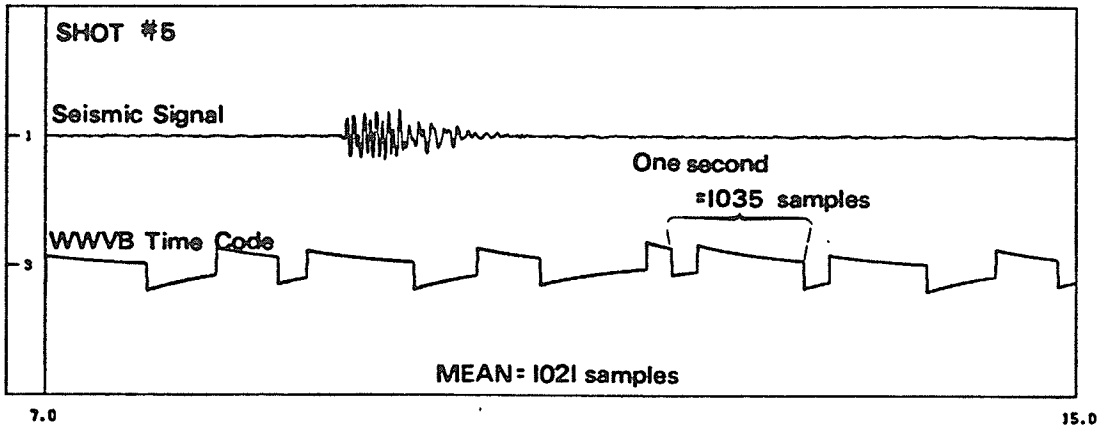

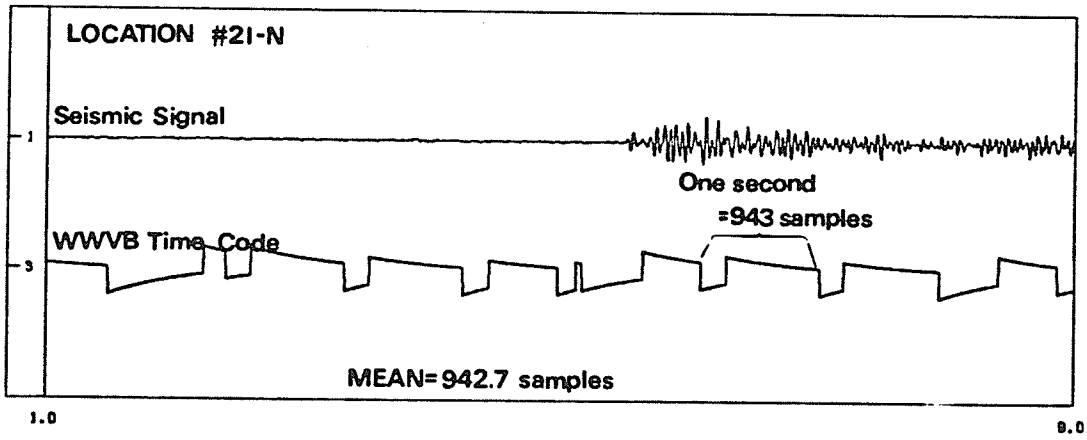

Figure 4.1: Variation of tape recorder speeds. The upper diagram illustrates the digitization rate of shot #5 using unit A. The lower diagram illustrates the rate of digitization of record 21-N recorded on unit F. Note that the polarity of the WWVB time code is such that second markers are designated by a sudden drop in the signal. The field examples given in this study are opposite in polarity to the example in figure 4.3 where second markers are designated by a rise in the signal.

program written by Anderson (1979) was modified and used to perform a linear interpolation on each section of each record. In order to interpolate the data it was necessary to find the number of digital intervals per second. This was accomplished by counting the samples from a dump of the time signal. The mean value was calculated and an interpolation constant was derived for each section of each record.

Another problem arose concerning the interpolation of the data. It was found that the WWVB time code was not reliable for exact timing information due to either the recording or the playback of the records. The rise of each square wave (marking the beginning of each second) was often delayed by a small amount, consequently this would increase the apparent length of one second and decrease the apparent length of the next (figure 4.3). It was therefore necessary to average the number of digital intervals per second over a large range in order to derive reliable interpolation constants. The interpolation constant was therefore derived over a range larger than the actual range of interpolation. The following illustrates the calculation of the interpolation constants necessary to interpolate each section of each record:

Apparent length of one second in digital intervals=Tn

Means for each section of each record are calculated by:

$$MEANm=\sum_{i}^{M} Ti/M$$

where: i=second counter

M=Total number of seconds used in calculation.

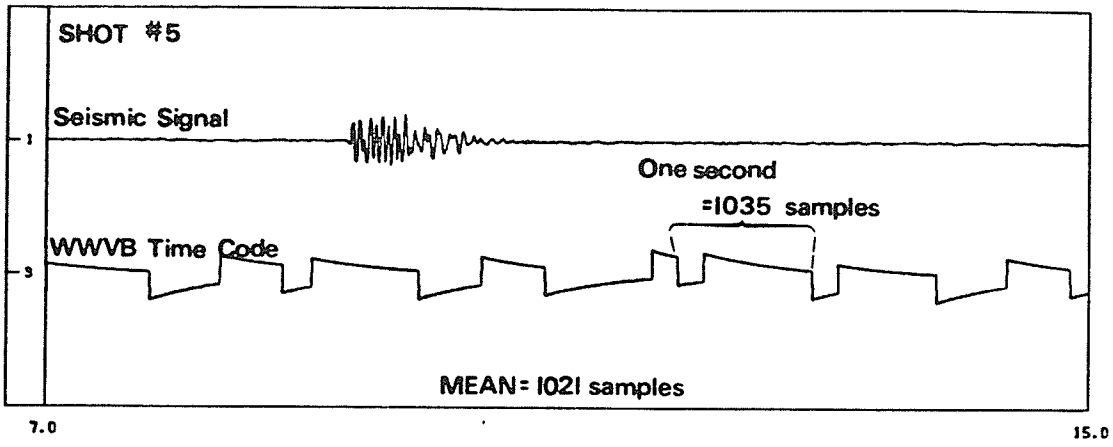

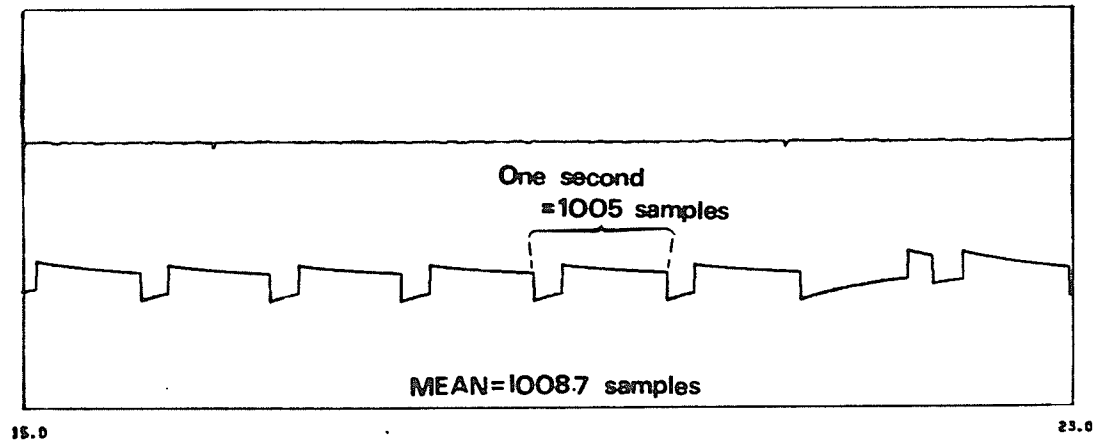

Figure 4.2: Variation of tape speed within a single recorder. This diagram illustrates the variation of the digitization interval at the beginning of shot #5 to that at the end. Again, note the polarity of the time code.

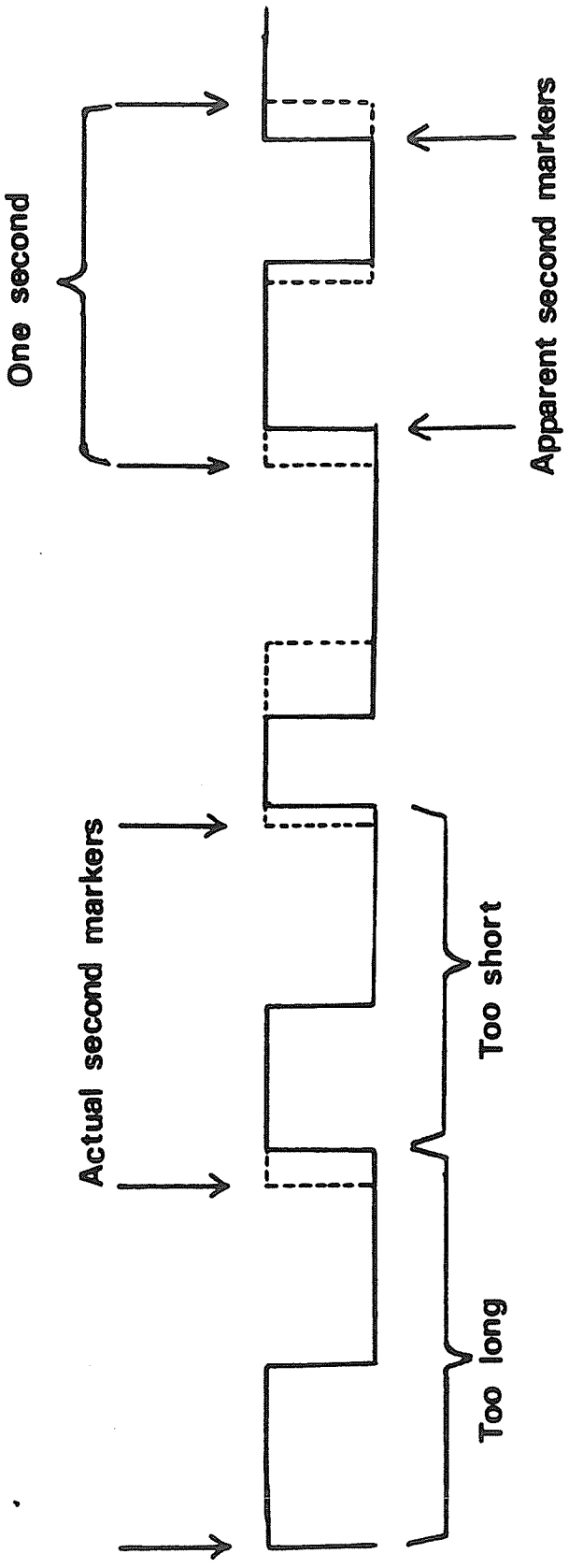

Figure 4.3: Unreliability of timing information.

m=Section number to be interpolated.

=1,2,...,N

N=Total number of sections to be interpolated.

Note: N was usually set at 3,4 or 5 depending on the length of the record.

Interpolation constants for each section are derived from the mean values representing the number of digital intervals per second:

Zm=interpolation constant

=MEANm/1000

Table 4.2 illustrates an example calculation of the interpolation constants.

Some records did not include a time signal due to equipment failure. These records were interpolated using the same interpolation constant throughout the entire record. The number of digital samples per second used in the derivation of the interpolation constant were taken from an average of records recorded on the same unit at near the same time. It was necessary to use records that were digitized near the same time as the speed of the playback unit also varied with time. At this point all of the records were consistent with one another within 1%.

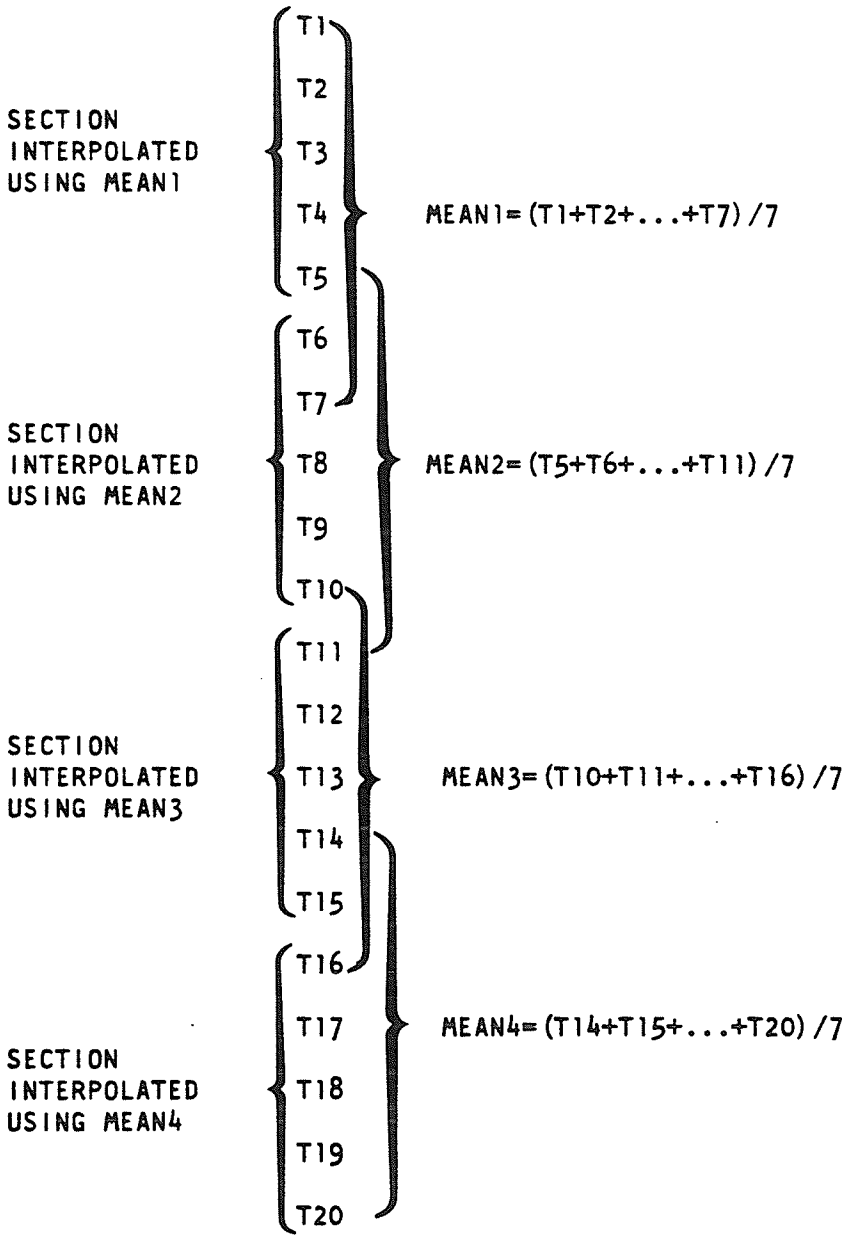

TABLE 4.2

Example of calculation of interpolation constants.

4.3 TIEING IN THE TRACES

Since the records were recorded individually it was then necessary to tie all records together. The first step involved tieing in records which were recorded at the same time (same shot). This was done using the absolute timing information of the WWVB time code. A reference point in the time code just before the shot time was chosen. This reference time was then located on each record of common shot point. Since the only consistent reference points on all records are the rises and falls of the square waves of the time code, it was necessary to choose the rise of a certain second marker as the common point on all traces. This was not as easy as first thought because of the unreliability of the WWVB time code (figure 4.3). The author's own discretion was used in picking a second marker in the code with a reliable square wave near the beginning of each record. The rise point of the square wave was then taken to be consistent with the actual rise time of all other square waves. This rise point could then be transformed to the chosen common second marker (figure 4.4). The time code channel was no longer required at this point and was therefore dropped.

The shot-receiver distances were measured directly from a 1:50,000 scale map. The error in measurement is $\pm$ 50 metres due to to the lack of major landmarks to locate many of the recorder locations. Appendix B gives these measured distances for all records. Figure 4.5 show the tied in records of all shots #1 and #2. The remaining shots are illustrated in Appendix C.

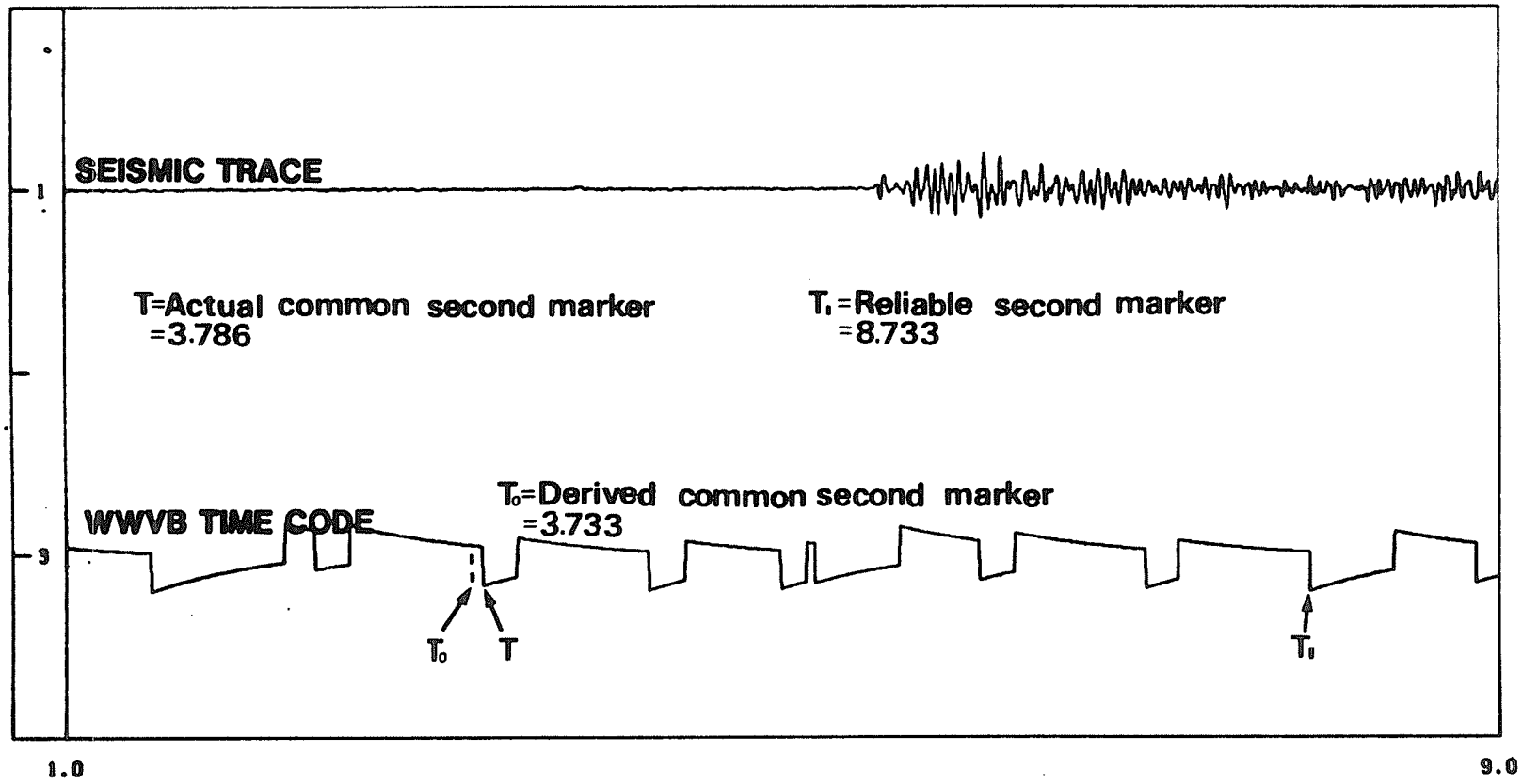

Figure 4.4: Locating a common second marker.

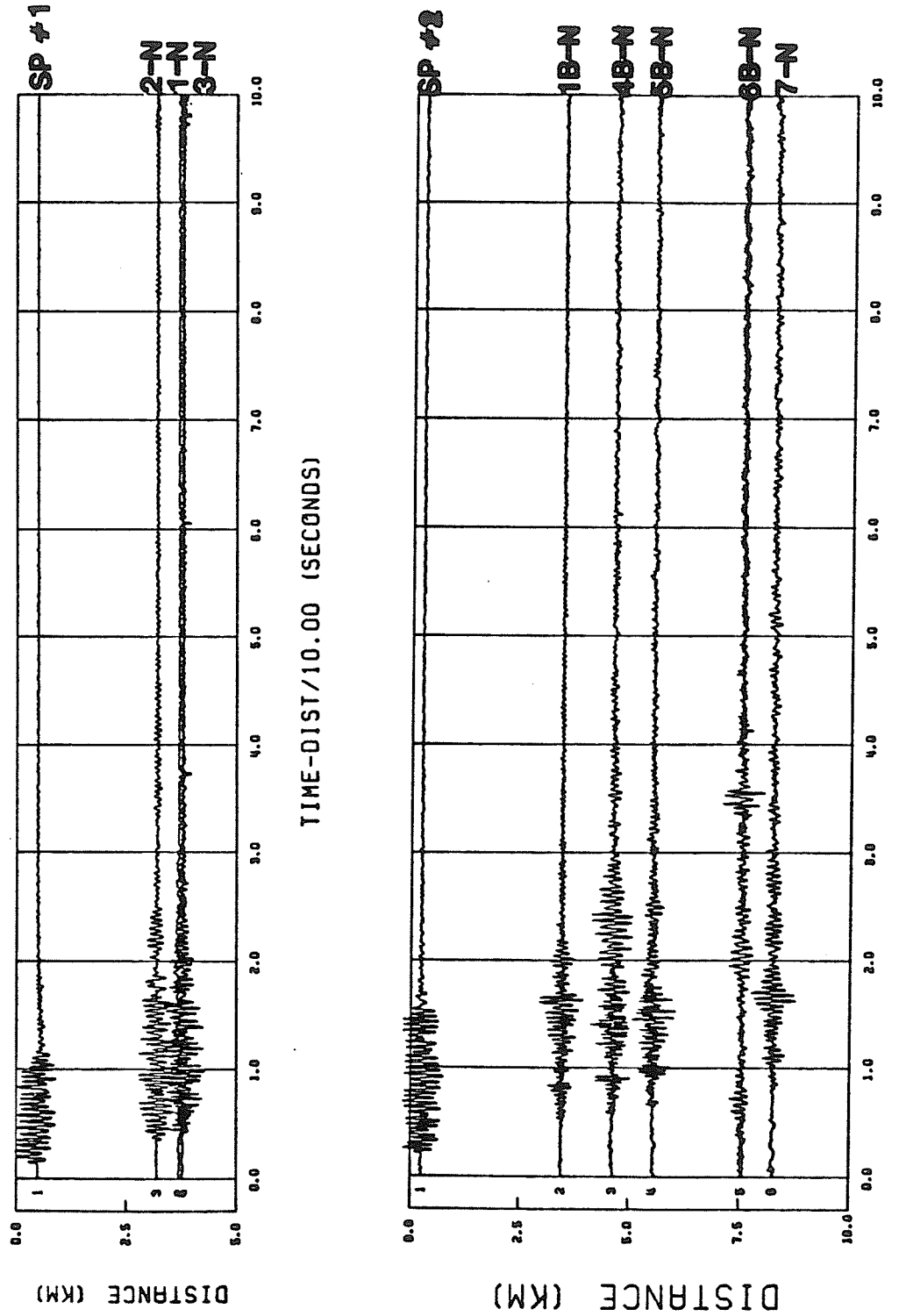

Figure 4.5: Raw records of shots #1 and #2.

Once all records of common shot point were tied in, it was then necessary to tie the records from the 16 shots together. This was accomplished by picking the first breaks off of the shot point records. Again, this was not as easy as first realized since the position of the first break was not obvious. In many cases the 'obvious' first break was not the actual first break. The actual first break was located before a large amplitude apparent first break sometimes just buried in the noise. By filtering the shot point record with a 6-40 Hz filter and plotting on a large amplitude plot, the first breaks of most shot point records could be located although it was still difficult to identify in many cases. Figure 4.6 illustrates the difficulty of locating first breaks. Figure 4.7 illustrates some of the more obvious examples that indicate more than one type of arrival at the source recorder. Possible explanations for these small amplitude first arrivals are discussed in Chapter 5. Note that the possibility of using the high amplitude apparent first breaks to tie in the shots was considered but this arrival was not apparent on many shot records. Also, since the exact nature of the arrival was not known, it was hard to extrapolate a shot time. In fact the use of this arrival was used in the beginning with no appreciable results.

Once the absolute time of the first break was known, the time of the shot could then be derived since the distance of shot point recorder and the approximate velocity of the medium was known. The shot time was then extrapolated to an accuracy of ± 10 msec. This shot time could then be found on all traces of common shot point and thus represent the start of all records.

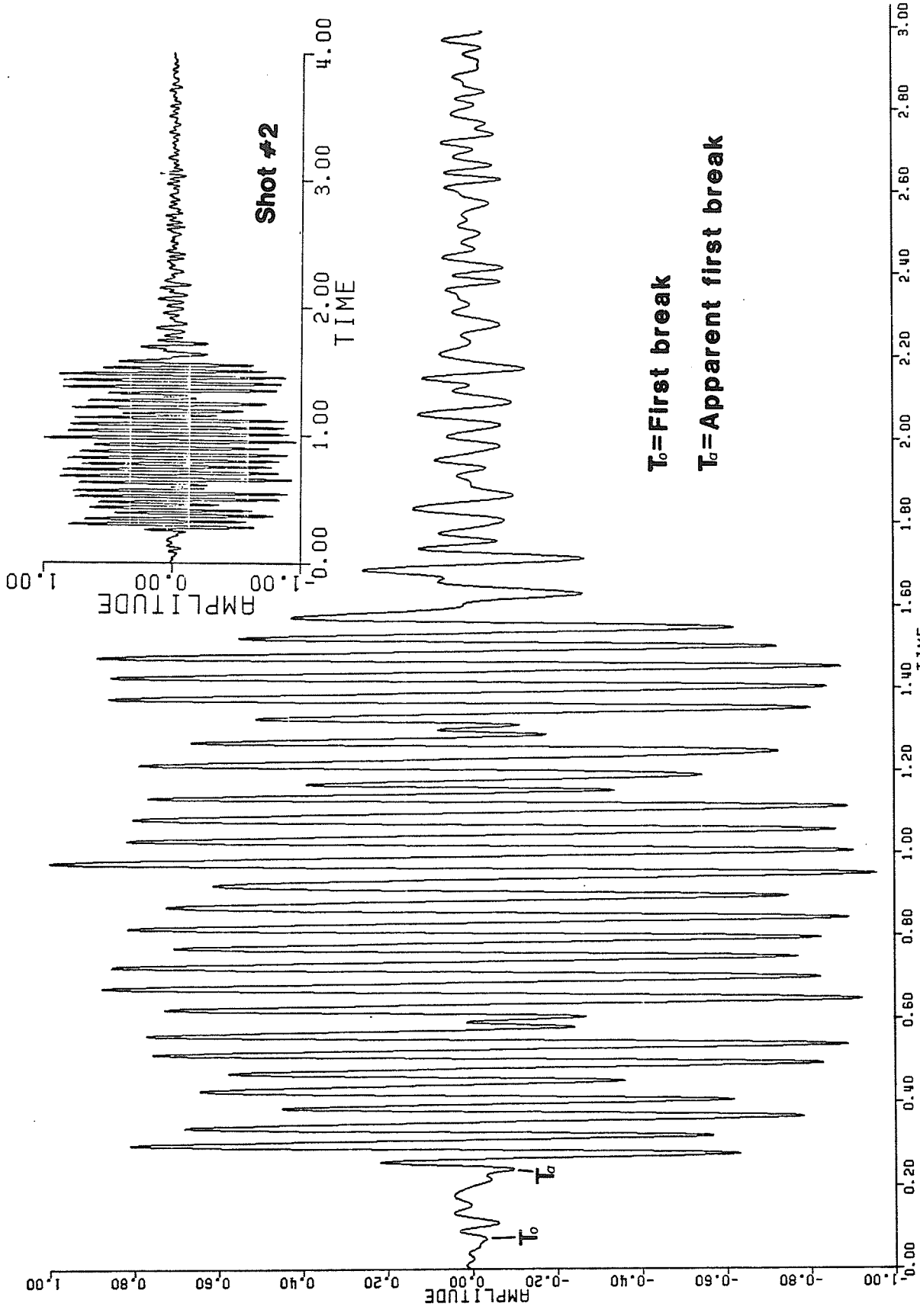

Figure 4.6: Difficulties in locating first breaks.

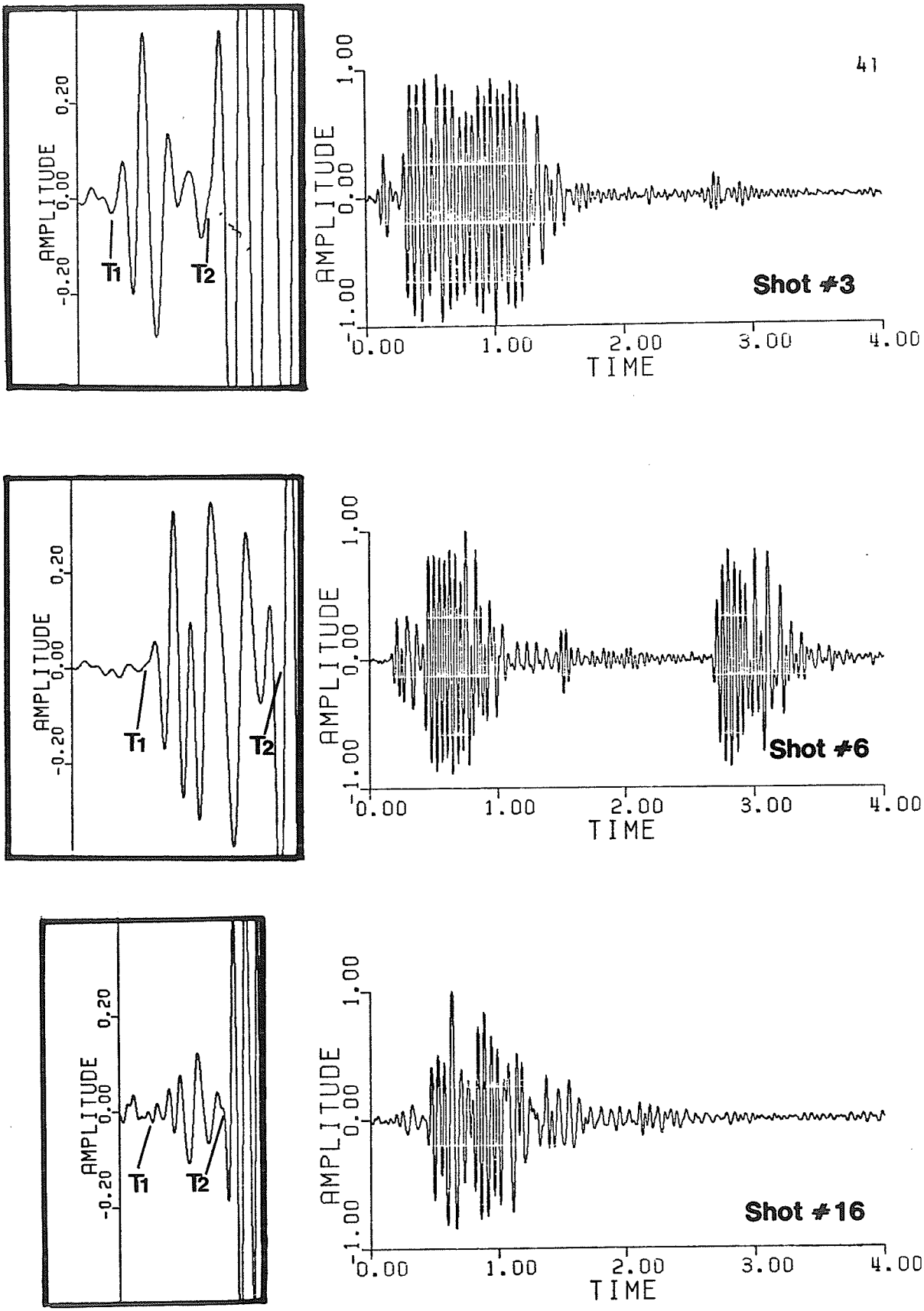

Figure 4.7: Examples of shot records showing more than one type of arrival.

Some of the shots did not include a shot point record, therefore it was necessary to tie these records in with the records of the other shots. This was done by using records that were repeated at a later shot for this purpose. Since the travel time of the record was known from the second shot, the shot time of the first shot could be derived by extrapolating this travel time back to the source. One problem was encountered using this technique. The location of the field recorder was the same for both shots but the location of the shot was not. This was because the location of each shot pattern was not the same from blast to blast. Since the velocity of medium was known from the travel time of the second record, the travel time of the first record could then be extrapolated from the difference in distances. The time of that shot could then be derived. Once the absolute time of all shots were derived, all of the records of all of the shots could be tied together. At this point the shot point records were not required other than for cross-correlation and for comparison with the models in Chapter 5. Figures 4.8 and 4.9 show the tied in records of both the North and South profiles. Table 4.3 indicates which records were included in the North and South profiles.

4.4 COMMENTS ON RAW DATA

The quality of data varies from good to very bad. The data from shots 1, 2, 3 and 8 are of good quality. Shots 4, 5 and 6 are poor in quality . The data from the remaining shots were of reasonable quality. The quality of each record is briefly summerized in Appen-

NORTH PROFILE			SOUTH PROFILE		
Shot number	Record number	Shot-receiver distance (Km)	Shot number	Record number	Shot-receiver distance (Km)
1	1-N	3.70	1	1-N	3.70
1	2-N	3.21	11	2D-S	3.00
1	3-N	3.80	7	3-S	3.37
2	4B-N	4.63	16	4F-S	4.94
3	5C-N	5.44	7	5-S	4.24
13	6F-N	7.28	11	6B-S	5.15
2	7-N	7.54	11	7B-S	5.67
2	8-N	8.25	8	8-S	7.79
12	9D-N	9.10	8	9-S	7.89
14	10F-N	10.98	8	10-S	8.37
12	11C-N	10.72	8	11-S	8.87
3	12-N	11.60	9	12-S	7.33
4	13-N	12.42	10	13B-S	10.17
4	14-N	13.51	10	14B-S	10.98
16	15C-N	14.30	10	15B-S	11.65
6	16C-N	15.38	10	16B-S	12.56
6	17B-N	16.45	13	17B-S	11.40
13	18C-N	18.35	--------	--------	---------
17	20D-N	19.75	--------	--------	---------
17	21-N	24.29	--------	--------	---------
17	23-N	31.82	--------	--------	---------
17	24B-N	35.48	--------	--------	---------

TABLE 4.3

Records used in the North and South profiles.

dix B. These records can be seen in Appendix C using Appendix B to locate them.

Shot #2 did not include a time signal while several other shots did not include a shot record. These include shots 4, 8, 9, 12, 14 and 17. Shot points 10 and 13 are poor in quality while the remaining shot point records were generally good in quality.

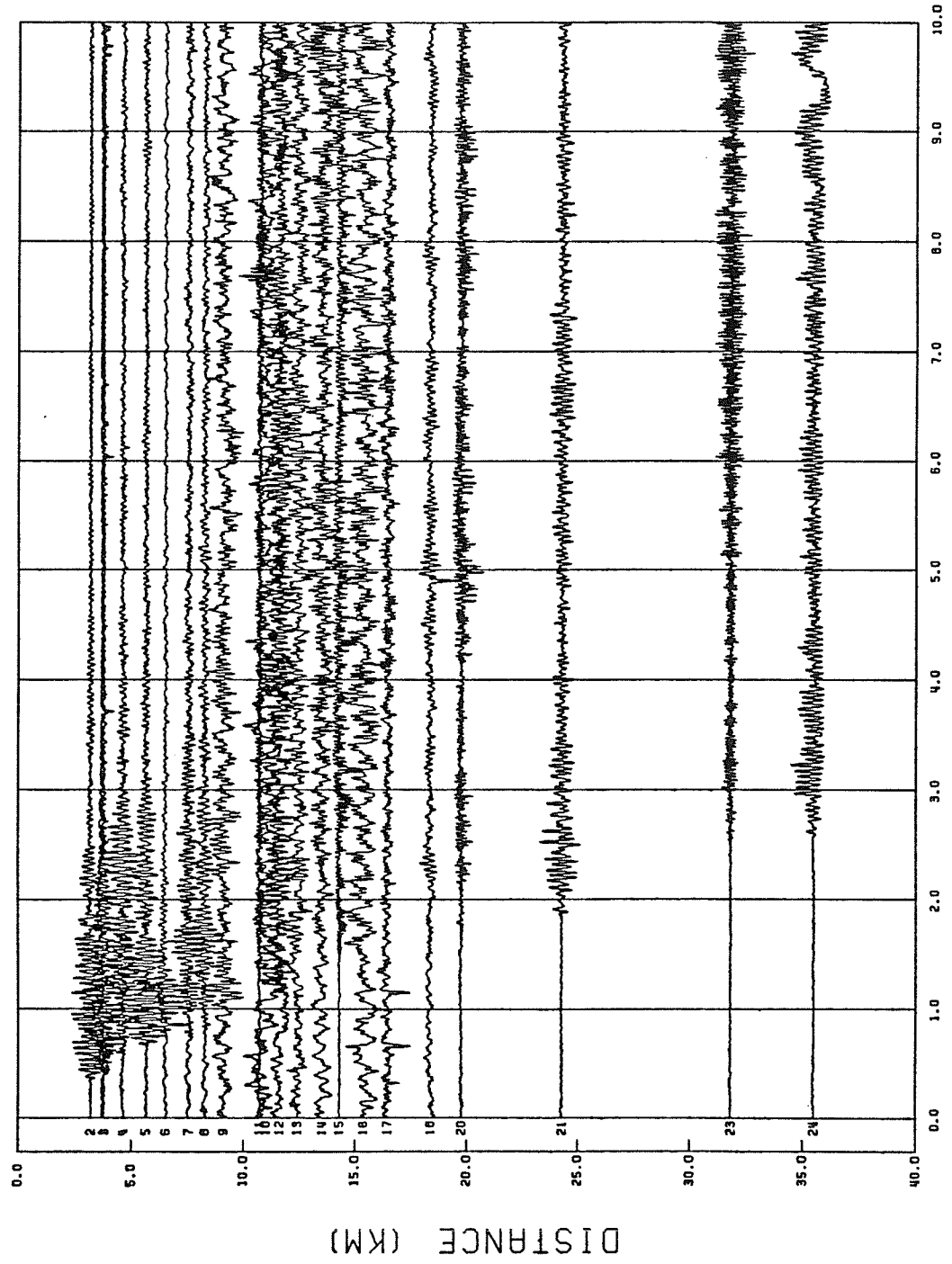

Figure 4.8: Raw records of the North profile.

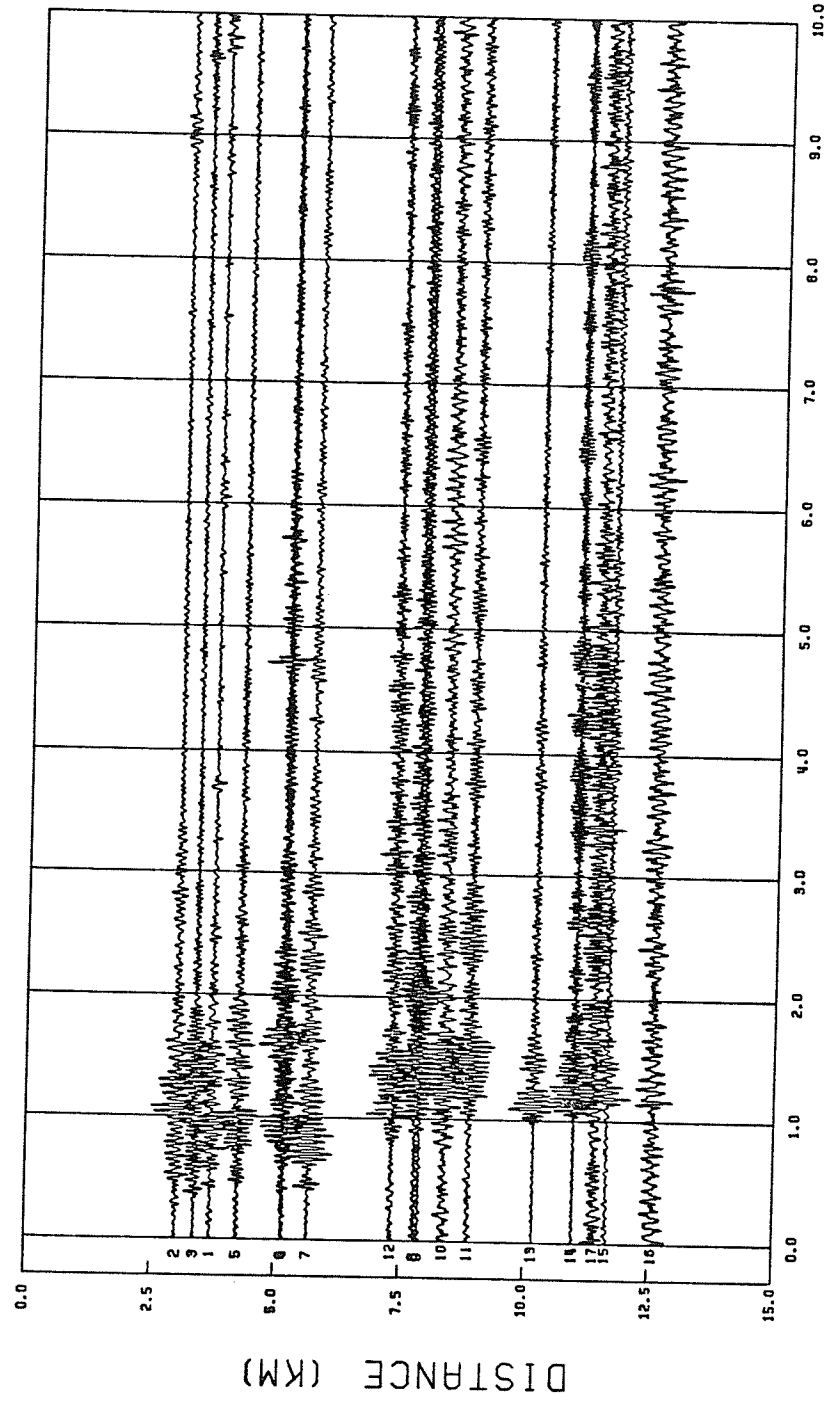

Figure 4.9: Raw records of the South profile.

The most serious problem encountered with the remaining field records was a low signal to noise ratio. This problem generally occurred on records with a shot-receiver distance of greater than 10 Km, although some of the other closer records are also affected. Some of these records include 6-S, 7-S, 10-S, 10C-S, 13-S, 14-S, 16B-S, 11-N, 11B-N, 12-N, 13-N, 14-N, 15-N, 16B-N, 16C-N, 17-N and 17B-N. These records as well as other records with low S/N can be found in Appendix C (use Appendix B to locate them).

Records 1 and 17B-N show spike problems which is noise generated from the playback unit. This problem was encountered often and when it occurred these records were played back and re-digitized. The spikes in records 1 and 17B-N could not be depressed due to poor quality cassette tapes.

The time channel on record 6E-N interferes with the seismic signal. This occurs occasionally in the playback if the cassette tape is not placed in the unit properly. Again, records of this type were re-digitized although record 6E-N resulted from the recording of the data rather than the playback. Record 2C-S shows a poor signal due to the shape of the source signal. Records 21-N, 23-N and 24B-N have questionable signals since an internal oscillation was thought to be set up within the recorder. These records were recorded on the experimental high gain recorders. Although it will not be possible to detect later events it is easy to pick first breaks on these records.

Many of the poor quality records are not included in the plots of the North and South profiles, but some records with low signal to noise ratios must be kept as the larger distances are essential to the interpretation of the data.

Chapter V

THE SOURCE

5.1 THE SHOT POINT

The seismic source used in this experiment is extremely complicated. In order to properly process and interpret the data a good understanding of the source and the physical conditions around it is necessary.

The quarry blasts were designed to break up rock and thus were not ideally suited for a seismic experiment. Each blast consists of one or more shot patterns in different parts of the pit. These individual shot patterns consist of 10-50 drill holes with 1000-1700 lbs of ANFO or Hydromex per hole. The ANFO which is a mixture of ammonia nitrate and fuel oil was used for most blasts. Hydromex was used for blasts in wet areas of the pit. Aluminum ANFO which is a mixture of ANFO and granular aluminum was also used in some blasts. The depth of the holes were generally 40-42 feet while the diameter ranged from 9 7/8 inches when Hydromex was used to 12 1/2 inches when ANFO was used. 1000-1100 lbs of ANFO was used for dry blasts while about 1700 lbs of Hydromex was used for wet blasts.

Individual shots within each shot pattern went off at 15, 25, 35, 40, 50 or 65 msec intervals. Figure 5.1 illustrates a simple example of one type of shot pattern. In this example, the shots in the

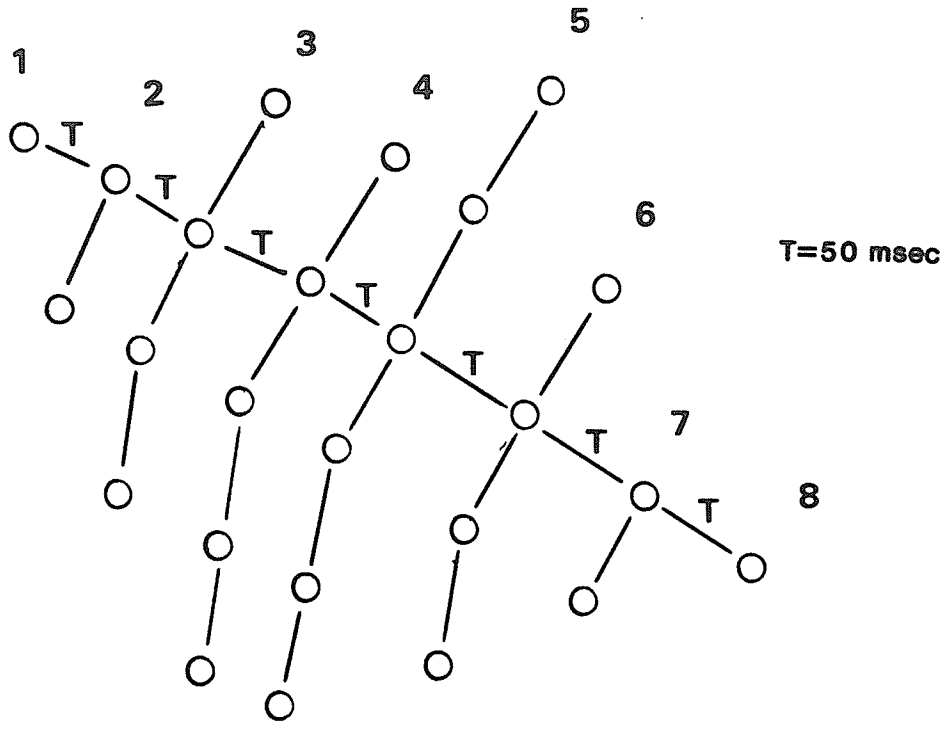

Figure 5.1: Simple example of a shot pattern-example 1.

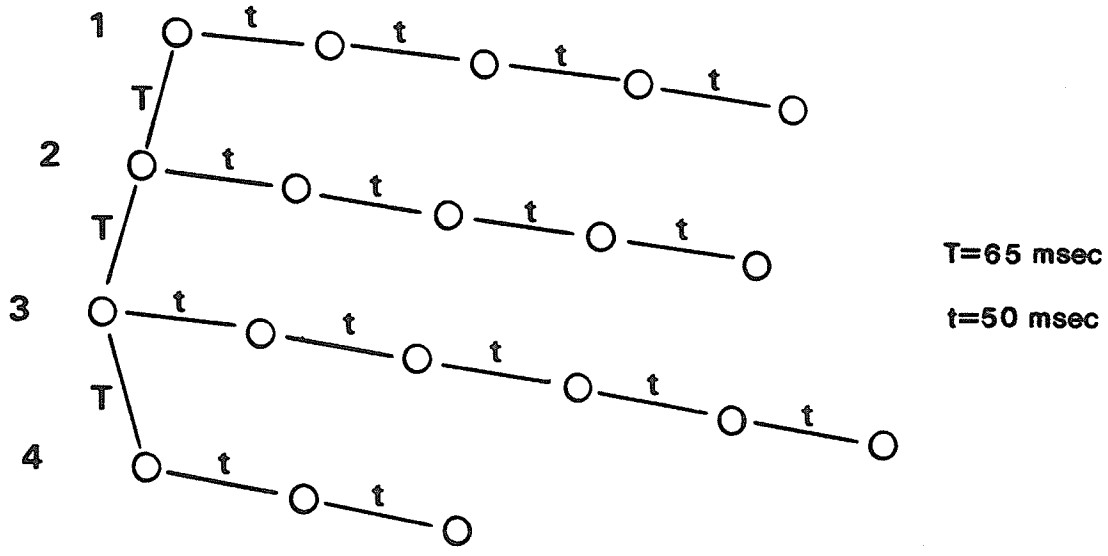

Figure 5.2: Simple example of a shot pattern-example 2.

first row explode first. The second row of shots then explodes 50 msec later, followed by the third row 50 msec after the second. This pattern continues until all of the rows of shots have exploded. Figure 5.2 illustrates another type of shot pattern. The individual shots in the first row of this type of shot pattern explode at a 50 msec interval. The second row starts in the same manner 65 msec after the first row starts. Similarly, the third row starts to explode 65 msec after the second row starts. This pattern is continued until all of the shots in all of the rows have exploded. The shot patterns used in this experiment consist of one of these types of patterns. Figure 5.3 illustrates the shot pattern used in shot #1. The remaining shot patterns used in the survey are illustrated in Appendix F.

The delays between the different shot patterns range from 0.2 to 2.5 seconds. Figures 5.4, 5.5 and 5.6 illustrate the actual signals recorded at the shot point recording site (300-1000 metres from the shot patterns).

In order to develope a good understanding of the source, an attempt to synthetically reproduce the source signal was made. Before the source signal could be synthetically modelled, different types of wavelets and their propagation through the earth were studied.

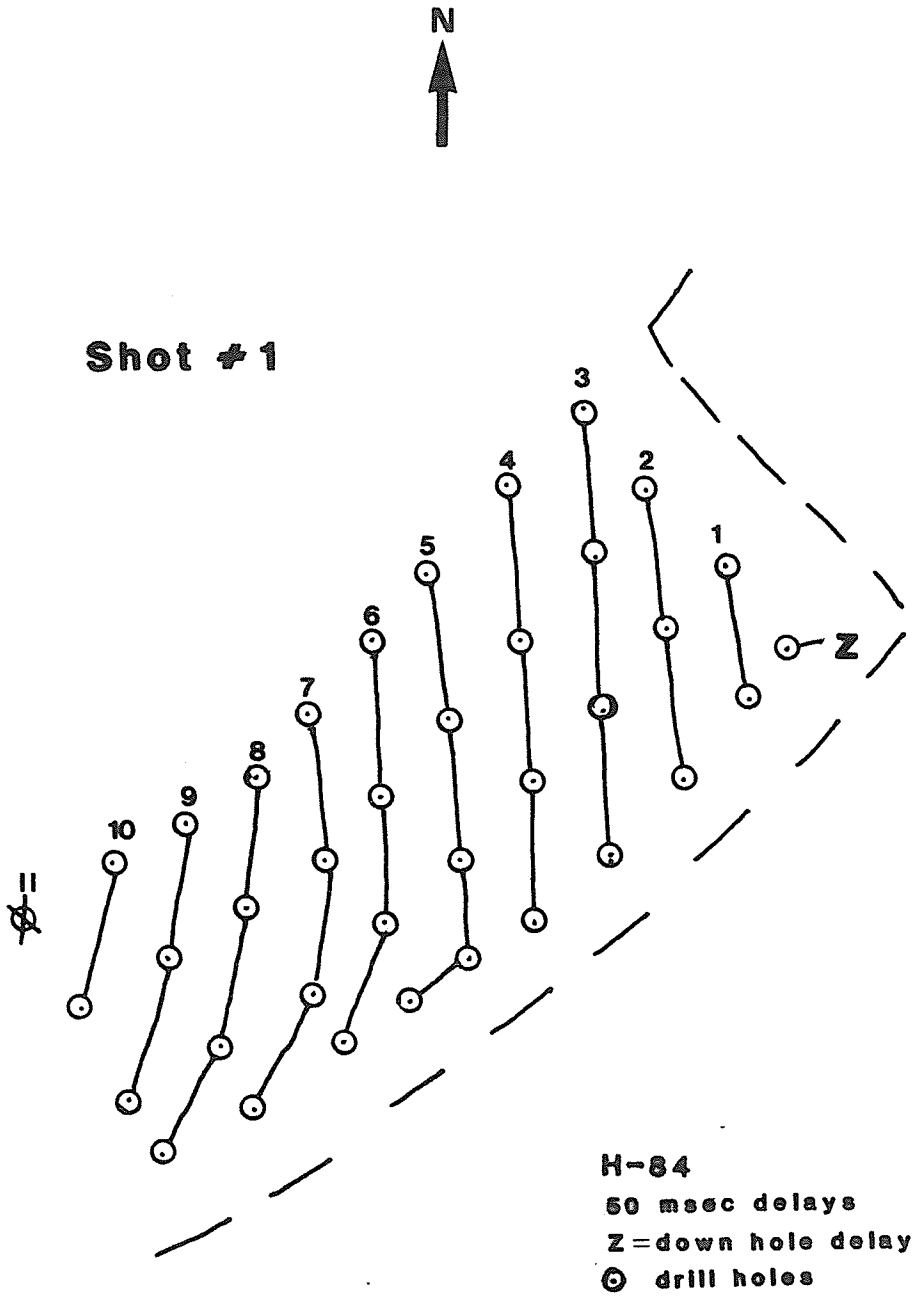

Figure 5.3: Shot pattern used for shot #1.

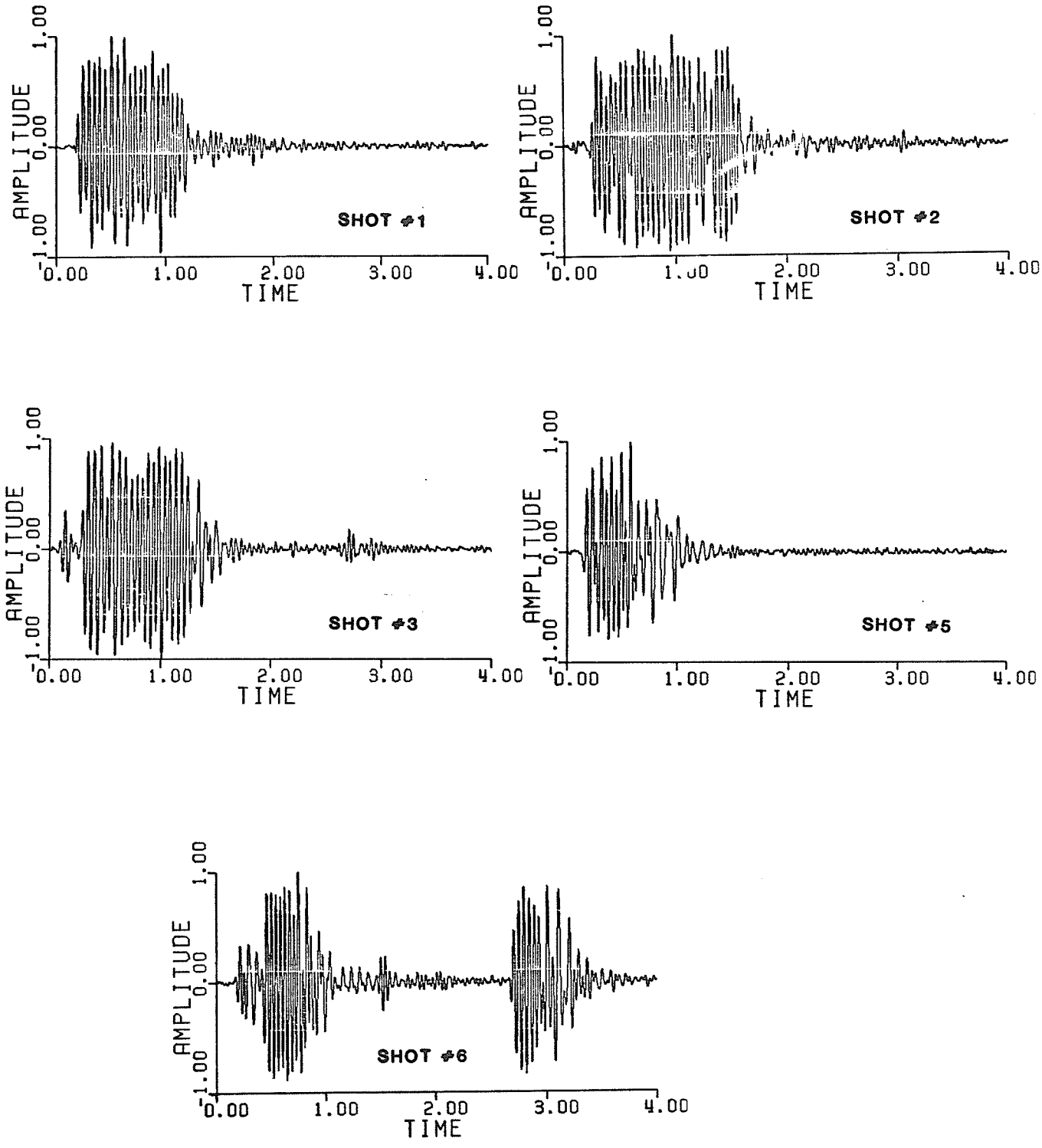

Figure 5.4: Shot records-1.

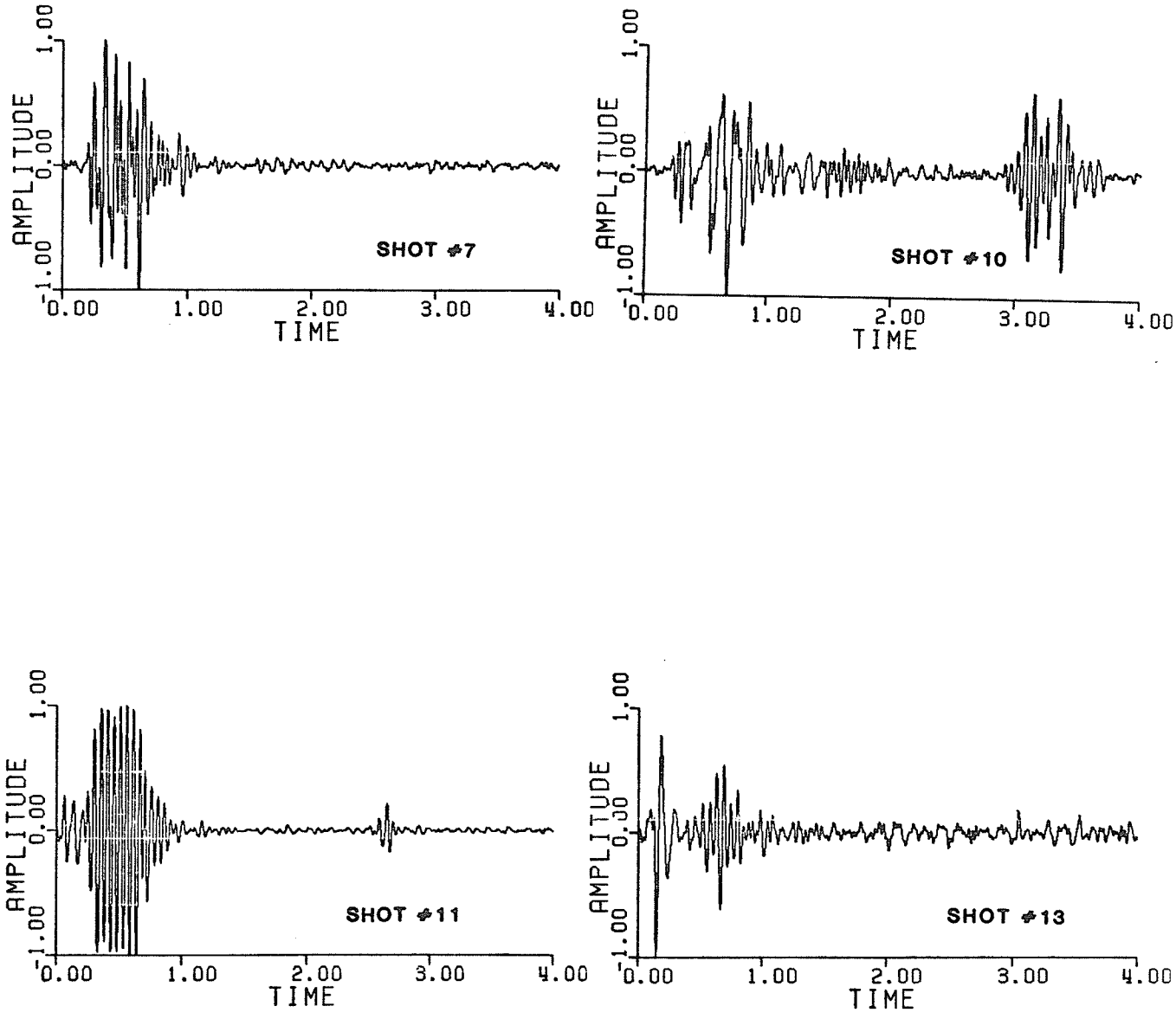

Figure 5.5: Shot records-2.

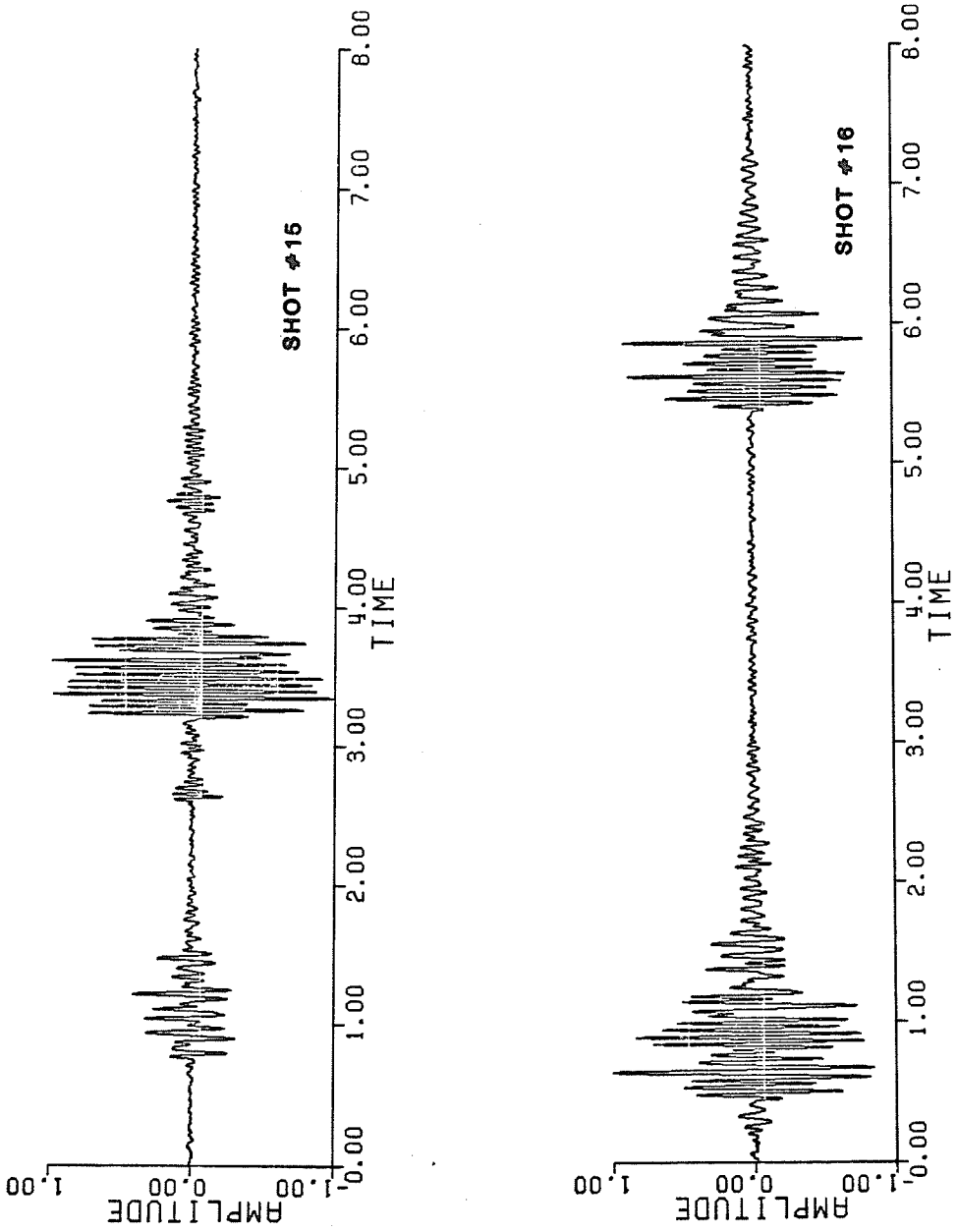

Figure 5.6: Shot records-3.

5.2 SEISMIC WAVELETS

Two types of seismic wavelets were considered in this study. The first is the more traditional Ricker wavelet (Ricker, 1940, 1944, 1953a, 1953b, 1977) and the second is a cylindrical source wavelet (Heelan, 1953).

5.2.1 Ricker Wavelet

The theoretical developement used here follows the work of N.H. Ricker (1940, 1944, 1953a, 1953b, 1977).

Briefly, the classical differential equation which is satisfied by the elastic displacement χ is:

$$(\lambda+2\mu)\nabla(\nabla\cdot\chi)-\mu\nabla\times\nabla\times\chi=\rho\frac{\partial^2\chi}{\partial t^2} \qquad 5\text{-}1$$

where: $\lambda=K+\frac{2}{3}\mu$

t=time

ρ=density of the medium

K=bulk modulus

μ=shear modulus

χ can be written as:

$$\chi=\chi_1+\chi_2$$

where: χ_1=compressional component

χ_2=shear component

Therefore the differential equation can be separated into two equations.

$$\nabla^2 \chi_1 = \frac{\rho}{\lambda+2\mu} \frac{\partial^2 \chi_1}{\partial t^2} \qquad 5\text{-}2\,(a)$$

$$\nabla^2 \chi_2 = \frac{\rho}{\mu} \frac{\partial^2 \chi_2}{\partial t^2} \qquad 5\text{-}2\,(b)$$

where: V_1 = compressional velocity $= \left(\frac{\lambda + 2\mu}{\rho}\right)^{1/2}$

V_2 = shear velocity $= \left(\frac{\mu}{\rho}\right)^{1/2}$

The general solution for (5-2) is:

$$\chi_1 = f_1(x - V_1 t) + f_2(x + V_2 t) \qquad 5\text{-}3$$

where: $f_1(x-vt)$ = wave travelling in the positive x-direction

$f_2(x+vt)$ = wave travelling in the negative x-direction

In order to find $f(x-vt)$ various physical effects of the earth must be considered. Before these effects are considered the initial waveform at the source must be approximated.

The initial wave at the source (figure 5.7) can be given by:

$f(x-vt) = b$ when $0<x<a$

$f(x-vt) = 0$ when $a<x<\infty$

$f(x-vt) = 0$ when $x=0$ 5-4

$f(x-vt) = -b$ when $-a<x<0$

$f(x-vt) = 0$ when $-\infty<x<-a$

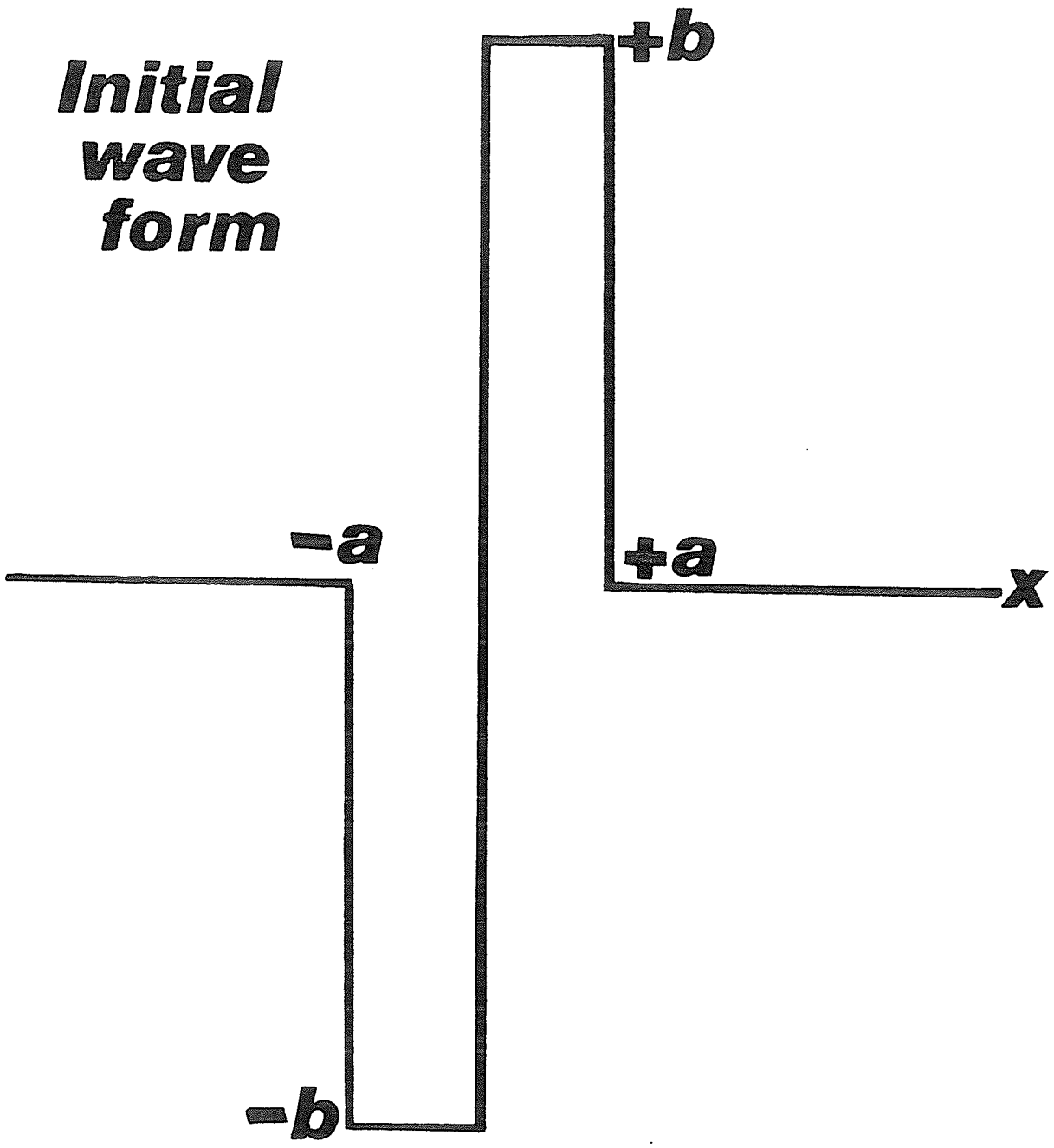

Figure 5.7: The initial wave at the source.

where: t=time

v=velocity

x=distance

f(x-vt) can be represented in a Fourier integral by:

$$f_1(x-vt) = \frac{2b}{\pi} \int_0^\infty \frac{[1 - \cos \frac{2\pi\nu}{v} x] \sin \frac{2\pi\nu}{v}(x-vt)\, d\nu}{\nu} \qquad 5\text{-}5$$

Since the earth absorbs higher frequencies more than lower frequencies, the absorption band can be represented by:

$$Tr = exp\left[-\left(\frac{\nu}{\nu_0}\right)^q \frac{x}{x_0}\right] \qquad 5\text{-}6$$

where: Tr=transmission factor

Xo=1/k=fixed reference distance

ν_o=constant reference frequency

q=constant integer

Assume that all of the single frequency components which make up the wave form all travel with the same velocity as the source wavelet $f_1(x-vt)$ passes through the earth. This is true for lower frequencies, therefore at larger distances this is generally true since higher frequencies are attenuated more. The displacement of the wavelet as modified by the earth's absorption at a distance (x) will then be:

$$f_1(x-vt)=\frac{2b}{\pi}\int_0^\infty \frac{[1-\cos\eta x]\, e^{-\left(\frac{\nu}{\nu_0}\right)^8 Kx} \sin\eta(x-vt)\, d\nu}{\nu} \qquad 5\text{-}7$$

where: $\eta=\frac{2\pi\nu}{V}$

This expression can be simplified such that the displacement observed at a distance x is:

$$f_1(x,t)=\frac{K}{x^{2/8}}H_8(u) \qquad 5\text{-}8$$

where: $H_8(u)=-\frac{dG_8(u)}{du}=\frac{1}{8}\left[\Gamma\left(\frac{3}{8}\right)u-\Gamma\left(\frac{5}{8}\right)\frac{u^5}{3!}+\Gamma\left(\frac{7}{8}\right)\frac{u^5}{5!}-\cdots\right]$

$$G_8(u)=\frac{1}{8}\left[\Gamma\left(\frac{1}{8}\right)-\Gamma\left(\frac{3}{8}\right)\frac{u^2}{2!}+\Gamma\left(\frac{5}{8}\right)\frac{u^4}{4!}-\cdots\right]\ \cdots\Big]$$

Γ =gamma function

$$K=\frac{4\pi a^2 b\,\nu_0}{V^2K^{2/8}}$$

$$u=\frac{\eta_0(x-vt)}{(Kx)^{1/8}}$$

$$\eta_0=\frac{2\pi\nu_0}{V}$$

Common electromagnetic geophones measure the velocity of displacement as opposed to the actual displacement, therefore we must consider:

$$\frac{\partial f_1(x,t)}{\partial t} = -\frac{KM}{x^{2/q}} I_q(u) \qquad 5\text{-}9$$

where: $I_q = \frac{d H_q(u)}{du}$

$$M = \frac{n_0}{K^{1/q}}$$

$$\therefore I_q = \frac{1}{q}\left[\Gamma\left(\frac{3}{q}\right) - \Gamma\left(\frac{5}{q}\right)\frac{u^2}{2!} + \Gamma\left(\frac{7}{q}\right)\frac{u^4}{4!} - \cdots\right] \qquad 5\text{-}10$$

Experimental studies by Ricker (1977) have shown that q=2 best represents the absorption of the earth:

$$G_q(u) = \frac{\sqrt{\pi}}{2} \exp\left(-\frac{u^2}{4}\right) \qquad 5\text{-}11\,(a)$$

$$H_q(u) = \frac{\sqrt{\pi}}{4} \exp\left(-\frac{u^2}{4}\right) \qquad 5\text{-}11\,(b)$$

$$I_q(u) = \frac{\sqrt{\pi}}{2}\left(\frac{u^2}{4} - \frac{1}{2}\right) \exp\left(-\frac{u^2}{4}\right) \qquad 5\text{-}11\,(c)$$

The far field velocity of displacement of the wave form can now be generated using equations (5-9) and (5-11(c)).

In order to generate a near field Ricker wavelet, the loss produced by viscosity must be considered. The classical wave equations therefore becomes:

$$\left(K+\frac{4}{3}\mu\right)\nabla^2\chi_1+\left(\eta_1+\frac{4}{3}\eta_2\right)\frac{\partial}{\partial t}\nabla^2\chi_1=\rho\frac{\partial^2\chi_1}{\partial t^2} \qquad 5\text{-}12\,(a)$$

$$\mu\nabla^2\chi_2+\eta_2\frac{\partial\nabla^2}{\partial t}\chi_2=\rho\frac{\partial^2\chi_2}{\partial t^2} \qquad 5\text{-}12\,(b)$$

where: η_1=viscosity associated with volume changes

η_2=viscosity associated with shear strains

The spherical wave expression can be derived from:

$$\frac{\partial\phi}{\partial T}=\frac{2}{R}\int_0^\infty \beta\ exp\left(-R\beta(1+\beta^2)^{-1/4}\ Sin\left(\frac{tan^{-1}\beta}{2}\right)\right.$$

$$\left.x\ Sin\left[R\beta(1+\beta^2)^{-1/4}Cos\left(\frac{tan^{-1}\beta}{2}\right)-\beta T\right]d\beta\right. \qquad 5\text{-}13$$

where: 0=generating function

$\beta=\omega/\omega_o$

R=numerical distance

$=\omega_o r/c$

r=true radial distance

T=numerical time

$=\omega_o t$

t=time

The generating function can be derived and therefore the velocity of displacement can be generated from:

$$\frac{\partial\chi}{\partial T}=A_o\omega_o\frac{\partial^2\phi}{\partial T^2} \qquad 5\text{-}14$$

Solving 5-13 and differentiating:

$$\frac{\partial \chi}{\partial T} = \frac{2\omega_o}{R}\int_0^\infty \beta \exp\left(-R\beta(1+\beta^2)^{-1/4} \sin\left(\frac{\tan^{-1}\beta}{2}\right)\right.$$

$$\left. \times \sin\left[R\beta(1+\beta^2)^{-1/4}\cos\left(\frac{\tan^{-1}\beta}{2}\right) - \beta T\right] d\beta \qquad 5\text{-}15$$

where: Ao=1

Ricker wavelets of various distances can therefore be generated from 5-15. Figure 5.8 illustrates how the form of the wavelet varies with (numerical) distance. The first four wavelets illustrates near field Ricker wavelets of varying numerical distance. Numerical distance is an expression used by Ricker (1953a,1977) for the convenience of disregarding units from the derivation of the wavelet expressions. The expression for numerical distance (R) is shown in equation 5-13. The variation in the shape of these wavelets is due to the different velocities of each single component of frequency. The bottom two wavelets in figure 5.8 are far field Ricker wavelets varying in propagation distance. The form of these wavelets are identical at large distances but the dominant frequency of the wavelet varies due to greater absorption at greater distances. Since at lower frequencies the velocities of each single frequency component are generally the same, then the waveform shape also remains the same at larger distances.

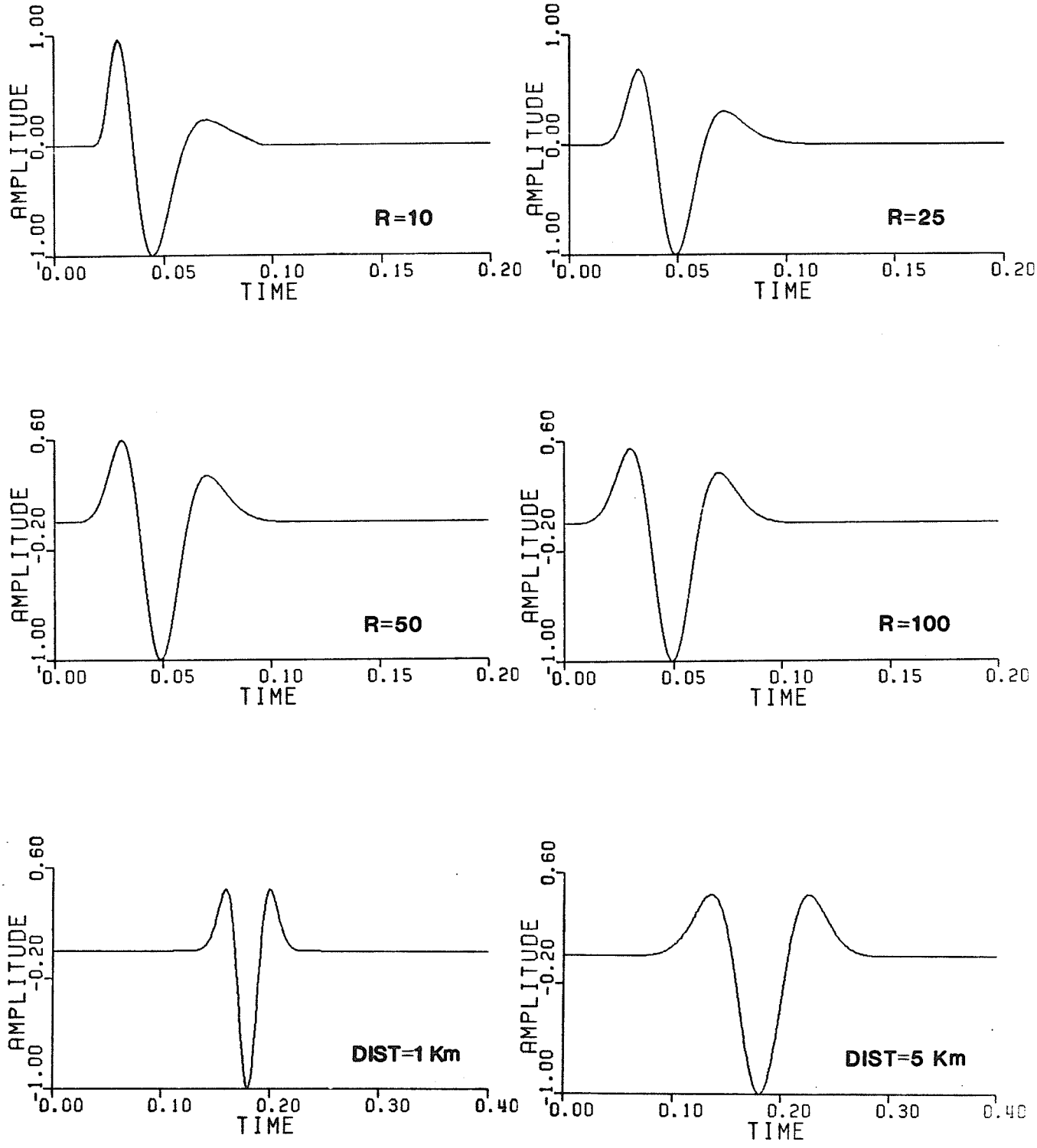

Figure 5.8: Examples of Ricker wavelets. R=numerical distance.

5.2.2 Cylindrical Source

A cylindrical source is useful as it best approximates the shape of each shot in the shot patterns. The following theoretical develop-ement of this source follows that of Heelan (1953).

The length of the cylinder is '2l' and the radius is given as 'a' (figure 5.9). The source is postulated to be centred at the origin of co-ordinates and is embedded ideally in an infinite medium. Stresses symmetric about the vertical axis act uniformly on the vertical walls of the cylinder. Stress conditions at the source are:

$[-\sigma rr]=p(t)$ or 0 as $|z|<l$ or $>l$ 5-16 (a)

$[-\sigma rz]=q(t)$ or 0 as $|z|<l$ or $>l$ 5-16 (b)

$[-\sigma r\theta]=s(t)$ or 0 as $|z|<l$ or $>l$ 5-16 (c)

$p(t)$, $q(t)$ and $s(t)$ are pressure functions at the source boundary and can be assumed to be proportional to one another.

The displacement can be expressed in terms of three wave functions ϕ_o, θ_o and χ_o. These wave functions satisfy the following three wave equations:

$$\phi_o'' - V_p^2 \phi_o = 0 \qquad 5\text{-}17\,(a)$$

$$\theta_o'' - V_s^2 \nabla^2 \chi_o = 0 \qquad 5\text{-}17\,(b)$$

$$\chi_o'' - V_s^2 \nabla^2 \chi_o = 0 \qquad 5\text{-}17\,(c)$$

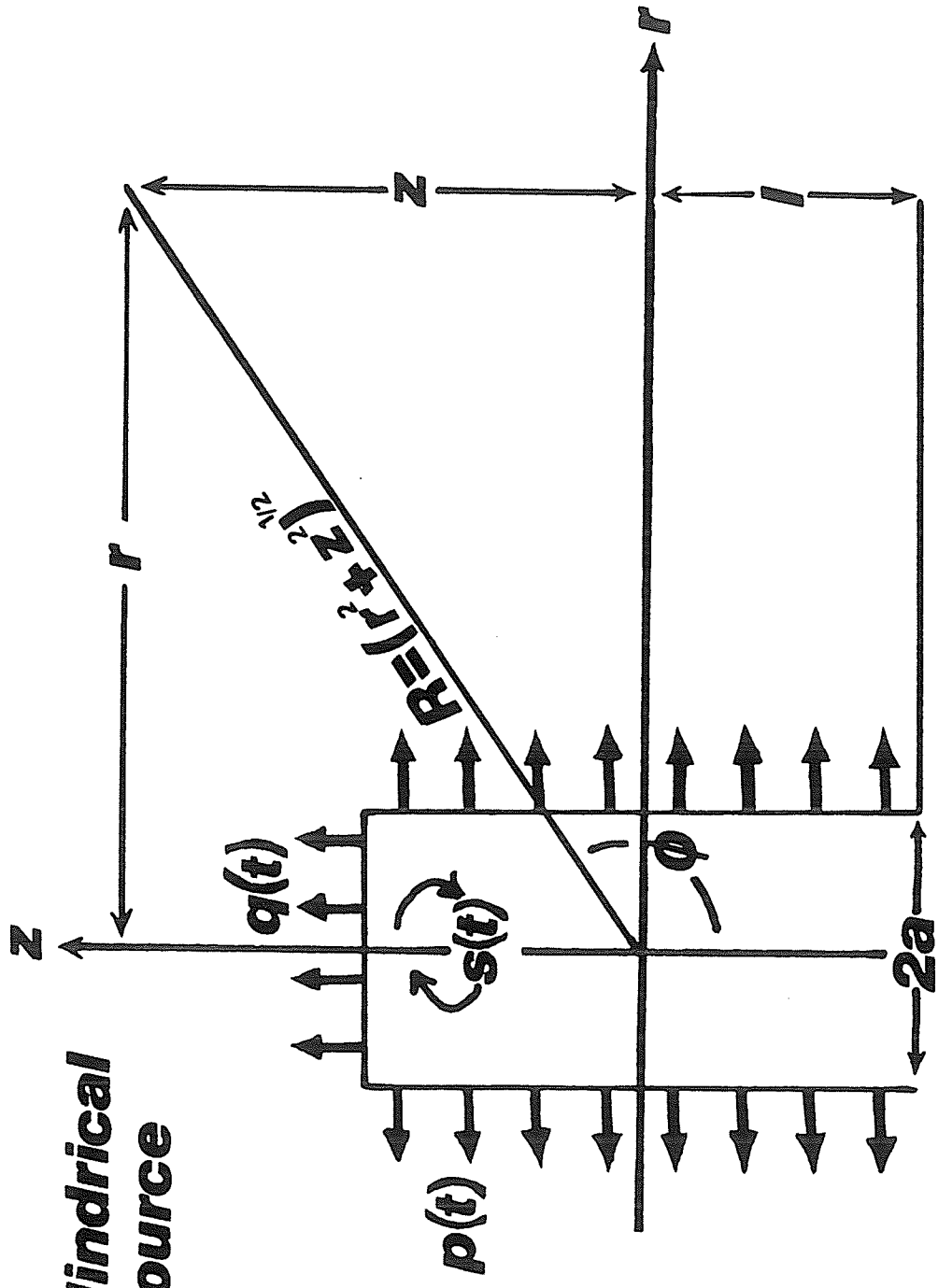

Figure 5.9: Cylindrical source. After Heelan, 1953.

where: V_P =compresssional velocity

V_{SV}=shear velocity

The displacements Ur, Ue and Uz are expressed as:

$$U_r = \frac{\partial \phi_0}{\partial r} - \frac{\partial^2 \Theta_0}{\partial r \partial z} \qquad 5\text{-}18\,(a)$$

$$U_\theta = \frac{\partial \chi_0}{\partial r} \qquad 5\text{-}18\,(b)$$

$$U_z = \frac{\partial \phi_0}{\partial z} + \frac{1}{r}\left(r \frac{\partial \Theta_0}{\partial r}\right) \qquad 5\text{-}18\,(c)$$

The stresses σrr, σrz, $\sigma r\theta$, σzz and $\sigma z\theta$ can be expressed as:

$$\sigma_{rr} = \lambda \nabla^2 \phi_0 + 2\mu \frac{\partial}{\partial r}\left(\frac{\partial \phi_0}{\partial r} - \frac{\partial^2 \Theta_0}{\partial r \partial z}\right) \qquad 5\text{-}19\,(a)$$

$$\sigma_{rz} = \mu \frac{\partial}{\partial r}\left(2\frac{\partial \phi_0}{\partial z} + \nabla^2 \Theta_0 - 2\frac{\partial^2 \Theta_0}{\partial z^2}\right) \qquad 5\text{-}19\,(b)$$

$$\sigma_{r\theta} = \mu\left(\frac{\partial^2 \chi_0}{\partial r^2} - \frac{1}{r}\frac{\partial \chi_0}{\partial r}\right) \qquad 5\text{-}19\,(c)$$

$$\sigma_{zz} = \lambda \nabla^2 \phi_0 - 2\mu \frac{\partial}{\partial z}\left(\frac{\partial \phi_0}{\partial z} - \nabla^2 \Theta_0 - \frac{\partial^2 \Theta_0}{\partial z^2}\right) \qquad 5\text{-}19\,(d)$$

$$\sigma_{z\theta} = \mu \frac{\partial^2 \chi_0}{\partial r \partial z} \qquad 5\text{-}19\,(e)$$

where: $\lambda = K - \frac{2}{3}\mu$

K=bulk modulus

μ=shear modulus

Solving the wave equations and equating the stress conditions at the source with the appropriate equations in figure 5.10, the far field vertical displacement can be approximated to be:

$$U_{z_p} = -\frac{F_1(\phi)}{R}\frac{d}{dt}\left[p\left(t-\frac{R}{V}\right)\right]\cos\phi - \frac{G_1(\phi)}{R}\frac{d}{dt}\left[q\left(t-\frac{R}{V}\right)\right]\sin\phi \qquad 5\text{-}20\,(a)$$

$$U_{z_{SV}} = \frac{F_2(\phi)}{R}\frac{d}{dt}\left[p\left(t-\frac{R}{V}\right)\right]\sin\phi + \frac{G_2(\phi)}{R}q\left(t-\frac{R}{V}\right)\sin\phi \qquad 5\text{-}20\,(b)$$

$$U_z = U_{z_p} + U_{z_{SV}} \qquad 5\text{-}20\,(c)$$

where: $F_1(\phi) = \Delta(1-2v^2\cos^2\phi/V^2)/4\pi\mu V$

$F_2(\phi) = \Delta \sin 2\phi/4\pi\mu V$

$G_1(\phi) = A\sin\phi/4\pi\mu$

$G_2(\phi) = -Av^2\cos\phi/4\pi\mu V$

Uz_p=vertical component of p-wave

Uz_{sv}=vertical component of s-wave

Uz=total vertical component

Δ=volume of the source

$= 2\pi a^2 \ell$.

A=area of the vertical walls of the source

$= 4\pi a \ell$

=shear modulus

p(t)=source function

a=radius of elastic boundary

Since electromagnetic geophones as used in this experiment measure the velocity of displacement, we must therefore consider:

$$\frac{\partial U_{zp}}{\partial t} = -\frac{F_1(\phi)}{R}\frac{d^2}{dt^2}\left[p\left(t-\frac{R}{V}\right)\right]\cos\phi - \frac{G_1(\phi)}{R}\,q\left(t-\frac{R}{V}\right)\cos\phi \qquad 5\text{-}21\,(a)$$

$$\frac{\partial U_{zsv}}{\partial t} = \frac{F_2(\phi)}{R}\frac{d^2}{dt^2}\left[p\left(t-\frac{R}{V}\right)\right]\sin\phi + \frac{G_2(\phi)}{R}\,q\left(t-\frac{R}{V}\right)\sin\phi \qquad 5\text{-}21\,(b)$$

$$\frac{\partial U_z}{\partial t} = \frac{\partial U_{zp}}{\partial t} + \frac{\partial U_{zsv}}{\partial t} \qquad 5\text{-}21\,(c)$$

The source function (figure 5.10) used in this study was:

$$p(t) = P_o \exp(-\pi t^2/t_o^2) \qquad 5\text{-}22$$

where: t_o=One half the period of the source function

P_o=Amplitude of the source function

For simplicity it was assumed in this study that q(t)=p(t). Using equation 5-20(a) as the source function, the far field velocity of vertical displacement therefore becomes:

$$\frac{\partial U_{zp}}{\partial t} = \frac{2\pi F_1(\phi)}{R}\cos\phi\left[\frac{2\pi t_1^2}{t_o^4} - 1\right]\exp\left(-\frac{\pi t_1^2}{t_o^2}\right)$$

$$-\frac{2\pi t_1 G_1(\phi)}{R}\exp\left(-\frac{\pi t_1^2}{t_o^2}\right)\cos\phi \qquad 5\text{-}23(a)$$

$$\frac{\partial U_{zsv}}{\partial t} = -\frac{2\pi F_2(\phi)\sin\phi}{R}\left[\frac{2\pi t_2^2}{t_o^4} - 1\right]\exp\left(-\frac{\pi t_2^2}{t_o^2}\right)$$

$$+\frac{2\pi t_2 G_2(\phi)}{R}\exp\left(-\frac{\pi t_2^2}{t_o^2}\right)\sin\phi \qquad 5\text{-}23(b)$$

$$\frac{\partial U_z}{\partial t} = \frac{\partial U_{zp}}{\partial t} + \frac{\partial U_{zsv}}{\partial t} \qquad 5\text{-}23(c)$$

where: t_1=t-R/V

t_2=t-R/vs

Po=1

A far field cylindrical source wavelet can be generated using the above expressions. Before the cylindrical source wavelet can be used to model the source signal it is important to study how the

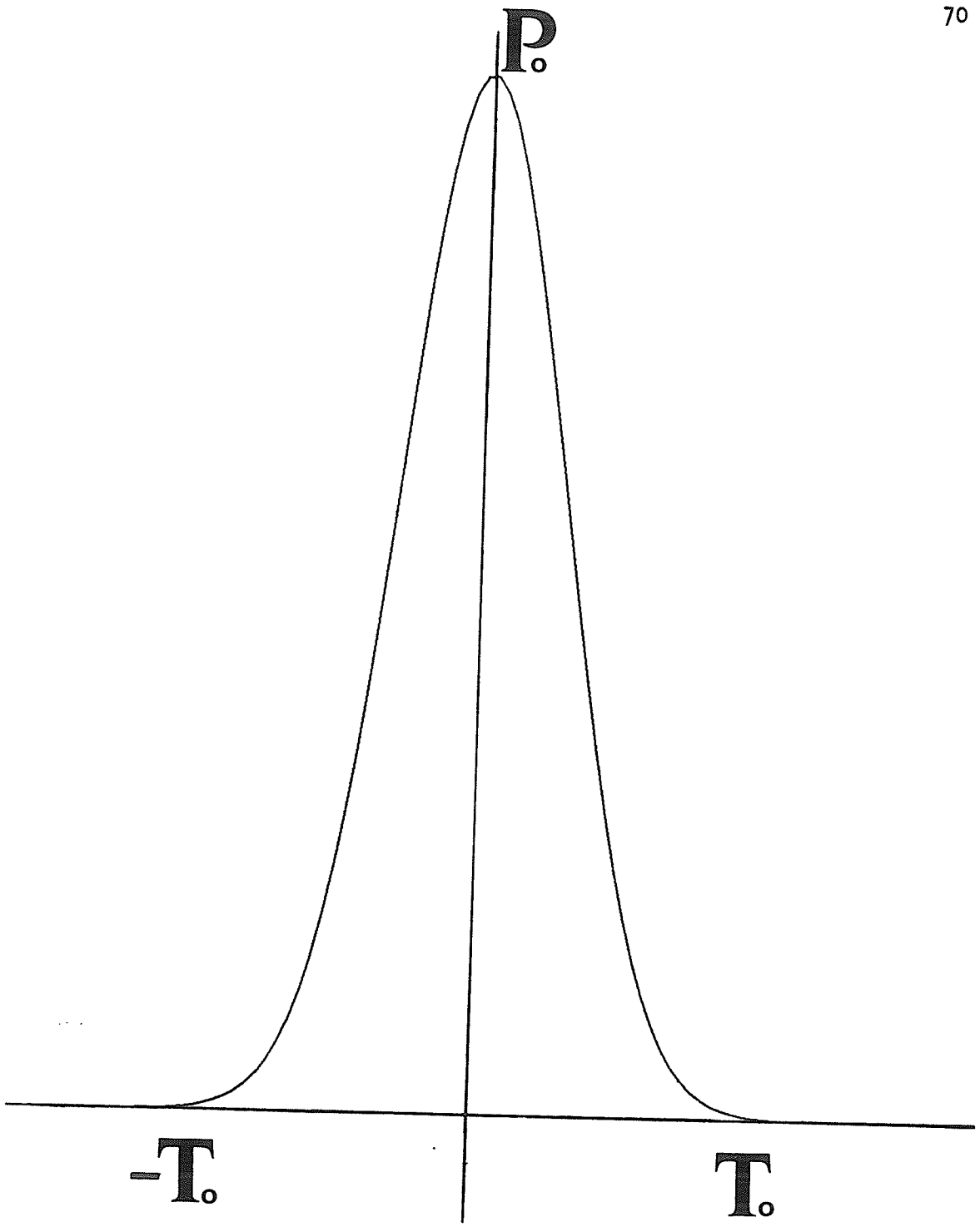

Figure 5.10: Source function used for cylindrical source.

various parameters of the expressions affect the shape of the wavelets. By studying these parameters some insight into the physical conditions present at the source as well as the type of wavelet to use may be gained.

After studying these expressions it was found that the most significant factors affecting the form of the wavelet are the initial period of the source function (To), the radius of the elastic boundary of the source (a), the angle of departure (ϕ) and the propagation distance of the wavelet (r). As expected, the effect of increasing the propagation distance is to decrease the dominant frequency (or period) of the wavelet. The shape of the wavelet approaches the shape of a far field zero phase Ricker wavelet (Ricker, 1940) as the distance of propagation increases. Figure 5.11 illustrates how the cylindrical source waveform varies with distance. Only p-waves are considered in this example.

The initial period of the source function (To) as expected determines the frequency of the wavelet as well as affecting the shape of the wavelet. At a fixed propagation distance, the effect of decreasing (To) causes the form of the wavelet to approach the shape of the far field Ricker wavelet. Figure 5.12 illustrates how the wavelet shape varies with (To). Again only p-waves are considered in this example as s-waves vary in a similar manner with (To).

The radius of the elastic boundary (a) primarily determines the shape of the cylindrical source wavelet, although it also varies inversely with frequency. As the radius of the elastic boundary (a)

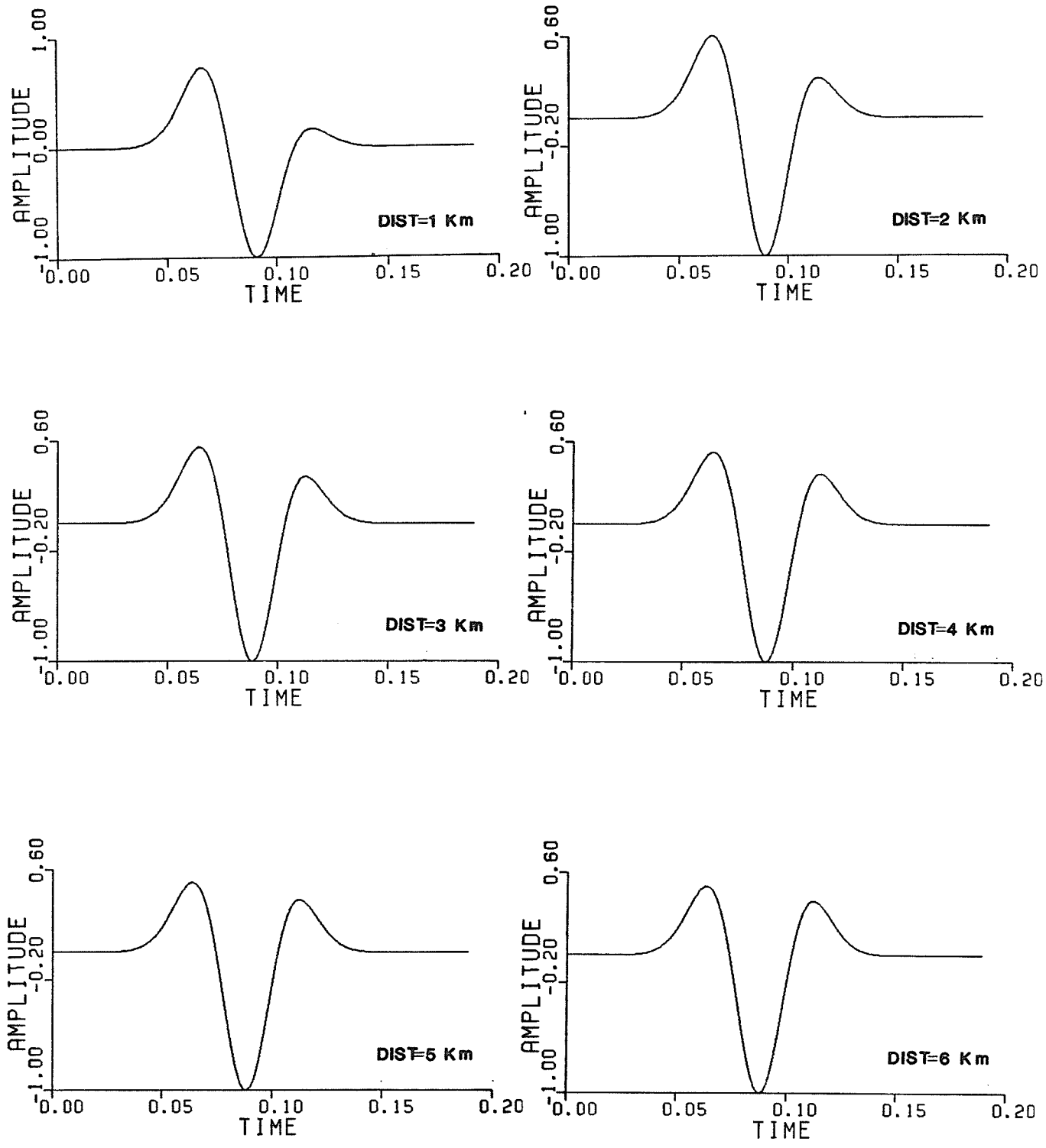

Figure 5.11: Variation of waveform with propagation distance.

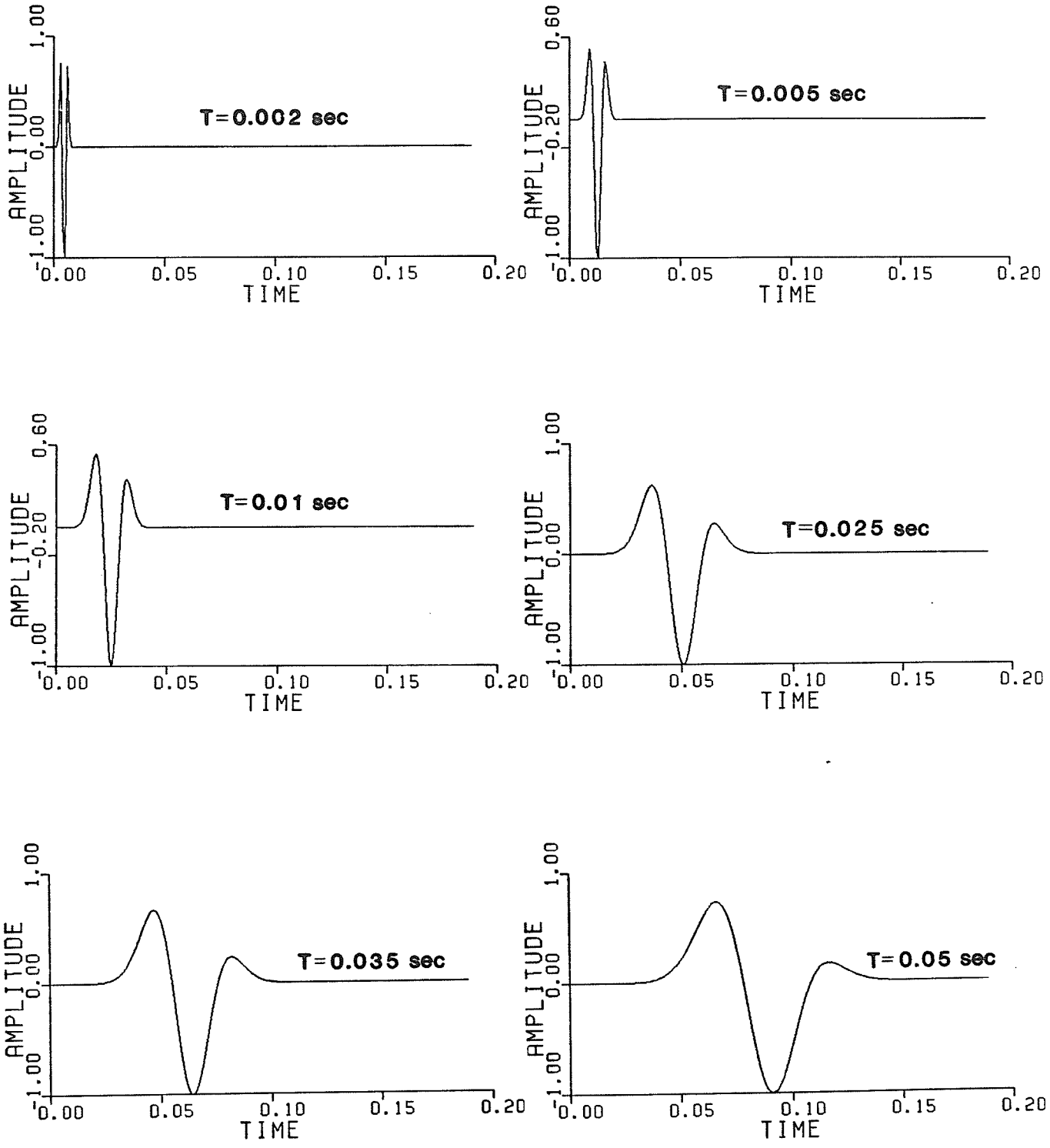

Figure 5.12: Variation of the waveform with (To).

is increased, the wavelet form again approaches the shape of the far field Ricker wavelet (figure 5.13). Again, only p-waves are considered.

The angle of departure (ϕ) affects the relative amplitudes as well as the relative shapes of the p and s-wave source wavelet. As the angle (ϕ) approaches 90 degrees (measured from the negative z-axis) the shape of the p-wave again approaches the shape of the far field Ricker wavelet. The s-wave on the other hand does not vary in wave shape with (ϕ) within the range of propagation distances used in this experiment. Figure 5.14 compares the shapes of the p and s-waves within the ranges of propagation distances (r) and angles of departures (ϕ) present in this study.

As concluded from the previous section, the shape of the wavelet is primarily due to the the amount of higher frequencies present in the signal. As the signal loses most of its higher frequencies it's shape approaches that of the far field (or zero phase) Ricker wavelet.

Although studies of the physical reactions of blasts of this kind have been undertaken (Sharpe, 1942 and Morris, 1950), it is not apparent what are reasonable values to assign to some of the physical cylindrical source parameters such as (a) or (To). By comparing the synthetic source signals with the actual source signals it may be possible to assign reasonable values to these parameters. The results of the study of the cylindrical source parameters have shown which physical parameters are the most suitable for the purposes of

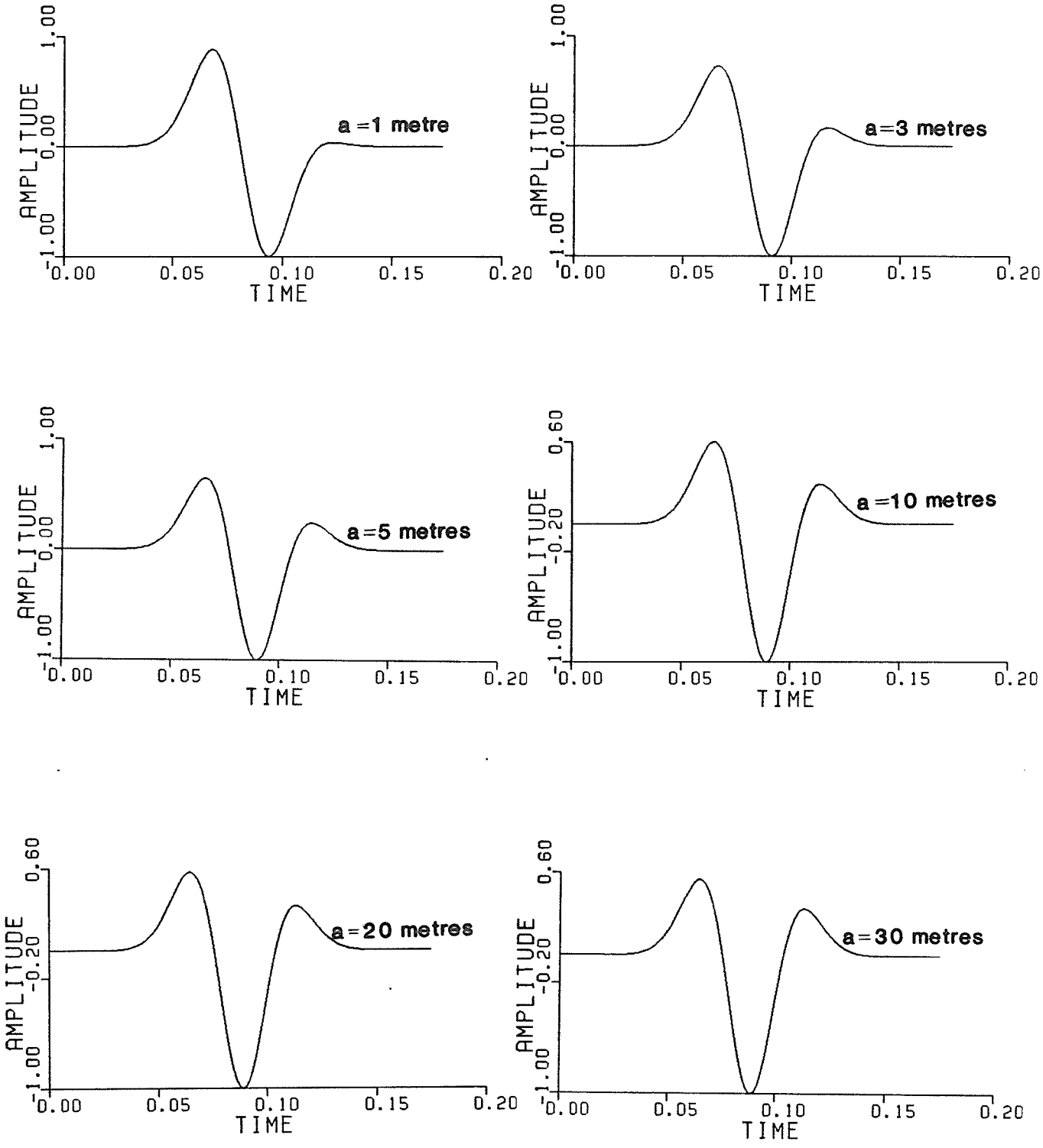

Figure 5.13: Variation of waveform with the radius of the elastic boundary.

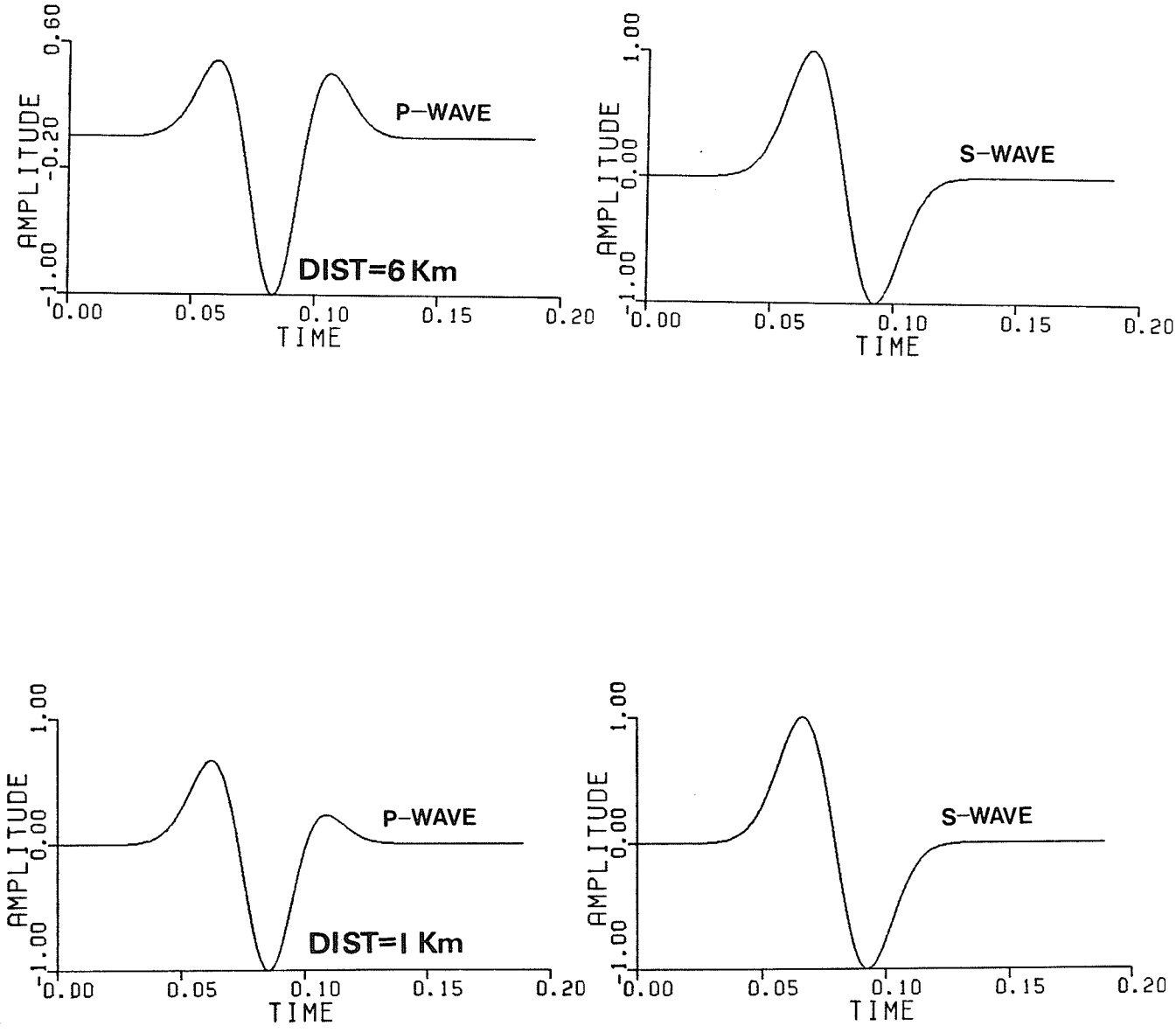

Figure 5.14: Comparison between the form of p and s-waves.

this study (a=5 metres, l=20 metres and To=0.035 seconds). The parameter 'l' is the length of the elastic boundary in the z-direction.

5.3 MODELLING THE SOURCE

The shot patterns used in this survey can be represented by a series of spikes with corresponding time delays. Every shot in a shot pattern can be represented by a unit spike since all of the shots in each shot pattern uses approximately the same amount of explosives. A series of spikes can then be generated for each shot pattern. Figure 5.15 gives an example of how such a series of spikes can be generated for a single shot pattern. Now, convolving this series of spikes with an appropriate wavelet will approximate the signal created by the blasting of the shot pattern.

Most of the mine blasts consist of two or more shot patterns. The signal of such a blast can be obtained by adding the signals from each shot pattern together. Consider the following:

$s(t)$=source signal

$w(t)$=single wavelet

$sp1(t)$=spikes generated from first shot pattern

$sp2(t)$=spikes generated from second shot pattern

then $s(t)=w(t)*sp1(t)+w(t)*sp2(t)$ 5-24(a)

Since convolution is distributive:

$$s(t)=w(t)*[sp1(t)+sp2(t)] \quad 5\text{-}24(b)$$

Therefore instead of adding the two signals from the two shot patterns together, the two sets of spikes can be added together first and then can be convolved with the wavelet.

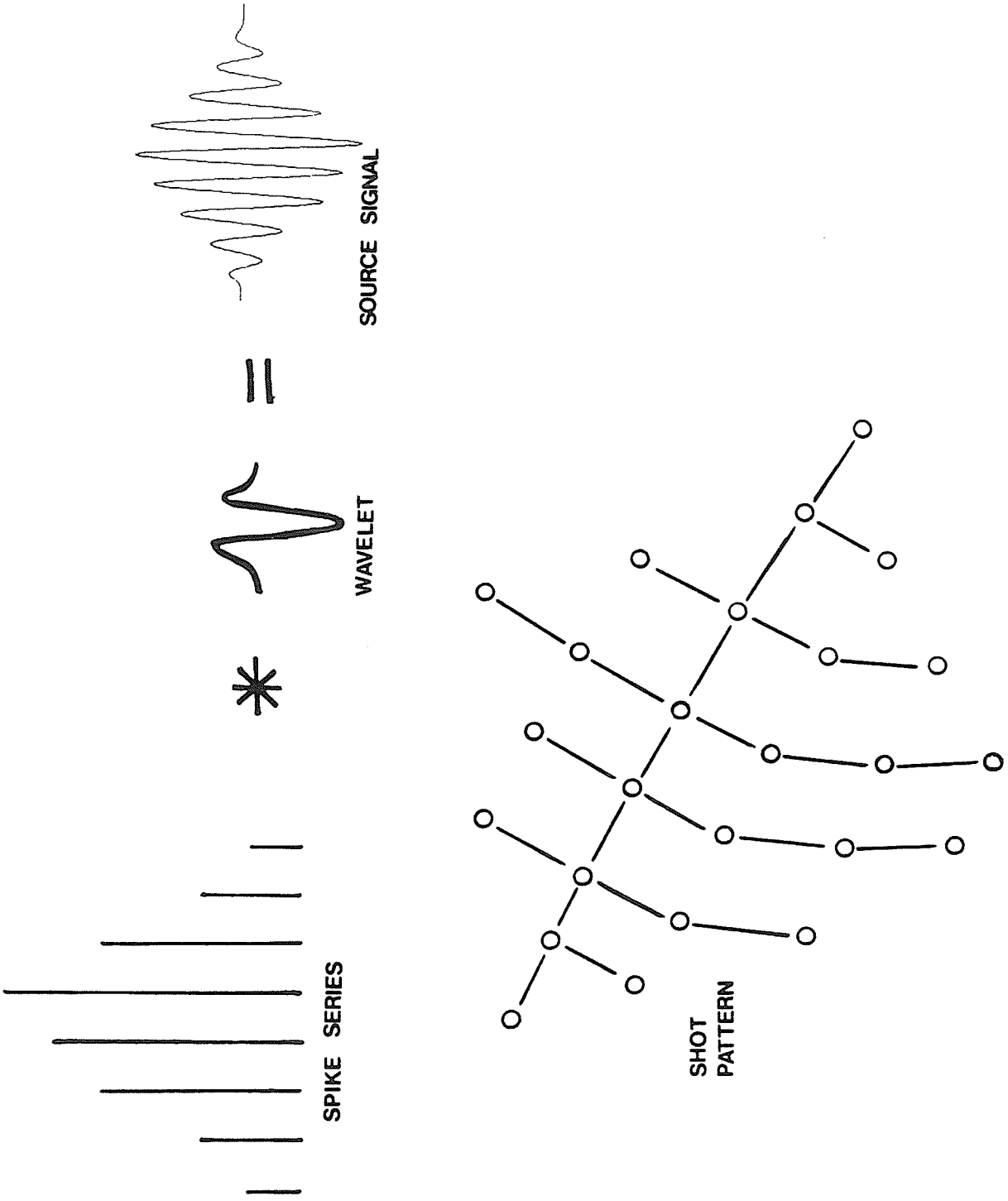

Figure 5.15: Generating spike series.

When the spikes from the different shot patterns are added together there are delay times between the shot patterns to consider. Two types of delays were used between shot patterns; the first called non-el delays and the second called period 10 delays. Also included in the delay between shot patterns is the downhole time to start the second shot pattern. The non-el delays are 2.275 seconds, the period 10 delays are 0.340 seconds and the downhole time is 0.230 seconds. Note that there may be one or more of non-el or period 10 delays between the shot patterns. Other important delays to consider are the delay created by the travel time of the signal in the primachord between shot patterns and the delay created by the difference in distance to the shot point recorder. The travel time of the signal in the primachord can be calculated by dividing the distance between the shot patterns by a velocity of 20,000 ft per second (6.56 Km/sec). The delay created by different travel times to the recorder can be derived by dividing the difference in distance by the velocity of the medium. A velocity of 4.70 Km/sec was used in this study. Table F1 in Appendix F shows each shot pattern of each shot as well as the delay type, the distances between shot patterns and distances to the shot point recorder. The following illustrates how the signals from the different shot patterns can be added together and how the delay can be calculated:

$$S(t)=S1(t)+[\ T+S2(t)\ ] \qquad 5\text{-}25$$

where: $S1(t)$=spikes generated for shot pattern #1

$S2(t)$=spikes generated for shot pattern #2

ΔT=delay between shot patterns

$T= t+dht+(D2-D1)/V+D0/6.56$

Δt=type of delay

dht=downhole time

DO=distance between shot patterns

D1=distance of shot point recorder from shot pattern #1

D2=distance of shot point recorder from shot pattern #2

V=velocity of medium

One of the wavelets previously discussed can now be convolved with the spike series to generate a synthetic source signal. A program written in this research (B.A. Maxwell) generates the spike series and convolves it with any wavelet that is input into the program. Programs were also written (in this research) to generate cylindrical source wavelets and Ricker wavelets and store them in a file to be read by the source generating program. Another program was written that reads in any desired wavelet and changes its dominant frequency (period) to any desired frequency. This program also stores the output into a file to be input later into the source generating program.

5.3.1 Types of First Arrivals

The nature of the first arrival recorded at the shot point is not known, but for the purposes of this study only the direct rays were considered. Since the relative amplitudes of p and s-waves for spherical and cyindrical sources are different, the following derivation is necessary in order to isolate the differences.

As described in the developement of the cylindrical source all angles are measured from the negative z axis (figure 5.6). The vertical displacement measured at the recorder is:

$$Uz=Uzp+Uzs \qquad 5\text{-}26\,(a)$$

$$Uzp=Wp(d,t,\phi_1)*\cos\phi_2 \qquad 5\text{-}26\,(b)$$

$$Uzs=-Ws(r,t,\phi_1)*\sin\phi_2 \qquad 5\text{-}26\,(c)$$

where: Uzp=vertical displacement of p-wave.

Uzs=vertical displacement of sv-wave.

Uz=total displacement.

$Wp(r,t,\phi_1)$=amplitude of the p-wave before it reaches the receiver.

$Ws(r,t,\phi_1)$=amplitude of the s-wave before it reaches the receiver.

r=distance travelled by wavelet=$(x^2+z^2)^{1/2}$

x=radial distance from the source.

z=vertical distance from source.

ϕ_1=angle of departure at the source. measured from the negative z axis.

ϕ_2=angle of arrival at the recorder measured from the negative z axis.

When generating the direct ray the angle of departure and the angle of arrival will be equal:

$$\phi_1=\phi_2 \qquad 5\text{-}27$$

The arrival time of the wavelet is:

$$t=r/V \qquad 5\text{-}28$$

where: V=velocity of medium.

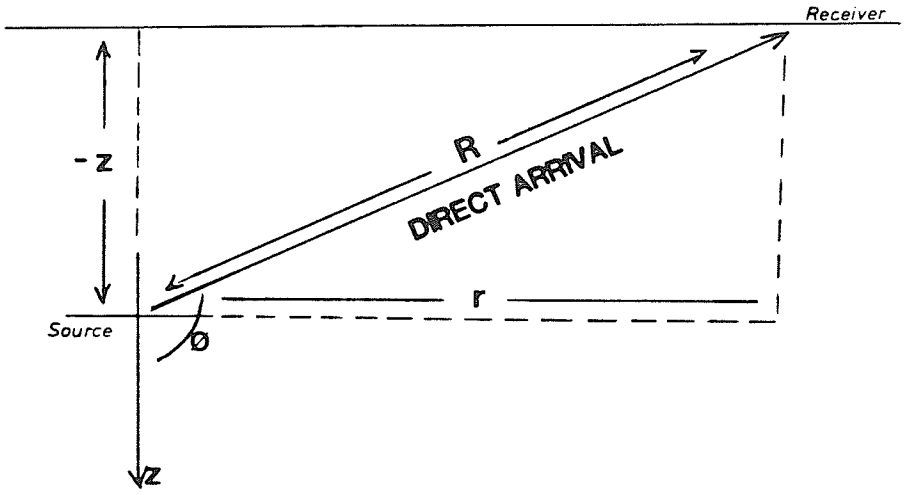

Figure 5.16: Direct arrivals.

The amplitude (of displacement) decay of a spherical wave is R**-1. When absorption is introduced, the amplitude of a spherical source decays as R**-3/2 (Ricker, 1940). For the amplitude of the velocity of displacement the decay rate is R**-5/2 (Ricker, 1940). The amplitude of a direct p-wave from a spherical source is therefore represented by:

$$A=Ao*\cos(\phi_2) \qquad 5\text{-}29\,(a)$$

where: $W(d,t,\phi_1)=Ao$

Ao=initial amplitude of wave minus absorption.

The amplitude of a direct s-wave from a spherical source is represented by:

$$A=Ao*\sin(\phi_2) \qquad 5\text{-}29\,(b)$$

For large distances, the amplitude of a direct ray of a cylindrical source decays the same as for the spherical source. The amplitude of a direct p-wave from a cylindrical source is therefore represented by:

$$A=Ao*\cos(\phi_1)*\cos(\phi_2) \qquad 5\text{-}30\,(a)$$

The amplitude of a direct s-wave from a cylindrical source is represented by:

$$A=Ao*\sin(\phi_1)*\sin(\phi_2) \qquad 5\text{-}30\,(b)$$

Note the differences between the equations representing the spherical source and the equations representing the cylindrical source. The difference between the two types of sources is that the amplitude of the signal from the cylindrical source depends on the angle of departure as well as the angle of arrival (angle of incidence). The amplitude of the spherical source signal is only dependant on the angle of arrival (angle of incidence). For this reason within the ranges of these angles in this study (approximately 90 degrees), the relative amplitudes of the p-wave to the s-wave is much larger for the spherical source than for the cylindrical source.

Figures 5.17 and 5.18 illustrate the direct ray signal generated from the program for shot #2 using various Ricker wavelets. Also shown in the diagrams is the signal recorded from that shot. Note that there is more to the actual signal than the synthetic signal,

consequently different types of arrivals must also be considered. Figure 5.19 illustrates signals generated using cylindrical source wavelets as well as the recorded signal for shot #2. Again, the actual signal is longer than the synthetic signal.

5.3.2 Discussion of the Program Options

The program can generate p and s-waves using any type of wavelet. The program will also read a series of spikes generated from other ray tracing programs in order to convolve with the resultant waveform. The resulting signal consisting of reflections, headwaves and other arrivals can then be generated for any geologic model. Note also that the cylindrical source program CYLSOURCE has many other options and can generate other types of wavelets which are not considered in the SOURCE program. The wavelet generating programs CYLSOURCE, RICKER and READ as well as the signal generating program SOURCE is listed in Appendix G.

5.4 DISCUSSION OF RESULTS

Shot #2 was used to study the source signal as it shows some evidence of two separate arrivals. It was also used because the shot patterns used were not as complicated as some of the other shot patterns used in other shots.

5.4.1 Source Signals considering p and s-waves

The synthetic signal (considering only p-waves) of shot #2 is shown in figures 5.17 and 5.19. Although the signal is not exactly reproduced, the general shape of the signal is present in most examples. Similarly, figures 5.18 and 5.19 show the synthetic signal considering both s and p-waves. Note that there is a small difference from the examples using only p-waves. The large amplitude arrival is the s-wave arrival while the p-wave arrival is a very small event just in front of this. The difference in the arrival amplitudes of the p and s-waves is due to the large angle of incidence of the direct ray. This has the effect of attenuating the p-wave more than the s-wave. Because the cylindrical source has an additional effect of (ϕ) (angle of departure) the p-wave is attenuated even more and is invisible in figure 5.19.

5.4.2 Other types of Arrivals

Other types of arrivals that may be affecting the shape of the source signal are turning rays, reflections, head waves and diffractions. Since the source area is geologically very complex, it is likely that other types of arrivals are contributing to the final form of the signal recorded by the source recorders. As mentioned in Chapter 3, the source area is located within a complexly folded iron formation along with intrabedded metasediments. Head waves and reflections will likely contribute to the form of the source signal as a result of the intrabedded metasediments and the iron formation. Ray tracing models in Chapter 7 show the presence of a very low ve-

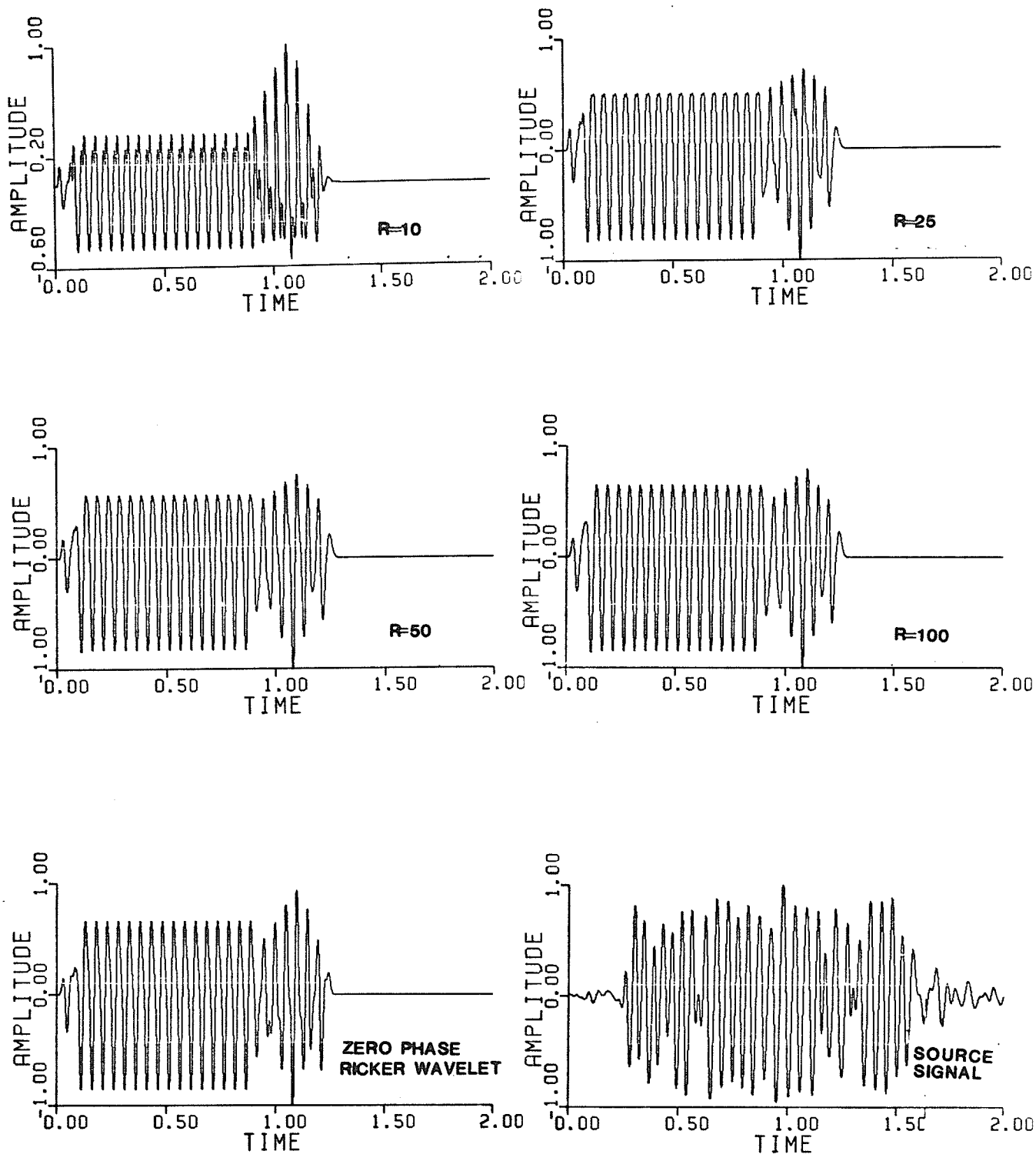

Figure 5.17: P-wave signal of shot #2 using Ricker wavelets. Only direct rays are considered.

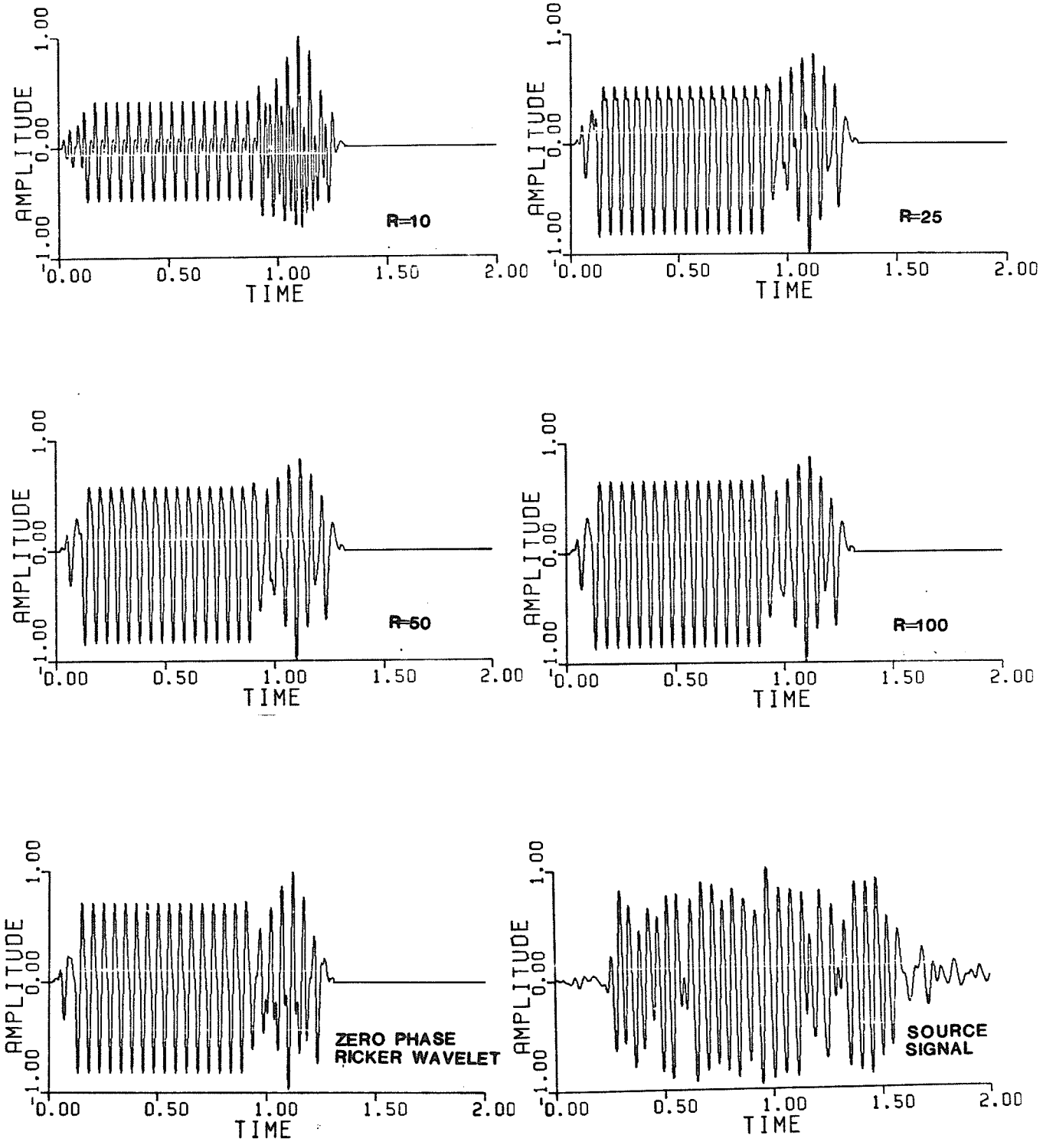

Figure 5.18: P and s-wave signals of shot #2 using Ricker wavelets. Only direct rays are considered.

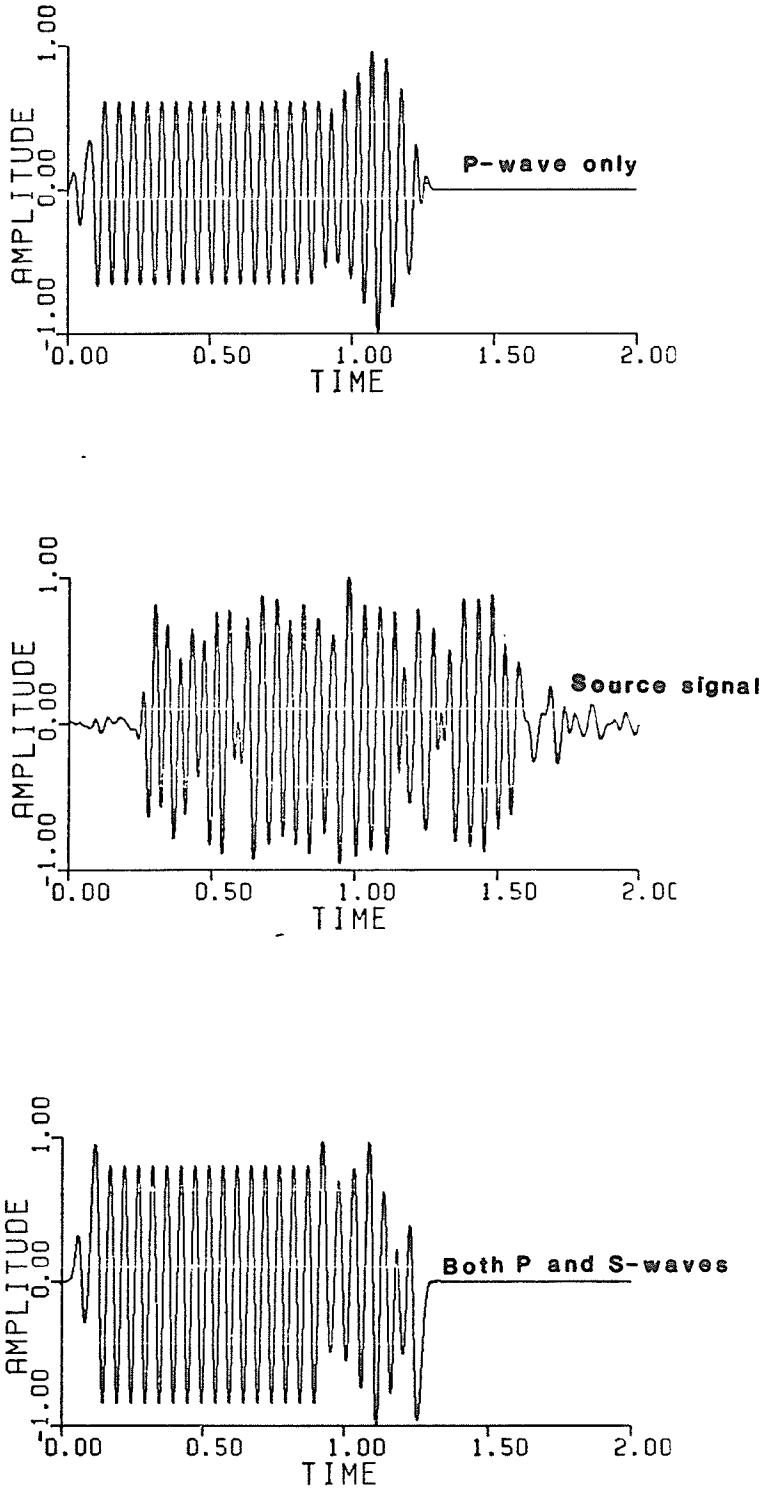

Figure 5.19: P and s-wave signal of shot #2 using cylindrical source wavelets. Only direct rays are considered.

locity weathered layer with a high velocity gradient throughout the area. For this reason, turning rays will affect the form of the source signal. Because the source recorders are less than 1 Km away from the source, the turning ray will essentially be equivalent to a direct ray for the source records.

Since the geology of the source area is very complex, diffrations, multiple reflections and reverberations will also affect the source signal. A good understanding of the local geology as well a more accurate study of the shot pattern information would be required. In any further studies of this kind, other types of arrivals, local geology and source radiation patterns would be important considerations for further investigation.

5.4.3 Radiation Patterns

Another factor that has not been considered in this study is the radiation pattern which depends on the relative positions of the recorder and the shot pattern. The radiation pattern was not considered because it makes the generation of source signals very complex since each shot in each shot pattern must be considered individually. Because the individual shots of each shot pattern are close together (less than 15 feet), the radiation pattern should only have a negligible effect on the generation of source signals. However, a more detailed study should consider it. Figure 5.20 illustrates how the radiation pattern might affect the arrival times to the shot and field recorders.

5.4.4 Source signals

For simplicity, only the direct p and s-wave arrivals are considered in the models of the remaining shot signals. Figures 5.21 to 5.26 illustrate the modelled signal from each of the shots using the cylindrical source wavelet. In each case, the general form of the modelled signal is similar to that of the recorded signal. Some recorded signals such as shot #2 indicate a close resemblance with the modelled signal. Other records such as shot #3 and shot #6 indicate two separate types of arrivals. This is not observed on the modelled signal. If the first smaller amplitude arrival is ignored, the modelled signal reasonably resembles the recorded signal. Other modelled signals such as that for shot #1 are considerably shorter in duration than the recorded signal. The above discrepancies are probably due to the local source conditions around each shot pattern. Because of the complex geology, different shots may be affected in different manners depending on the local geology around the individual shot patterns.

In order to better understand the source signal used in experiments of of this kind, a more thorough study is necessary. A study of the local geology, the physical conditions around each shot and much more accurate representations of the shot patterns and different arrival types will be important in such a project. The results of this study of the source are preliminary but encouraging. This study has at least shown that the p-wave arrival is very small in amplitude compared to the s-wave arrival. This was important in locating first breaks in order to assemble the profiles (Chapter 6).

In many cases the p-wave may have been buried in the noise preceding the large amplitude s-wave arrivals. Because of this, much care was taken in order to try to isolate the p-wave arrival. Despite the care taken to pick first breaks, this may have been a source of some errors in assembling the profiles. These errors would also affect the velocities used in this study. Another important result of the source study is that it shows that the source can be modelled. This indicates that future surveys of this kind are possible and can be used again to provide an inexpensive seismic source.

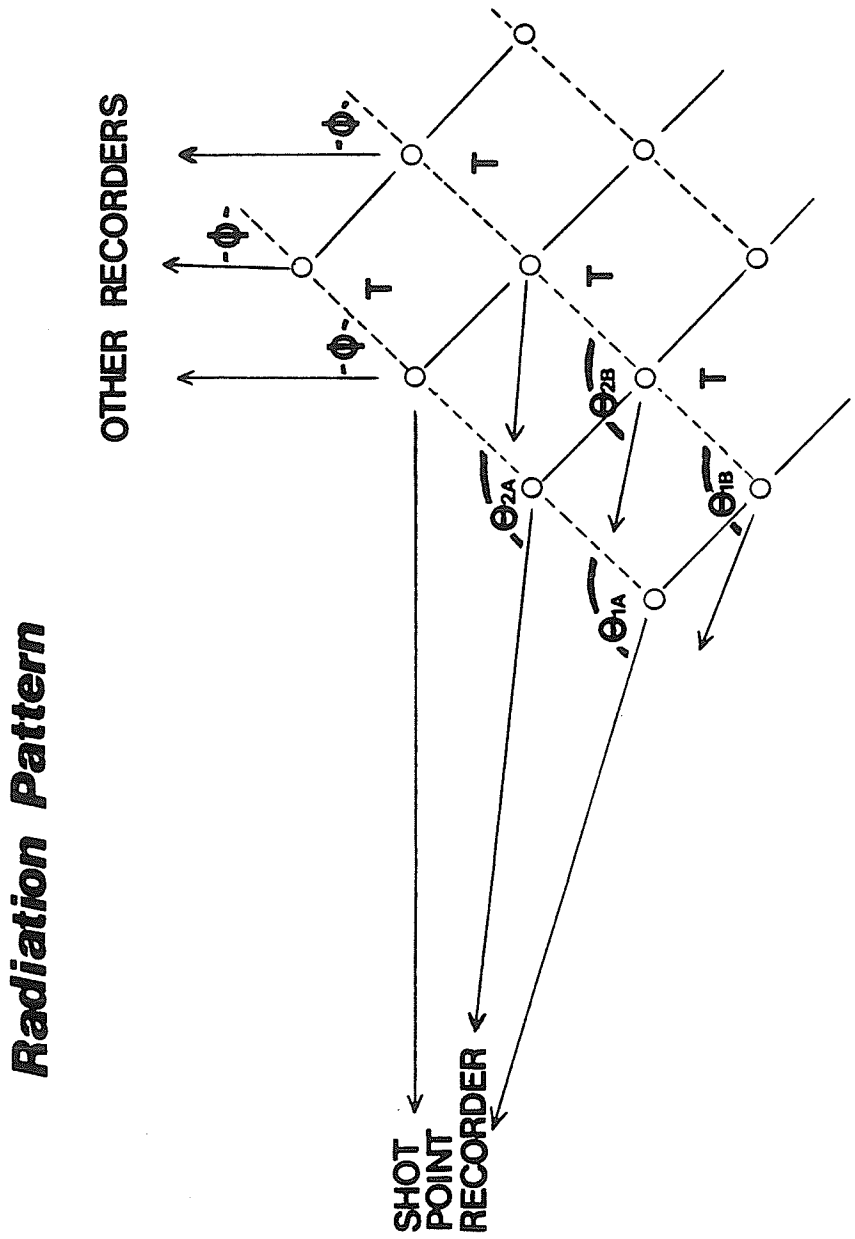

Figure 5.20: Radiation pattern.

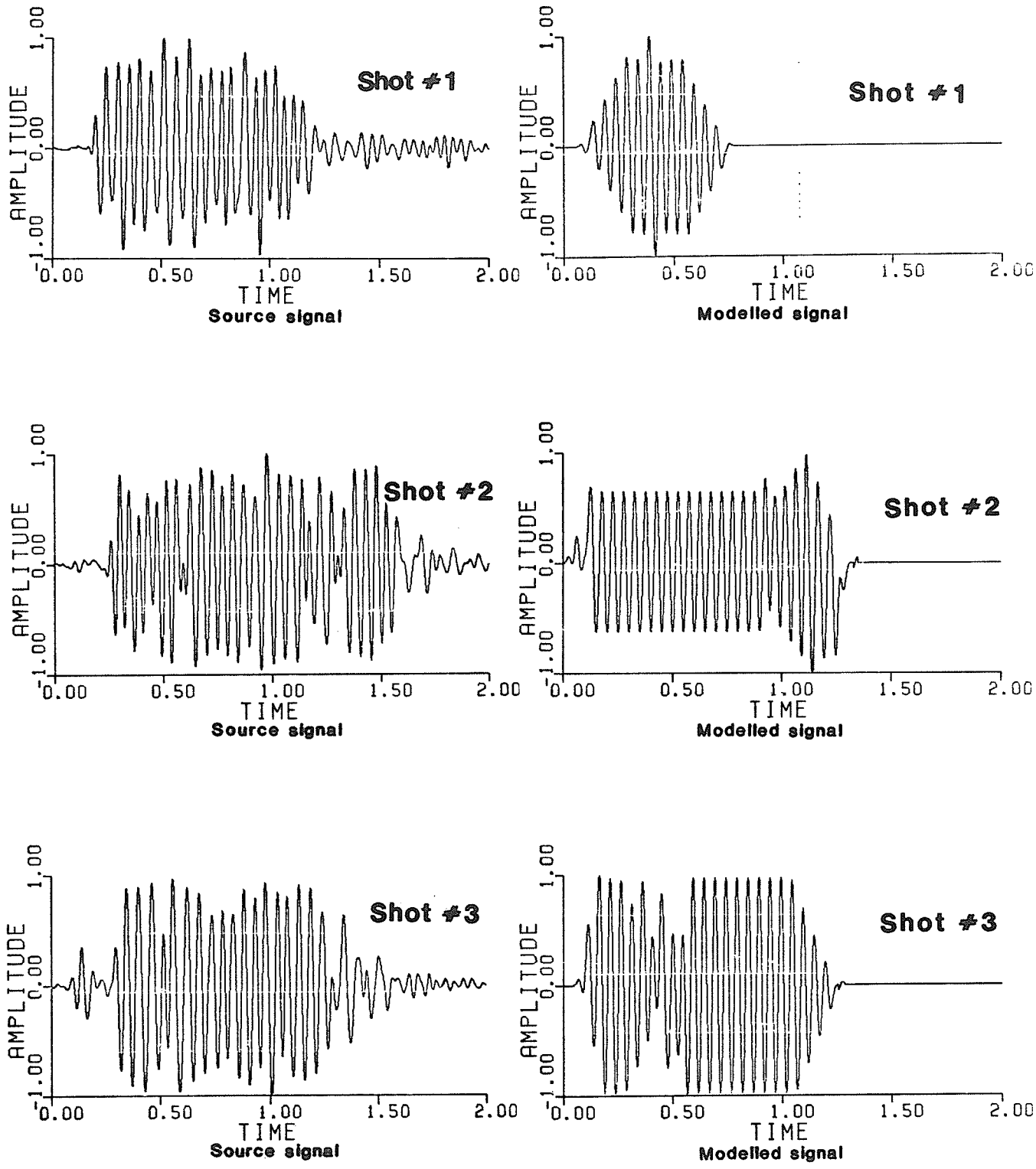

Figure 5.21: Modelled source signals of shots #1, #2 and #3. The recorded signals are also illustrated for comparison.

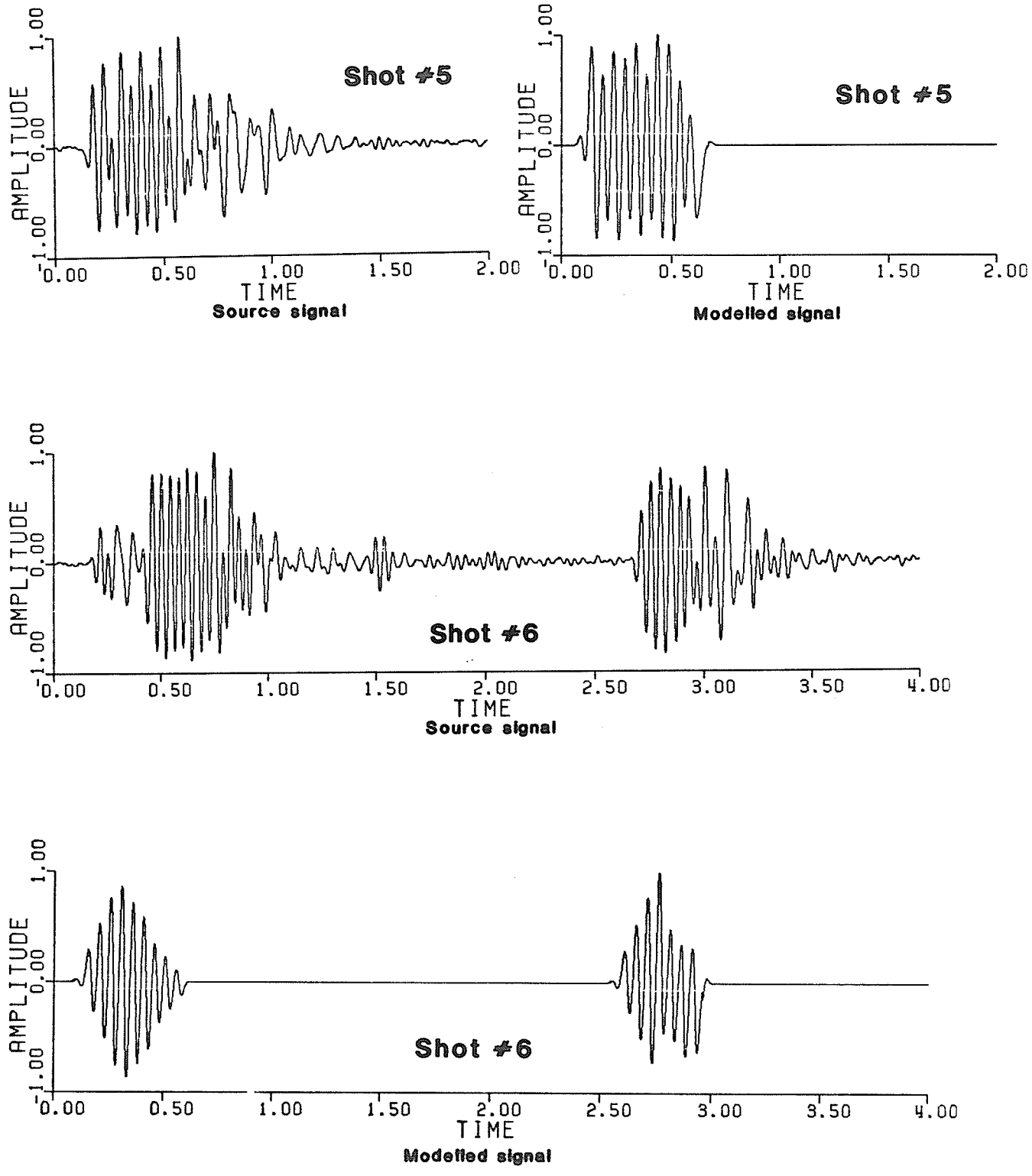

Figure 5.22: Modelled source signals of shots #5 and #6. The shot records are also illustrated.

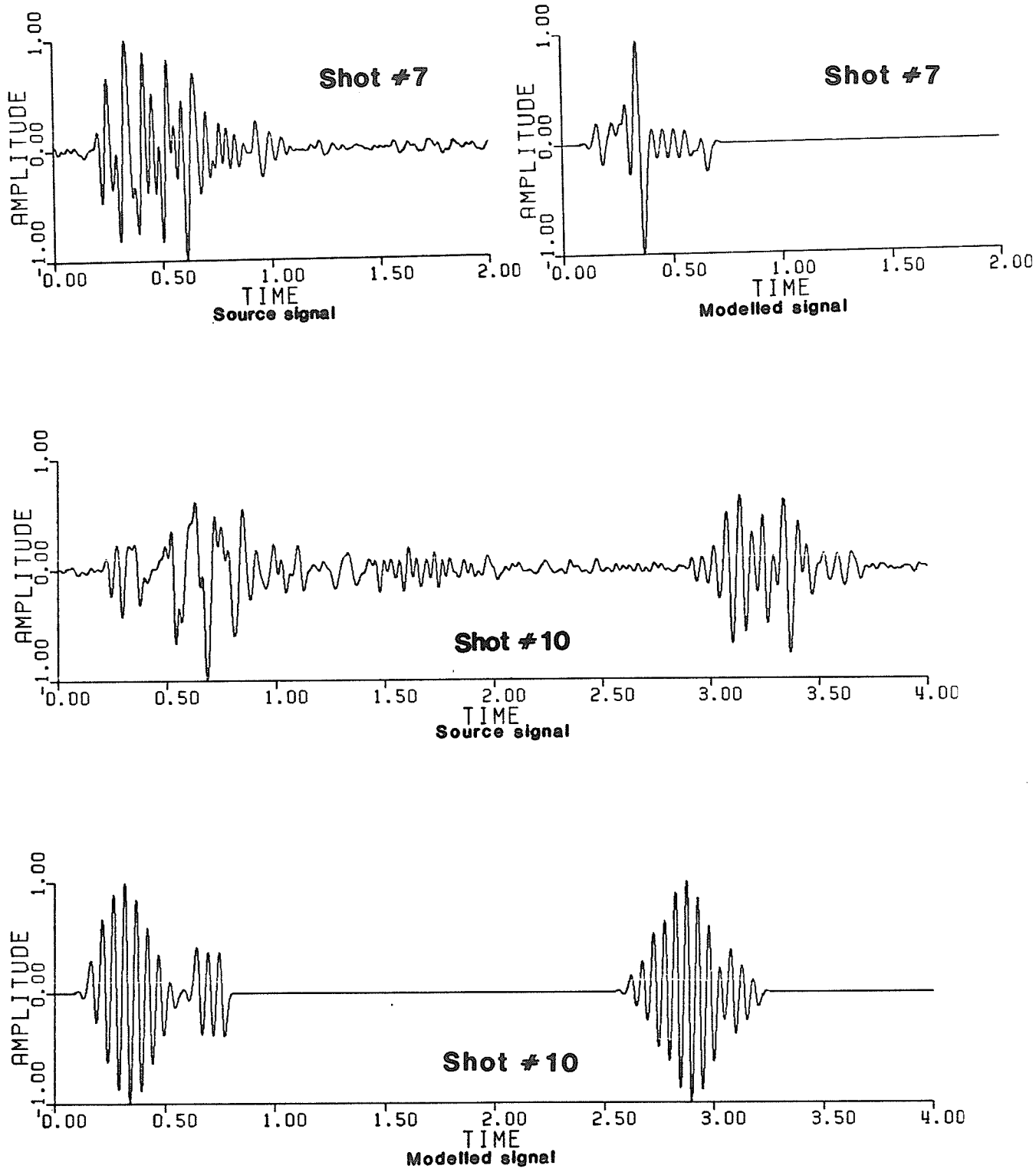

Figure 5.23: Modelled source signals of shots #7 and #10. The shot records are also illustrated.

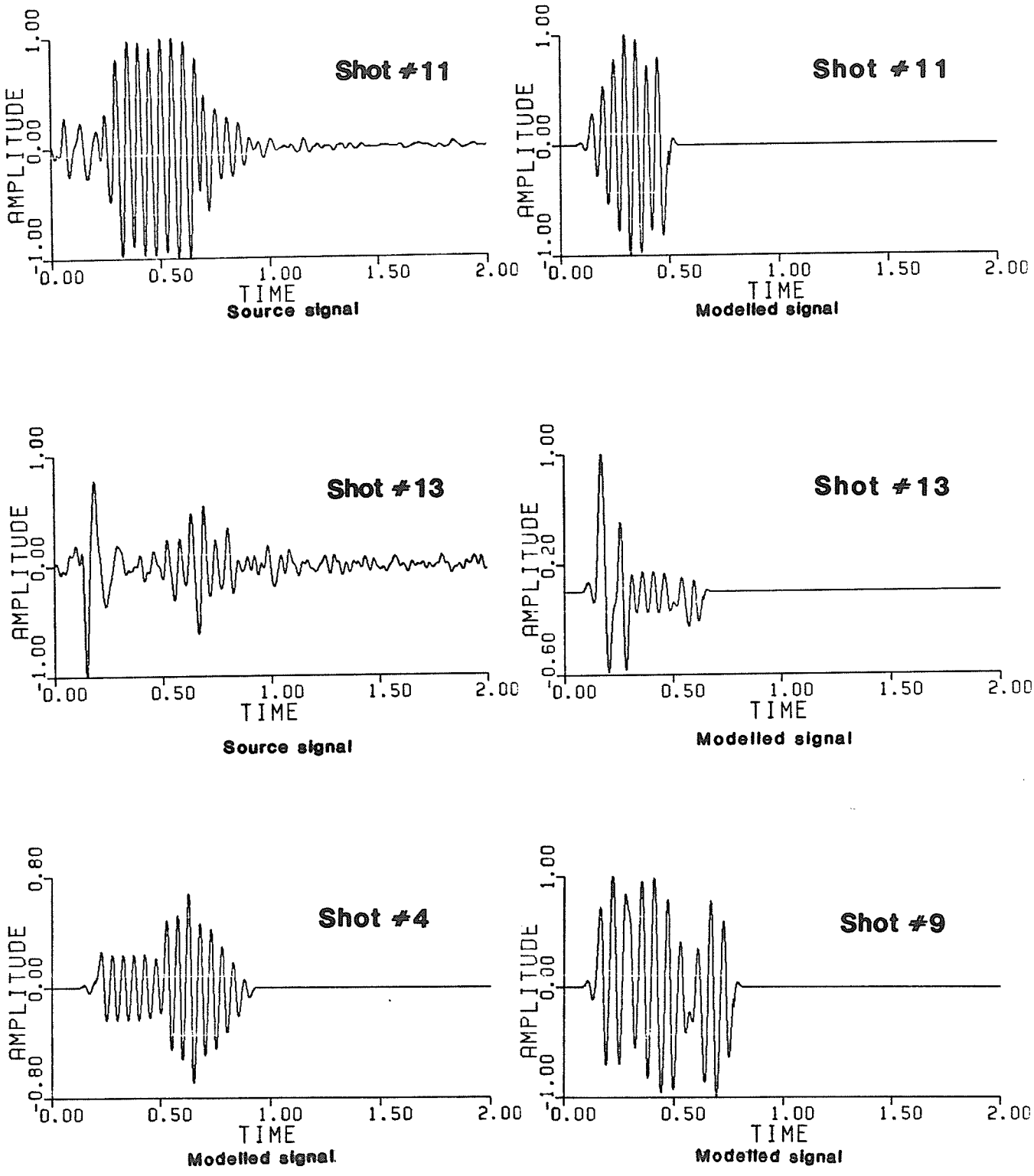

Figure 5.24: Modelled source signals of shots #4, #9, #11 and #13. The shot record for shots #11 and #13 are also illustrated. Shot records for shots #4 and #9 were not recorded.

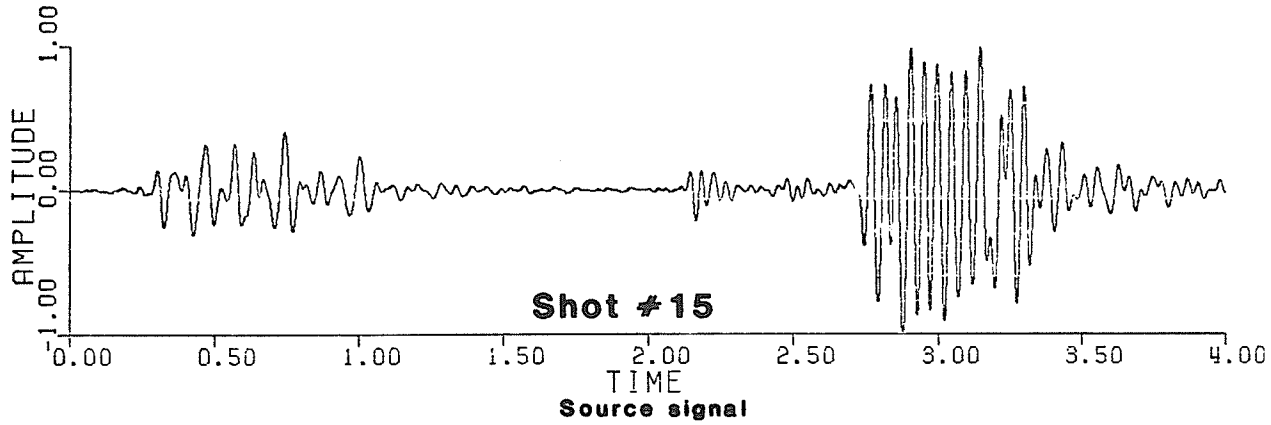

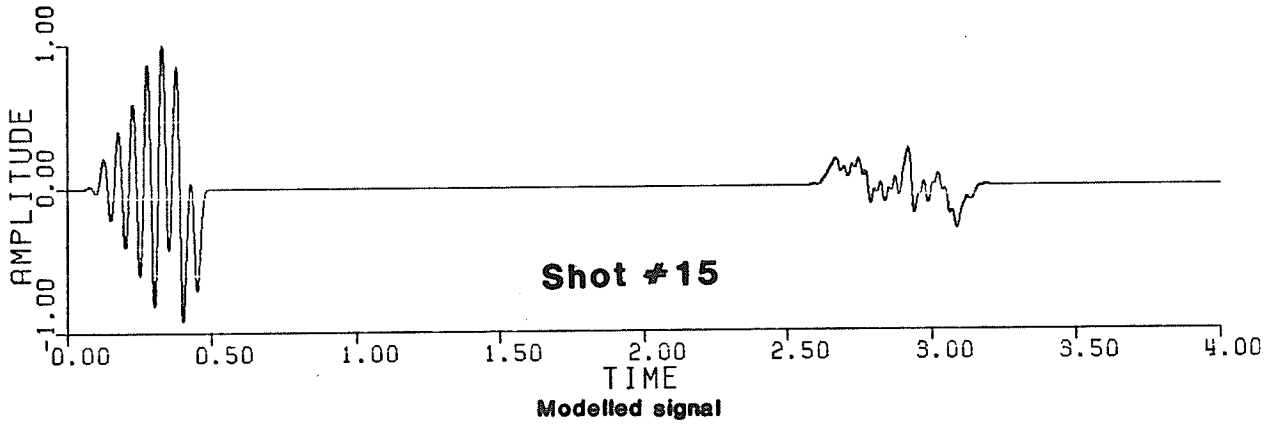

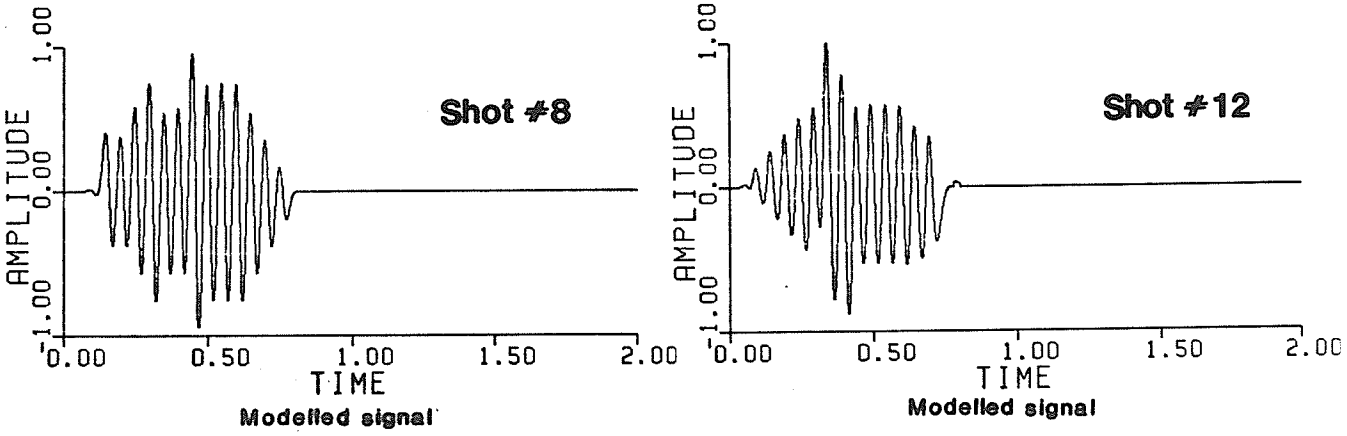

Figure 5.25: Modelled source signals of shots #8, #12 and #15. The shot record is also illustrated for shot #15. Shot records for shots #8 and #12 were not recorded.

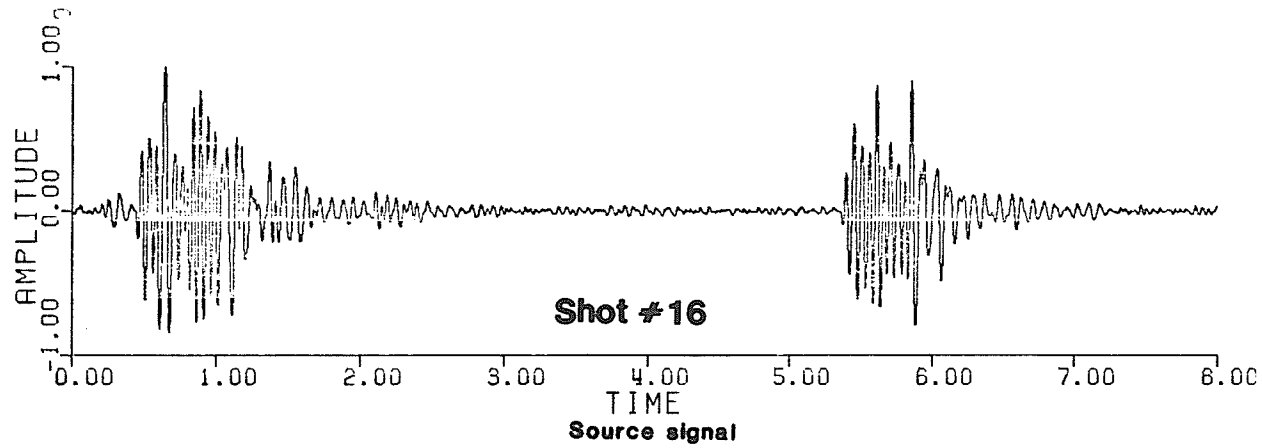

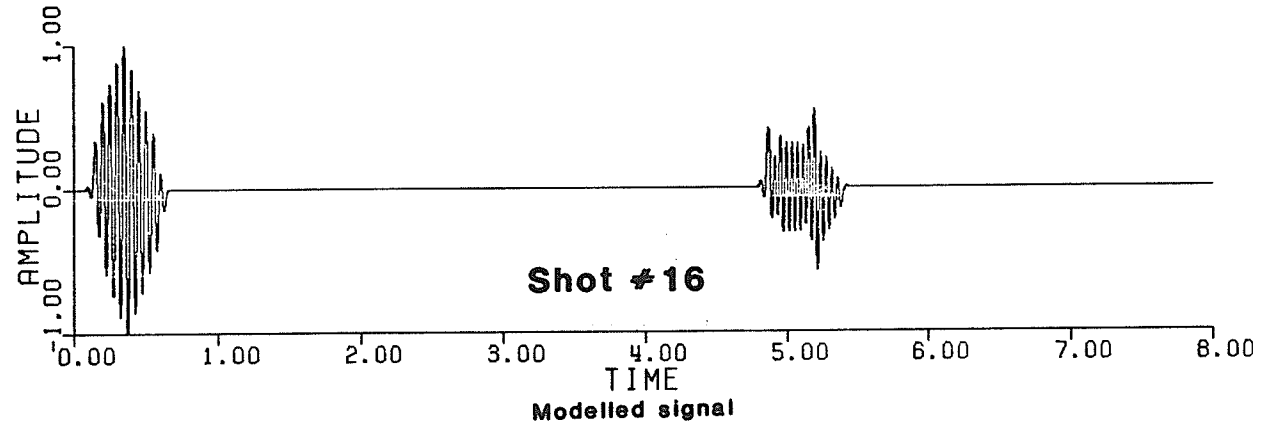

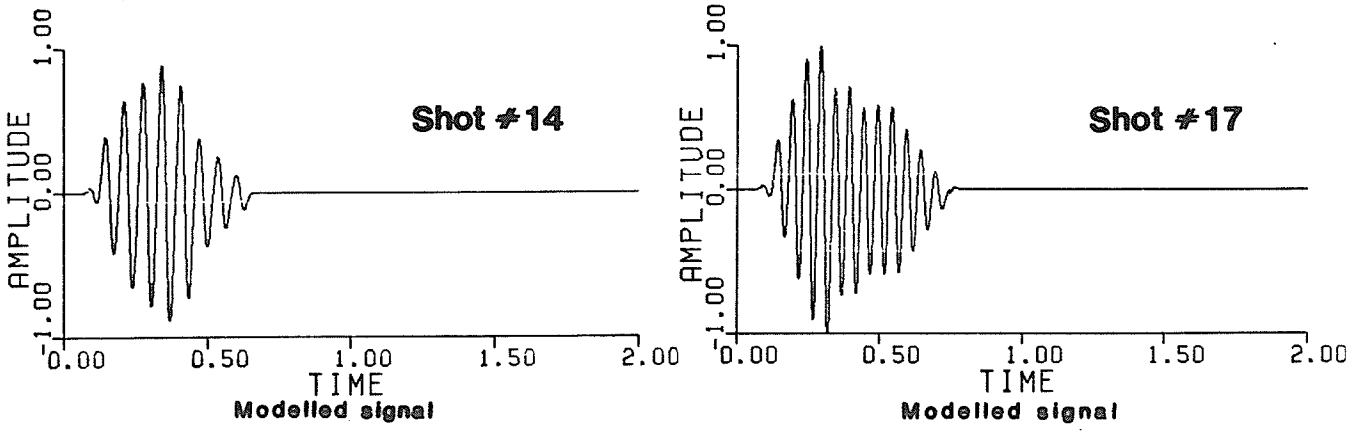

Figure 5.26: Modelled source signals of shots #14, #16 and #17. The shot record for shot #16 is also illustrated. Shot records for shots #14 and #17 were not recorded.

Chapter VI

DIGITAL PROCESSING TECHNIQUES

The source signal used in this experiment is complex and usually a second or more in duration, consequently many of the early arrivals may be buried in the signal. At intermediate distances (5-10 Km) the p-wave and the s-wave separate making arrivals up to 5 seconds (near surface reflections and refractions) difficult to identify. The separation of the p-wave and the s-wave can be seen in most records although it is more apparent on records 6F-N and 4F-S. Even at large distances (>10 Km) as the s-wave is further separated from the p-wave, low amplitude later arrivals are buried. Later events of interest that may be buried in the signal are the reflections from the Riel and the Mohorovicic discontinuities. To further complicate the source signal, the mine blast may consist of two shot patterns separated by several seconds. The subsequent separation of the s-wave and the p-wave at intermediate and large distances only increases the difficulty in locating later arrivals. Therefore the purpose of any processing techniques applied to this data will be to try to recover some of these buried arrivals.

Digital processing techniques that may be useful are vertical stacking, cross-correlation and deconvolution. Since the signal to noise ratio of the data was often low, it was first necessary to filter the data to improve the quality of the data before any of these methods could be applied.

6.1 FILTERING OF THE DATA

The filter used in this study was the Butterworth band pass filter. The Butterworth filter is useful because of its close approximation to an ideal band pass filter which has a response of one in the band pass region and zero in all other regions. The expression for the Z-transform of an 8-pole Butterworth band pass filter used for digital data is (Kanasewich, 1978 after Butterworth 1930):

$$W(z) = \frac{(1-z^2)}{B_1(z)\,B_2(z)\,B_3(z)\,B_4(z)} \qquad 6\text{-}1$$

where: $B_j = 1 - D_{1j}z + D_{2j}z^2$

$$D_{1j} = \frac{(c_j \Delta t - \frac{4}{\Delta t})}{a_j}$$

$$D_{2j} = \frac{\frac{2}{\Delta t} - b_j + c_j \frac{\Delta t}{2}}{a_j}$$

$$a_j = \frac{2}{\Delta t} + b_j + c_j \frac{\Delta t}{2}$$

Δt=sampling interval

b_j, c_j=coefficients obtained from the pole positions of the corresponding 8-pole Butterworth low pass filter.

Since the natural frequency of the Hall-Sears geophones is 1 Hz and the frequency response of the portable recording units is about 60 Hz, then suitable high and low cut frequencies for the filter

must be between these frequencies. After experimenting with several band widths between 1 and 60 Hz a 10 to 35 Hz band pass filter was found to be most effective on the data.

The S/N ratio was greatly enhanced by the filter as first breaks previously unrecognizable could be identified. The filtered records for shots #1 and #2 are shown in figure 6.1, while those for the remaining shots can be located in Appendix D. The quality of both the North and South profiles were subsequently greatly enhanced by the Butterworth filter (figures 6.2 and 6.3).

6.2 VERTICAL STACK

A vertical stack involves the "mixing together of the records of several shots made in nearly the same location without corrections for offset differences" (Sheriff, 1976). Vertical stacks have been studied and used successfully in crustal studies by Brown (1977) and Green et al (1978).

The source signal from each shot is different, consequently vertical stacking may be a useful technique in processing this type of data. Since the source signals of two different shots may be dissimilar in form, other records from the shots will also be different. Generating a vertical stack of traces recorded at the same recording site (common receiver location) but recorded from different shot signals results in the initial pulse of each arrival to be completely stacked. Succeeding pulses in the signal will be stacked to a lesser degree depending on the similarity between each source sig-

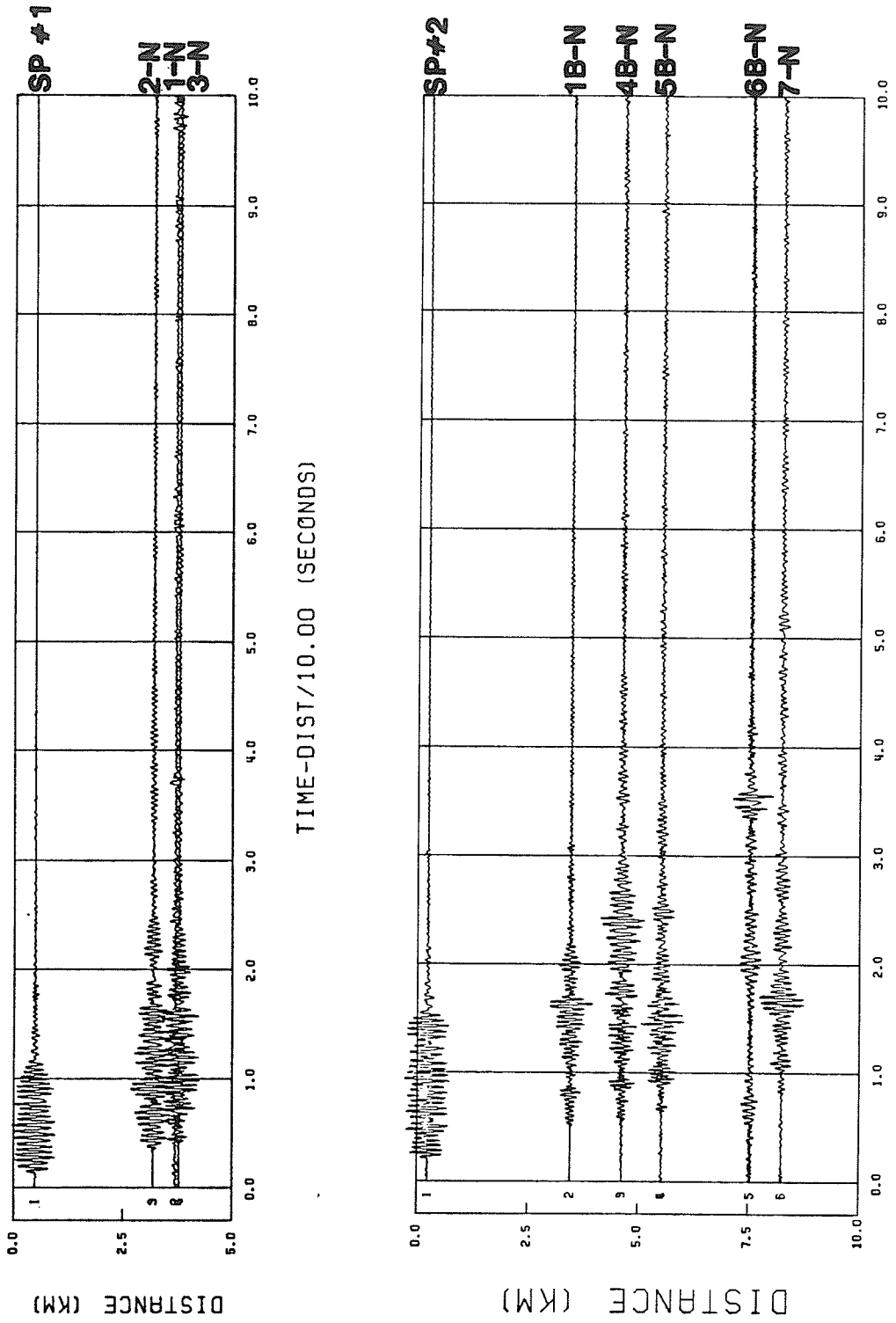

Figure 6.1: Filtered records of shots #1 and #2.

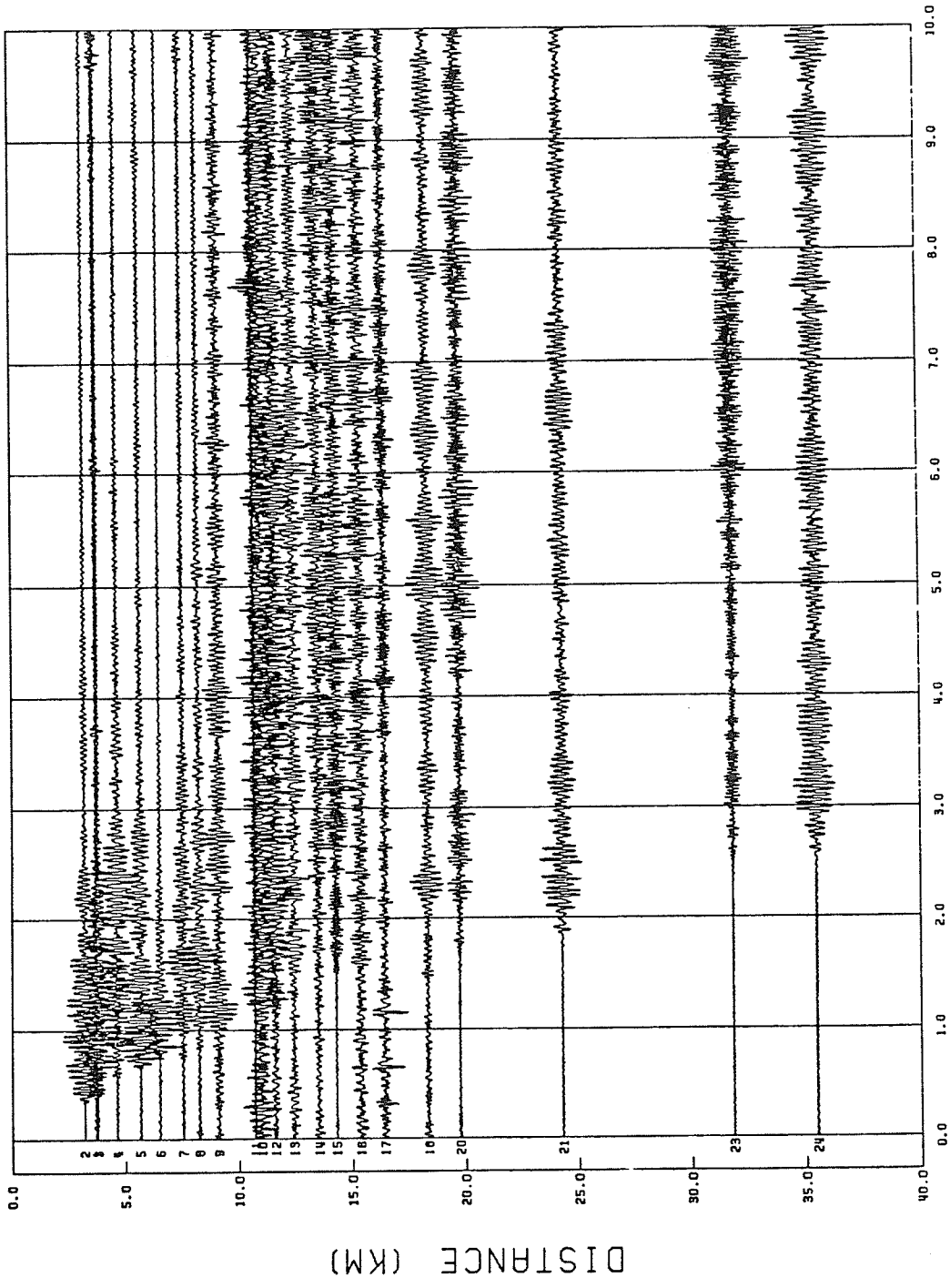

Figure 6.2: Filtered records of the North Profile.

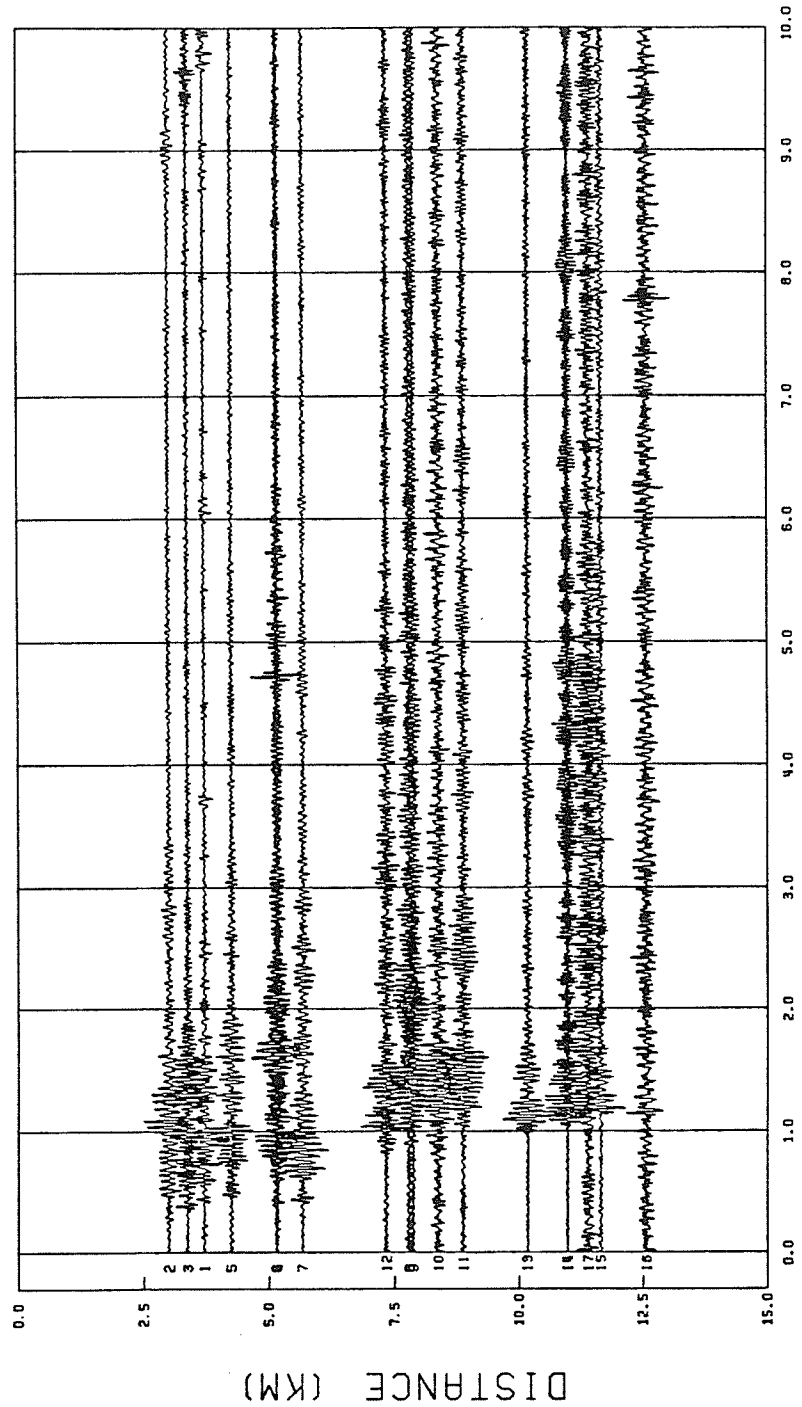

Figure 6.3: Filtered records of the South Profile.

nal. By stacking a large number of records, the initial pulse in each arrival may be stacked enough to be identified. Since only a limited number of records were repeated, this method will not be totally useful for this data, although enough repeated records were collected to test the usefulness of the technique for future studies of this kind.

Two methods of stacking the data were attempted. The first method involved stacking records recorded at common receiver locations. It was hoped that this method of stacking would make it possible to locate first breaks using records with low S/N. The second method of stacking the data involved stacking records recorded from different recording sites but with similar shot-receiver distances in order to try to enhance near vertical reflections. Records with shot-receiver distances between 3 and 5 Km were used for the stacks. It was hoped that this method of stacking the data would make it possible to locate deep reflections. Table 6.1 lists the repeated records that were stacked as well as the records of the different recording sites that were stacked.

The results of the vertical stack of records at common receiver sites show that the timing of the data was not accurate enough as no increase in the amplitude of first breaks was apparent. Figures 6.4 and 6.5 illustrate some examples of stacked records of common recorder locations. In each example the upper traces represent the records that were stacked. The lower trace in each example represents the result of vertically stacking the upper traces. Figure 6.6 illustrates examples of stacked records between 3 and 5 Km. The

results of stacking these records again emphasize the inadequate timing as no reflections were recognized.

6.3 CROSS-CORRELATION

Cross correlation is a measure of the similarity between two sets of data. A correlation coefficient can be generated from two aligned data sets by multiplying corresponding data points together and summing the products. The cross-correlation coefficient can be obtained from (Telford et al, 1976):

$$XC = \sum_{K=-N}^{N} G_K H_{K+T} \qquad 6\text{-}2$$

Similarly, a normalized cross-correlation may be derived using (Telford et al, 1976):

$$XC_n = \sum_{K=-N}^{N} G_K H_{K+T} / \left(\sum_{K=-N}^{N} G_K^2 \sum_{K=-N}^{N} H_K^2 \right)^{-1/2} \qquad 6\text{-}3$$

If two data sets are similar in a certain alignment, the correlation coefficient is high when cross correlated. Similarly, if two data sets are not similar in a certain alignment, the correlation coefficient is near zero when cross-correlated. If one data set is inverted or 90 degrees out of phase, the cross-correlation coefficient is negative. Cross-correlating two sets of data involves the generation of correlation coefficients at different alignments by shifting one of the data sets by some constant interval.

Cross correlation is used extensively in vibroseis and in other seismic techniques involving long source signals. It is useful in vibroseis as the source used is a frequency varying sweep, conseq-

Stack number	File number	Record number	Shot number	File number	Shot-receiver distance (Km)
1	1	5B-N	2	4	5.53
	2	5C-N	3	2	5.44
2	1	5B-N	2	4	5.53
	2	5C-N	3	2	5.44
	3	5D-N	4	1	5.44
3	1	16B-N	5	3	15.53
	2	16C-N	6	4	15.38
4	1	4B-S	8	1	5.12
	2	4F-S	16	2	4.94
5	1	4B-S	8	1	5.12
	2	4D-S	12	1	5.16
	3	4F-S	16	2	4.94
6	1	17-S	11	6	11.77
	2	17B-S	13	2	11.40
7	1	2D-S	11	2	3.00
	2	3D-S	17	1	3.37
	3	3B-S	14	1	3.23
	4	2-S	7	2	3.25
	5	2B-S	9	1	3.32
	6	3-S	7	3	3.37
	7	5-S	7	4	4.24
	8	4F-S	16	2	4.94
8	1	2D-S	11	2	3.00
	2	3D-S	17	1	3.37
	3	3B-S	14	1	3.23
	4	2-S	7	2	3.25
	5	2B-S	9	1	3.32
	6	3-S	7	3	3.37

TABLE 6.1

Records used in vertical stacks.

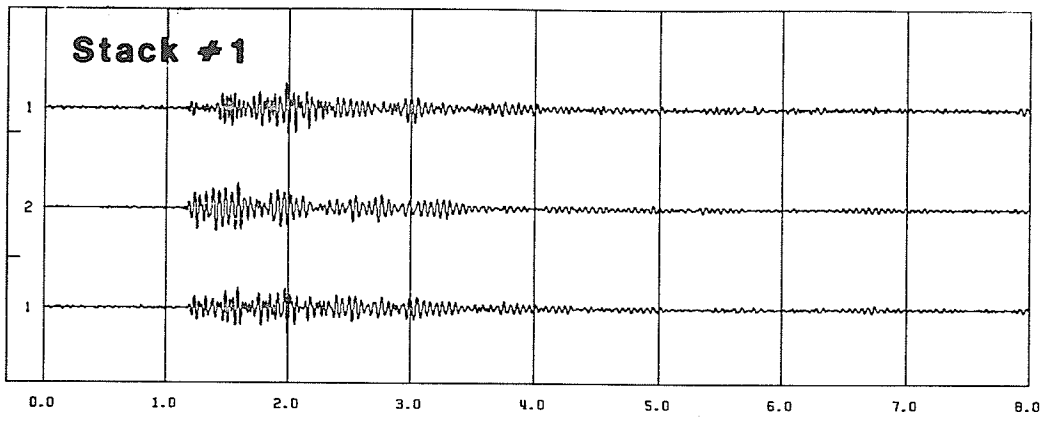

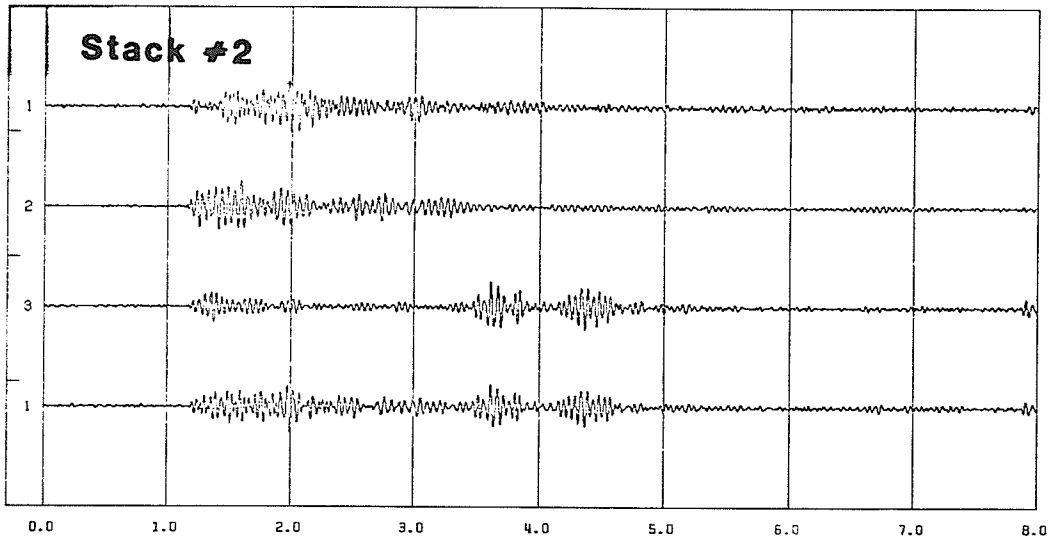

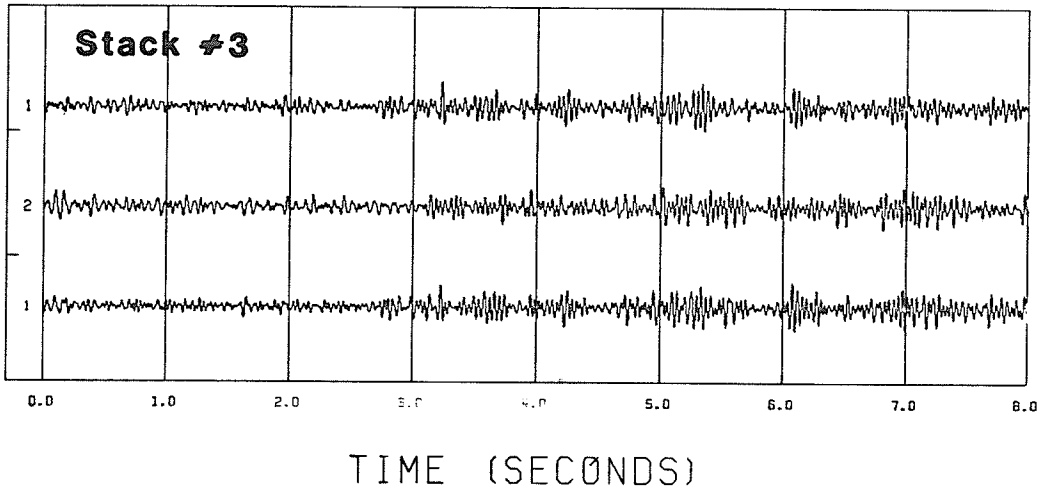

Figure 6.4: Vertical stack of common receiver locations of the North profile. Stacks #1, #2 and #3 are illustrated (table 6.1).

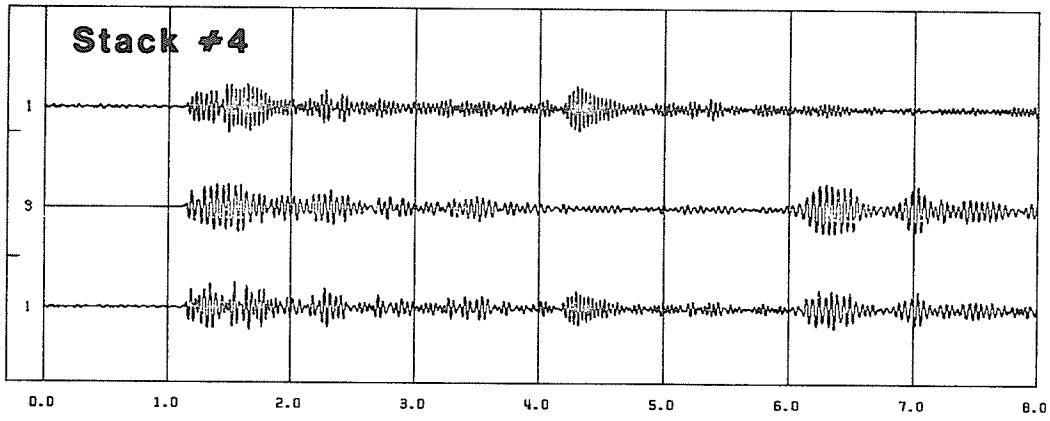

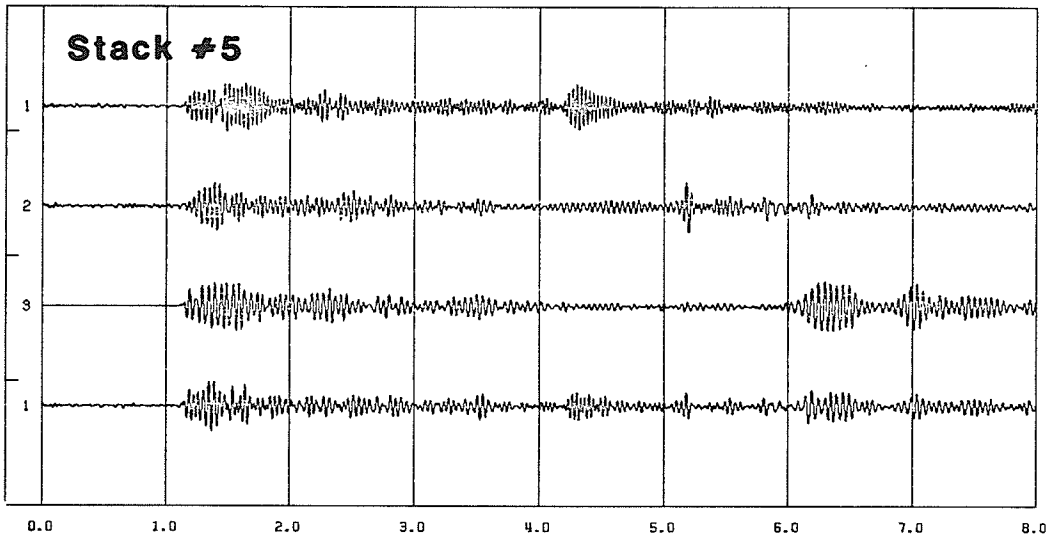

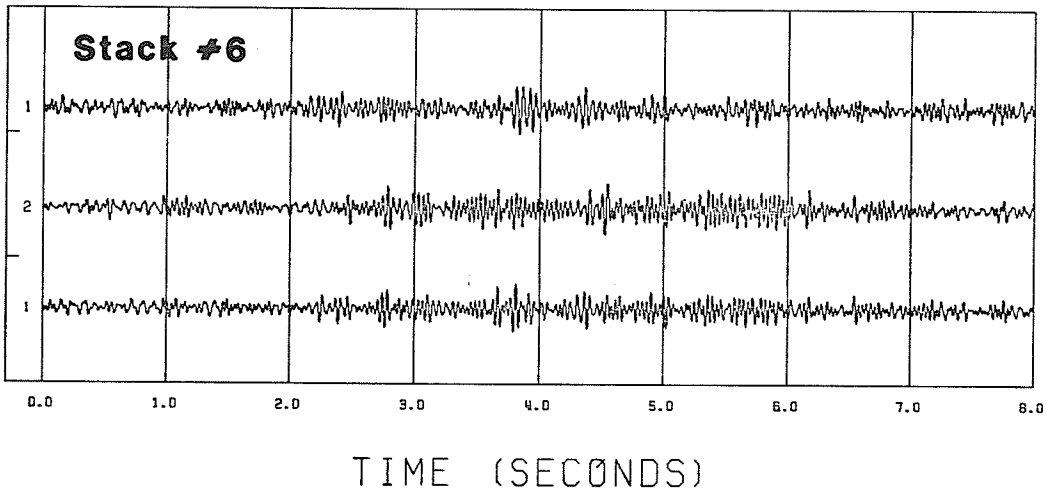

Figure 6.5: Vertical stack of common receiver locations of the South profile. Stacks #4, #5 and #6 are illustrated (table 6.1).

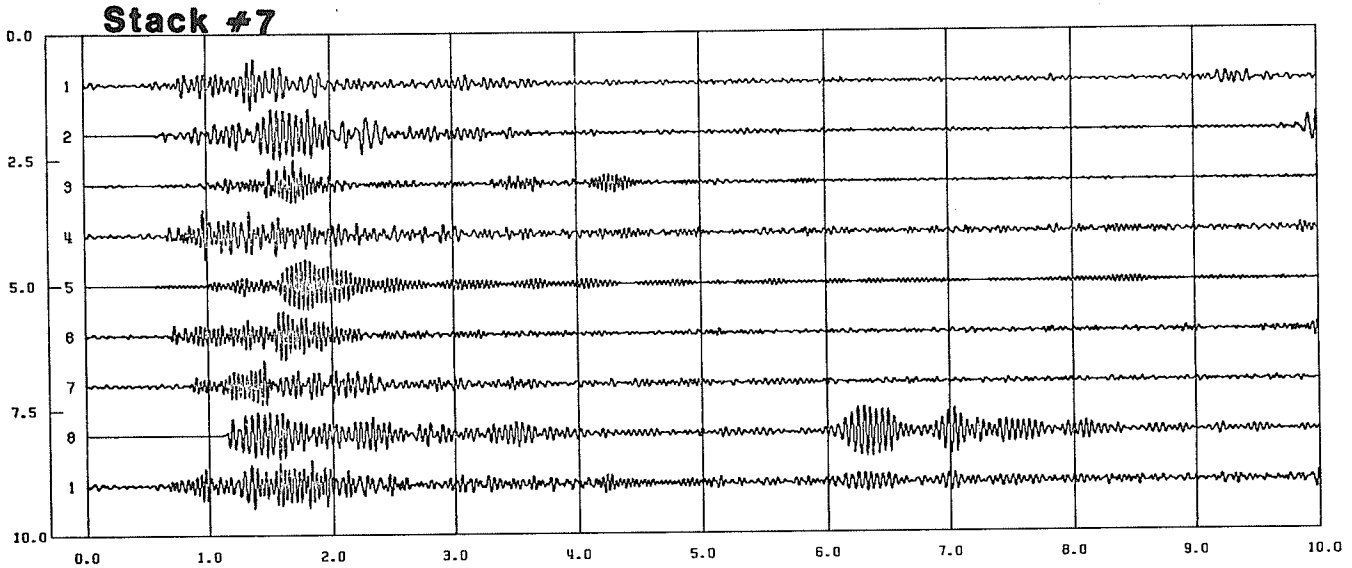

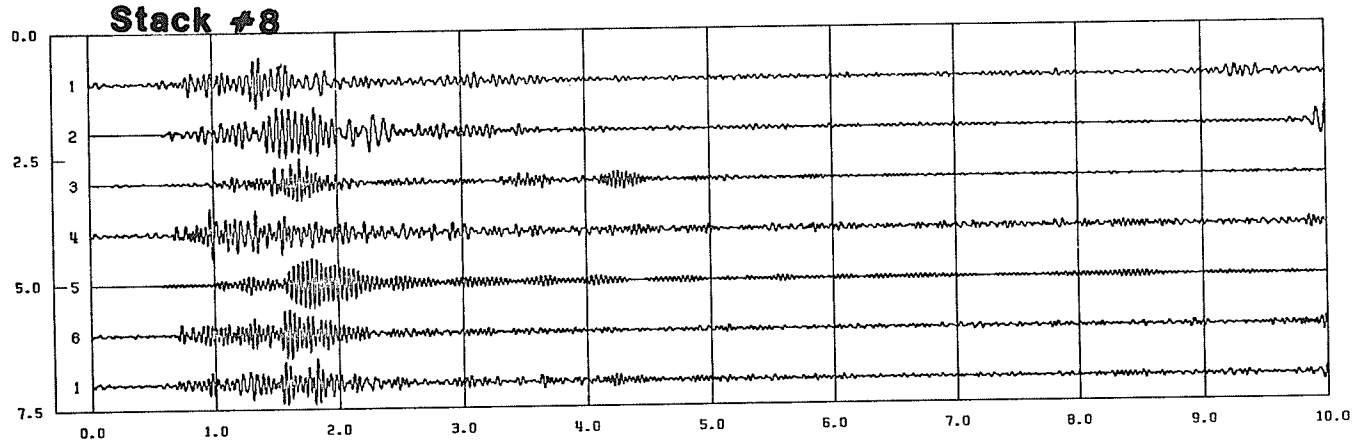

Figure 6.6: Vertical stack of records from different recording sites. Stacks #7 and #8 are illustrated (table 6.1). Records from the North profile at distances between 3 and 5 Km were used for the stacks.

uently there is only one alignment with the source signal that generates a high correlation coefficient.

Cross-correlation can also be useful using a long random source signal. As in the vibroseis signal, there will only be one alignment with the source signal that generates a high correlation coefficient, consequently if the complex source signal of the data collected in this experiment is random in nature, cross-correlation may be a useful technique to apply.

The cross-correlated traces of shots #1 and #2 are shown in figure 6.7 while the cross-correlated records of some of the other shots are illustrated in Appendix E. The cross-correlation of records involving shots with no shot point records were carried out using the nearest record to the shot.

The results of the cross-correlation show that the source signal is not random in nature. There is a high correlation for each shot or group of shots in the blast. Figure 6.8 illustrates in a simplified manner what is occurring during the cross-correlation of the data. As the operator is shifted down the trace the first high correlation occurs when the last shot in the operator is aligned with the first shot in the signal. The second high correlation is larger than the first and occurs when the last two shots in the operator (source signal) are aligned with the last two shots of the signal. This trend continues until the maximum correlation occurs when the entire operator and the signal are aligned. The opposite trend occurs as the operator is further shifted past the signal.

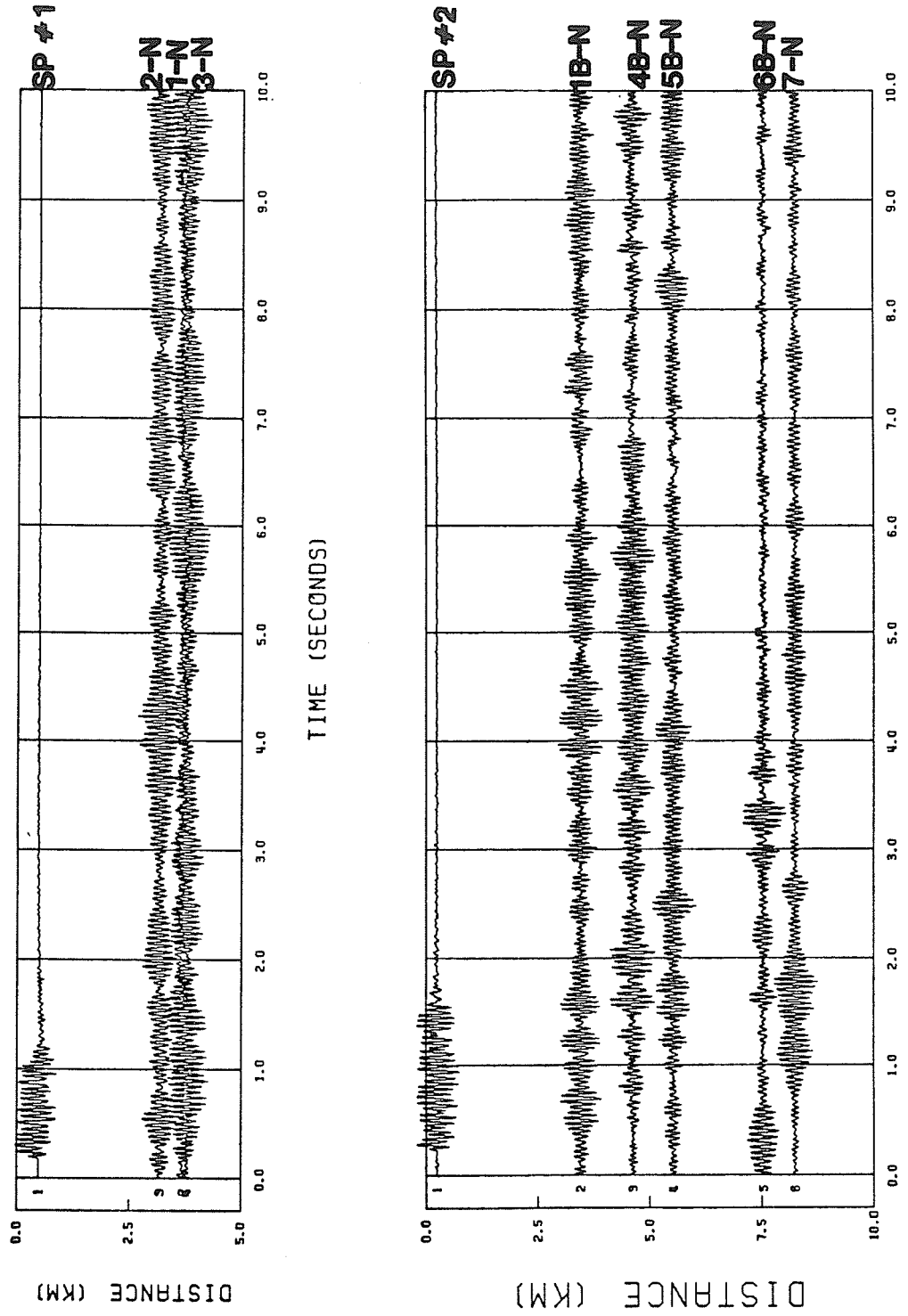

Figure 6.7: Cross-correlated records of shots #1 and #2.

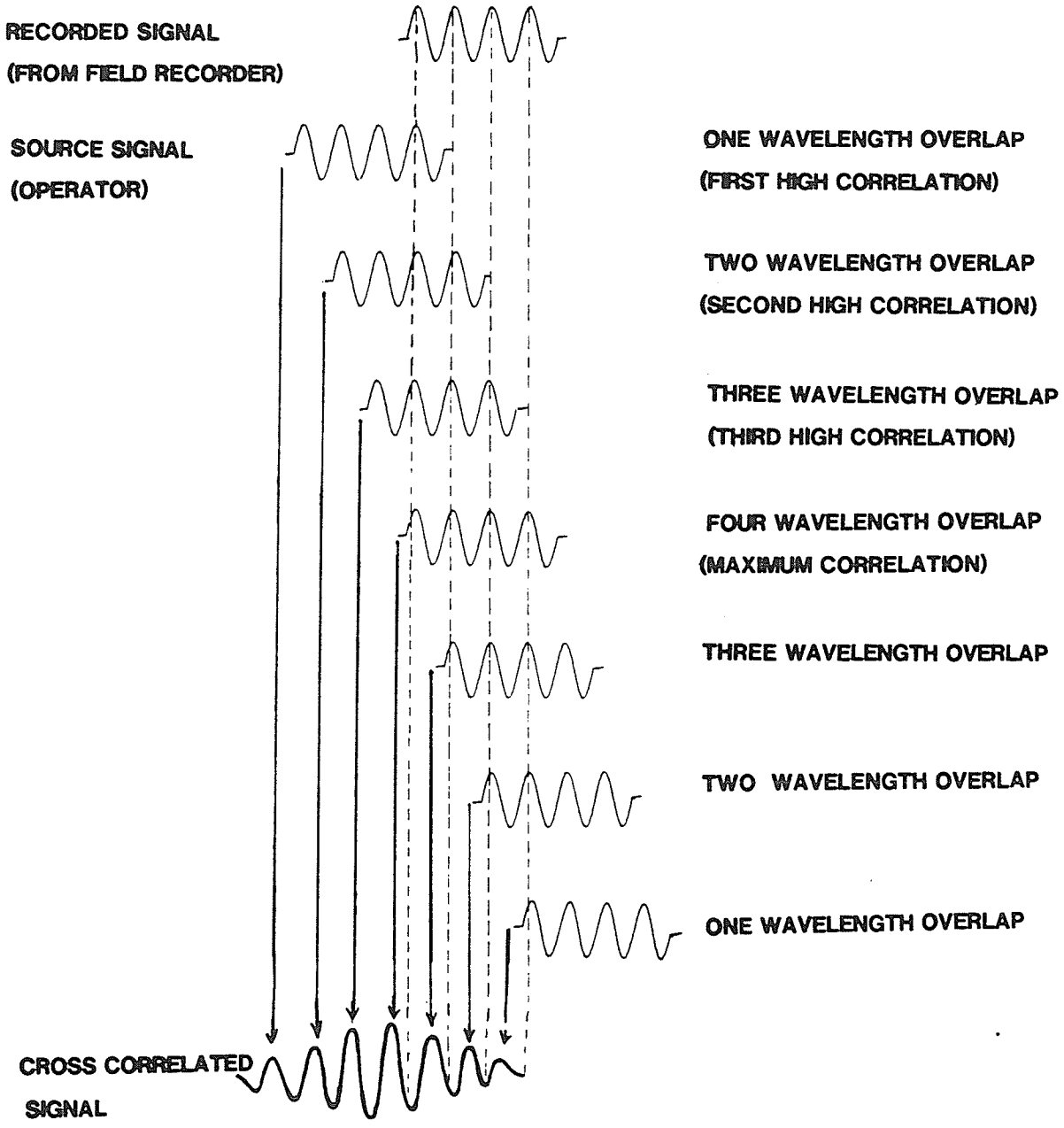

Figure 6.8: Cross-correlation of similar records.

Another factor affecting the cross-correlation of the data is the radiation pattern. Since most of the mine blasts consist of multiple shot patterns, the time delay between the signals of the shot patterns may vary depending on the relative positions of the shot point recorder, the field recorder and the shot patterns. The radiation pattern from single shot patterns can also cause the signals recorded at the shot point and at the field recorders to be different depending on their relative positions.

The final factor affecting the cross-correlation of the data involves the nature of the first break. Since the type of arrivals at the shot point and at the field recorders are different, the actual signal is similar but not the same, consequently the signal recorded at the shot point is not adequate for cross-correlation.

6.4 DISCUSSION OF RESULTS

The results of this study have shown that neither vertical stacking or cross-correlation were effective methods to process this data, however under planned source conditions both methods may be effective.

Although the vertically stacked records of this experiment failed to bring out first breaks or later events it may be possible to use these techniques with better planning of the shot signal. Most importantly, the times of each shot must be measured more accurately. This might be accomplished by timing the plunger or the electrical system used to ignite the blast rather than using first breaks of a

record near the blast. Also, it is important that all the data to be stacked have recorded shot signals that originate in a similar location in the pit. Finally, it may be possible to plan the shot signal so that a large group of shots in a shot pattern ignite simultaneously followed by a delay of greater than 10 seconds in order that the arrivals from this blast can be recorded before the remaining portion of the shot pattern is set off. This would be a more effective way of obtaining good results from a survey of this type as most of the problems are due to the complex nature of the blasts. In fact with a series of smaller blasts each 10 seconds apart, it may be possible to record a suitable number of records for stacking if necessary at a later time. At this time however, it is not apparent whether this type of blast would be suitable to the mine's production needs. If some or all of these shot conditions are met then vertically stacking records can be a viable method of processing data recorded from quarry blasts.

The cross-correlated traces of this data is also not suitable for normal interpretion, although with better planning of the shot patterns this method may be effective. First, the shot time must be known more accurately. As mentioned in the preceding paragraphs, this might be accomplished by timing the plunger or the electrical system of the blast. The shape of the source signal must also be recorded more accurately. A technique whereby only the direct p-wave is recorded would be best suited as multiple arrivals at the shot recorder results in an inadequate source signal. Perhaps if the horizontal component of the source signal was recorded, other

arrivals such as the direct sv-wave and head waves would be suppressed enough to record a signal suitable for cross-correlation. Also, if the source signal could be accurately reproduced, it may be adequate for cross correlation of the data. This has been attempted in Chapter 5 and requires further study.

Once the source signal can be accurately recorded it is important that the individual shots in the shot patterns be arranged such that a random signal is created. Also, the location of the shot point recorder should be pre-planned such that the radiation pattern does not affect the signal. If all of the preceding conditions are realized, cross-correlation can be a viable method for the processing of complex data sets such as this.

6.5 ALTERNATE PROCESSING TECHNIQUES

A technique that would have been useful is deconvolution, however due to time constraints this method was not attempted. With proper planning of the shot signal, this method would probably have been more effective than the two processing techniques used in this study.

Another technique that may have been useful to apply to this data is a combination of stacking and cross correlating. The first step required of this technique would be to stack all records of common receiver location. If the source signals were also stacked then perhaps the resultant signal may be random enough that cross correlation of the stacked data may be effective. Due to a lack of repeated records and poor timing information, this was not attempted.

Chapter VII

INTERPRETATION

The interpretation of this data was attempted in two parts. First, a first break analysis was applied to study shallow refractors using the ray tracing technique of Whittal and Clowes (1979). The WKBJ method derived by Chapman (1978) was then applied to interpret later reflections. The WKBJ method considers only horizontal reflectors consequently the ray tracing method was better suited to interpret the near surface events.

7.1 RAY TRACING METHOD

The Whittal-Clowes (1979) technique is a ray tracing method which computes travel times of head waves, turning rays and post critical reflections for any pre-determined subsection. First, any subsection can be derived by using plane interfaces of any dip. Velocities at these interfaces are constant while a linear velocity gradient is set up perpendicular to the direction of dip of the interfaces. The ray path is a circular arc through each layer. The path of various rays can be traced and the travel time within each layer can be derived using:

$$dT=\frac{1}{GRAD}*(ARCTANH(COS(IOUT))-ARCTANH(COS(IIN)) \qquad 7\text{-}1$$

where: VEL=the velocity in the layer

GRAD=the velocity gradiant in the layer

IOUT=the initial ray departure angle measured with respect to the gradient.

IIN=the ray intersection angle on the next boundary measured with to the gradient.

By tracing each ray through the subsurface, travel times for any turning rays, head waves or post critical reflections can be computed. A time-distance plot can then be generated illustrating these arrivals. Applying this technique, best fit models for both the North and South profiles were generated. Figures 7.1 and 7.2 illustrates these models while the first break picks are shown in figures 7.3 and 7.4.

The best fit model of the North profile (figure 7.1) consists of an upper layer which varies in depth from 0.9 Km at the source to 0.75 Km at an 8.5 Km distance. The velocity of this low velocity layer is 4.7 Km/sec at the surface with a velocity gradient of 0.5 Km/sec/Km. This layer is interrupted by a very low velocity layer extending from 8.5 Km to 15.0 Km. This low velocity zone varies in depth from 3.0 Km at an 8.5 Km distance to 3.3 Km at a distance of 15.0 Km. The velocity of this zone is 3.2 Km/sec at the top of the zone but has a very high velocity gradient of 0.65 Km/sec/Km. The original low velocity zone then resumes across the rest of the profile to a 40.0 Km distace. The depth varies from 3.3 Km at a distance of 15.0 Km to 2.25 Km at a 40.0 Km distance. The velocity of the second layer is 6.16 Km/sec at its upper interface and has a velocity gradient of 0.075 Km/sec/Km. The top of the third layer is 2.75 Km deep at the source and then dips to a depth of 4.45 Km at

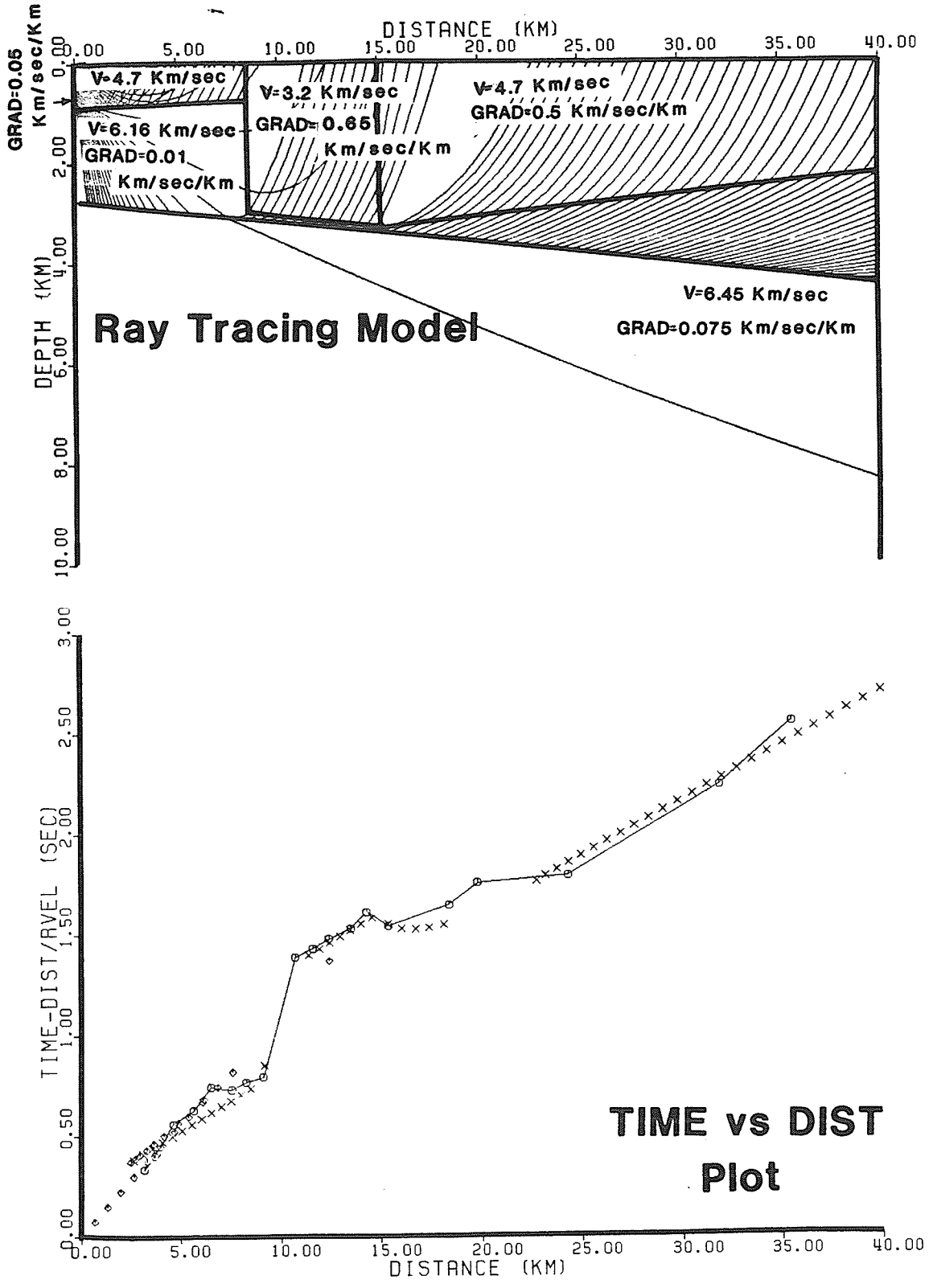

Figure 7.1: Ray tracing model for North Profile.

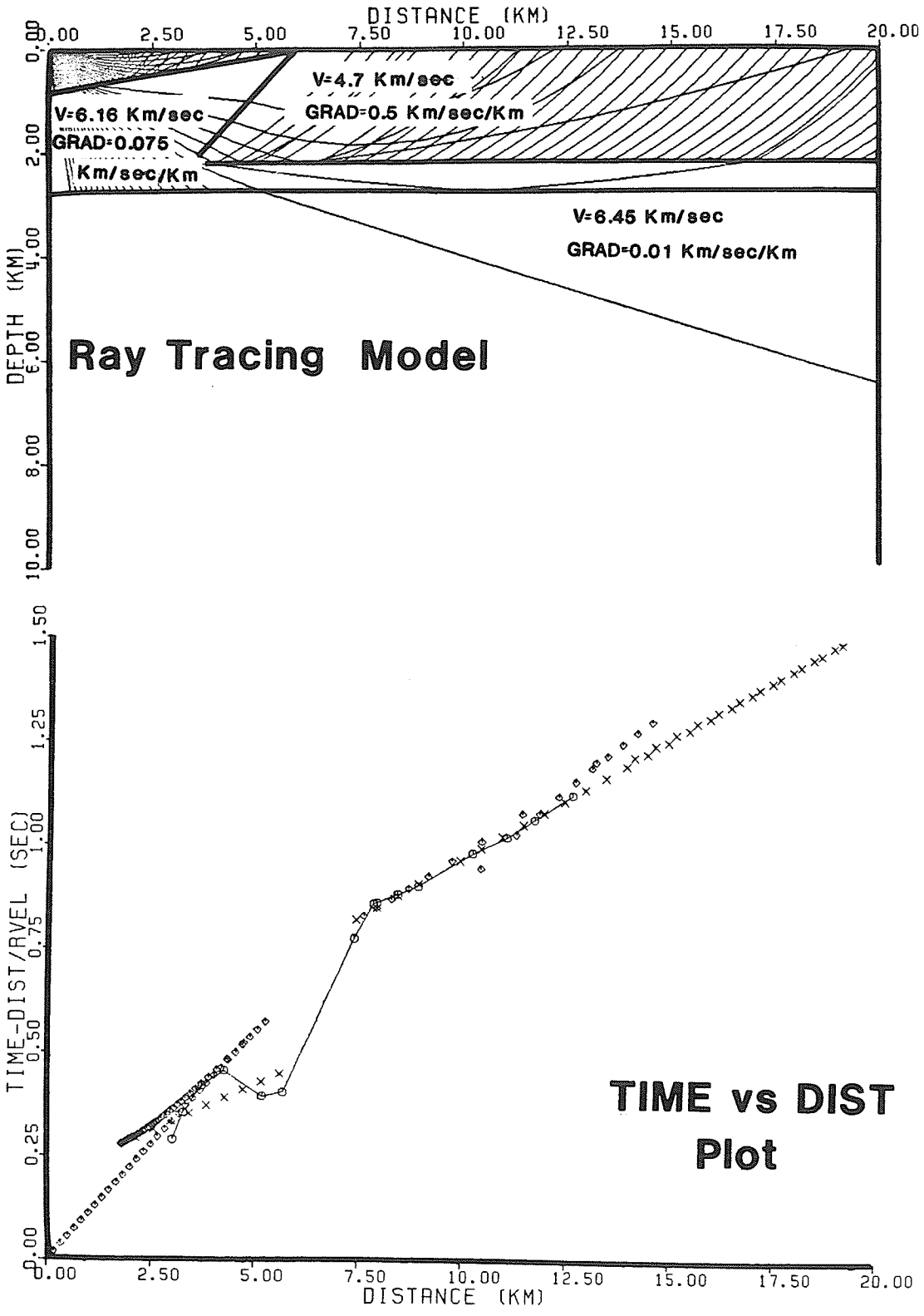

Figure 7.2: Ray tracing model for South Profile.

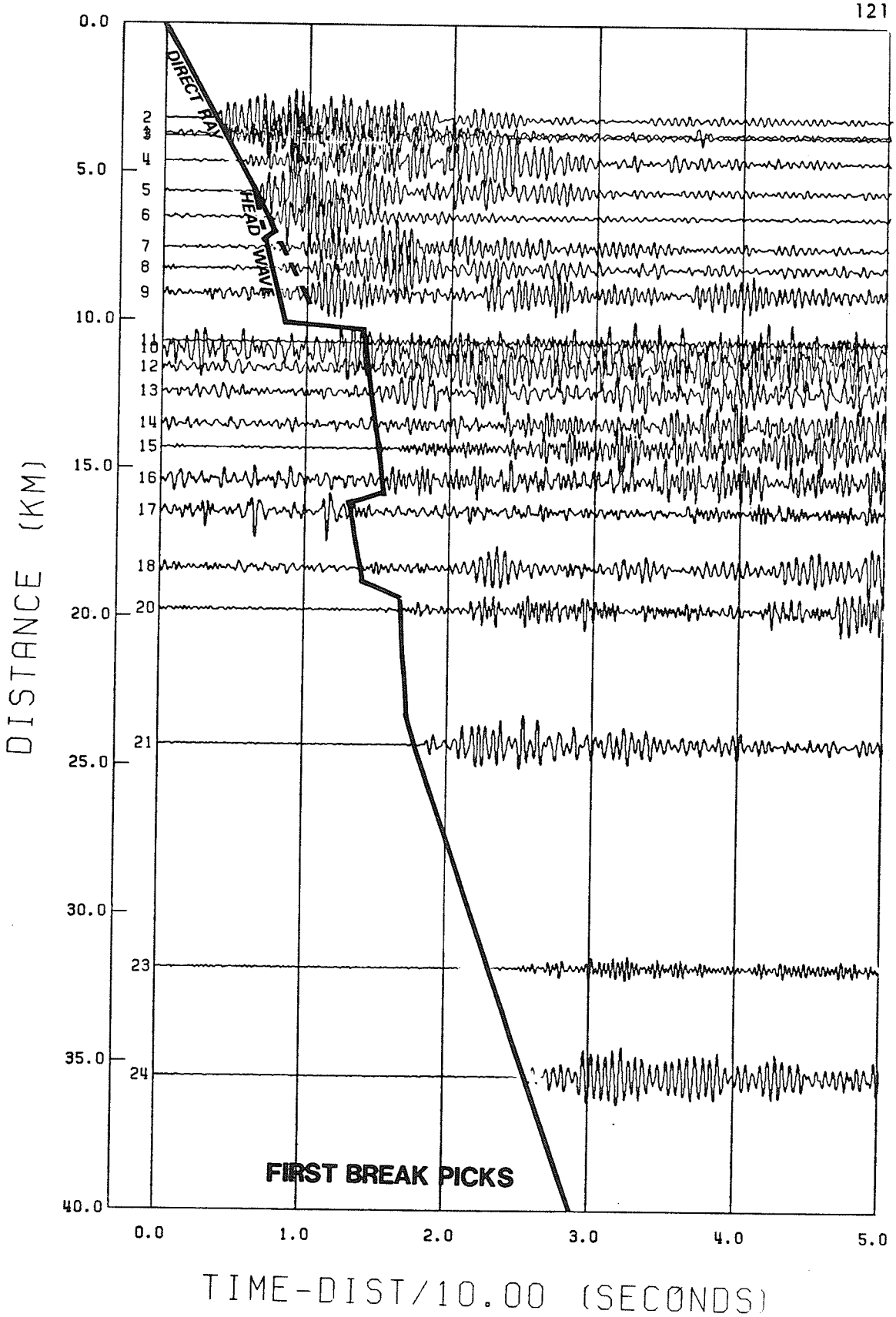

Figure 7.3: First break picks from the North profile.

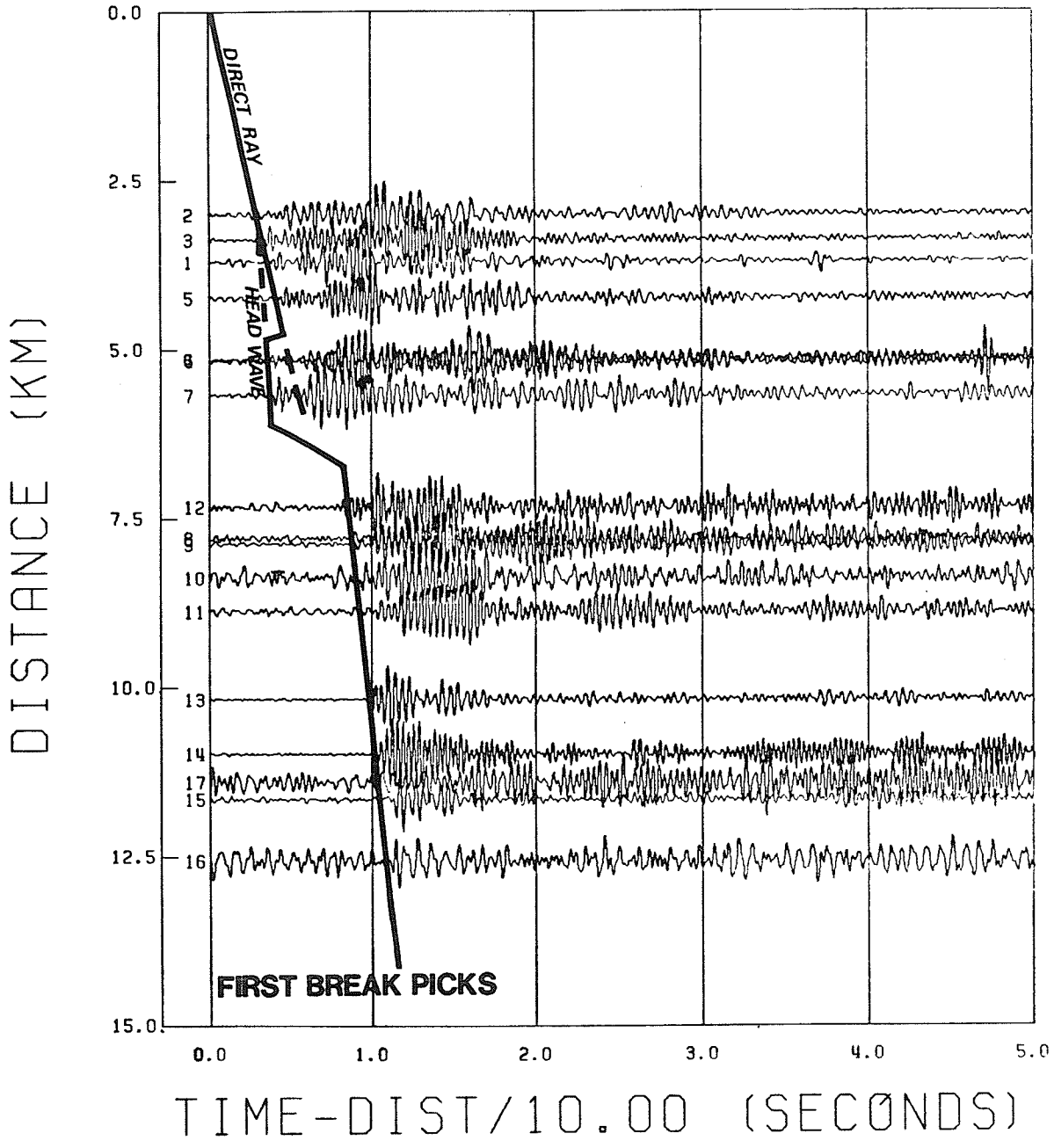

Figure 7.4: First break picks from the South profile.

the end of the profile (40.0 Km). The velocity at the top of this layer is 6.45 Km/sec, while the velocity gradient is 0.01 Km/sec/Km.

The best fit model of the South profile (figure 7.2) is similar to that of the North profile. The model consists of a low velocity layer near the surface which varies from 0.8 Km in depth at the shot point to 0.01 Km at a distance of 6.0 Km. The lower interface then dips from this point to a depth of 2.3 Km at a 3.25 Km distance. This interface then extends from 3.25 Km to 20.0 Km which is at a depth of 2.2 Km. The low velocity layer has a velocity of 4.7 Km/sec at the surface with a high velocity gradient of 0.5 Km/sec/Km. The second layer has a velocity of 6.16 Km/sec at its upper interface and a velocity gradient of 0.075 Km/sec/Km. The top of the third layer extends across the profile at a constant depth of 2.75 Km. The velocity of this layer is 6.45 Km/sec at the top with a velocity gradient of 0.01 Km/sec/Km. The ray tracing models of both the North and South profiles will be discussed further section 7.3.

Since the ray tracing method does not consider pre-critical reflections and because the profiles are short, the deeper reflections are not considered using this technique. The WKBJ synthetic seismogram method was therefore applied to interpret these arrivals. The WKBJ method is suitable to interpret the deep reflections from near horizontal reflectors such as the Moho and the Riel discontinuities.

7.2 WKBJ SYNTHETIC SEISMOGRAM METHOD

The WKBJ technique is one of several methods that is available to generate synthetic seismograms. This method uses the WKBJ approximate solution of the wave equation. The method is valid only if the frequencies are high compared to the velocity gradients. Using the WKBJ solution the displacement of the seismogram is:

$$U(t,x)=\left(\frac{1}{2\pi}\right)\dot{S}(t)\sum_{t=\theta(p,x)}R(p)/\theta'(p,x) \qquad 7\text{-}2$$

where: $S(t)$=source function which includes the transform function of the geophones.

$\theta=px+T(p)$

$T(p)$=vertical slowness integral.

$$=2\int_{Za}^{Zb}q(p,E)\,dE$$

The method can generate direct rays, turning rays, reflections and head waves. Because of the complex nature of the data collected in this experiment, later events were hard to locate, consequently various earth models were considered to generate synthetic seismograms.

The Earth models used were those of Hall and Hajnal (1969,1973), Berry and Fuchs (1973) and DeLandro (1981). The ray tracing models for the upper layers were averaged and the Earth models were applied at lower depths in order to generate the synthetic seismograms. Deep reflections were generated using the WKBJ method and the re-

sulting seismograms were used to locate these events in the actual data. The Earth models of Hall and Hajnal (1969,1973) as well as the seismograms that were generated from them are shown in figure 7.5. The Hall and Hajnal (1969,1973) model is illustrated here because of its close proximity to the survey area.

The model consists of a low velocity layer on the surface which has an initial velocity of 4.7 Km/sec. This layer has a velocity gradient of 0.5 Km/sec/Km, consequently the velocity is increased to 5.45 Km/sec at a 1.5 Km depth. The density over this interval is 2.69 gm/cm**3. At this depth the velocity increases to 6.16 Km/sec and the density increases to 2.75 gm/cm**3. Both the velocity and the density is constant to a 3.0 Km depth. At a 3.0 Km depth the velocity is increased to 6.45 Km/sec and the density is increased to 2.8 gm/cm**3. The velocity and density is constant to a depth of 24.0 Km. From this depth, the Hall and Hajnal (1969,1973) model was used. At 24.0 Km the velocity increases to 6.85 Km/sec and the density increases to 2.9 gm/cm**3. This again is constant to a depth of 31.0 Km where the velocity increases to 7.92 Km/sec and the density increases to 3.1 gm/cm**3. The velocity and density is constant to a depth of 45.0 Km.

The densities used for the shallow layers in these models were estimated from Gupta and Barlow(1984) and Berry and Fuchs (1973). The densities from the deeper layers were approximated from Stacey (1977) and Berry and Fuchs (1973). Figures 7.5 and 7.6 illustrate the expected arrival times of the Riel and Moho events as taken from the WKBJ model. These events are indicated on both the North and South profiles.

7.3 DISCUSSION OF RAY TRACING RESULTS

The best fit models of both the North and South profiles generally fit with the surrounding geology, although there are some unnatural structures associated with the models that must first be explained.

7.3.1 The North Profile

The first major problem with the ray tracing model of the North profile is a delay in arrival of the first breaks on a few records at distances less than 10 Km from the source. Fortunately, this can be explained by the presence of the Pakwash Lake Pluton. The pluton seems to be causing a delay of first arrivals to certain recording locations. Figure 7.7 illustrates the effect of the pluton. The first arrivals of the first four recording sites is a direct ray (or turning ray) therefore the pluton does not significantly affect these records. The first arrival at the fifth and sixth recording sites should be a head wave however this arrival has been delayed. This delay is a result of the pluton interrupting the interface that the head wave is propagating along. Since this interface is cut off by the pluton the head wave must travel in the low velocity upper layer causing a small delay in the arrival of the first break. The pluton does not lie in the path of records #7, #8 and #9 therefore the wave is allowed to reach these sites with no delay. The head waves of the remaining recording sites are impeded in the same manner as records #5 and #6 as the pluton lies in the direct path between the source and receiver.

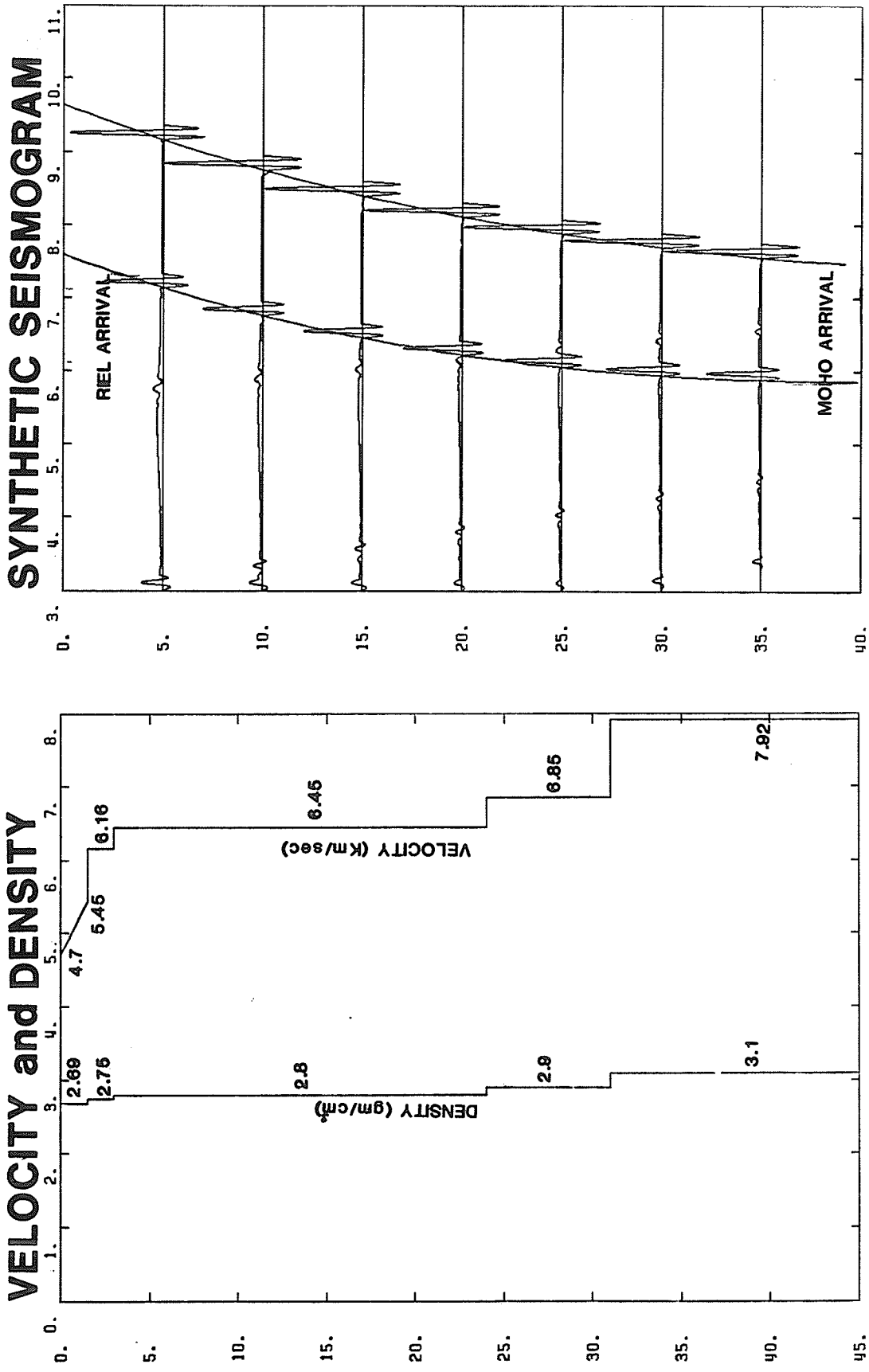

Figure 7.5: WKBJ Earth model.

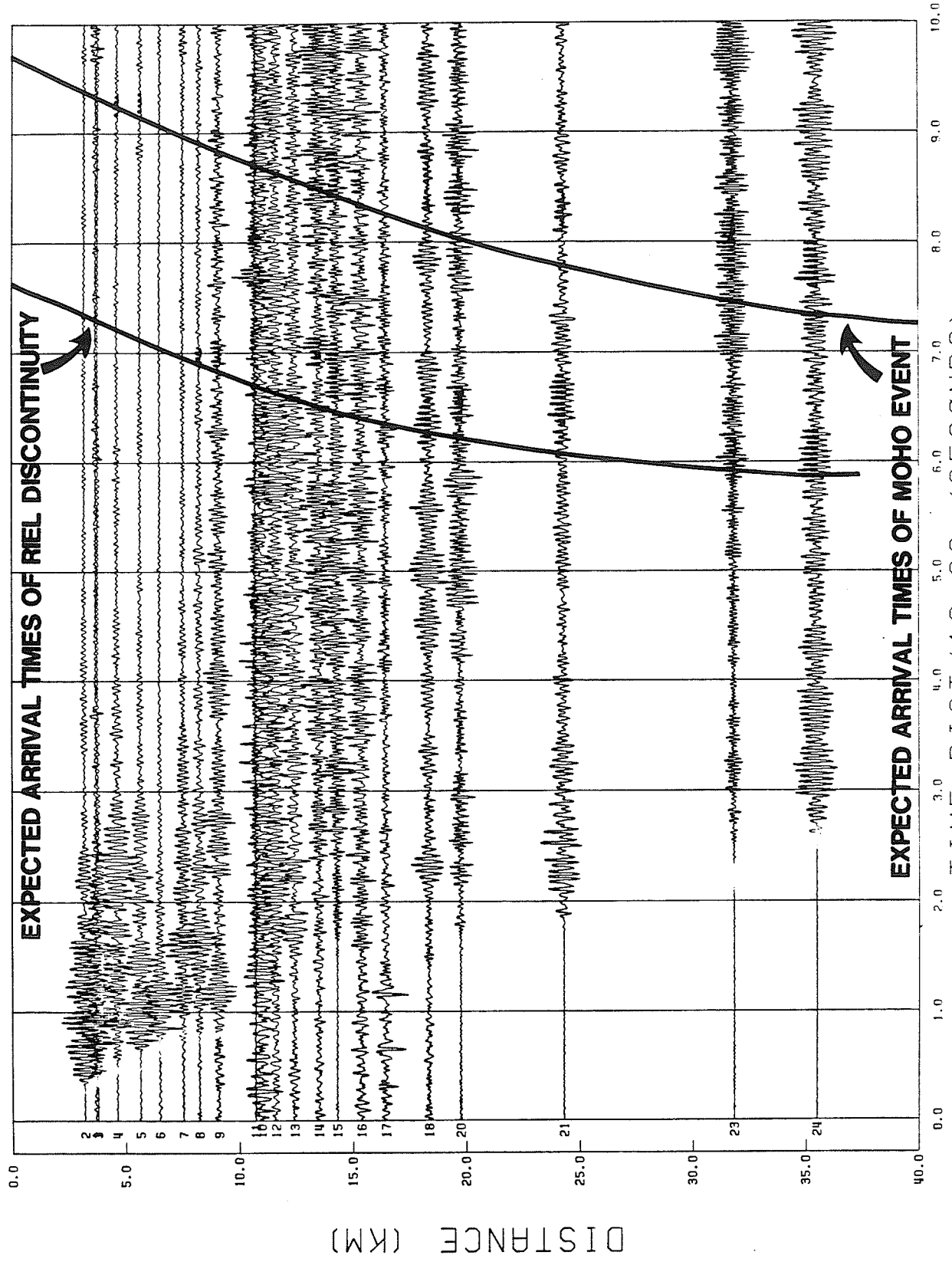

Figure 7.6: Expected arrival times of Riel and Moho events on North profile.

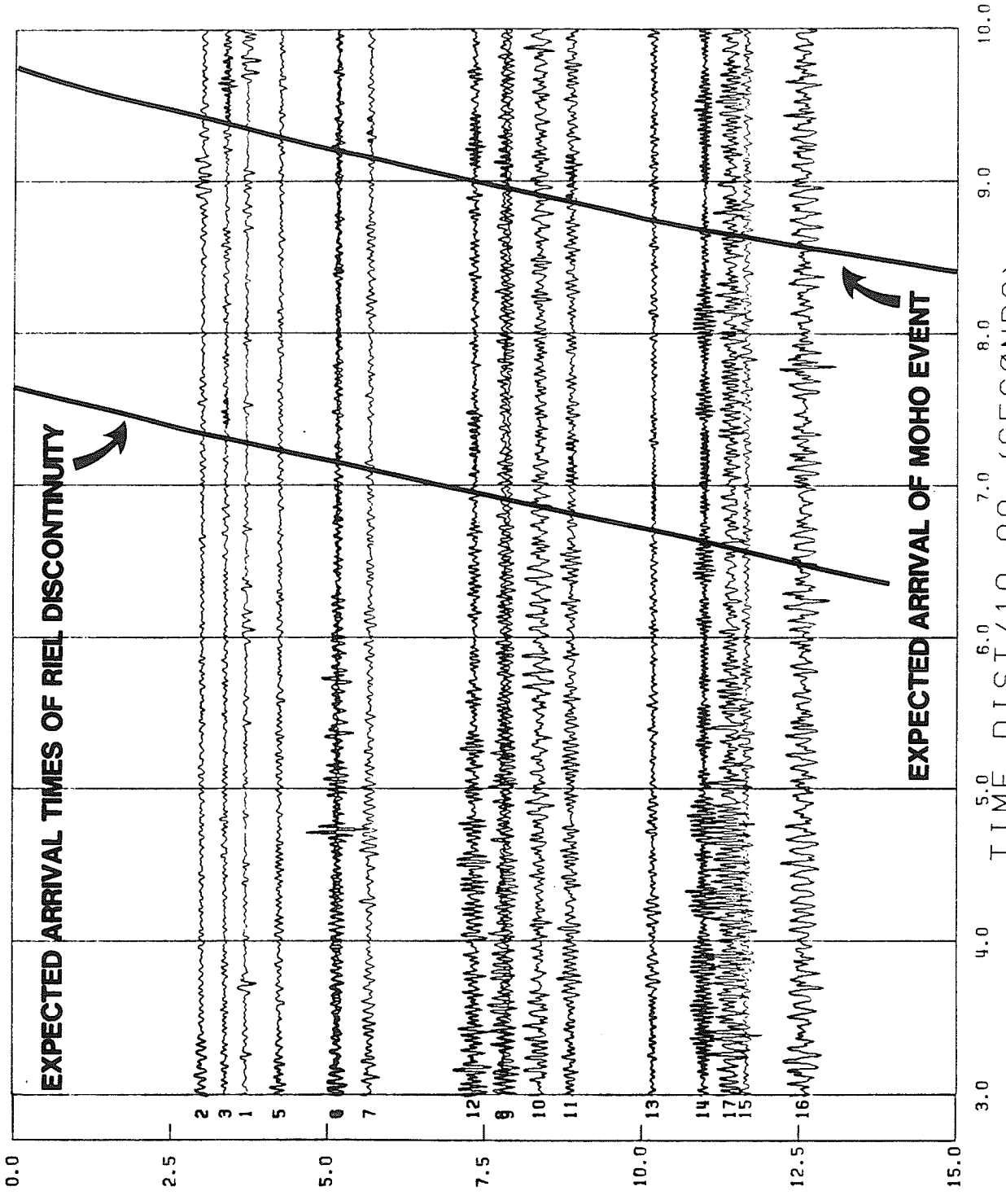

Figure 7.7: Expected arrival times of Riel and Moho events on South Profile.

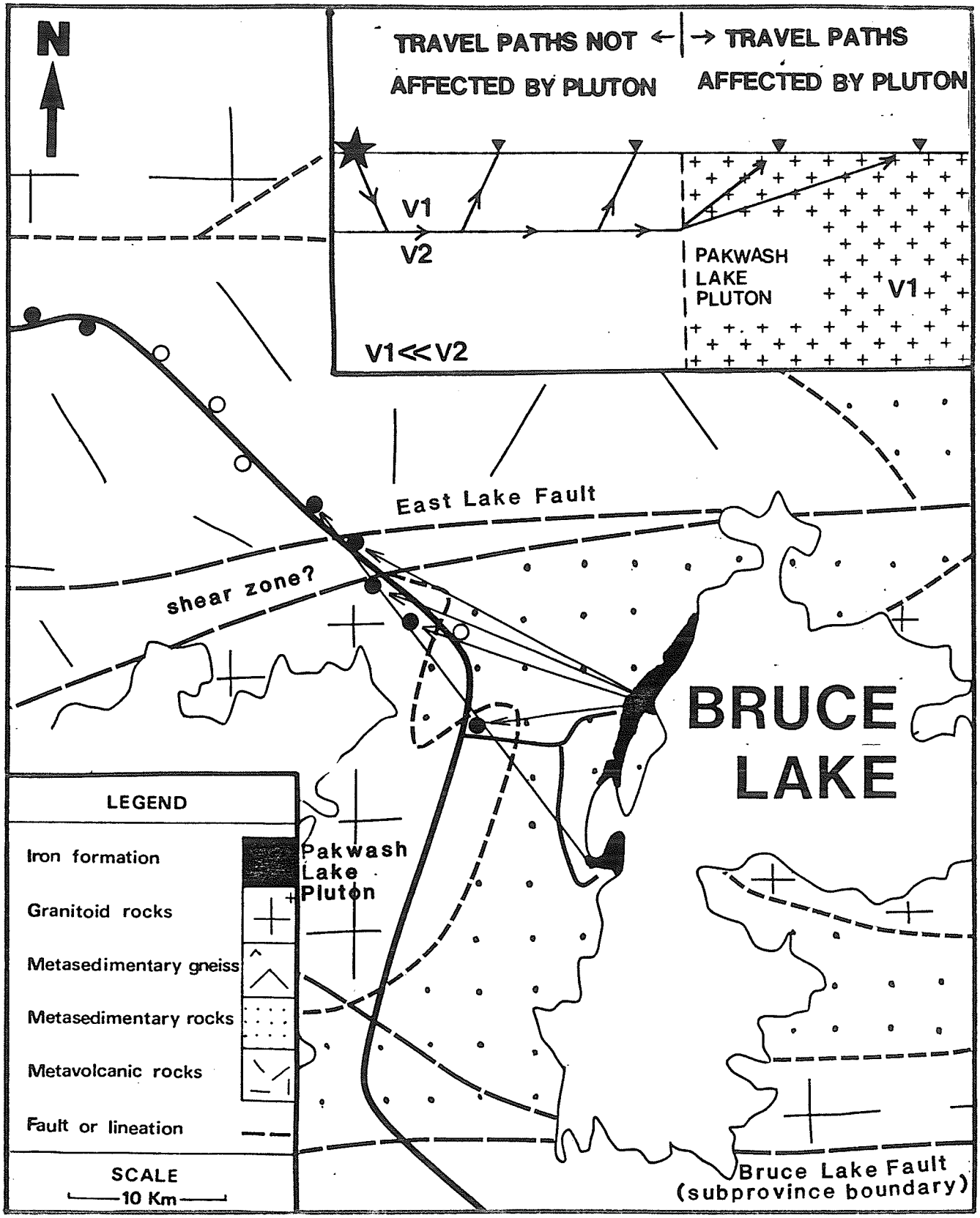

Figure 7.8: Effect of the Pakwash Lake Pluton on the North profile. Arrows indicate the raypaths of near records affected by the pluton. The receiver locations that record raypaths that travel through the pluton are indicated by black dots.

The occurence of this head wave indicates that the low velocity layer is thinner in the sedimentary terrain than in the Pakwash Lake Pluton and that there is an abrupt lithologic change to a much higher velocity material at a depth of about 0.8 Km under the metasedimentary terrain. The Pakwash Lake Pluton must have intruded through this interface as indicated in figure 7.8.

It has now been shown above that delays in first breaks in the profile may be due to the Pakwash Lake Pluton and the fact that the profile is not straight. Although these delays can be explained by the presence of the pluton, a second large delay in the first arrivals occurs between 10 and 11 Km indicating the presence of a low velocity zone between the shot point and the recording sites. Because there was no reverse profile, the exact location of the low velocity zone is not known. Possible locations of this low velocity zone include:

1) the Pakwash Lake Pluton,
2) the area around the East Lake Fault and
3) a subsurface zone.

The first possibility is unlikely as the pluton is composed of quartz diorite which is not a low velocity material. The occurrence of a large shear zone around the East Lake Fault makes the second possibility the most likely. The third possibility is unlikely as no evidence of a subsurface structure has been detected in previous geophysical work in the area. If in fact the area around the East Lake Fault is the low velocity zone affecting the data, its effect must be greater on the records further to the west. This can be ex-

plained by the fact that the East Lake Fault divides into two separate sections just north of the metasedimentary-metavolcanic boundary (figure 7.8). If a shear zone exists between these two sections of the fault, the western records will be affected more by the shear zone because it is wider in the west. Also, since the profile trends in an east-west direction, the raypath through the shear zone would be along its length rather than along its width, causing a significant delay for the records further to the west.

The profile turns in a more westward direction at about 10 Km from the source. The bend in the profile at this point is probably a major cause of this delay. The East Lake Fault shear zone and the bend in the profile at 10 Km from the source only partially explains the large delay as the low velocity shear zone (Vp=3.2 Km/sec) required to fit the model is not physically probable. For this reason there are probably some other factors contributing to this delay. At the present time, it is unknown what might be contributing to this delay as no previous geophysical or geological work has indicated evidence of a large low velocity structure. It should be noted that this delay may also be partially due to the poor timing information causing errors in assembling the records of the profile. Because of the magnitude of the delay, it is unlikely that it was caused entirely by errors in assembling the profiles as the procedure has been checked many times.

The velocity of the weathered layer measured from this study is lower than those measured in other crustal studies in northwestern Ontario and southeastern Manitoba (Hall and Hajnal, 1969,1973, Green

et al, 1978, Green et al, 1979 and Anderson, 1979). Green et al (1978) calculated a near surface p-wave velocity of 6.07 Km/sec from first breaks in a crustal survey carried out on the Aulneau batholith which is located to south of Kenora, Ontario. This indicates that the weathered layer is very thin in this area. Anderson (1979) measured a velocity of 6.19 Km/sec from initial first breaks in the Snake Bay-Kakagi Lake area also to the south of the Kenora region. He estimates that the low velocity weathered layer is approximately 60 metres thick.

The Red Lake-English River subprovince boundary area seems to be much more susceptible to weathering as the low velocity layer in this region is much thicker than in the areas of the surveys to the south (Green et al, 1978, Green et al, 1979 and Anderson, 1979). The initial velocity of 4.7 Km/sec is extremely low but a high velociy velocity gradient of 0.5 Km/sec/Km makes the velocity increase quickly with depth. The reason for the low velocity and thick weathered layer is probably due to the presense of extreme deformation and faulting around the Red Lake-Enlish River subprovince boundary making the area more susceptible to weathering.

7.3.2 The South Profile

As in the North profile, the Pakwash Lake pluton also affects the records of the South profile in a similar manner. Figure 7.9 illustrates the effect of the pluton on the South profile. The first and second records are not affected by the pluton as the first arrivals are direct or turning rays. Records #3, #4 and #5 are affected by

the pluton in the same manner that the records of the North profile were affected. The pluton does not lie in the path of recording sites #6 and #7 consequently the head wave reaches these locations with no delay. Note that records #3, #6 and #7 are slightly ahead of the trend of the remaining records. Since all of these records were recorded from the same shot point (shot #11), this may be due to a small error in the tieing in of this shot with the rest of the shots. The remaining records are not affected by the pluton but are delayed due to a steeply dipping structure at a 6 Km distance. Geologically, this structure corresponds to the southern extension of the Bruce Lake Fault.

The results of the best fit model shows that the velocity conditions on either side of the Bruce Lake Fault are radically different. This indicates that there is a distinct boundary between the Red Lake and English River Subprovinces.

The large delay located at a distance of 6 Km from the source may be due to a cataclastic zone associated with the Bruce Lake Fault. Since the Bruce Lake fault is part of the Sydney Lake fault system which is a cataclastic zone consisting of low density material then the Bruce Lake fault and surrounding area will likely also consist of low density and low velocity material.

The model also shows that the low velocity zone is much thicker in the gneissic terrain south of the fault than in the metasedimentary terrain north of the fault. As indicated in the North profile, the metasedimentary terrain sits on top of a high velocity zone at a

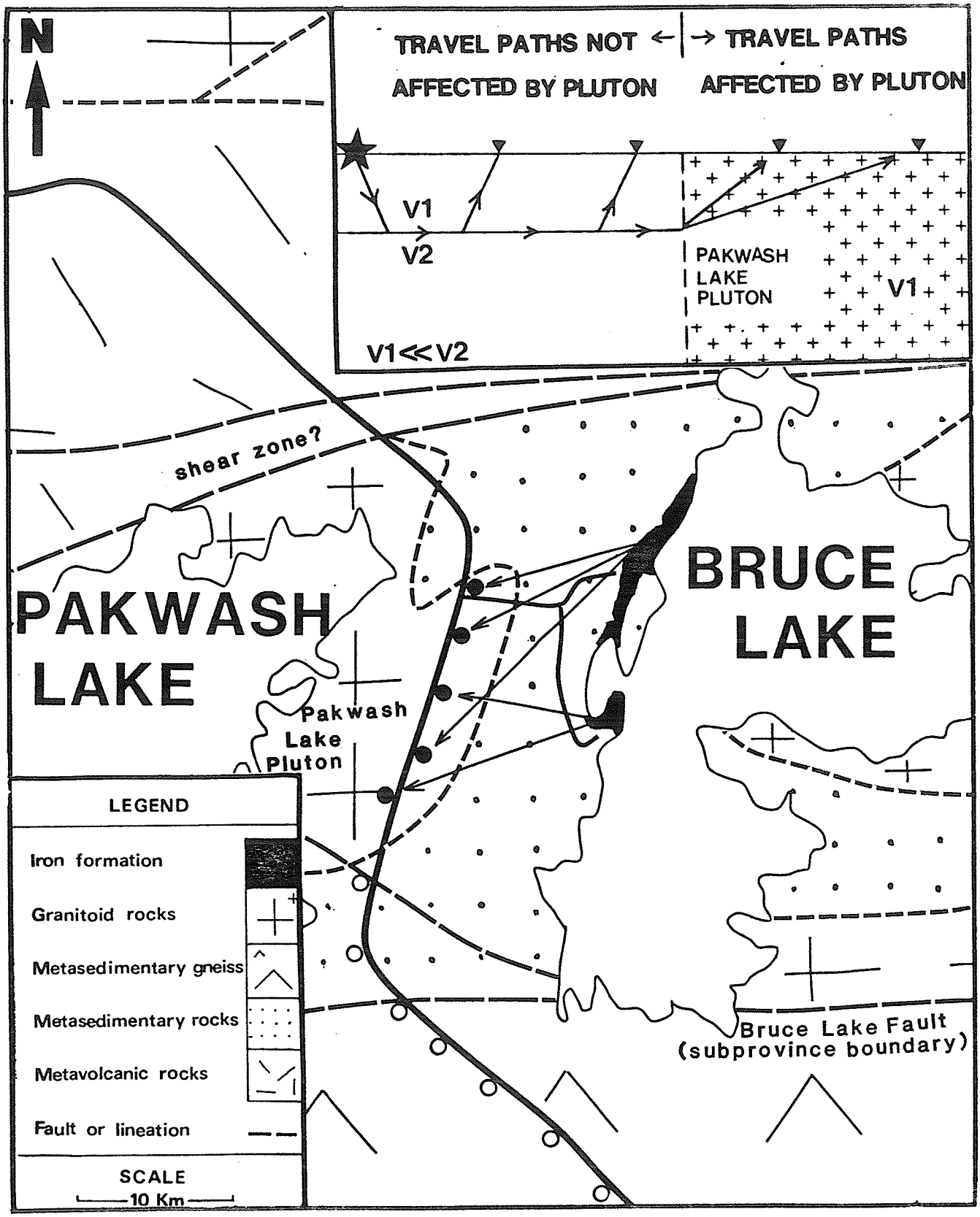

Figure 7.9: Effect of the Pakwash Lake Pluton on the South profile. Arrows indicate the raypaths of near records affected by the pluton. The receiver locations that record raypaths that travel through the pluton are indicated by black dots.

0.8 Km depth. The shape of the models between the Bruce Lake Fault and the East Lake Fault show evidence of a metasedimentary basin between these points.

7.3.3 Other Ray Tracing Model Considerations

Although the model 'looks' as if the upthrown side of the fault is on the north side, this is in disagreement with the actual geology which indicates that the upthrown side is south of the fault. Since the best fit model is a very simple model, it should not be assumed that the shape of the model is the exact shape of the actual geologic structure. The seismic survey only maps large velocity contrasts and cannot detect much of the smaller structural detail of the area. The best fit model therefore indicates only that there is a large difference in velocity conditions on either side of the fault and that the upper low velocity zone is much thicker on the south side of the fault perhaps indicating that the gneissic rock is more susceptable to extreme weathering on the surface. This is in agreement with the magnitude of displacements expected from the faults as vertical displacements on the order of 4.0 Km (Thurston and Breaks, 1978) should yield drastic contrasts over the fault.

Also to be taken into account in any interpretation of these models is the fact that the profiles are not straight. This fact indicates that the ray paths to each recorder may or may not travel through the same geology. Therefore variations in the depth profile as well as any lateral variations could cause delays in travel times to the recorders. Also, since no reverse profiles were shot it is

impossible to indicate where some of the structures are located along the profile. All that can be assumed from the models is that the structures affecting the records are somewhere between the source and the recorder of interest. The degree of dips of the various interfaces are also affected by both the fact that there is no reverse profile and that the profile is not straight. Velocities will also be affected by apparent dips as well as the fact that the profiles are not straight.

Another factor to be taken into consideration is the location of the source. The source is located in a very complexly folded iron formation intruded by many dikes (Shklanka, 1970). The location of the different shot patterns of the different shots within this complex geology may complicate the ray paths to the various recorders.

Another important consideration is that ray tracing does not yield a unique model. Another modelling approach using different velocity and structural conditions may also yield a model which also match the first breaks. For these reasons, the ray tracing models should be accepted only as a general indication of the shallow structure of the survey area.

7.4 DISCUSSION OF WKBJ RESULTS

The WKBJ reflection times show marginal results when compared to the data from the South profile while data from the North profile indicates some minor evidence of Riel and Moho reflections.

7.4.1 The North Profile

Figure 7.6 illustrates the expected arrival times of the Riel and Moho p-wave reflections. The first few pulses of the signals where there is evidence of these arrivals are shaded. As expected, most of the evidence for these arrivals occur on the far offset recorders although some of the near records indicate some evidence of these arrivals. The complex source signal as well as poor S/N made it impossible to detect these deep reflections on many of the records.

7.4.2 The South Profile

As indicated in figure 7.7, there is little evidence of either Riel or Moho p-wave reflections in the South profile. At first glance this is surprising as the data quality of the South profile is generally better than the north. A possible explanation for this is that the Bruce Lake Fault is affecting the deep reflections in some manner. The size of the fault and the effect that it had on the ray tracing model indicate that this is quite possible. The other probable cause of the poorer results in the South profile is that the maximum offset is only 12.5 Km. Most of the best evidence of deep reflections in the North profile occurred on records with farther offsets than 12.5 Km. Although the evidence of deeper reflections in the South profile is generally poor, there is some minor evidence for these reflections as indicated in figure 7.7. Some of the apparent arrivals do not correspond exactly to the model but this may be due to the fault or small errors in assembling the profile.

7.4.3 Other WKBJ Model Considerations

The evidence of deep refections should not be thought of as direct evidence for arrivals as there are many other complications to consider. Although it is encouraging that these arrivals occur at about the expected arrival times as derived from the models, there are other possible origins for these events. Because the source signal and the geology are both very complicated, these events may correspond to interference patterns associated with other events such as s-wave arrivals or other arrivals associated with near surface interference.

The fact that the far offset traces show the best evidence for these reflections is not surprising. Because the far offset records will have a higher angle of incidence on the reflection surface, the reflection amplitude from these reflectors will be larger for longer offsets.

Another factor to consider is that the Riel and Moho discontinuities are not flat in the survey area (figure 3.3). Since the WKBJ model is required to be flat, the earth model of Hall and Hajnal (1969,1971) was averaged over the survey area. This again will be a source of discrepancies between the model and the actual data.

Finally, it should be noted that the marginal results resulting from this interpretation is not a result of the WKBj technique or the earth models used but a direct result of the marginal quality of the data.

Chapter VIII

CONCLUSIONS

Because of the nature of this project, this study has covered a wide variety of topics. For this reason the conclusions will be discussed in five sections. The first section will consider the results of the source modelling while the second part will make comments on the quality of the survey. Processing techniques will then be discussed followed by comments on the interpretation of the data. This will be followed by some general concluding remarks.

8.1 SOURCE MODELLING

Although only preliminary results were obtained, this may have been the most important part of the study. The source modelling was important in all aspects of the study. The profiles would not have been assembled properly if the source signal was not studied. Distinguishing between the low amplitude p-wave arrival and the high amplitude s-wave arrival was essential in assembling the profiles. The study was also useful in understanding the results of the processing. It was found that in future studies of this kind a better understanding of the source signal is necessary in order to process the data properly. Also, the interpretation of the data would be very difficult without some understanding of the source signal.

The results of the source modelling have shown that the signal recorded at the shot recorder is much more complex than a single direct p-wave arrival since the recorded source signals were usually longer in duration than the modelled signal. Since some modelled signals fit the recorded source signals better than others, the local geology between the source shot patterns and the source recorder plays a large part in the type of arrivals that are recorded.

Despite this study, much more work of this type is necessary in order to pursue other surveys of this kind. The source study carried out in this project was very general in nature. Future studies of this type would have to be done in much greater detail and requires the use of more accurate computer algorithms.

8.2 DATA QUALITY

The data quality in this experiment was generally disappointing. In order to properly interpret this type of data, timing information must be accurate. The equipment and procedures used in this survey were not adequate to properly study this area. The major faults with the portable analogue units were a poor timing system and an unreliable tape drive system. The procedures used in this study were inadequate mostly because this type of survey is not often carried out and it was hard to anticipate the types of problems that would occur. Also, since this was a regional reconnaissance survey, the need for accuracy was not initially realized.

8.3 PROCESSING

The processing procedures followed in this survey are only a few of many possibilities for reducing the data to an interpretable form. Although the procedures used in this study were not successful, much information was gained on how to process future studies of this kind.

Two methods were attempted for the processing of the data. The first technique used was a vertical stack of the data in order to try to recover deep near vertical reflections such as the Riel and Moho discontinuities. The results showed that the timing of the data was inadequate. The second technique tried was cross-correlation in order to try to simplify the complex signal. In order for cross-correlation to be successful, the source signal must be random so that there is only one high correlation corresponding to the onset of each arrival. It was found that the source signal was not random consequently cross-correlation did not simplify the signal.

In order for this type of survey to be successful in the future it is important that careful planning of the shot patterns and a better method of measuring the shot time be derived. The simplest method to use in future surveys may be to set off one single blast 10 seconds before the main blast. It is important to plan the blast to suit the mine's production needs as well as the needs of the seismic survey.

8.4 INTERPRETATION

Since the quality of the data was marginal, the interpretation was quite general. Many of the initial aims of the project could not be attained due to the data quality. Two methods were used in the interpretation of the data. The first method used was ray tracing using first breaks to delineate the shallow crustal structure. Although smaller features were not visible on the seismic data, some of the larger structures were apparent in the ray tracing models. Large features attributed to the Bruce Lake Fault and the East Lake Fracture zone were very apparent in the ray tracing results. The method also showed the presense of a very low velocity weathering layer with a high velocity gradient near the surface. It was found that this layer was much thicker over the gneissic and metavolcanic terrains than over the metasedimentary terrain at the source. This weathered layer was found to be much lower and much thicker than those measured in other surveys in northwestern Ontario (Green et al, 1978, Green et al, 1979 and Anderson, 1979). This discrepancy may be due to the area around the Red Lake-English River subprovince boundary being much more susceptible to weathering due to the extreme deformation and faulting. Other velocity layers were also defined using the ray tracing method. It should be noted that since the profiles were not straight and since there was no reverse profile, the velocities may not be exact. Also, because of the lack of reverse profiles the structure at the ends of the profiles (North and South profiles) are not seen on the models. Therefore structures such as the Red Lake greenstone belt would not be visible in the models. The WKBJ synthetic seismogram method was also used to

try and locate deep near vertical reflections from the Riel and Moho discontinuities. The model of Hall and Hajnal (1969,1973) was used because of its close proximity to the survey area. The data showed only minor evidence of Moho and Riel arrivals when compared to the synthetic models thus illustrating the marginal quality of the data.

8.5 FINAL CONCLUSIONS

Despite the lack of quality in the data it was encouraging that some results could be attained from the data. Much was learned about what is necessary for future studies of this kind. Some final recommendations for future seismic studies of this kind include:

1) pre-plan the shot patterns to suit both the mine's production needs as well as the survey needs,
2) carry out an extensive source study in order differentiate between the different types of arrivals that are being recorded at the source recorder,
3) carry out a detailed geologic study of the source area in order to assist the source study,
4) develope a better method of measuring the shot times and
5) try deconvolution to see if it is more effective than the methods used in this study (vertical stack and cross-correlation).

With careful planning and following the above recommendations, it will be possible to use mine blasts as an inexpensive seismic source for future seismic surveys.

Appendix A

RECORDER AND SHOT PATTERN INFORMATION

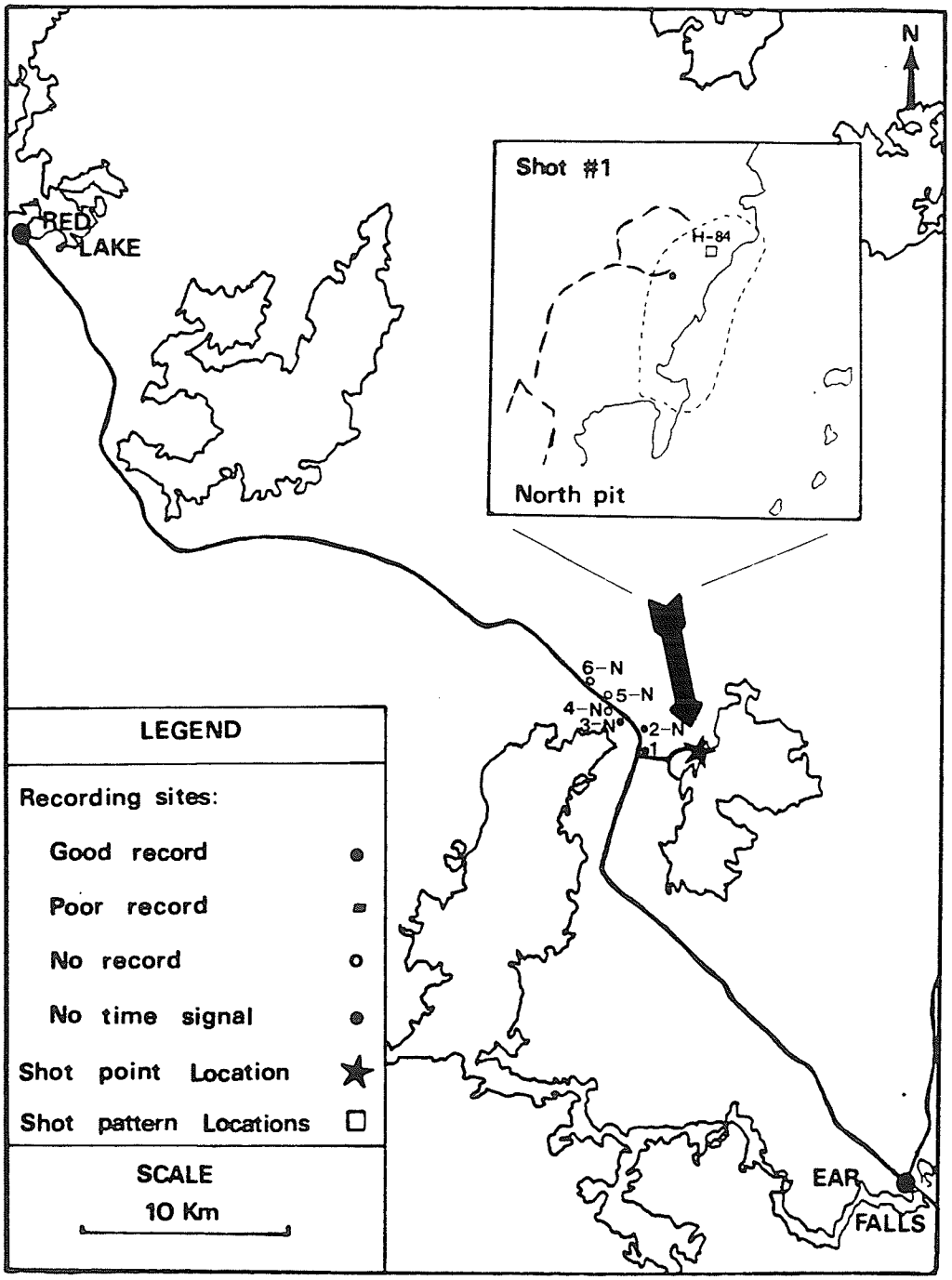

Figure A.1: Recorder and shot pattern locations of shot #1.

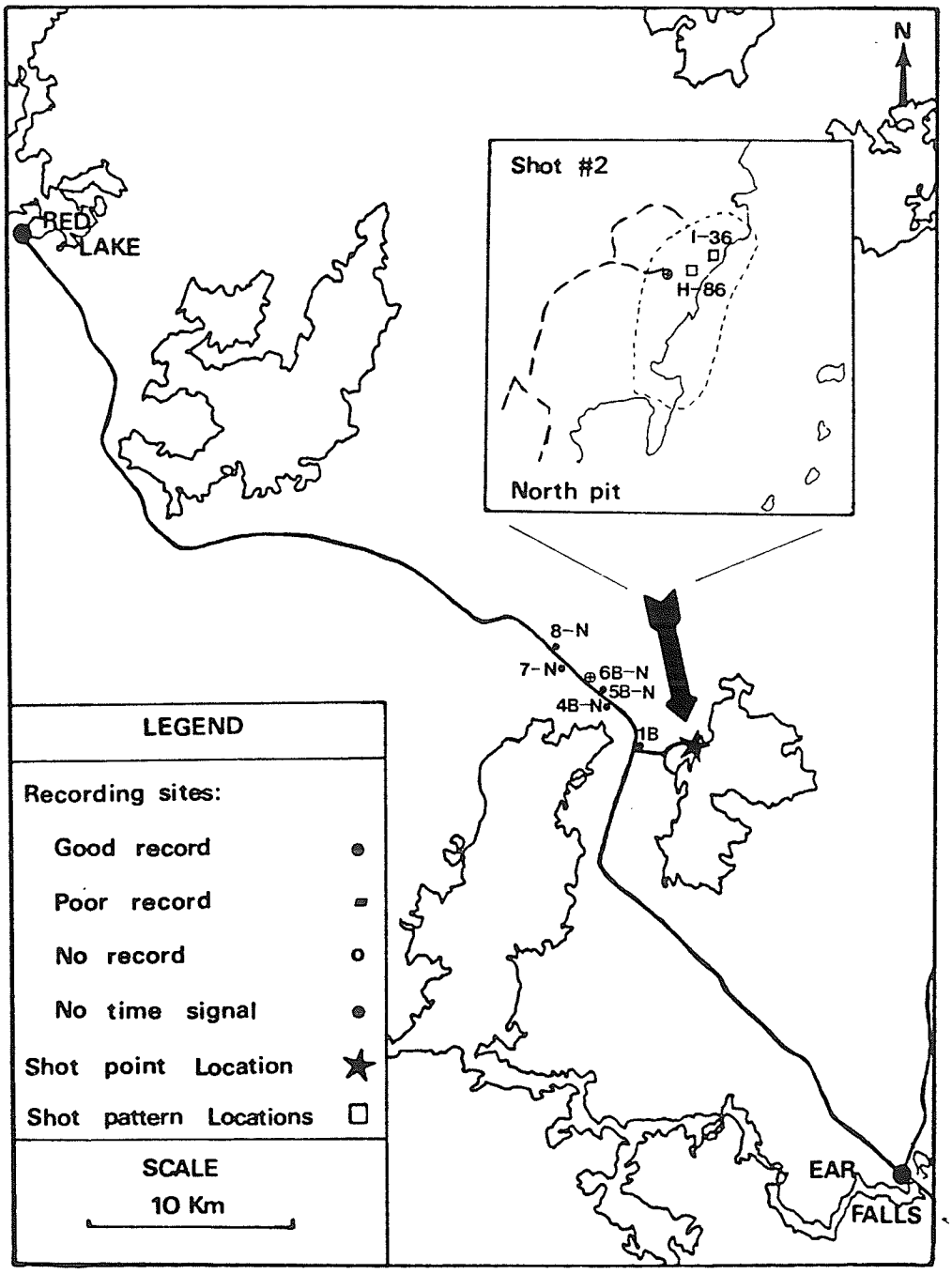

Figure A.2: Recorder and shot pattern locations of shot #2.

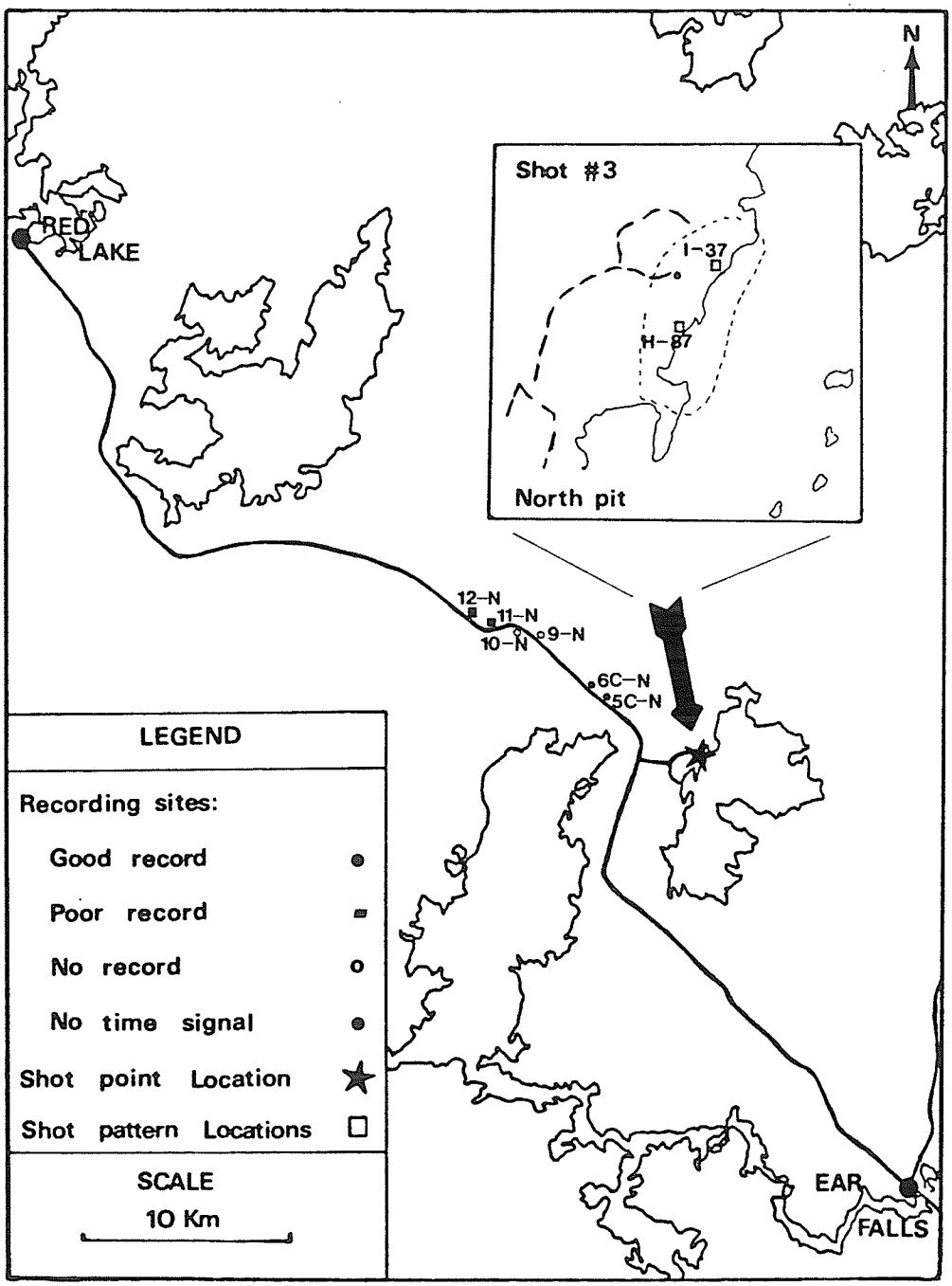

Figure A.3: Recorder and shot pattern locations of shot #3.

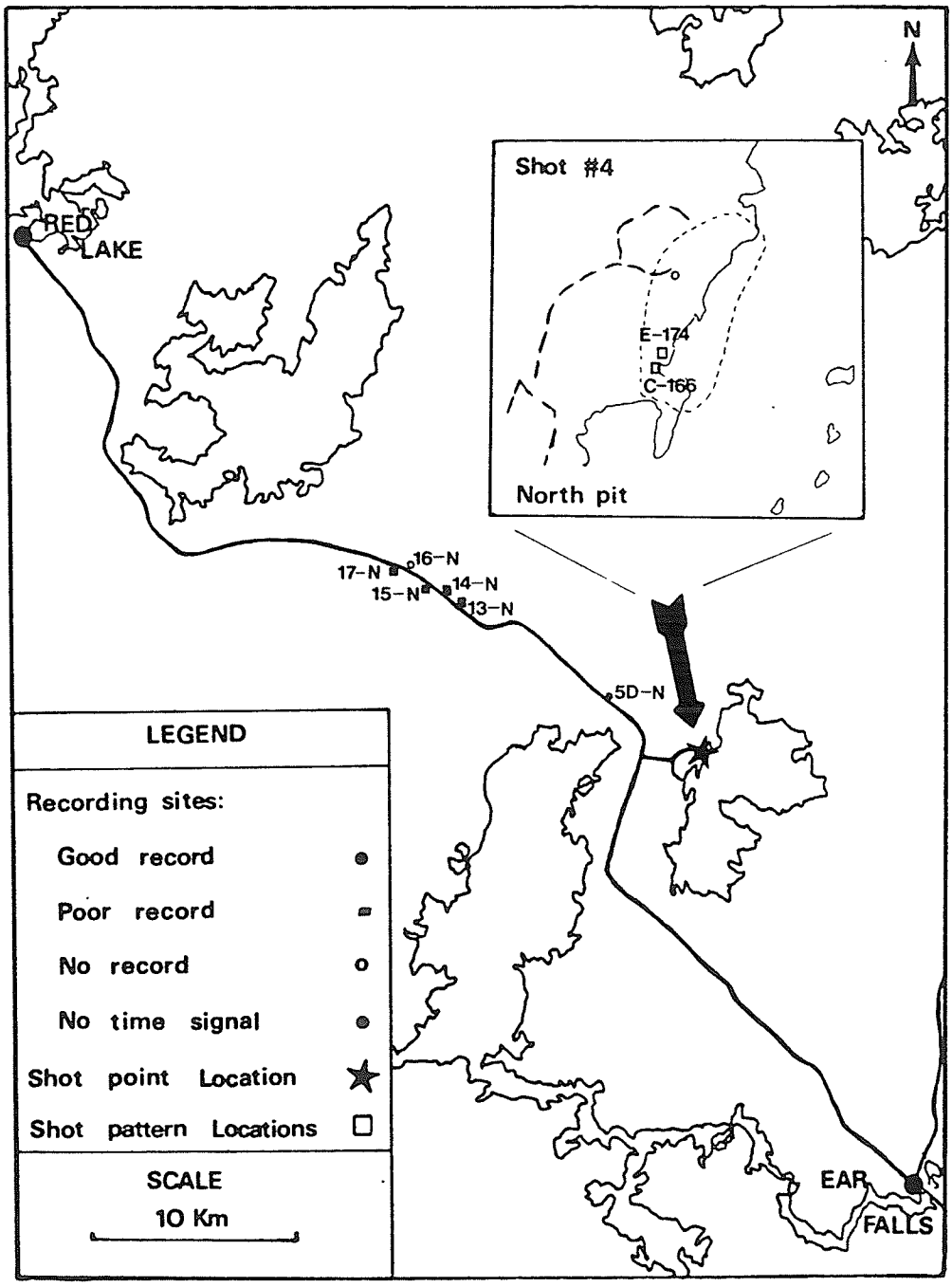

Figure A.4: Recorder and shot pattern locations of shot #4.

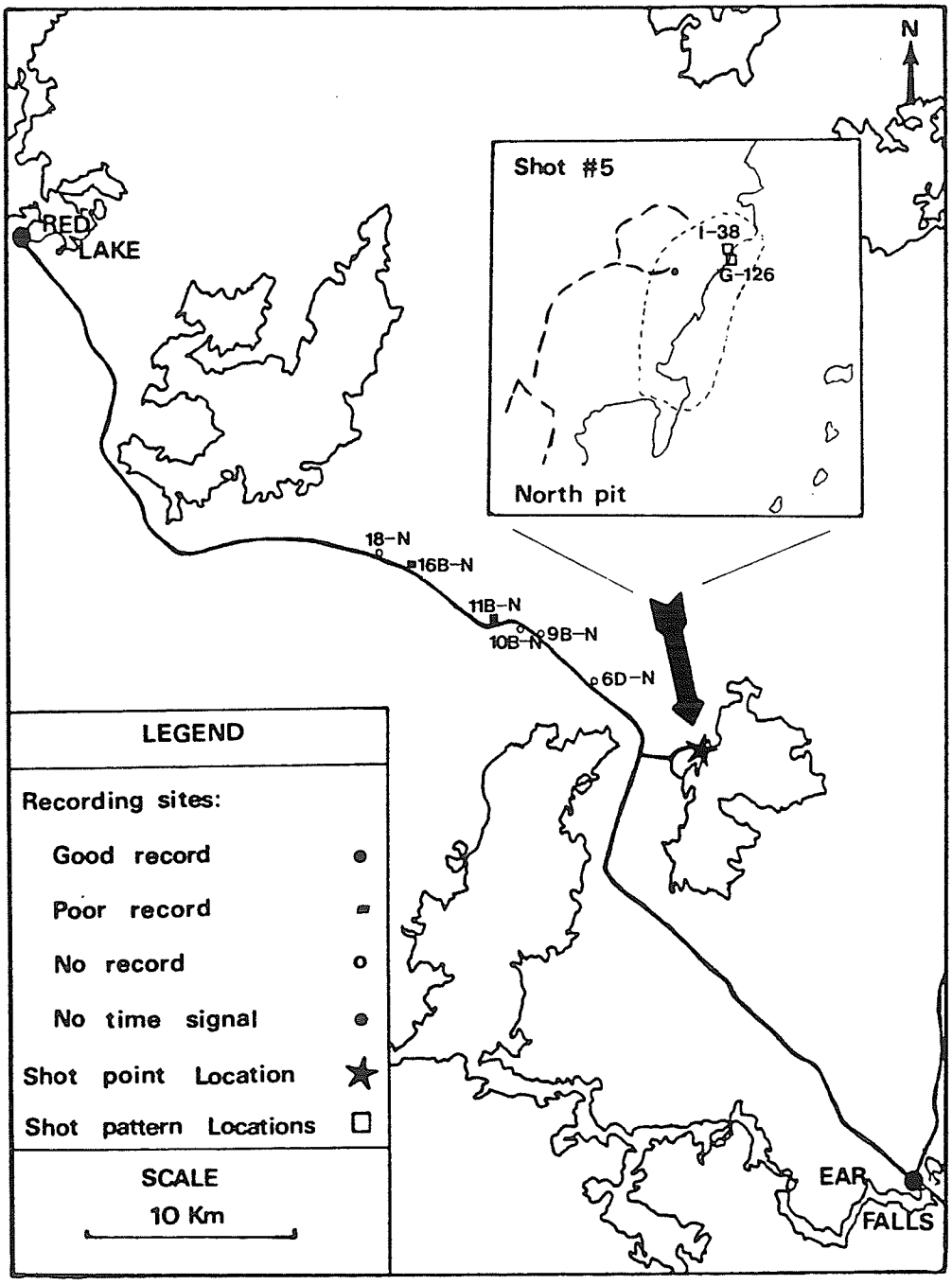

Figure A.5: Recorder and shot pattern locations of shot #5.

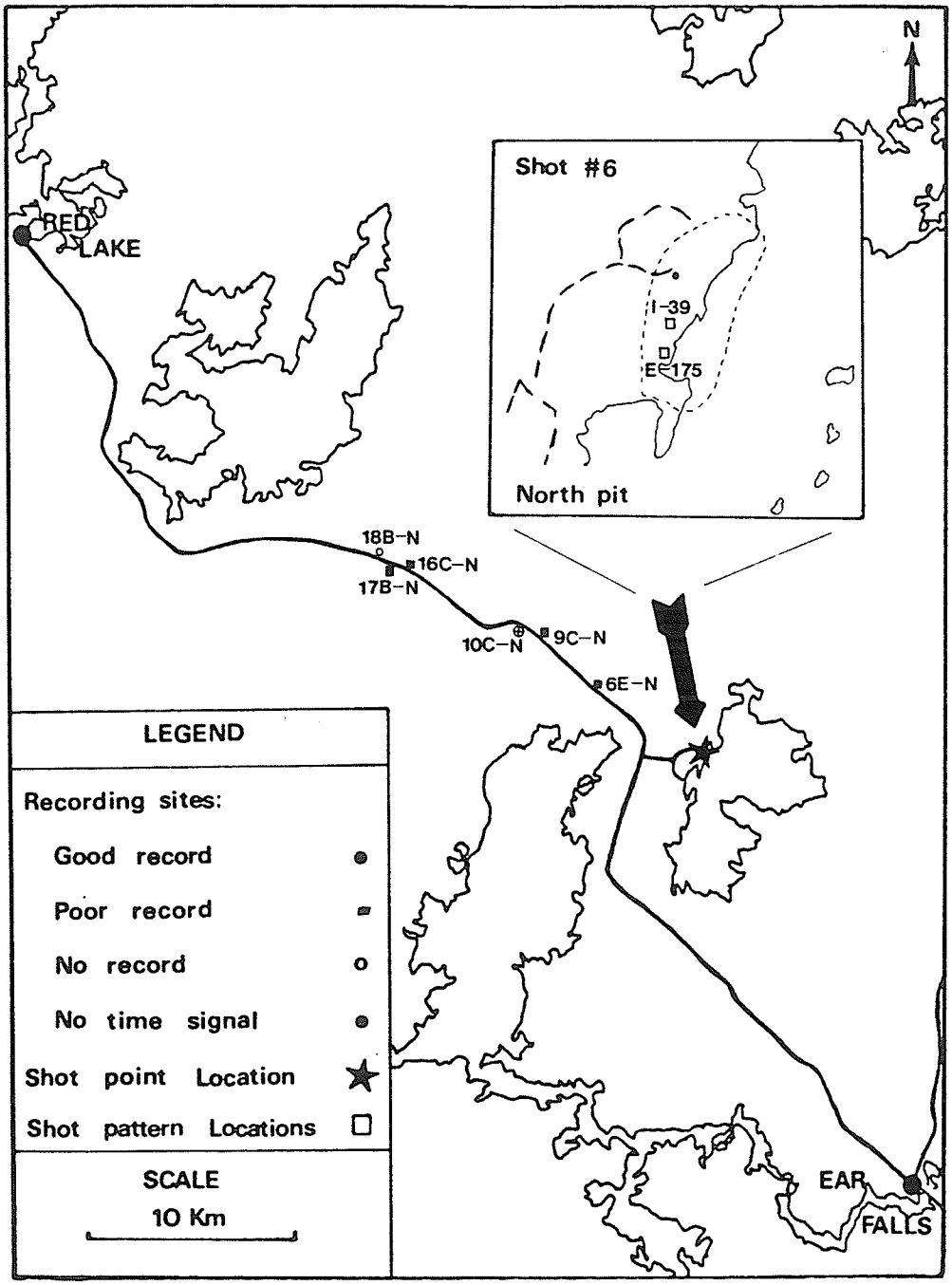

Figure A.6: Recorder and shot pattern locations of shot #6.

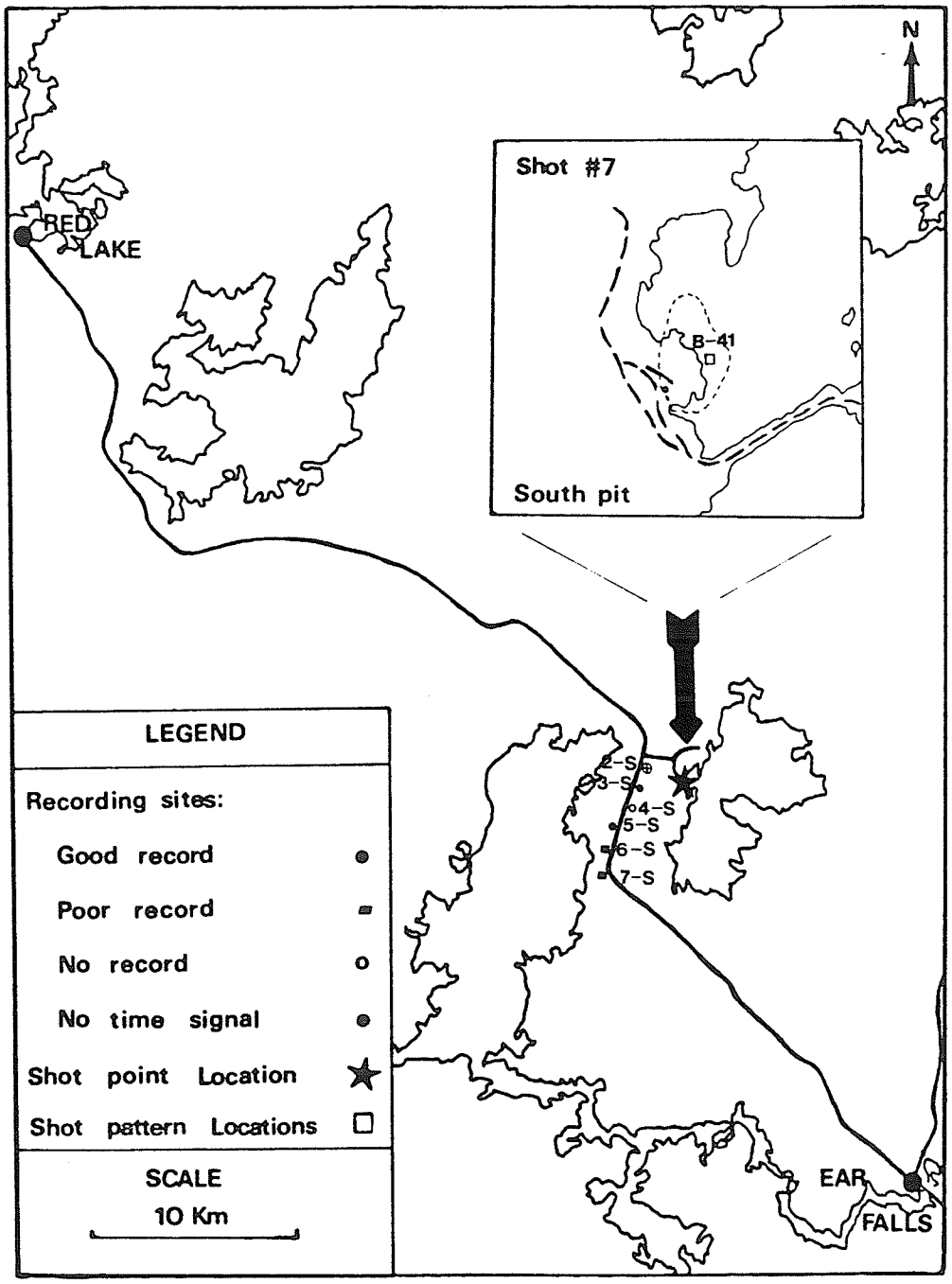

Figure A.7: Recorder and shot pattern locations of shot #7.

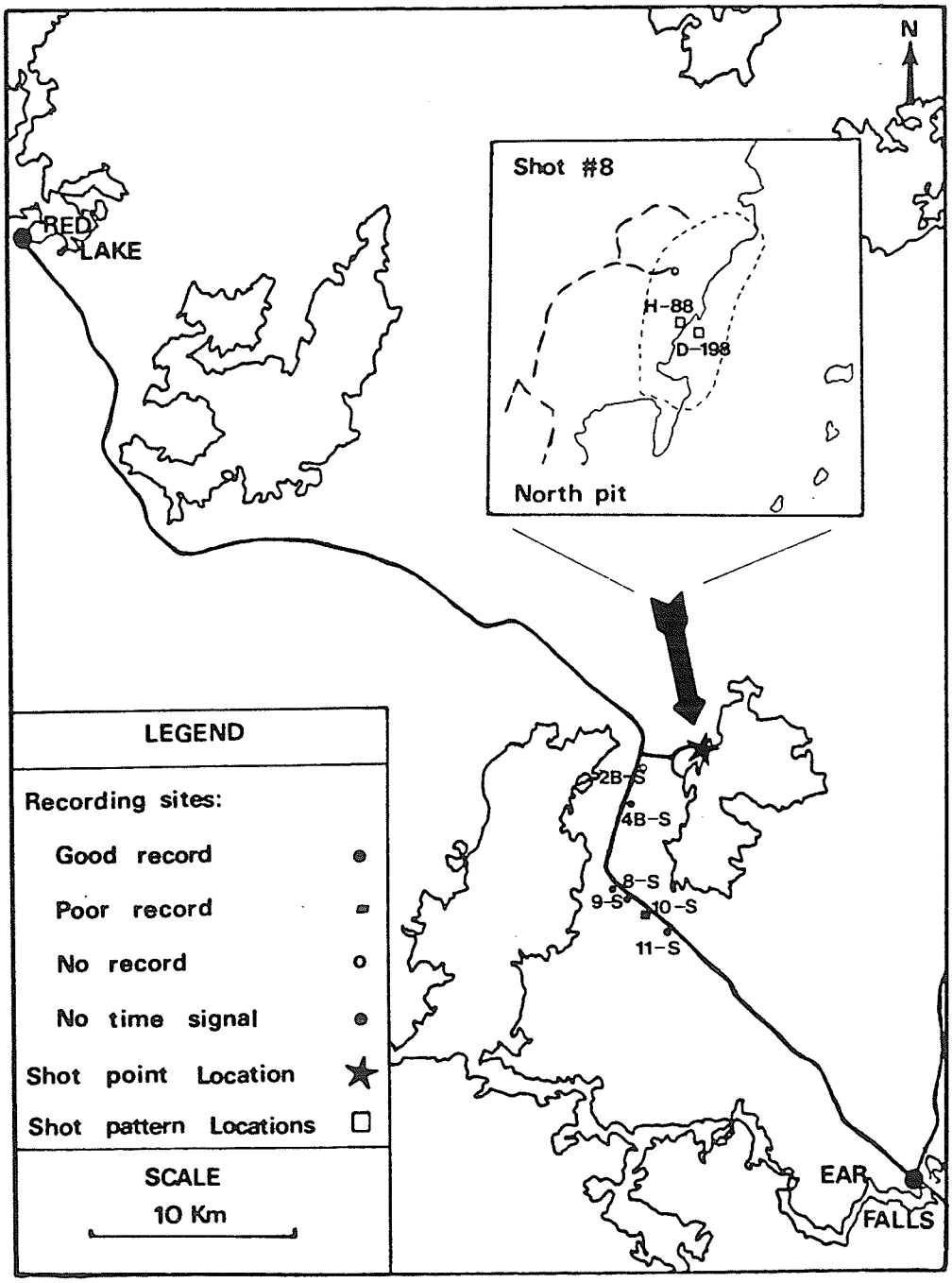

Figure A.8: Recorder and shot pattern locations of shot #8.

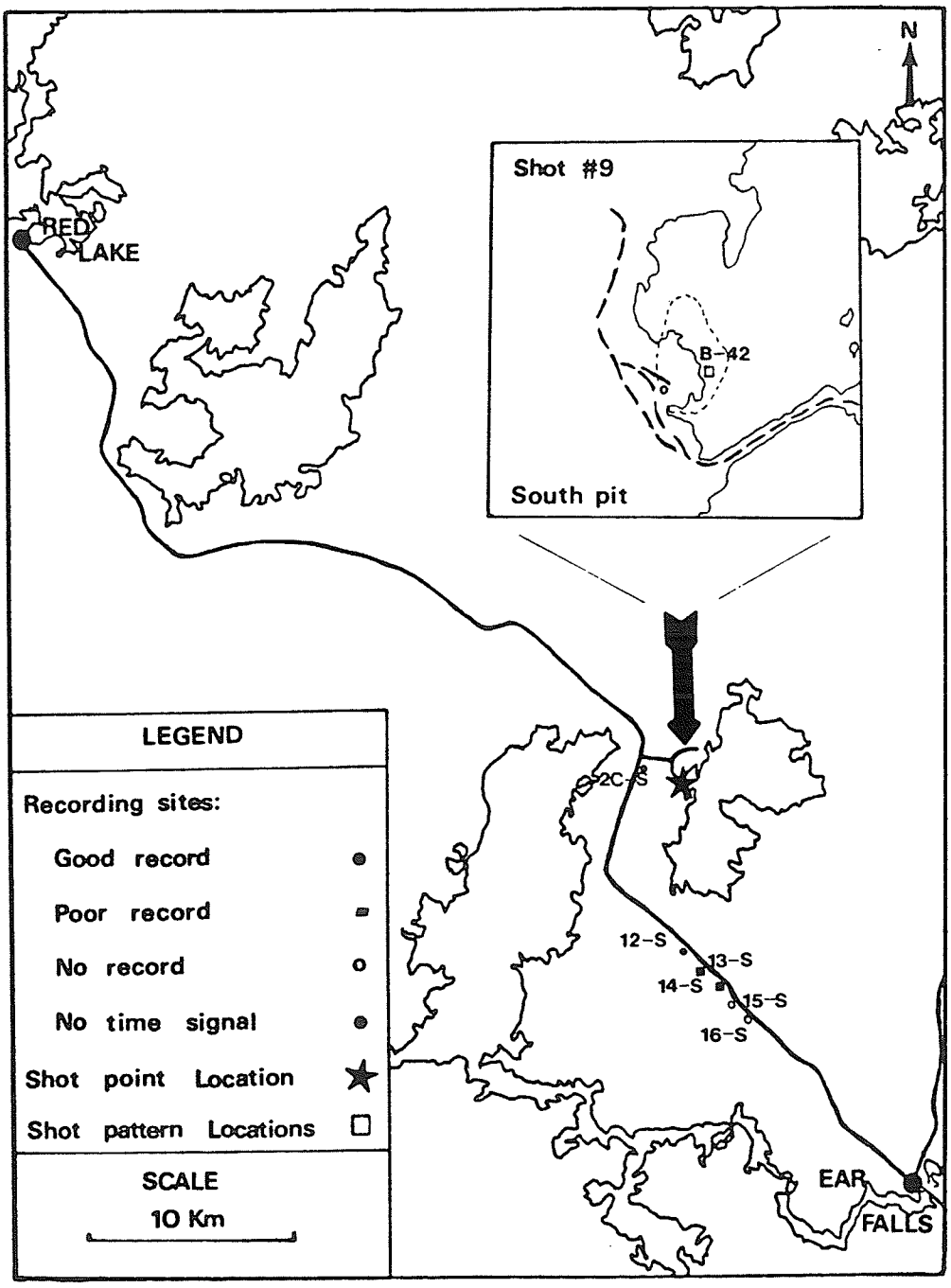

Figure A.9: Recorder and shot pattern locations of shot #9.

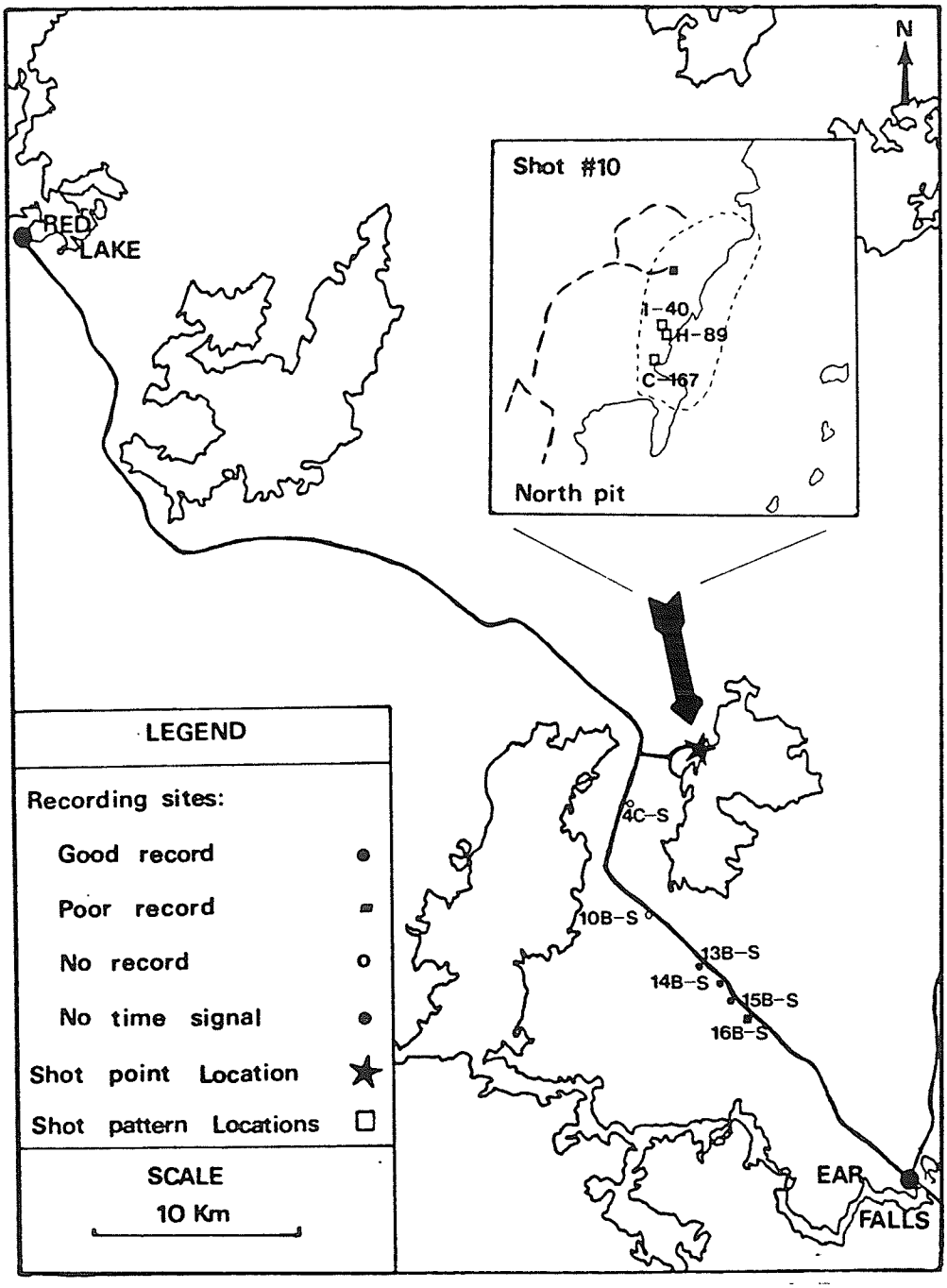

Figure A.10: Recorder and shot pattern locations of shot #10.

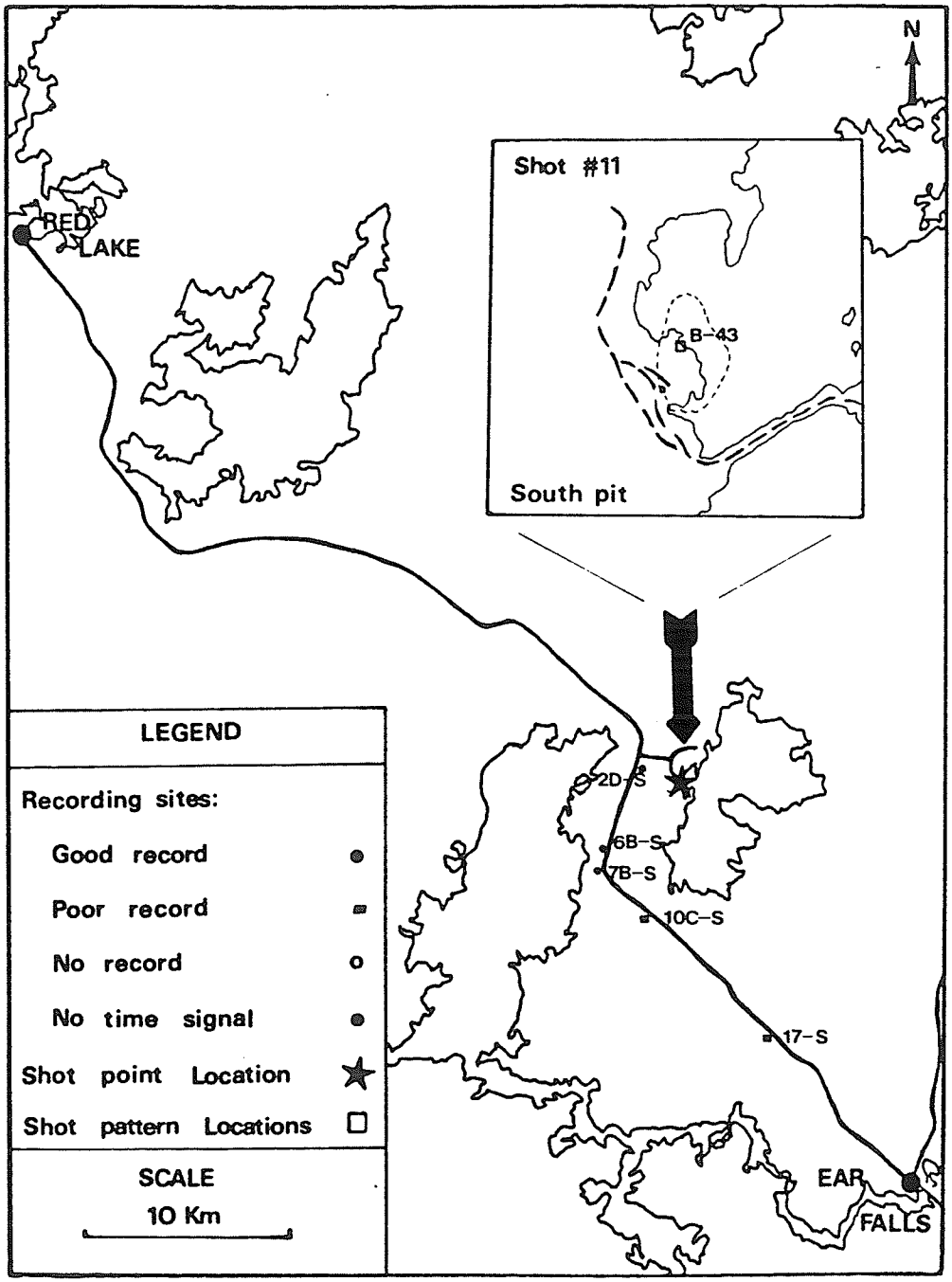

Figure A.11: Recorder and shot pattern locations of shot #11.

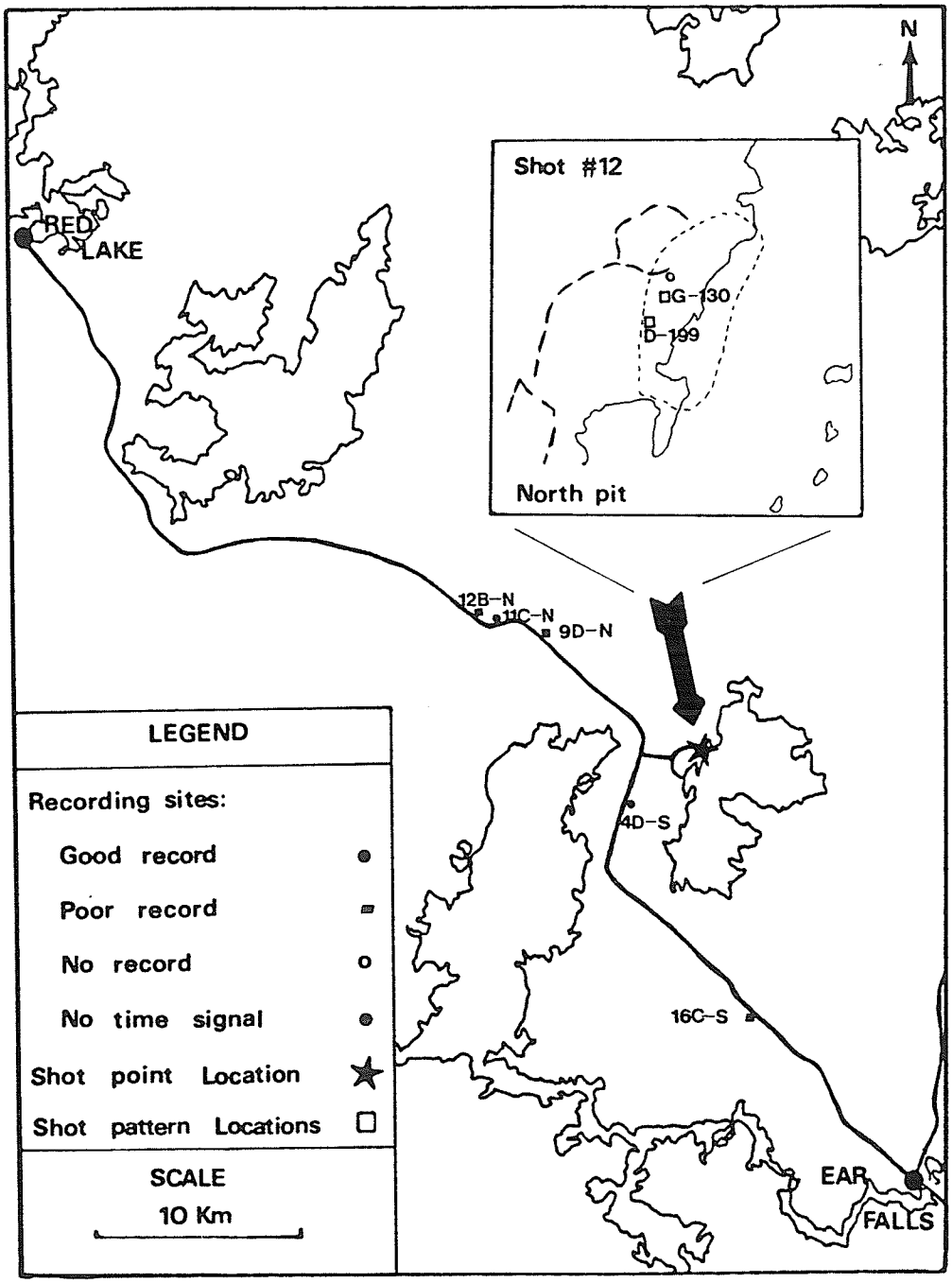

Figure A.12: Recorder and shot pattern locations of shot #12.

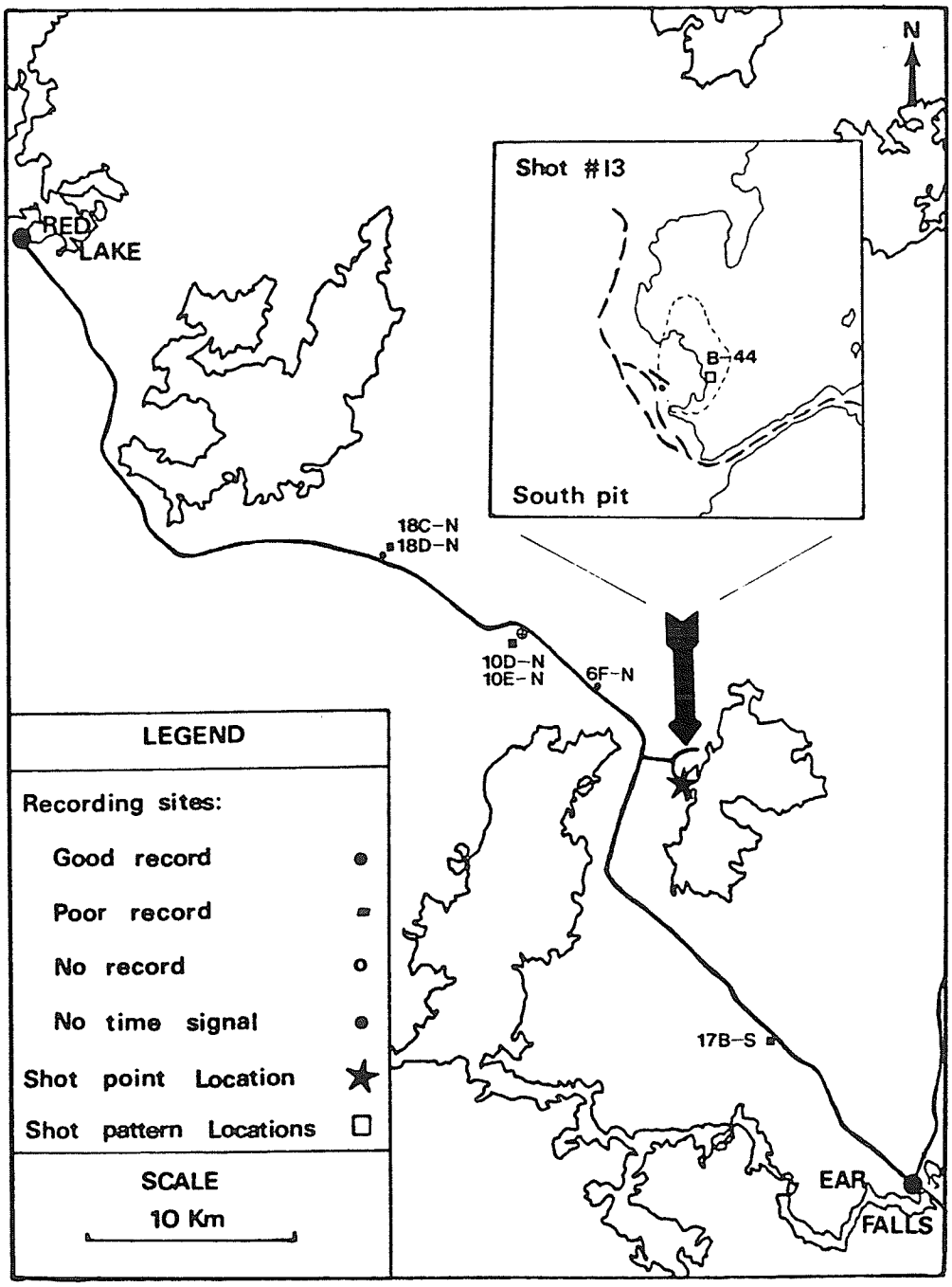

Figure A.13: Recorder and shot pattern locations of shot #13.

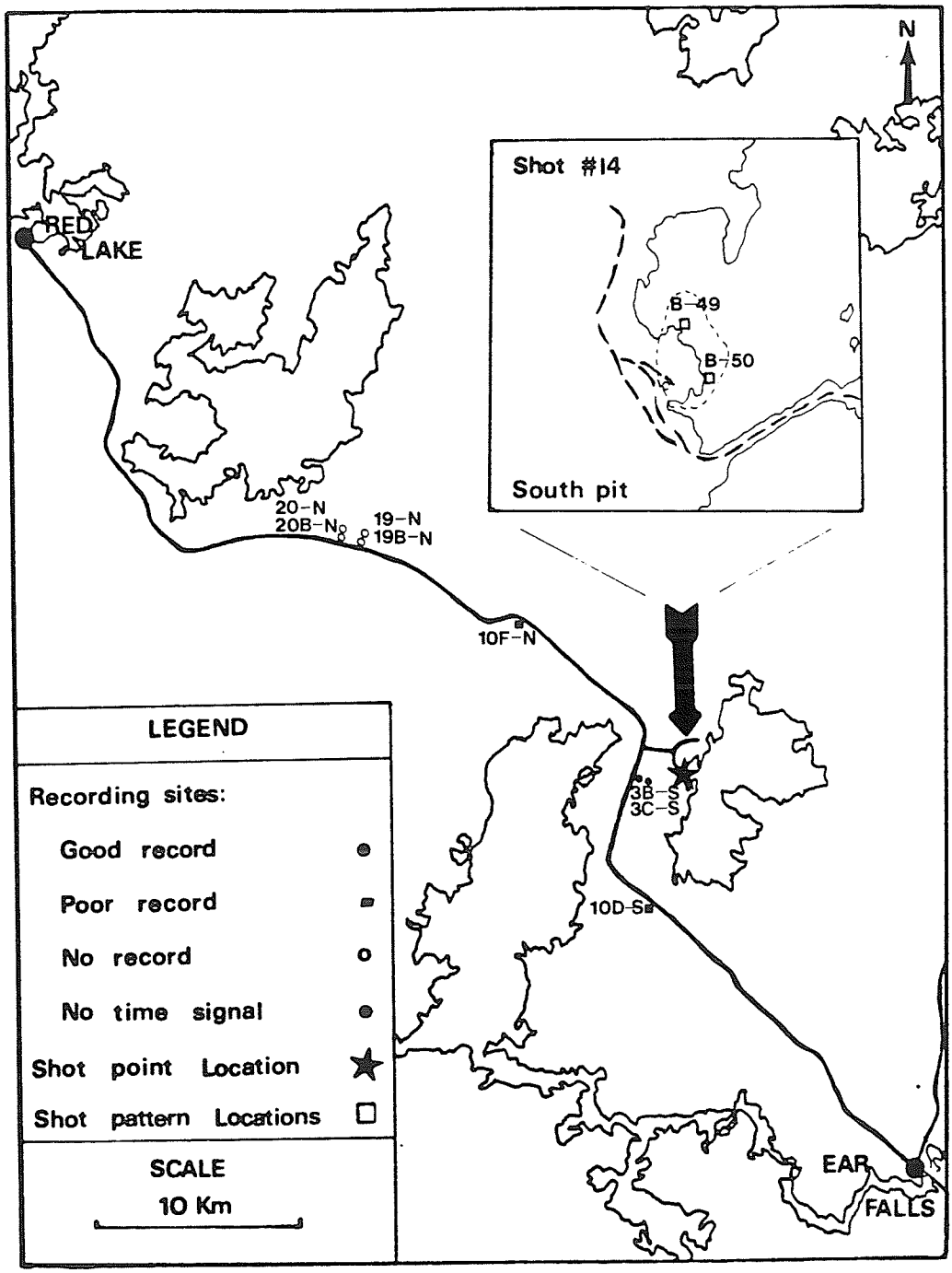

Figure A.14: Recorder and shot pattern locations of shot #14.

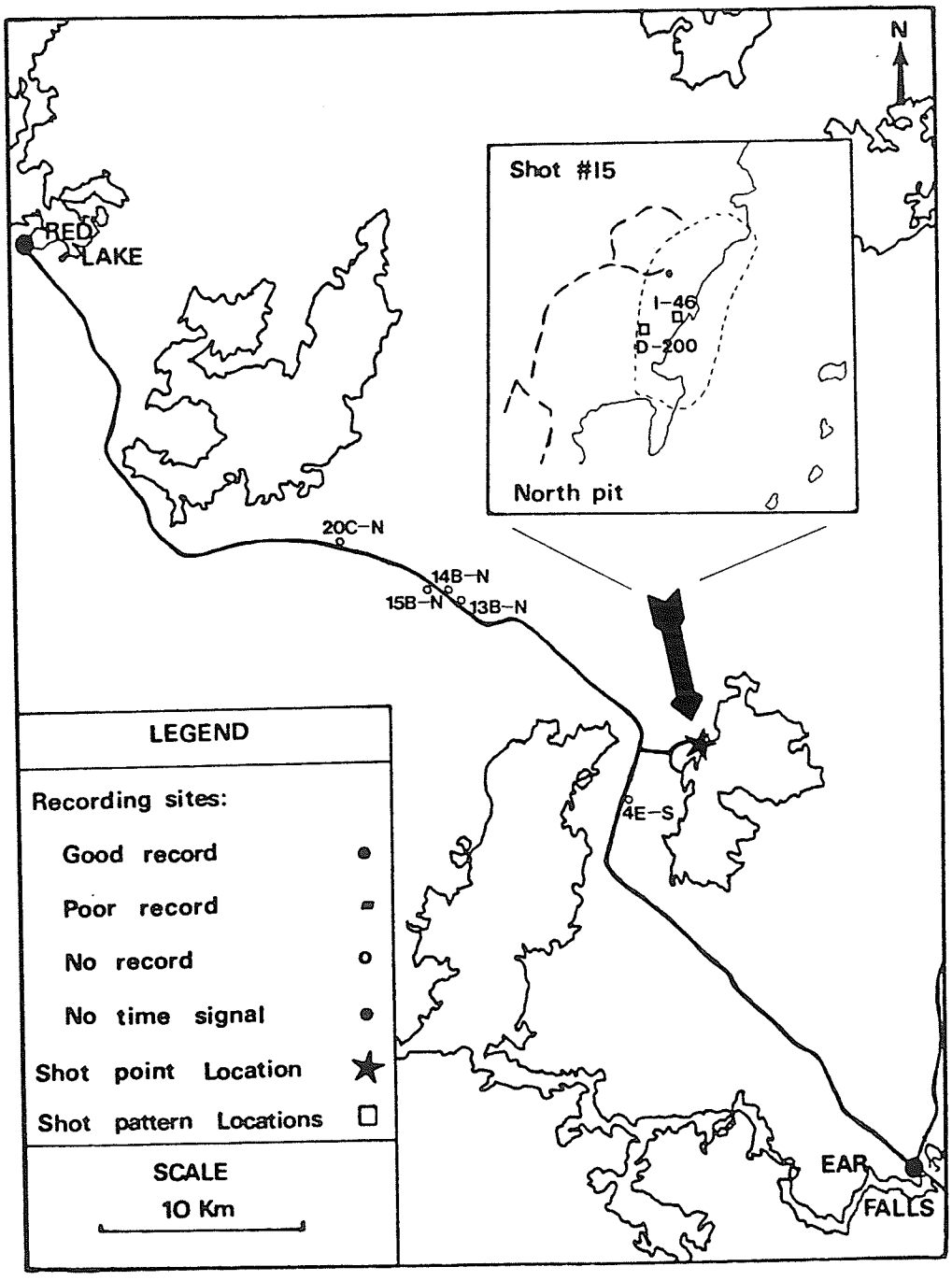

Figure A.15: Recorder and shot pattern locations of shot #15.

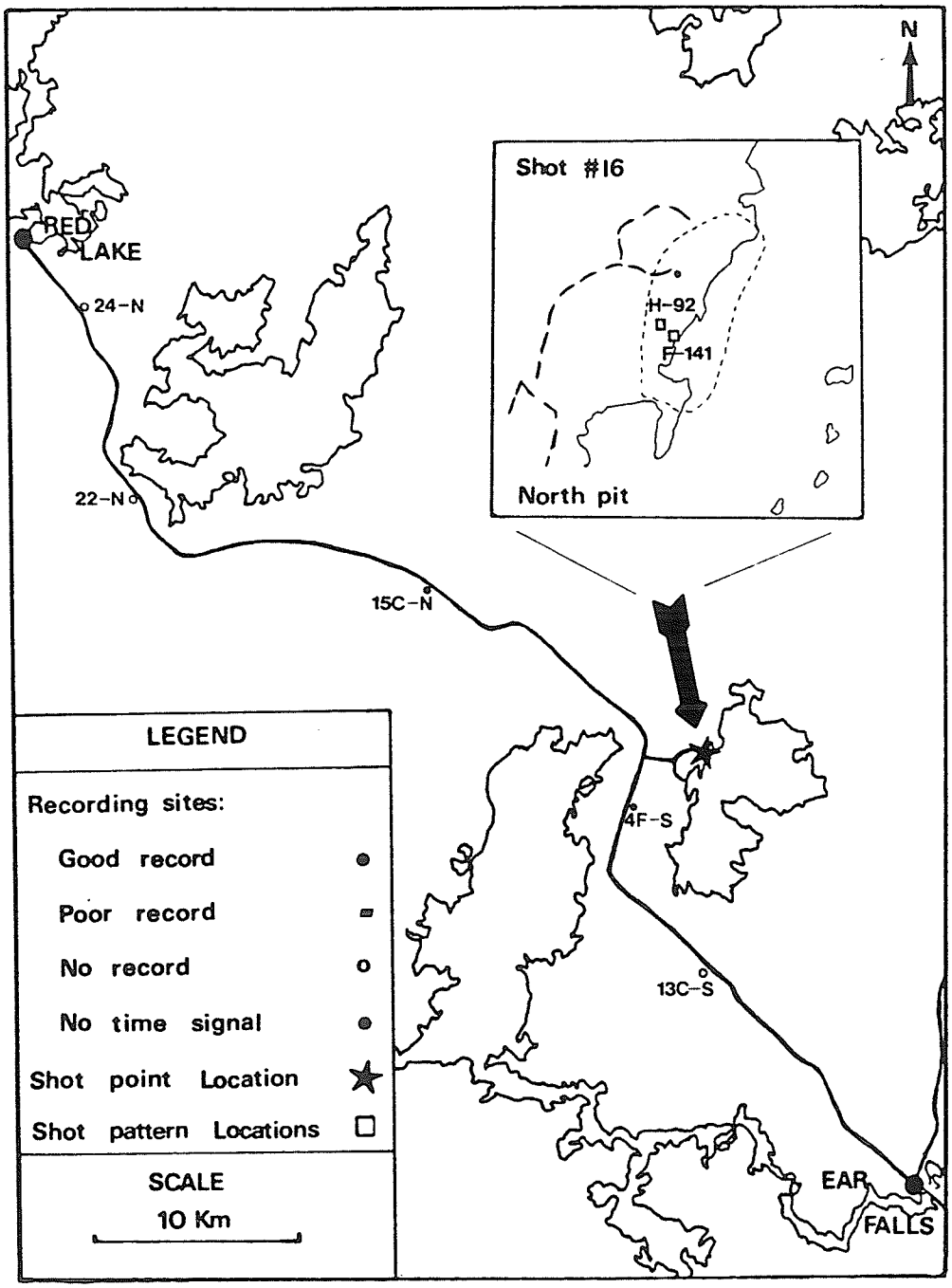

Figure A.16: Recorder and shot pattern locations of shot #16.

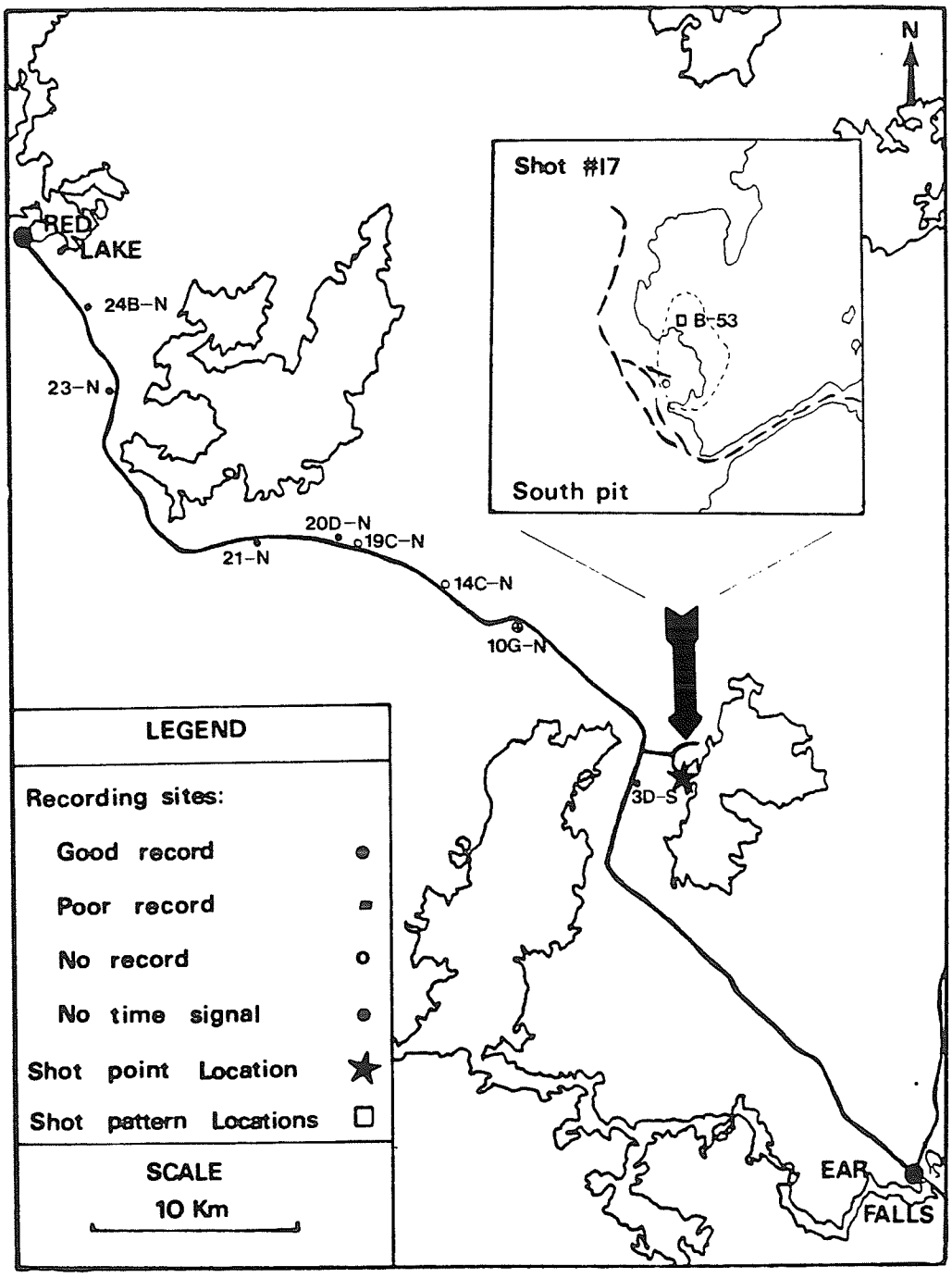

Figure A.17: Recorder and shot pattern locations of shot #17.

Appendix B

RECORD INFORMATION.

Shot number	File number	Record number	Shot-receiver distance (Km)	Quality of data
1	1	SP #1	0.33	good
	2	1-N	3.70	poor
	3	2-N	3.21	good
	4	3-N	3.80	good
2	1	SP #2	0.44	no time signal
	2	1B-N	3.46	good
	3	4B-N	4.63	good
	4	5B-N	5.53	good
	5	6B-N	6.38	no time signal
	6	7-N	7.54	adequate
	7	8-N	8.25	?
3	1	SP #3	0.33	good
	2	5C-N	5.44	good
	3	6C-N	6.51	poor (DC shift)
	4	11-N	10.97	poor (low S/N)
	5	12-N	11.60	poor (low S/N)
4	1	5D-N	5.44	good
	2	13-N	12.42	poor (low S/N)
	3	14-N	13.51	poor (low S/N)
	4	15-N	14.47	poor (low S/N)
	5	17-N	16.57	poor (low S/N)
5	1	SP #5	0.22	good
	2	11B-N	10.95	poor (low S/N)
	3	16B-N	15.53	poor (low S/N)
6	1	SP #	0.33	good
	2	6E-N	6.27	poor
	3	9C-N	9.20	poor
	4	16C-N	15.38	poor (low S/N)
	5	17B-N	16.45	poor (low S/N)

TABLE B.1

Shot and record information-table 1.

Shot number	File number	Record number	Shot-receiver distance (Km)	Quality of data
7	1	SP #7	0.55	good
	2	2-S	3.25	good
	3	3-S	3.37	good
	4	5-S	4.24	good
	5	6-S	5.22	poor (low S/N)
	6	7-S	5.69	poor (low S/N)
8	1	4B-S	5.12	good
	2	8-S	7.79	good
	3	9-S	7.89	good
	4	10-S	8.37	adequate
	5	11-S	8.87	adequate
9	1	2B-S	3.32	good
	2	12-S	7.33	good
	3	13-S	8.06	poor (low S/N)
	4	14-S	8.91	poor (low S/N)
10	1	SP #10	0.57	poor
	2	13B-S	10.17	good
	3	14B-S	10.98	good
	4	15B-S	11.65	good
	5	16B-S	12.56	poor (low S/N)
11	1	SP #11	0.50	good
	2	2D-S	3.00	good
	3	6B-S	5.15	adequate
	4	7B-S	5.67	adequate
	5	10C-S	6.37	poor (low S/N)
	6	17-S	11.77	poor (low S/N)

TABLE B.2

Shot and record information-table 2.

Shot number	File number	Record number	Shot-receiver distance (Km)	Quality of data
12	1	4D-S	5.16	good
	2	16C-S	12.81	low S/N
	3	9D-N	9.10	?
	4	11C-N	10.72	poor (low S/N)
	5	12B-N	11.34	poor (low S/N)
13	1	SP #13	0.57	poor
	2	17B-S	11.40	poor (low S/N)
	3	6F-N	7.28	good
	4	10D-N	11.41	poor (low S/N)
	5	18C-N	18.35	good
	6	18D-N	18.35	good
14	1	3B-S	3.23	good
	2	3C-S	3.23	good
	3	10D-S	6.49	poor
	4	10F-N	10.98	low S/N
15	1	SP #15	0.43	good
16	1	SP #16	0.56	good
	2	4F-S	4.94	good
	3	15C-N	14.30	adequate
17	1	3D-S	3.18	good
	2	10G-N	10.94	no time signal
	3	20D-N	19.75	adequate
	4	21-N	24.29	good
	5	23-N	31.82	oscilation?
	6	24B-N	35.48	oscilation

TABLE B.3

Shot and record information-table 3.

Appendix C

RAW RECORDS.

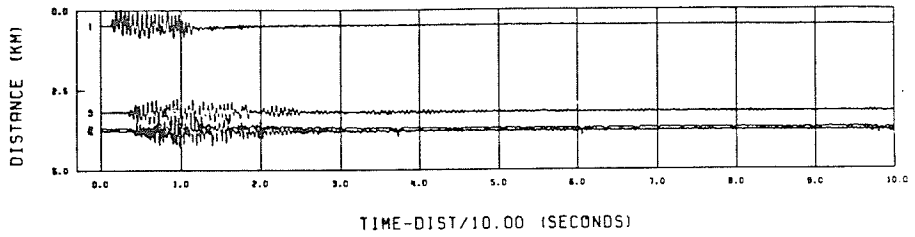

Figure C.1: Raw records of shots #1.

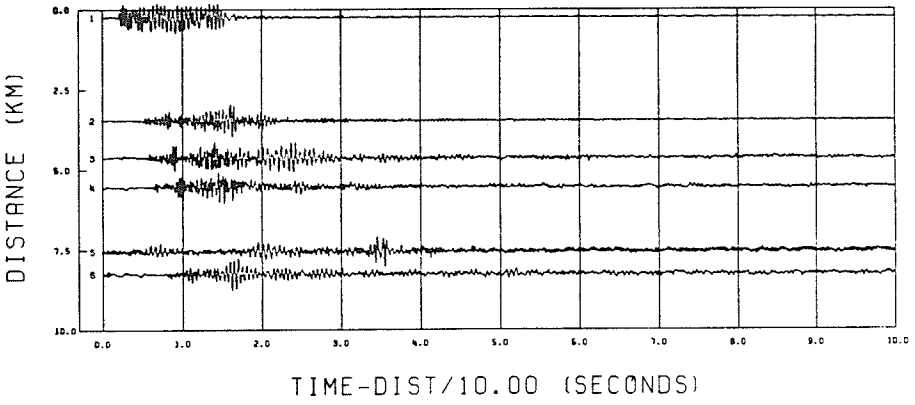

Figure C.2: Raw records of shots #2.

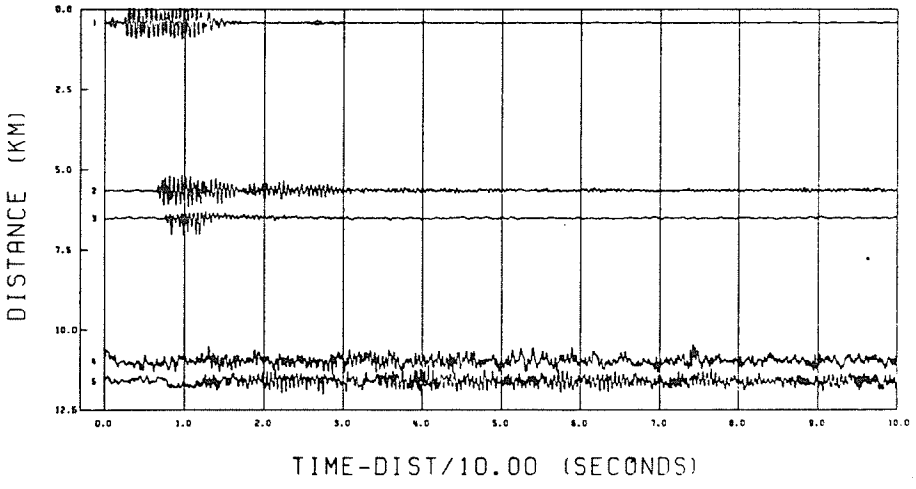

Figure C.3: Raw records of shot #3.

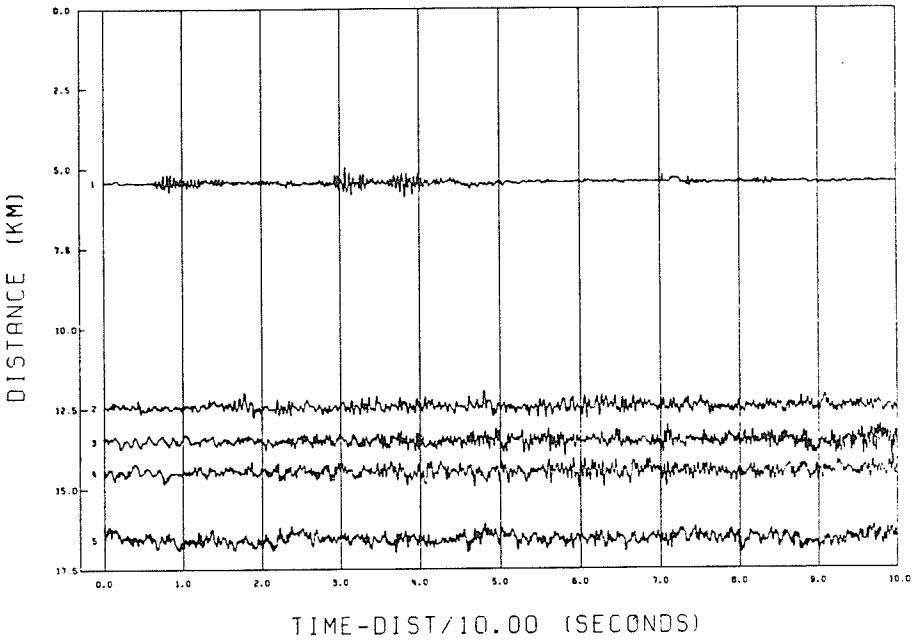

Figure C.4: Raw records of shot #4.

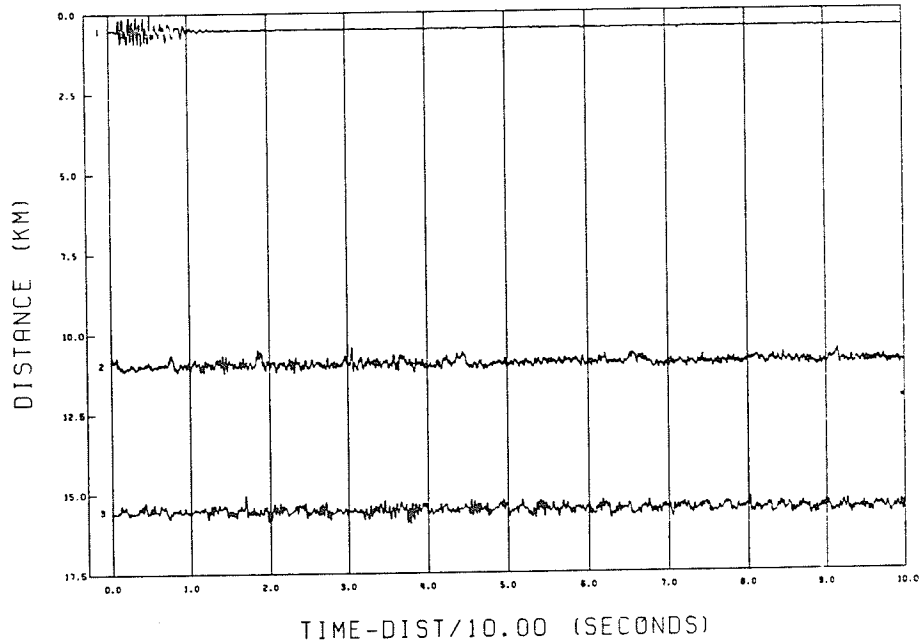

Figure C.5: Raw records of shot #5.

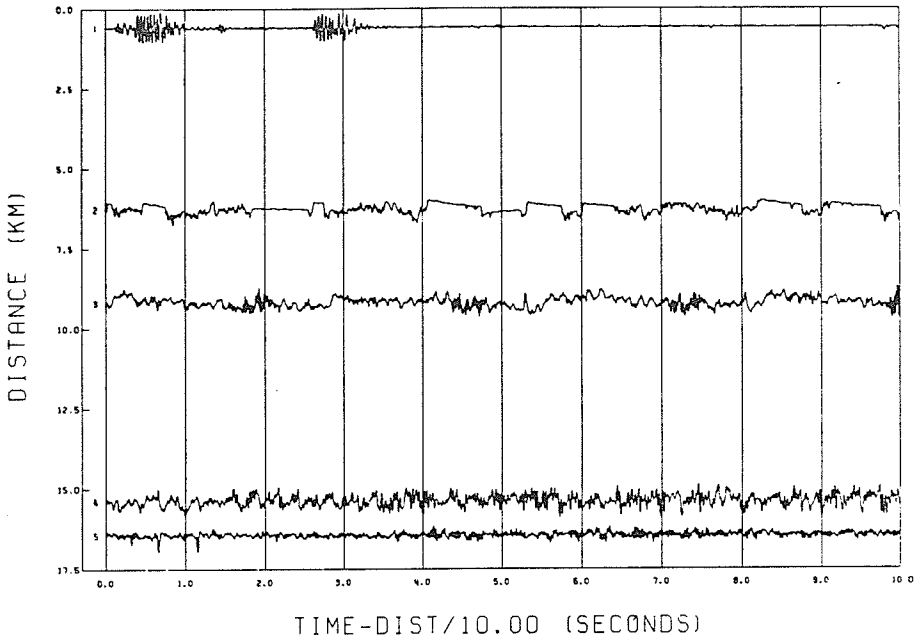

Figure C.6: Raw records of shot #6.

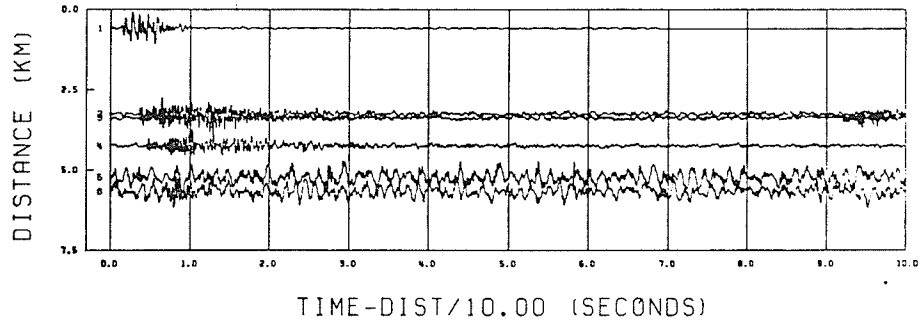

Figure C.7: Raw records of shot #7.

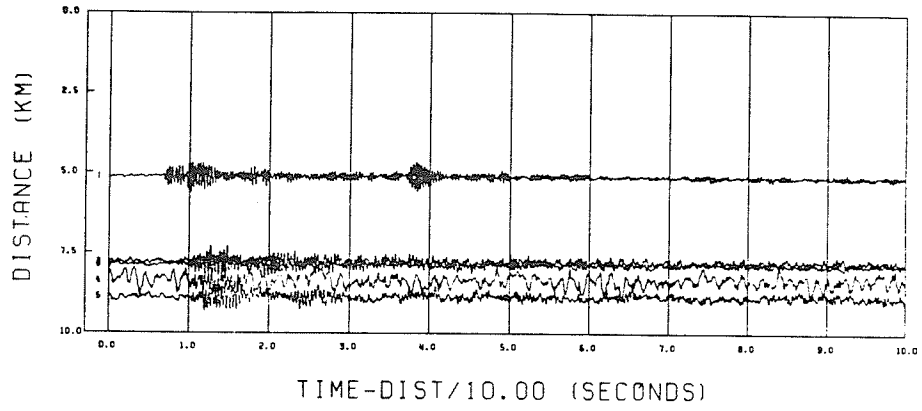

Figure C.8: Raw records of shot #8.

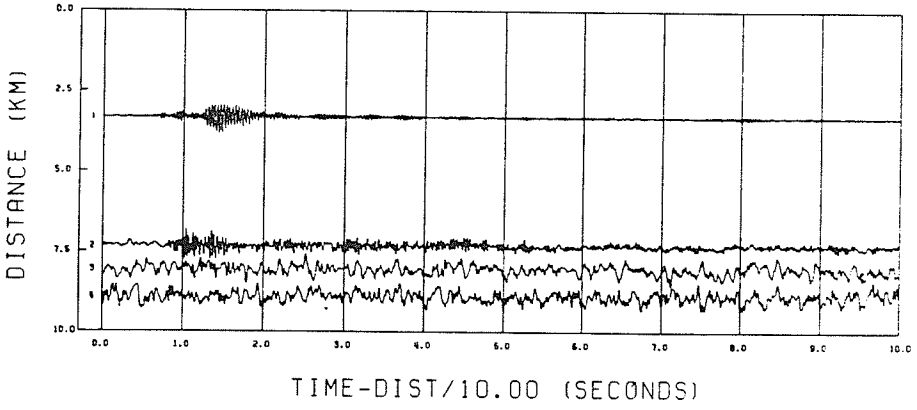

Figure C.9: Raw records of shot #9.

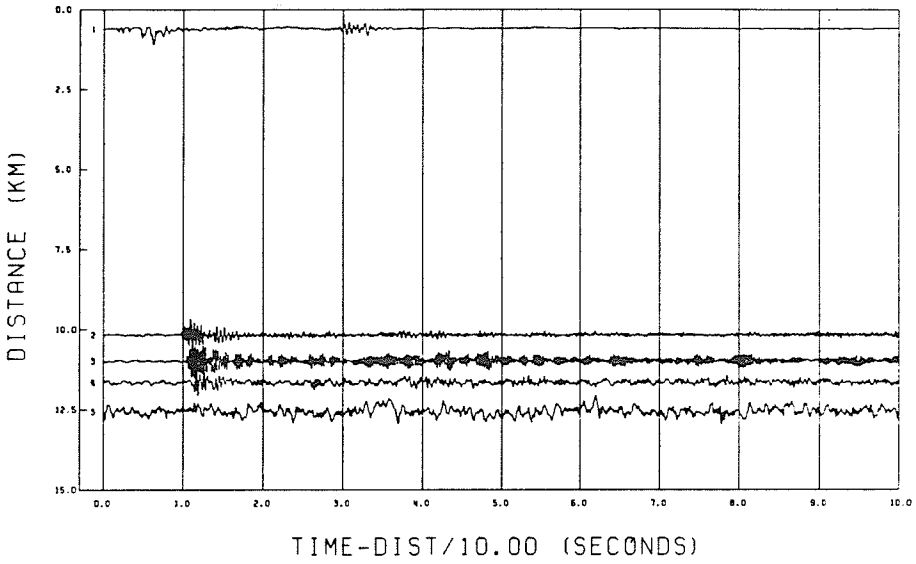

Figure C.10: Raw records of shot #10.

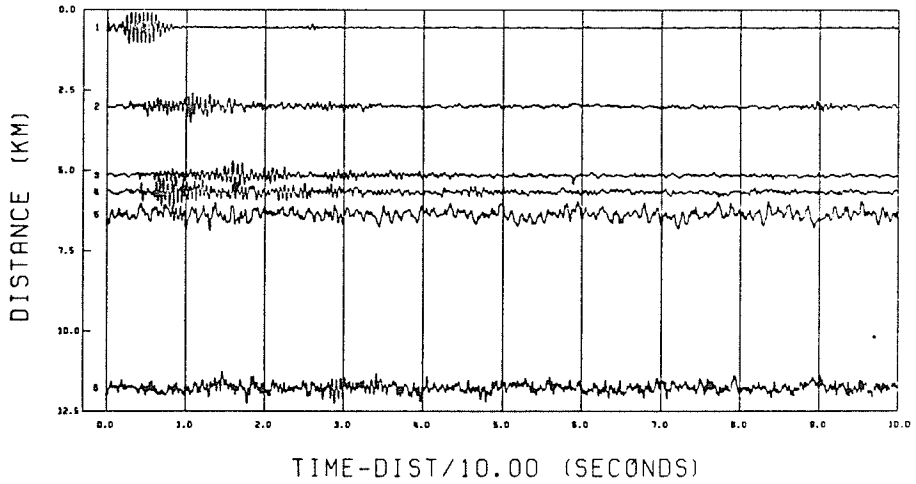

Figure C.11: Raw records of shot #11.

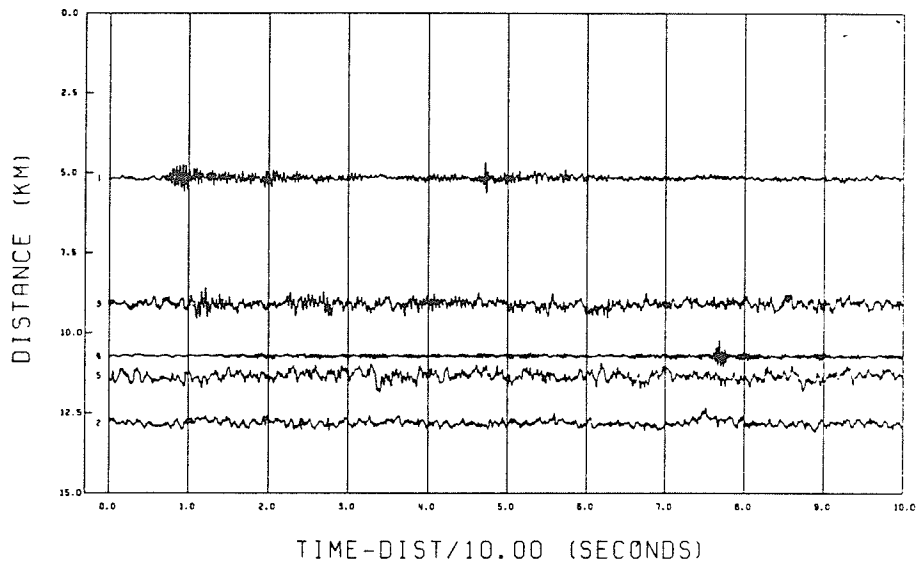

Figure C.12: Raw records of shot #12.

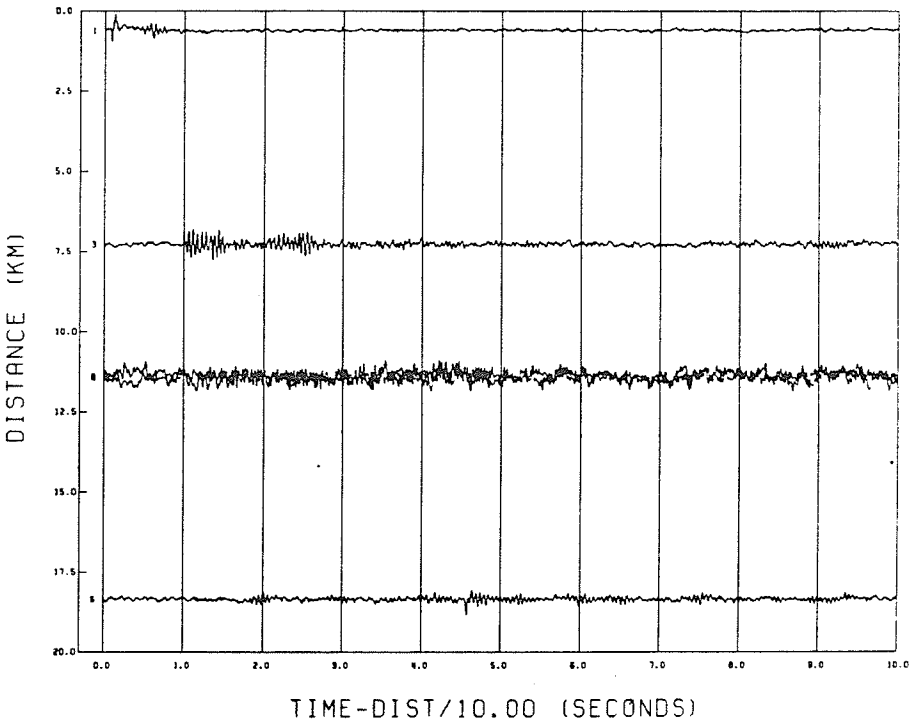

Figure C.13: Raw records of shot #13.

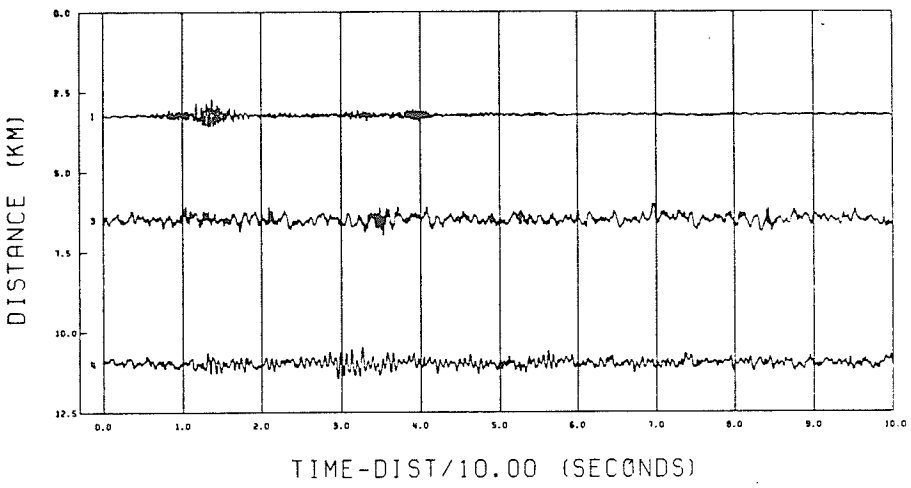

Figure C.14: Raw records of shot #14.

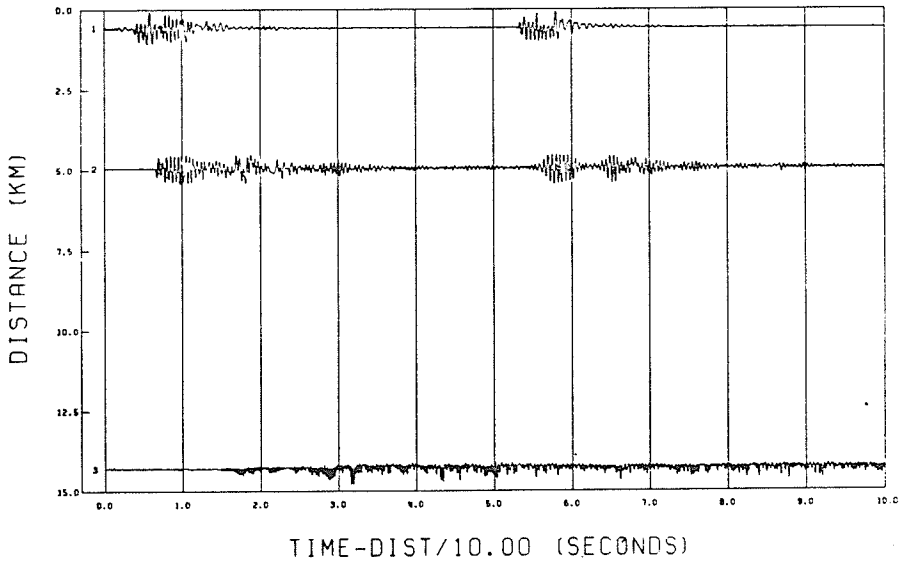

Figure C.15: Raw records of shot #16.

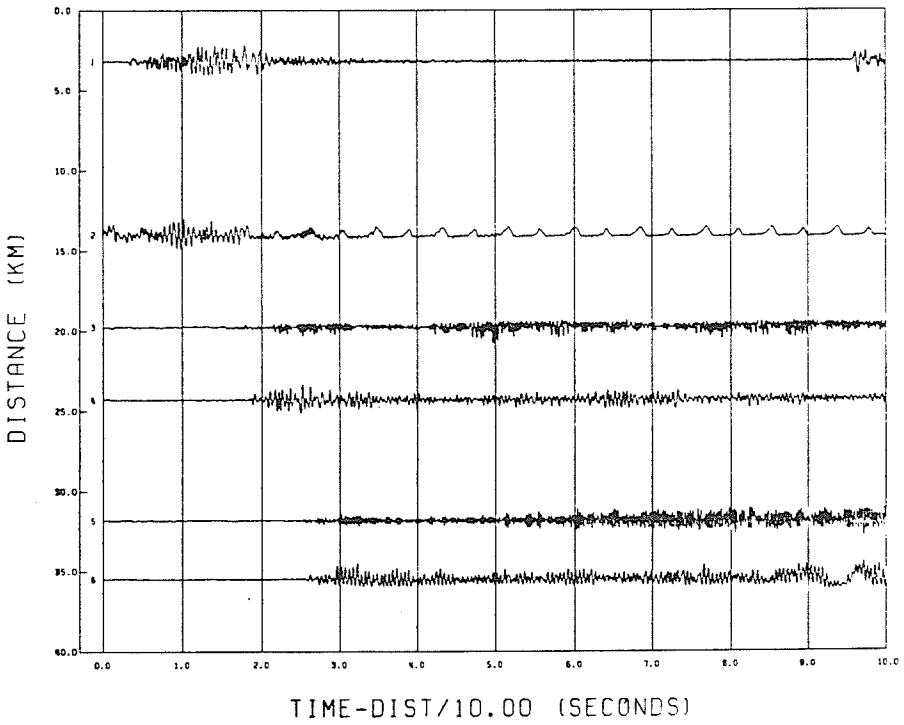

Figure C.16: Raw records of shot #17.

Appendix D

FILTERED RECORDS.

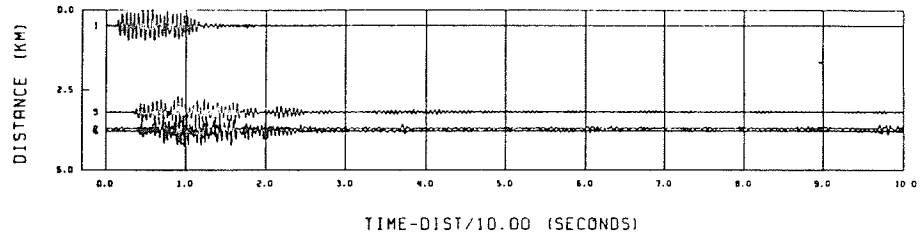

Figure D.1: Filtered records of shots #1.

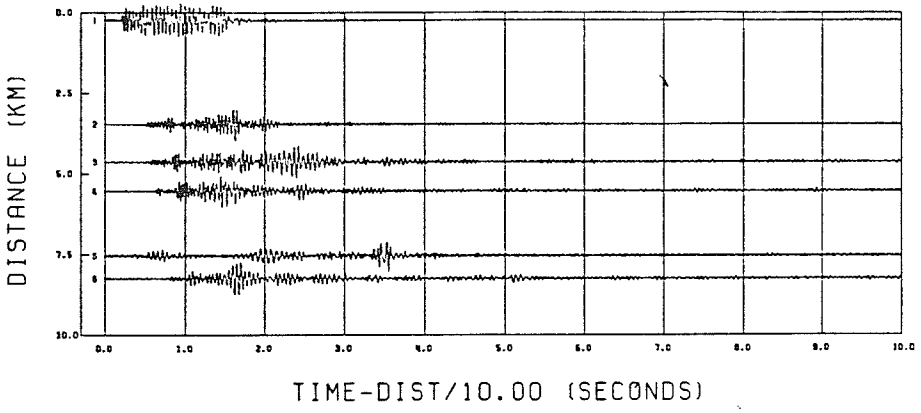

Figure D.2: Filtered records of shots #2.

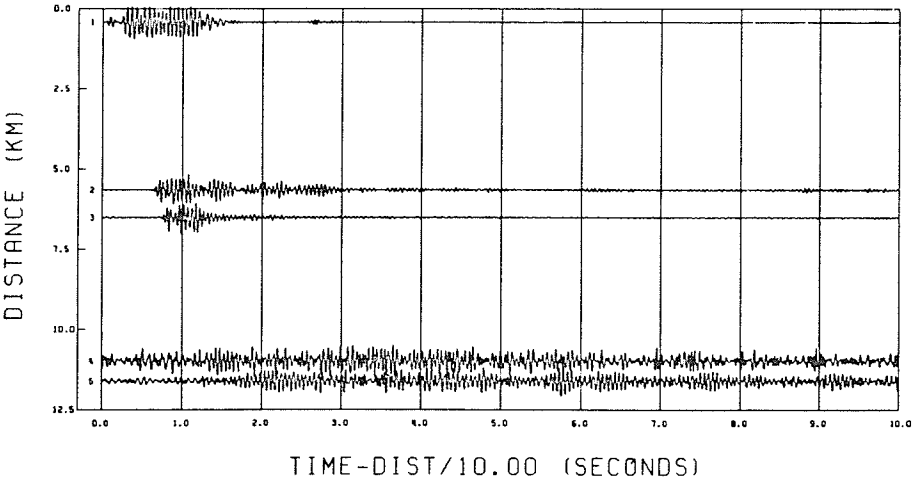

Figure D.3: Filtered records of shot #3.

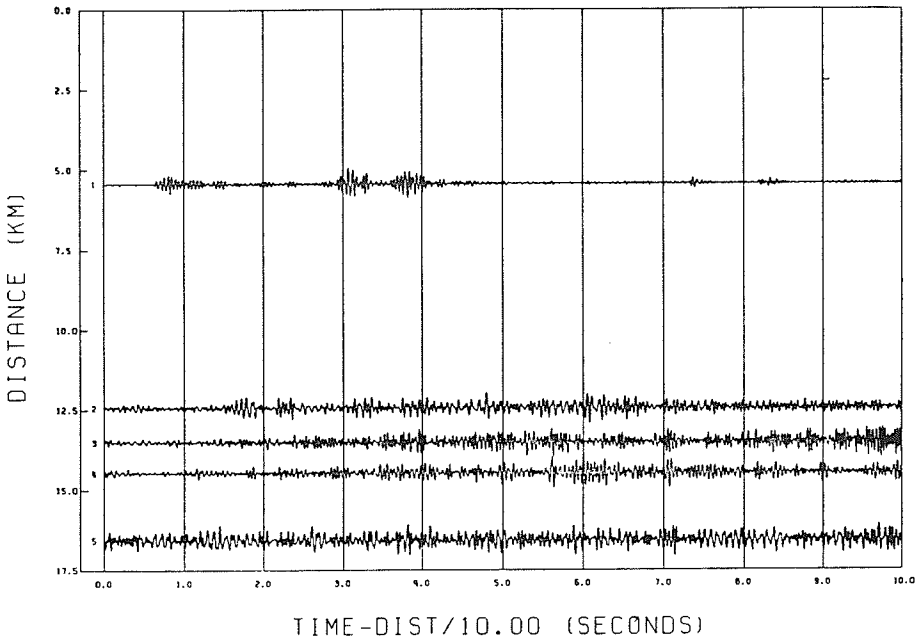

Figure D.4: Filtered records of shot #4.

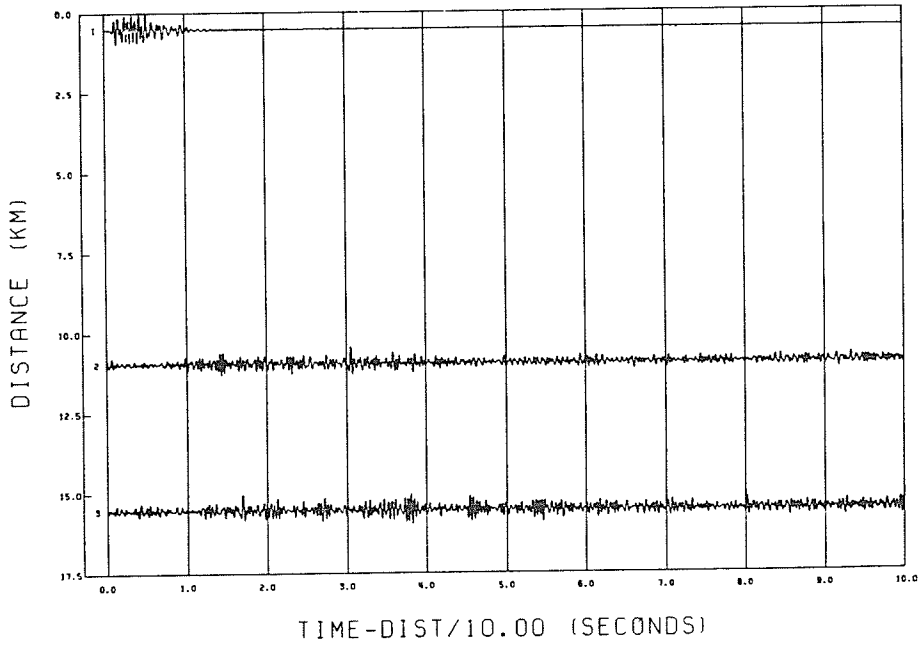

Figure D.5: Filtered records of shot #5.

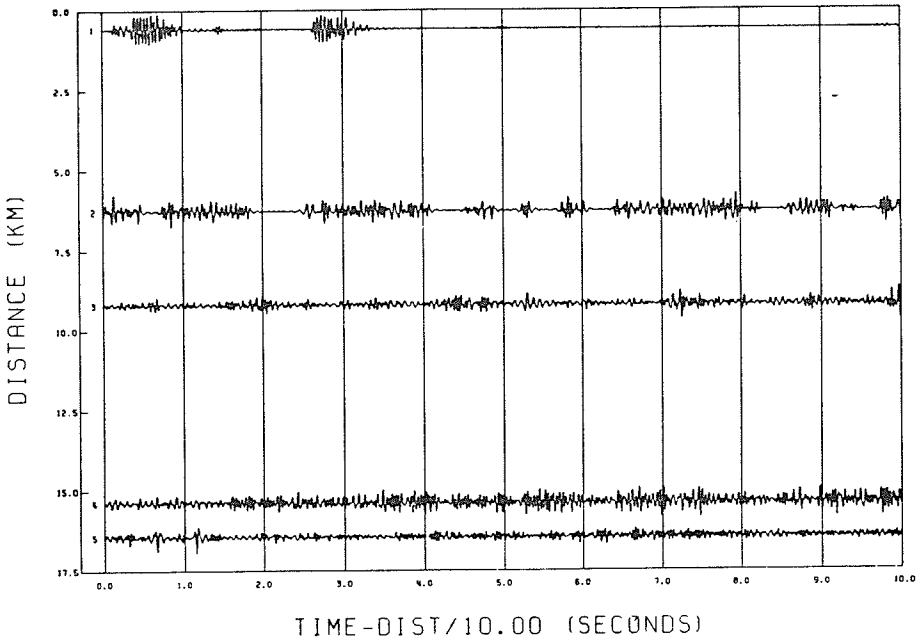

Figure D.6: Filtered records of shot #6.

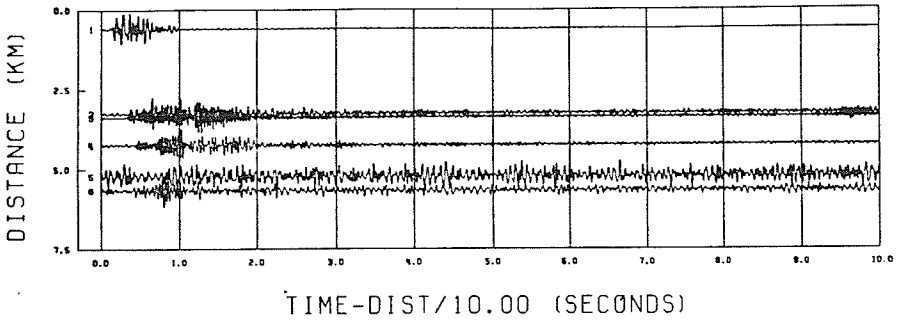

Figure D.7: Filtered records of shot #7.

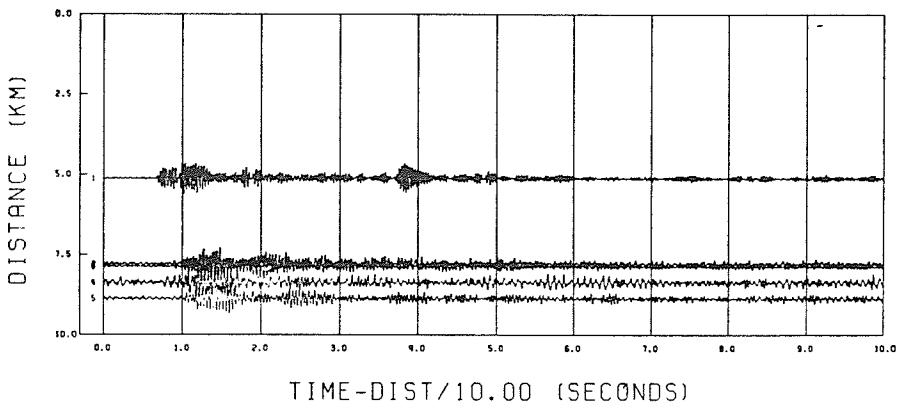

Figure D.8: Filtered records of shot #8.

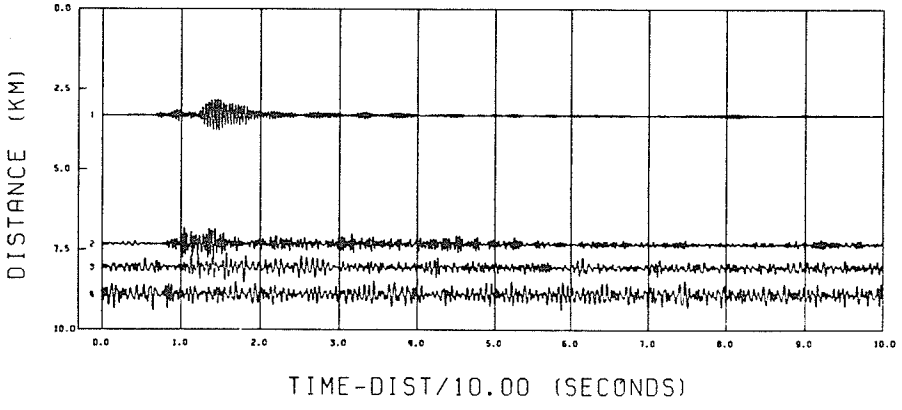

Figure D.9: Filtered records of shot #9.

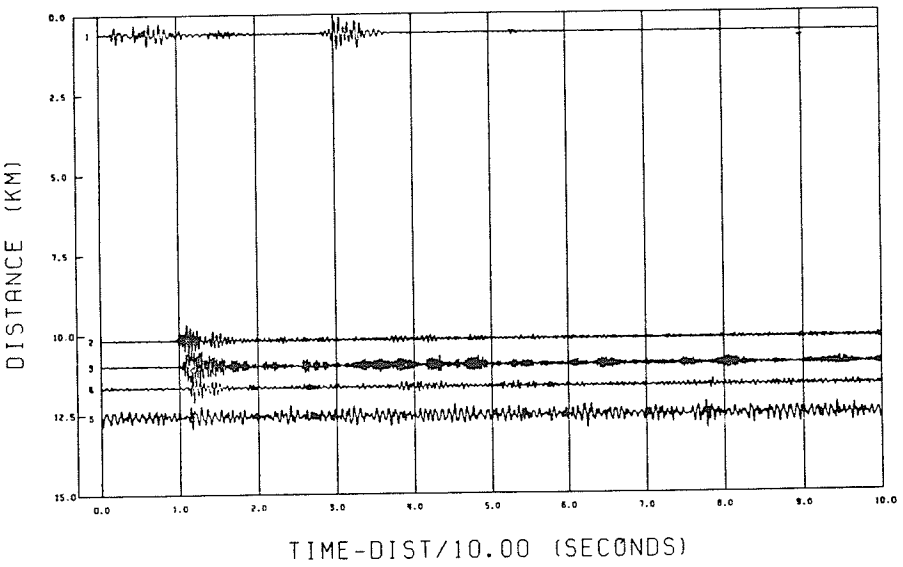

Figure D.10: Filtered records of shot #10.

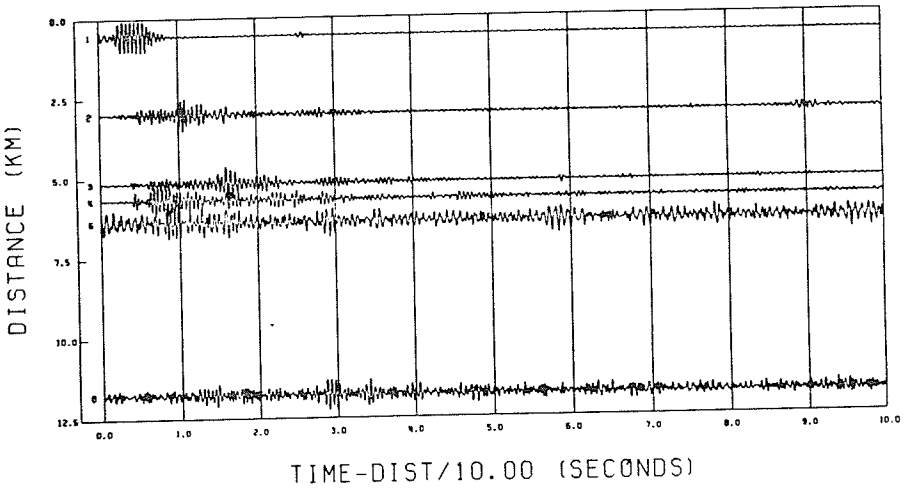

Figure D.11: Filtered records of shot #11.

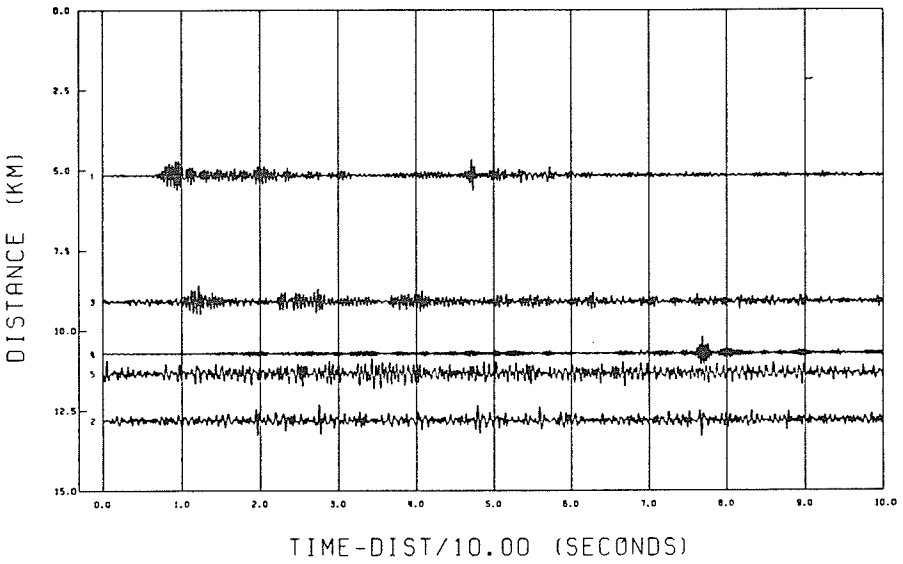

Figure D.12: Filtered records of shot #12.

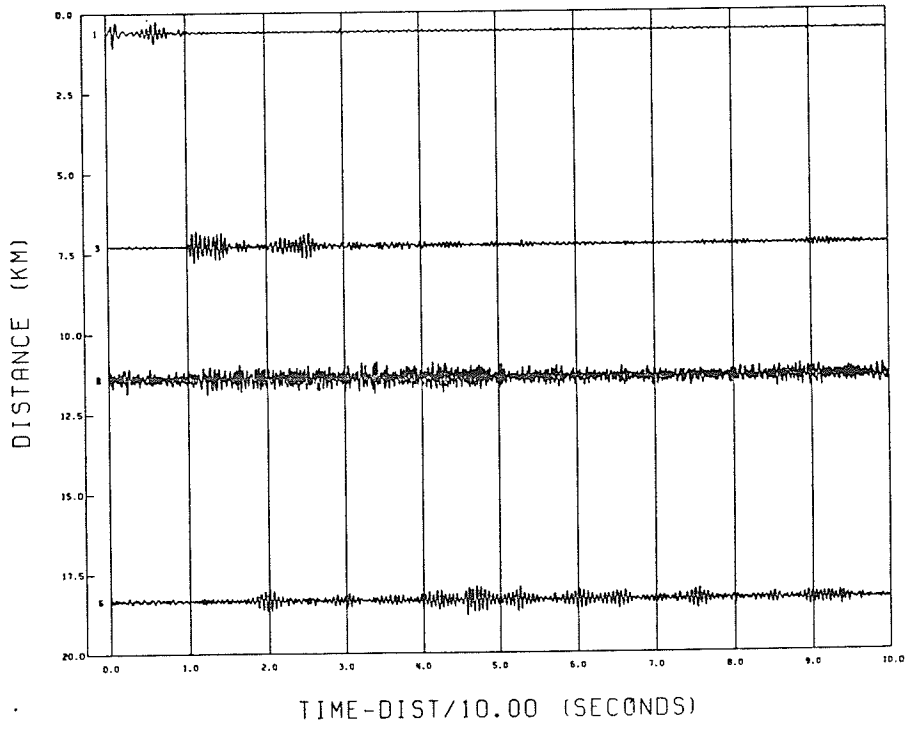

Figure D.13: Filtered records of shot #13.

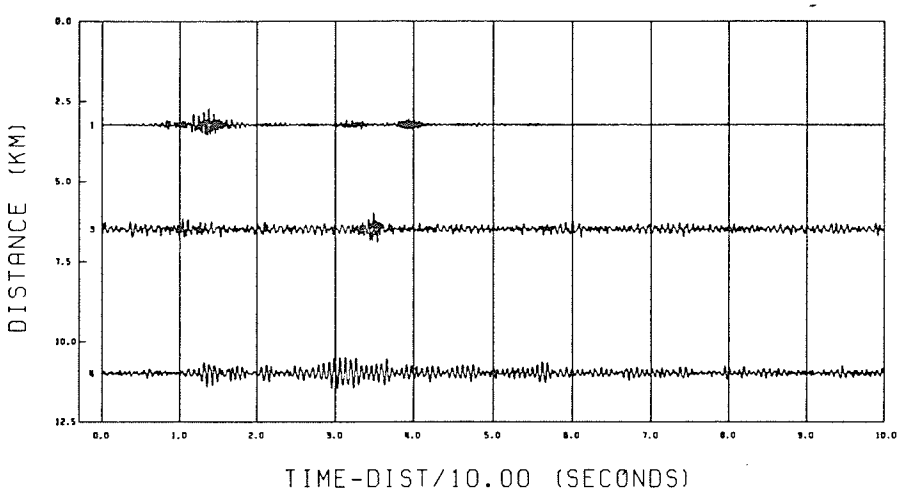

Figure D.14: Filtered records of shot #14.

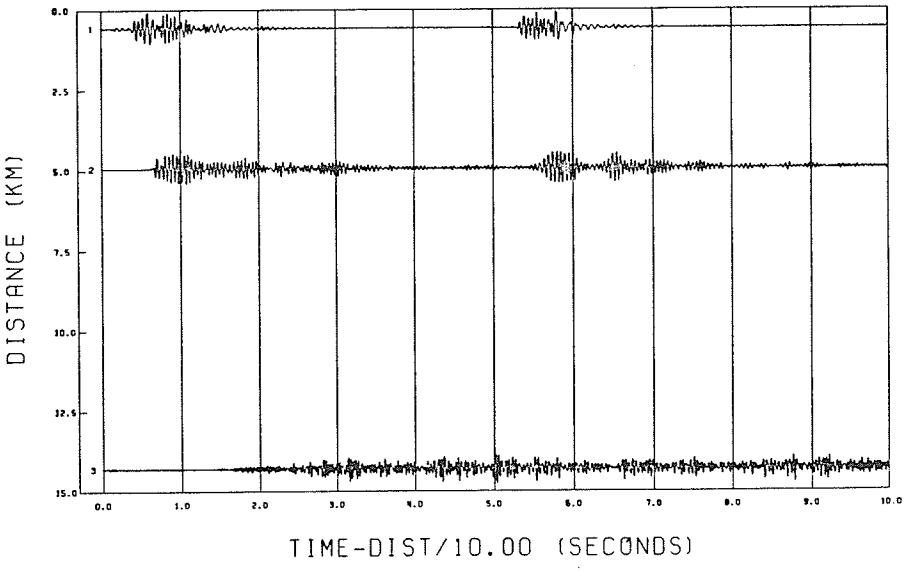

Figure D.15: Filtered records of shot #16.

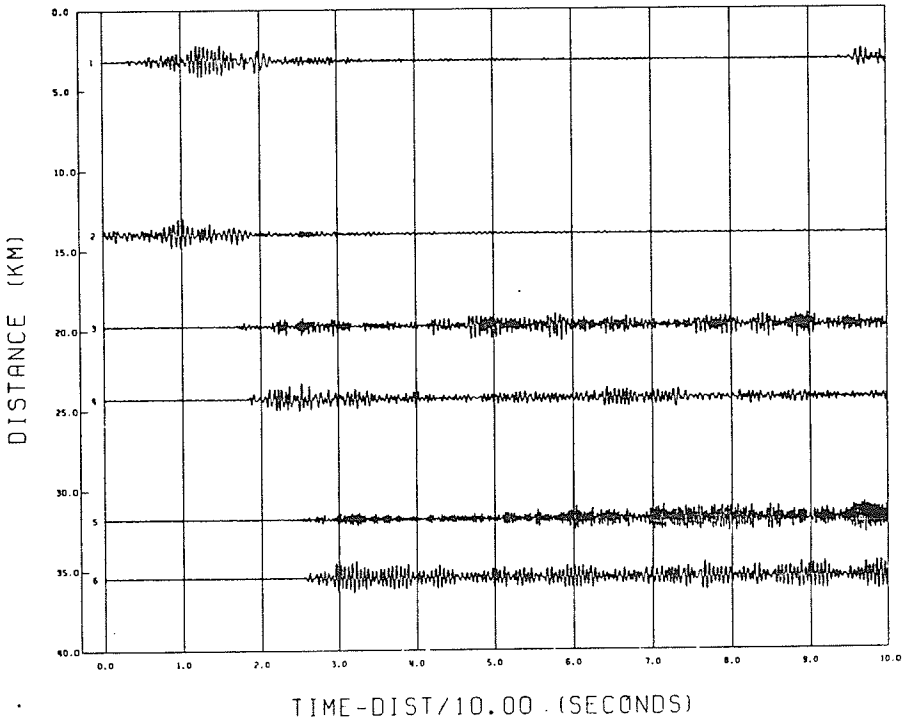

Figure D.16: Filtered records of shot #17.

Appendix E

CROSS-CORRELATED RECORDS.

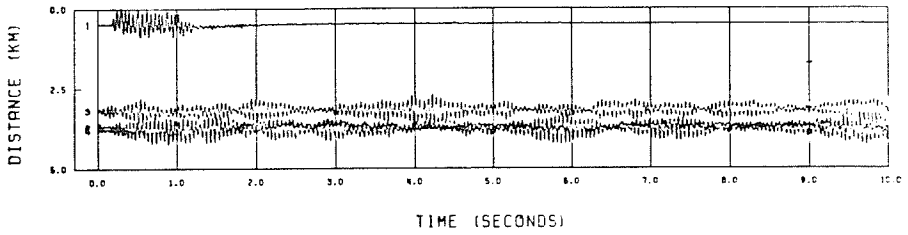

Figure E.1: Cross-correlated records of shots #1.

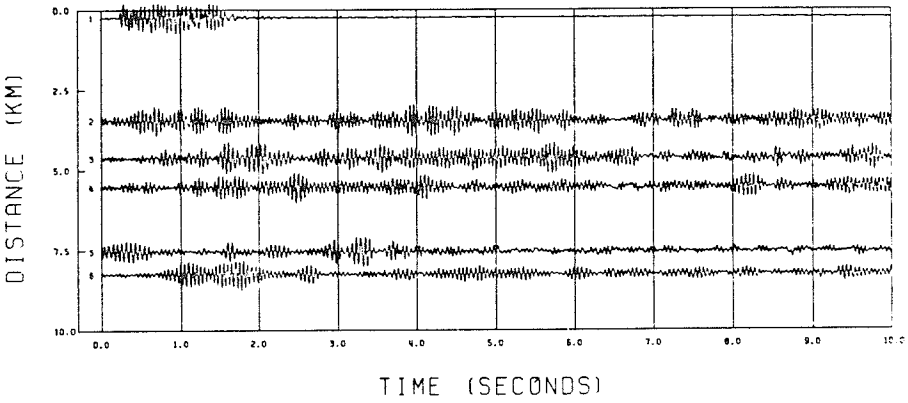

Figure E.1: Cross-correlated records of shots #2.

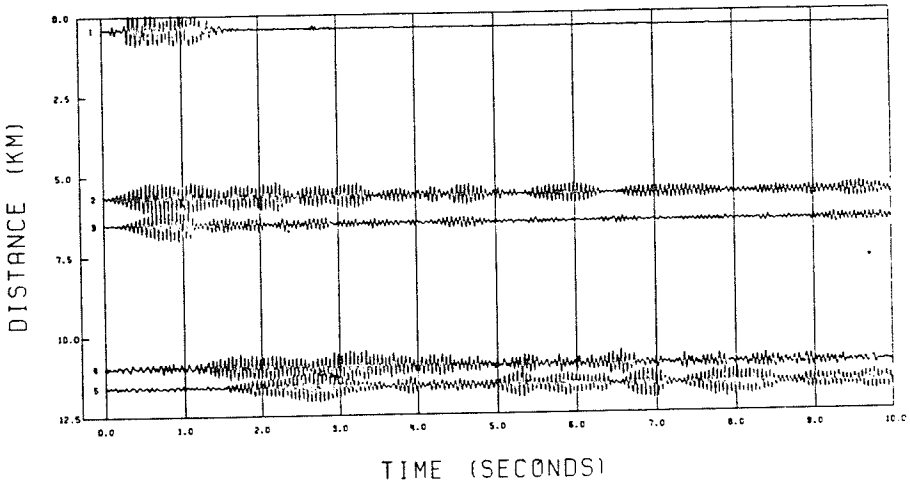

Figure E.3: Cross-correlated records of shot #3.

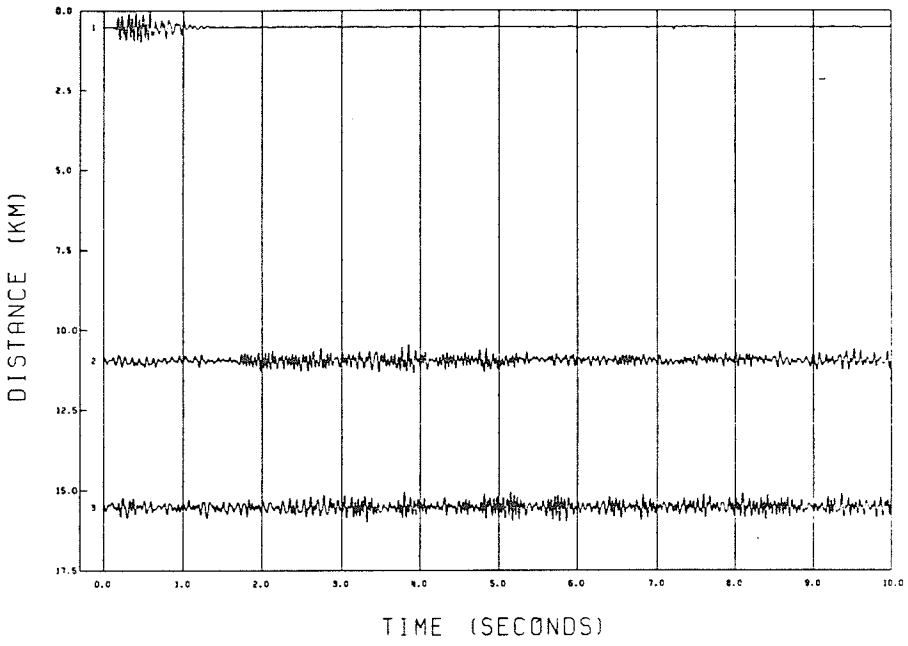

Figure E.4: Cross-correlated records of shot #5.

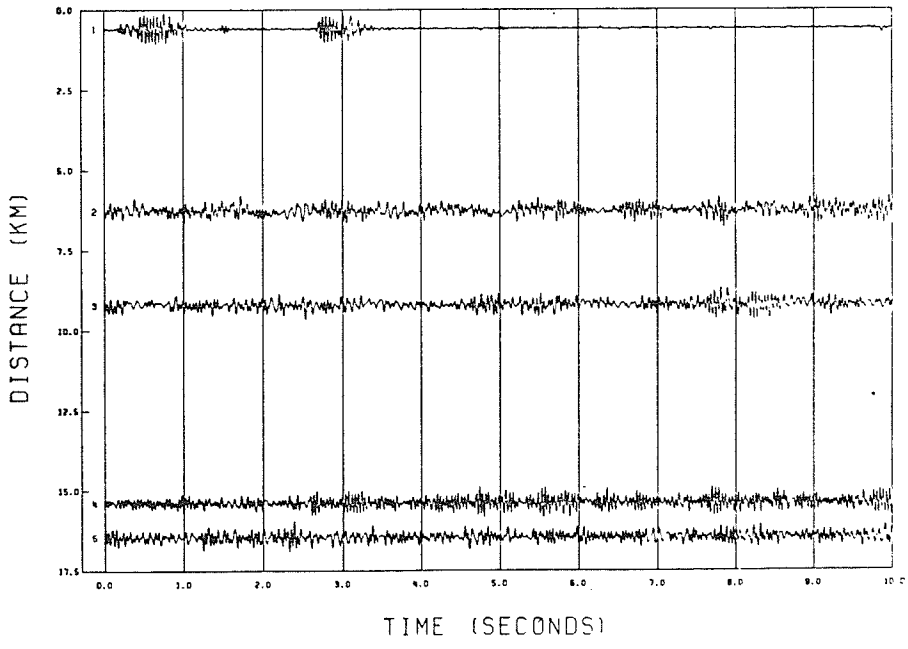

Figure E.5: Cross-correlated records of shot #6.

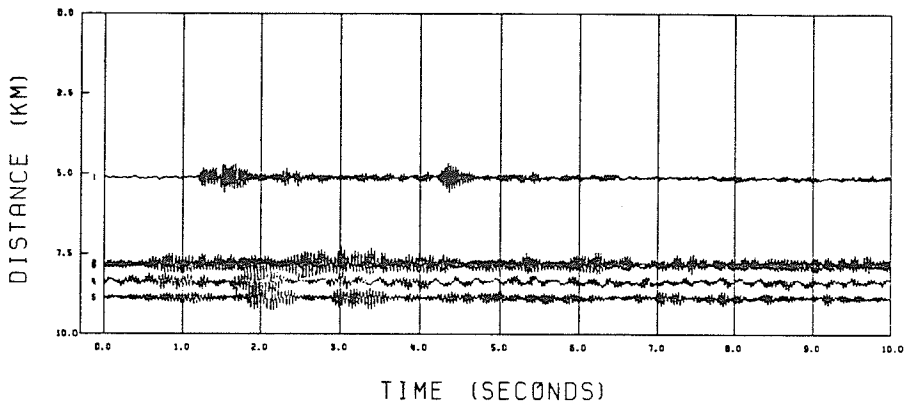

Figure E.6: Cross-correlated records of shot #8.

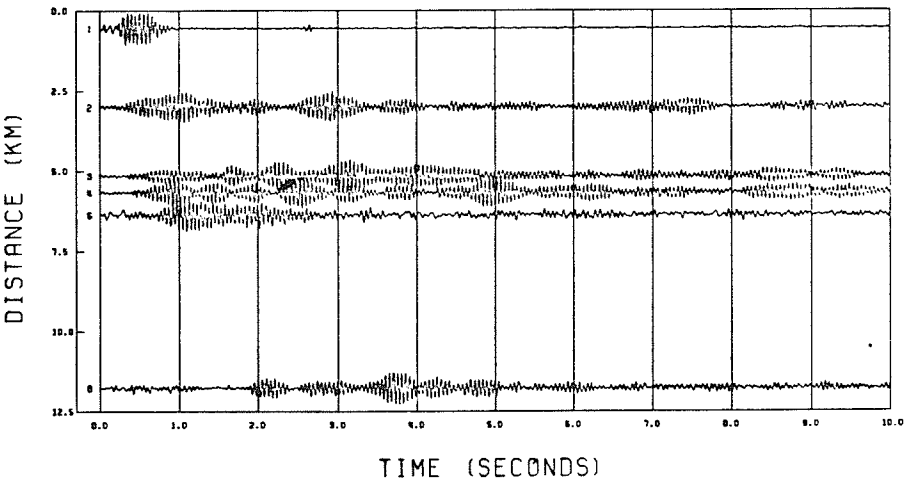

Figure E.7: Cross-correlated records of shot #11.

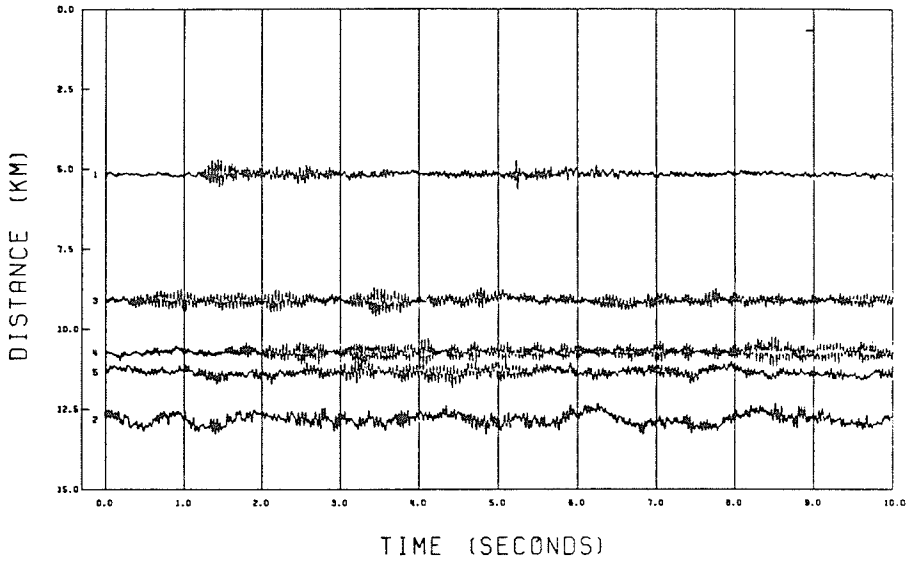

Figure E.8: Cross-correlated records of shot #12.

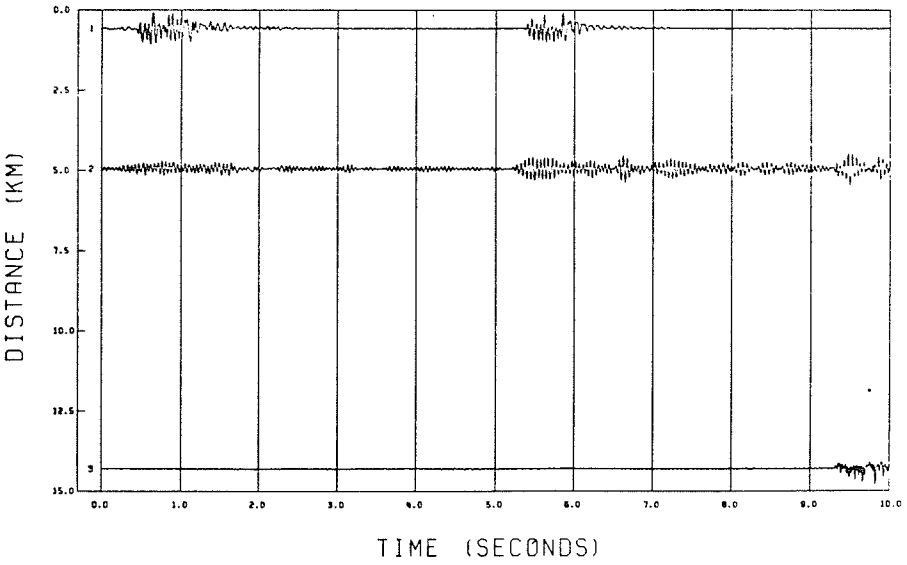

Figure E.9: Cross-correlated records of shot #16.

Appendix F

SHOT PATTERNS

Shot number	Number of shot patterns	Shot pattern number	Type of delays between shot patterns	Distance to receiver (metres)	Distance between shot patterns
1	1	H-84	----------	442.0	--------
2	2	H-86 I-36	period 10 (2) ----------	219.5 405.4	73.0 --------
3	2	H-87 I-37	---------- ----------	390.1 499.9	753.0 --------
4	2	E-174 C-166	Non-El ----------	777.2 923.4	280.0 --------
5	2	I-38 G-126	period 10 (3) ----------	475.5 490.7	94.0 --------
6	2	I-39 E-175	Non-El ----------	545.6 810.8	296.0 --------
7	1	B-41	----------	545.6	--------
8	2	H-88 D-198	Non-El ----------	506.0 670.6	140.0 --------
9	1	B-42	----------	570.0	--------
10	3	I-40 H-89 C-167	period 10 (3) Non-El ----------	578.0 606.6 969.3	64.0 365.0 --------
11	1	B-43	----------	509.2	--------
12	2	G-130 D-199	Non-El ----------	310.9 713.2	344.0 --------
13	1	B-44	----------	560.8	--------
14	2	B-49 B-50	Non-El ----------	509.0 548.64	546.0 --------
15	2	I-46 D-200	Non-El (2) ----------	435.9 548.6	546.0 --------
16	2	H-92 F-141	Non-El ----------	530.4 694.9	201.0 --------
17	1	B-53	----------	496.8	--------

TABLE F.1

Source information.

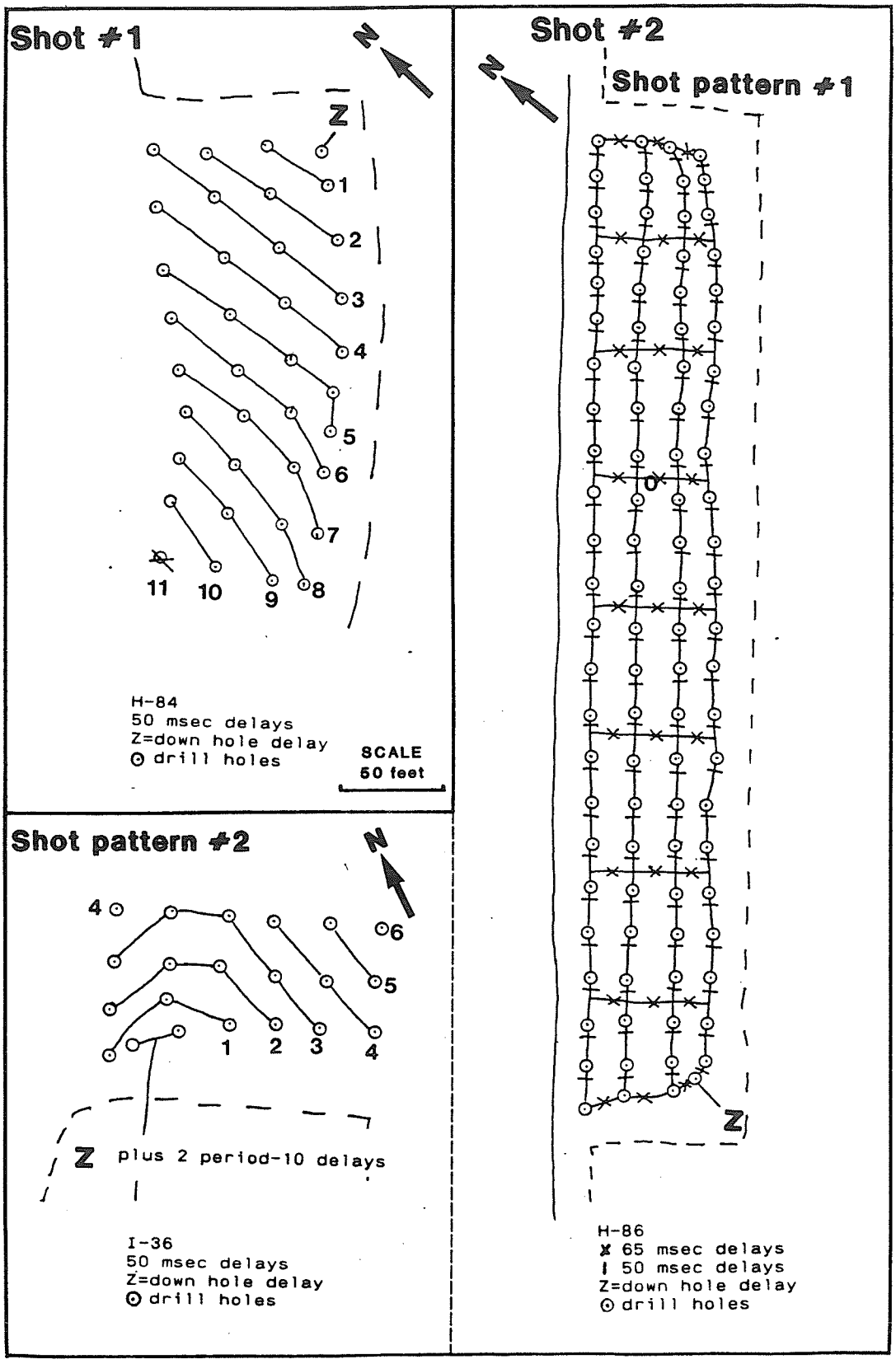

Figure F.1: Shot patterns used for shot #1 and #2.

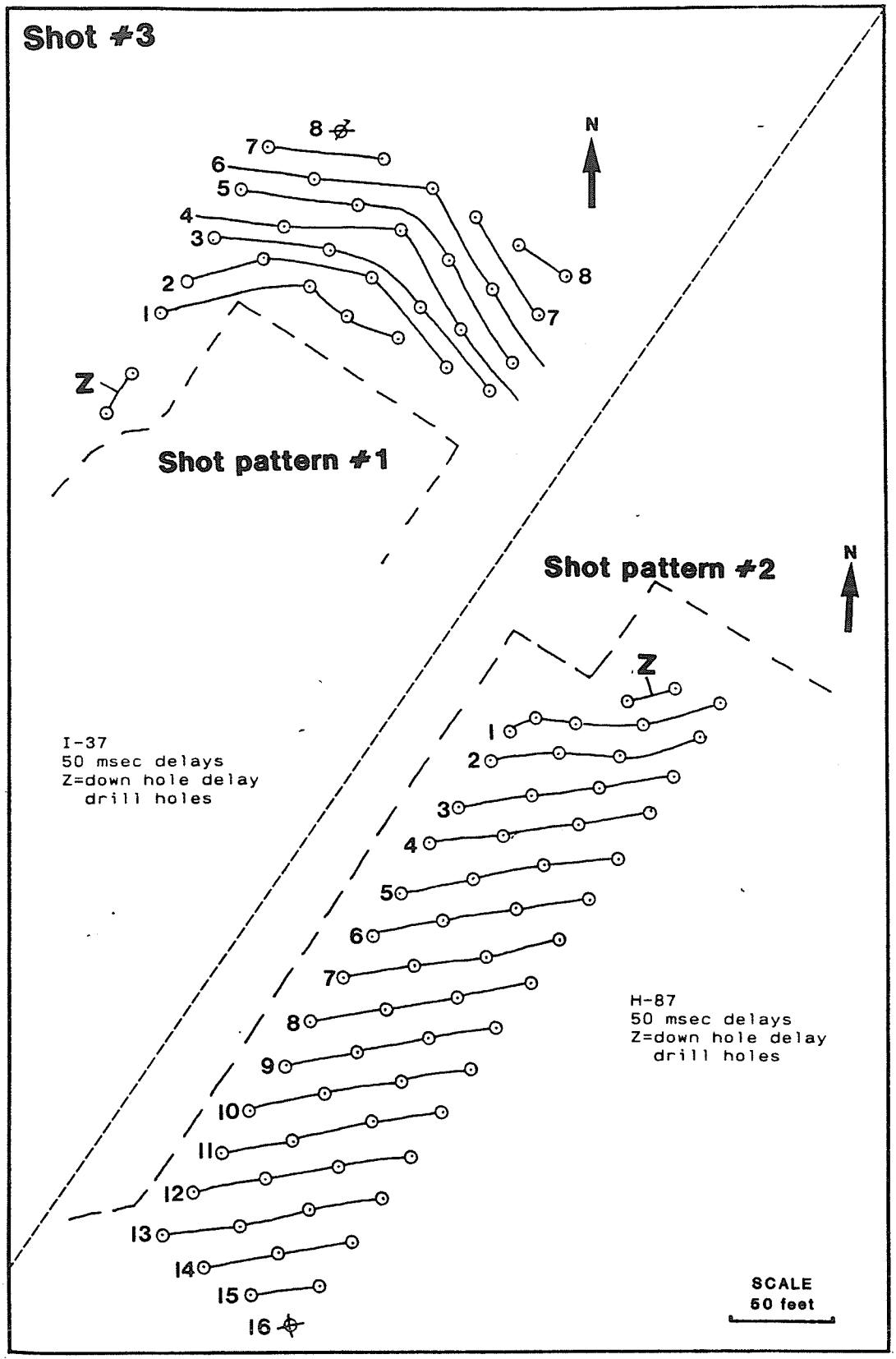

Figure F.2: Shot patterns used for shot #3.

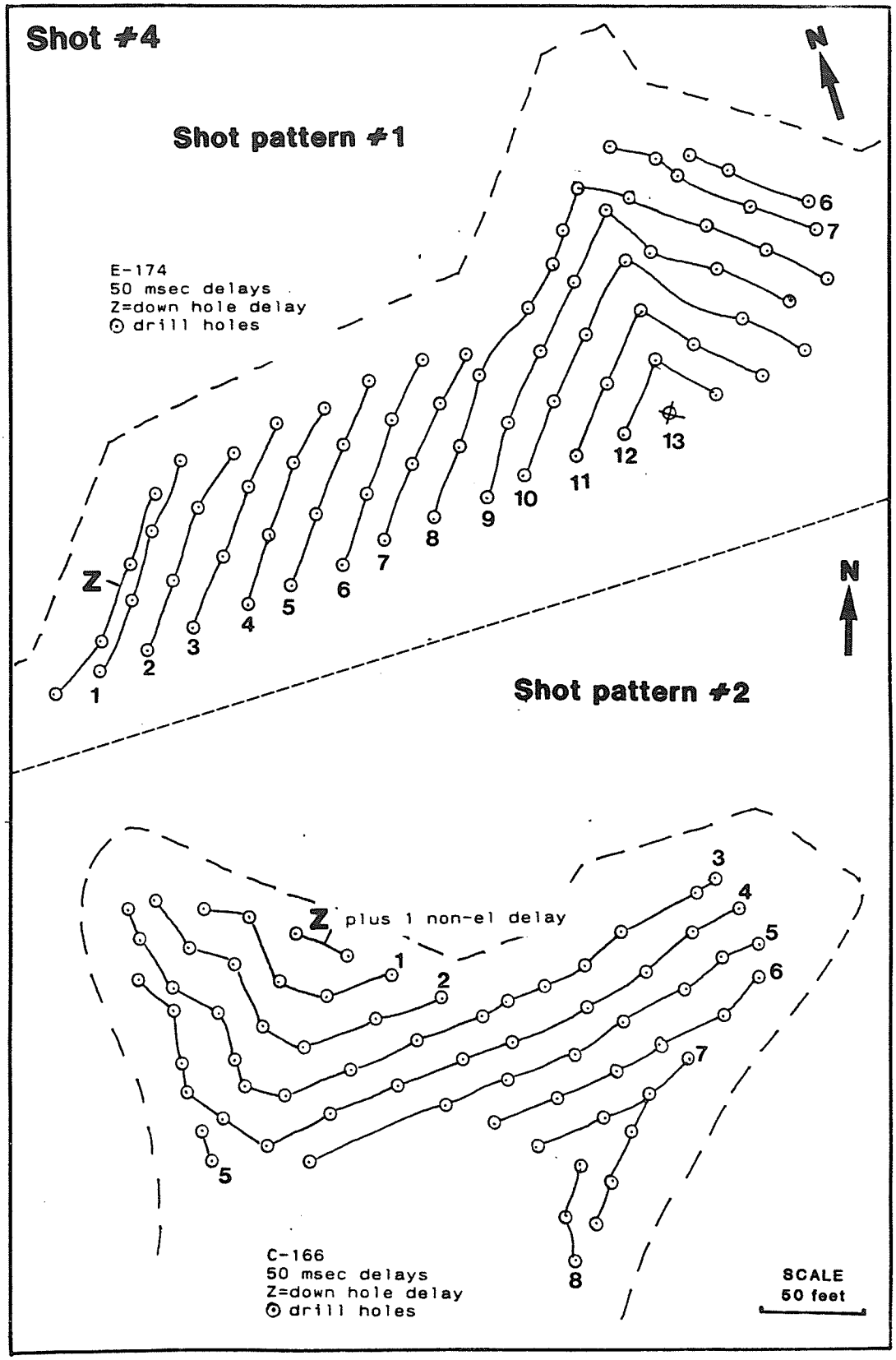

Figure F.3: Shot patterns used for shot #4.

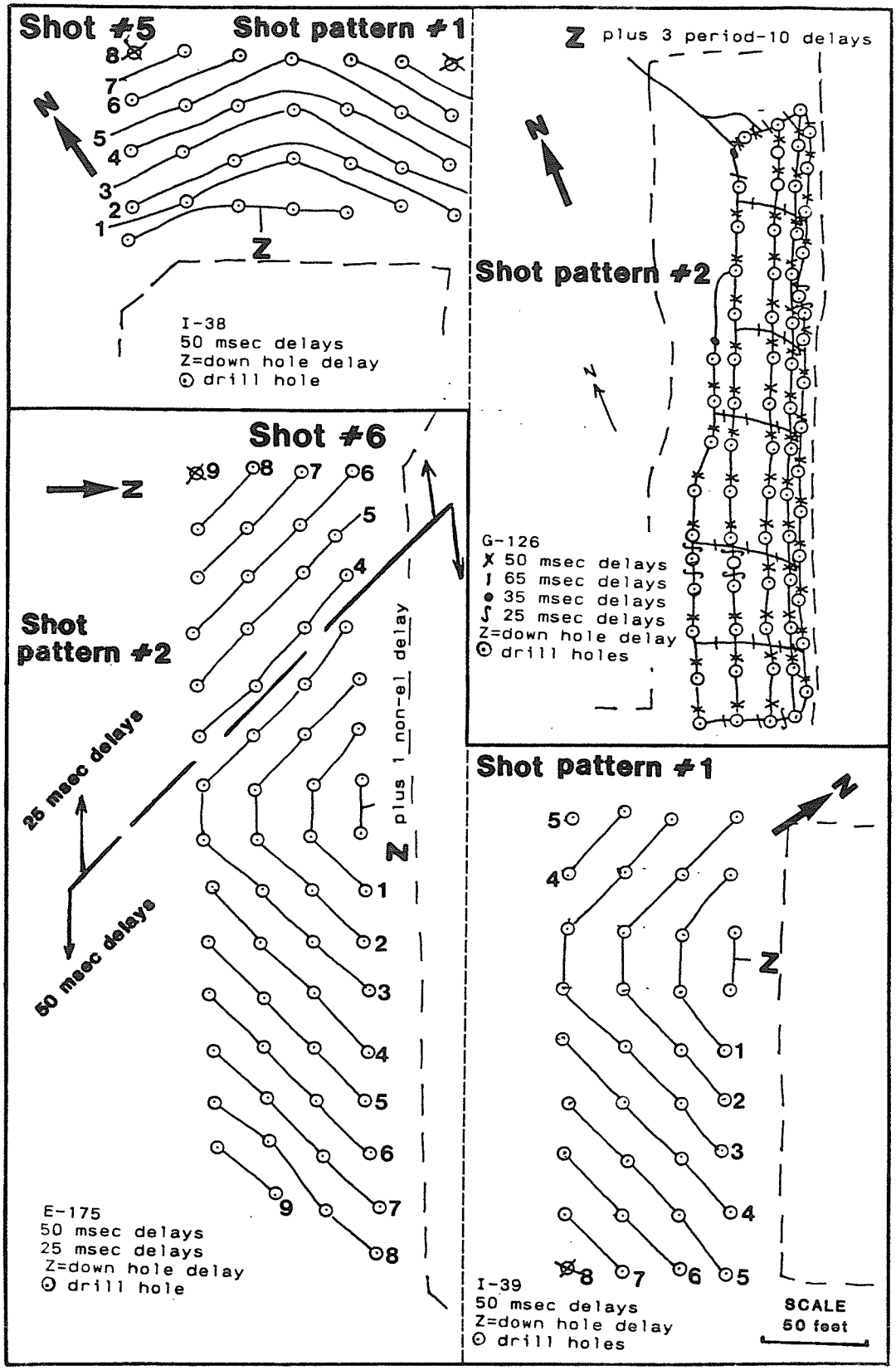

Figure F.4: Shot patterns used for shots #5 and #6.

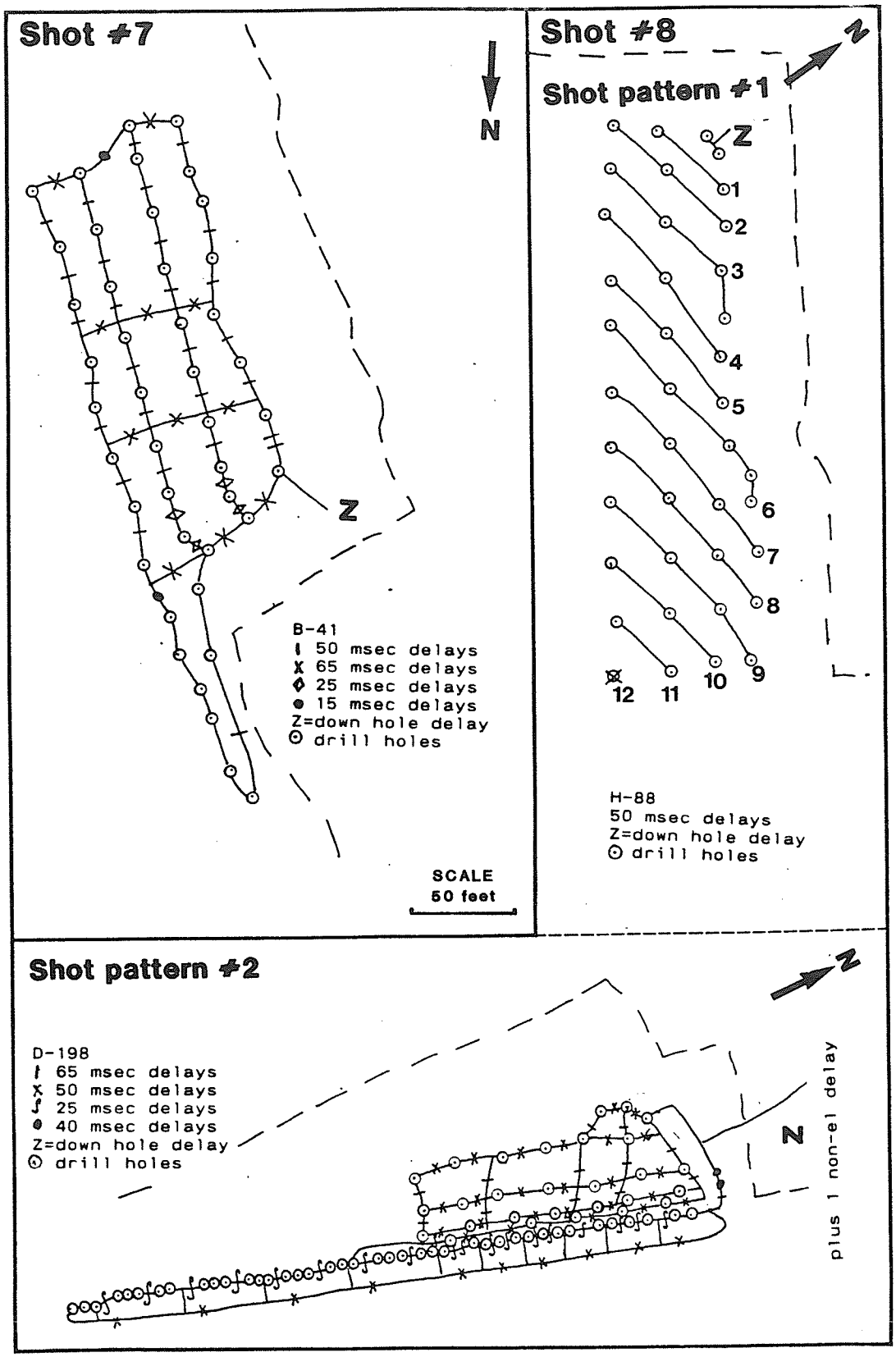

Figure F.5: Shot patterns used for shots #7 and #8.

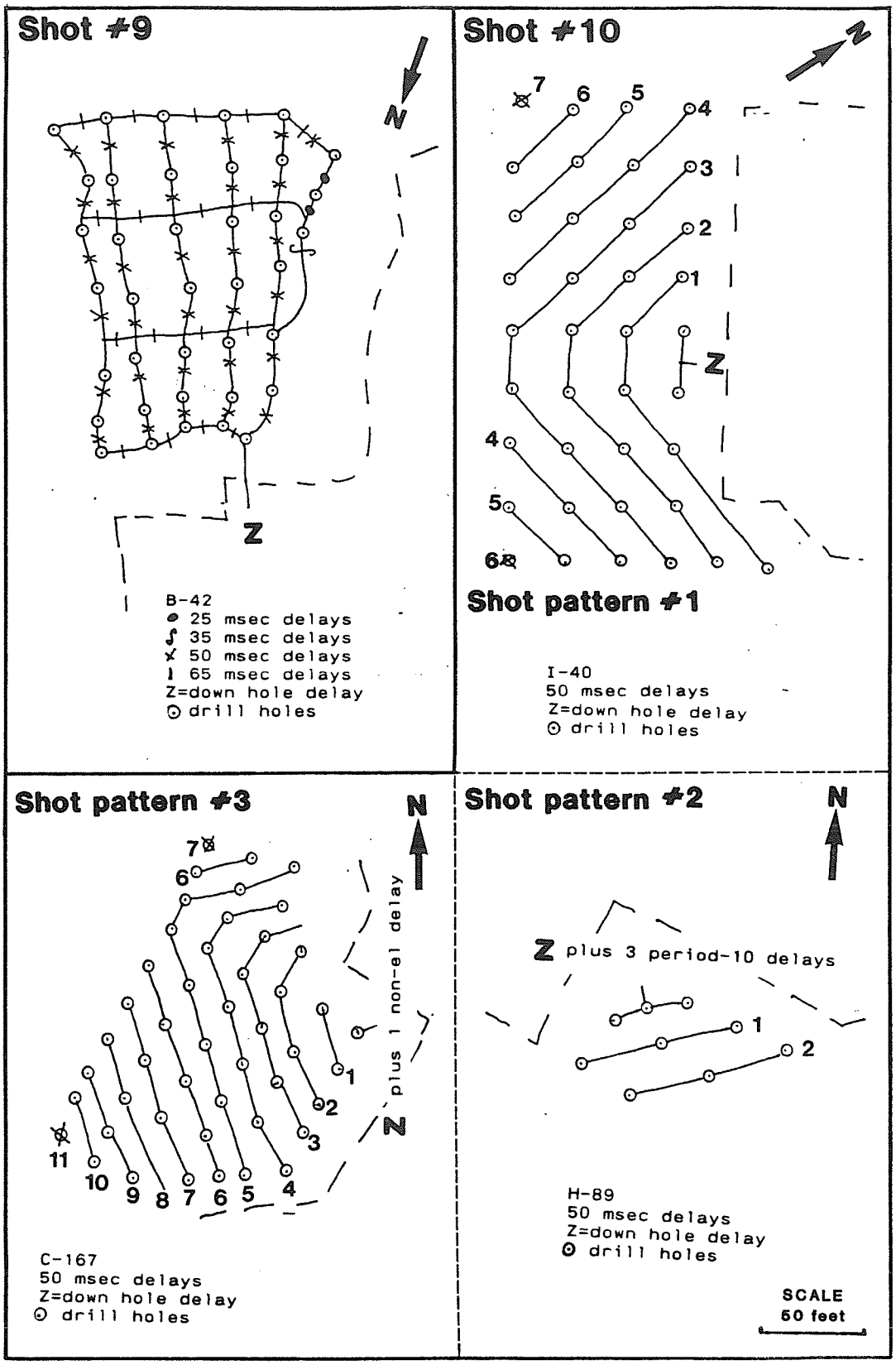

Figure F.6: Shot patterns used for shots #9 and #10.

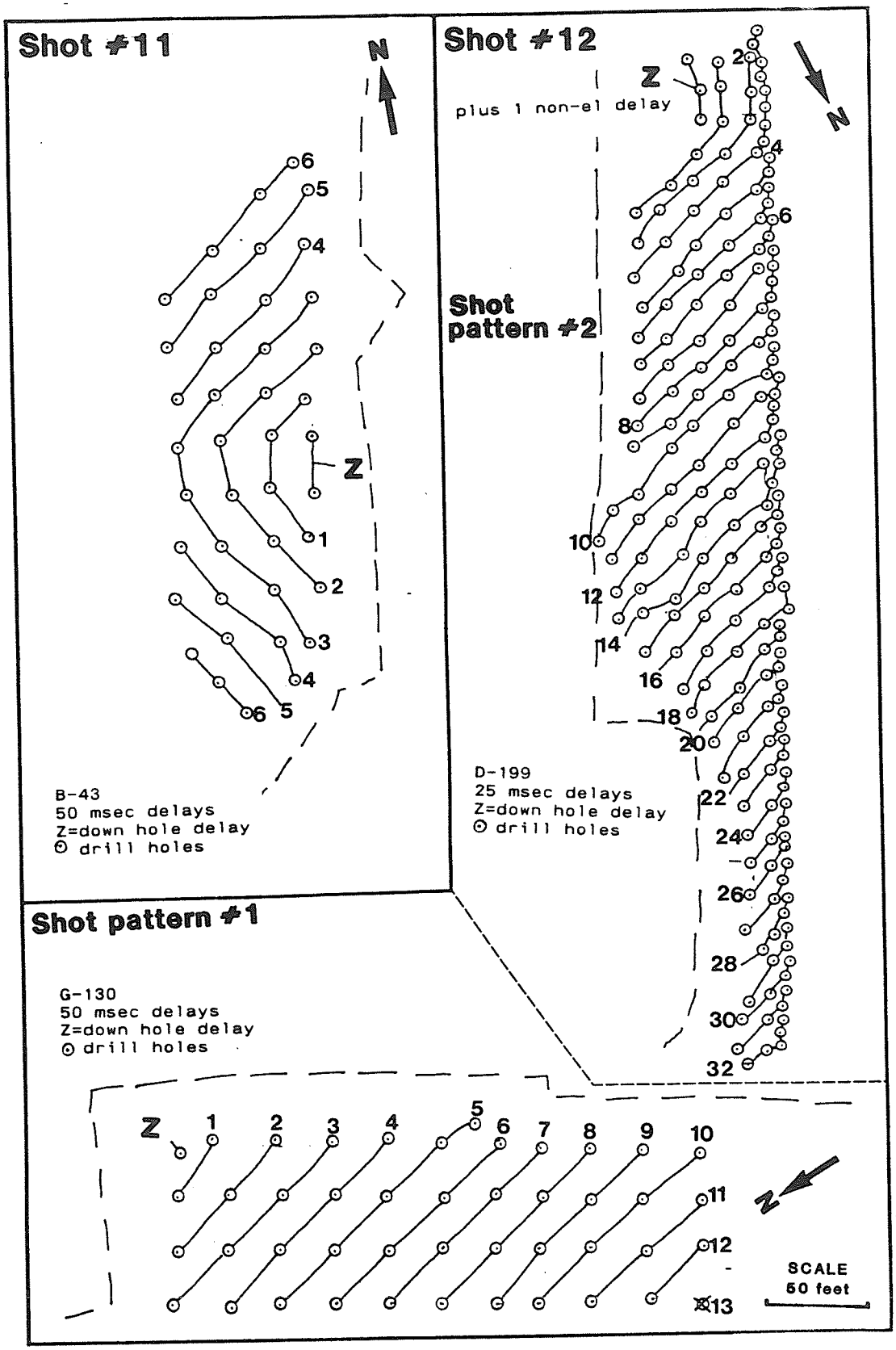

Figure F.7: Shot patterns used for shots #11 and #12.

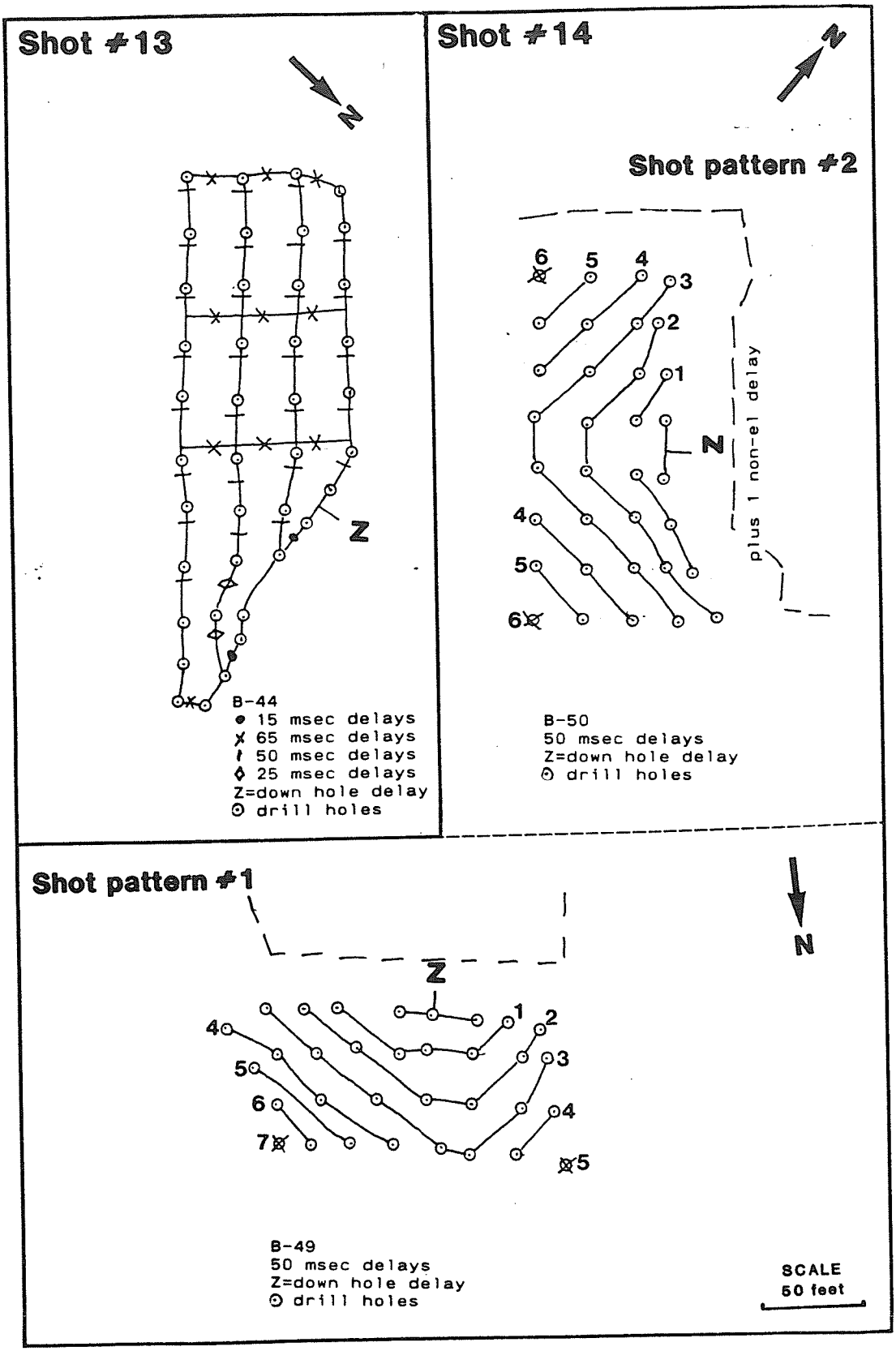

Figure F.8: Shot patterns used for shots #13 and #14.

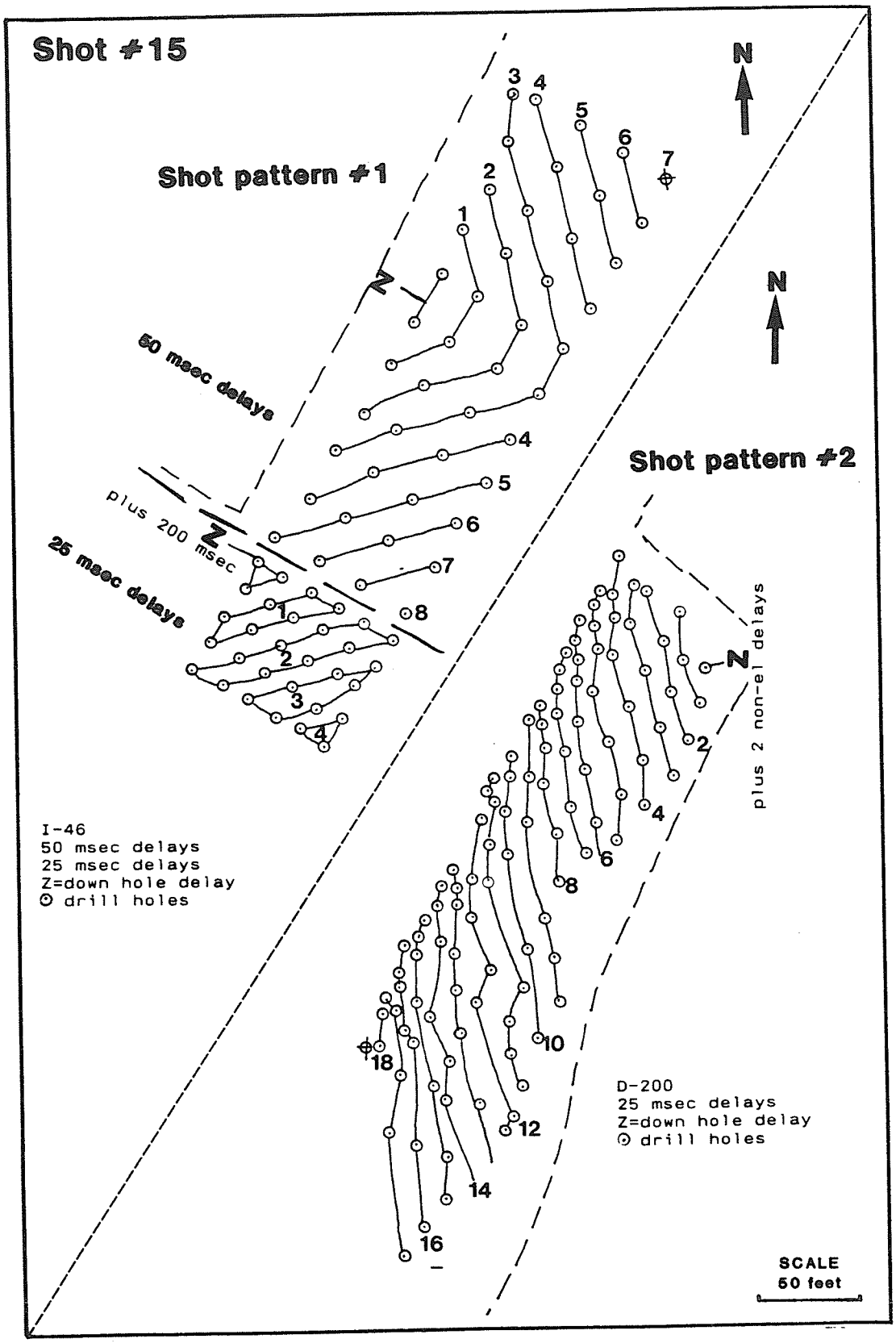

Figure F.9: Shot patterns used for shot #15.

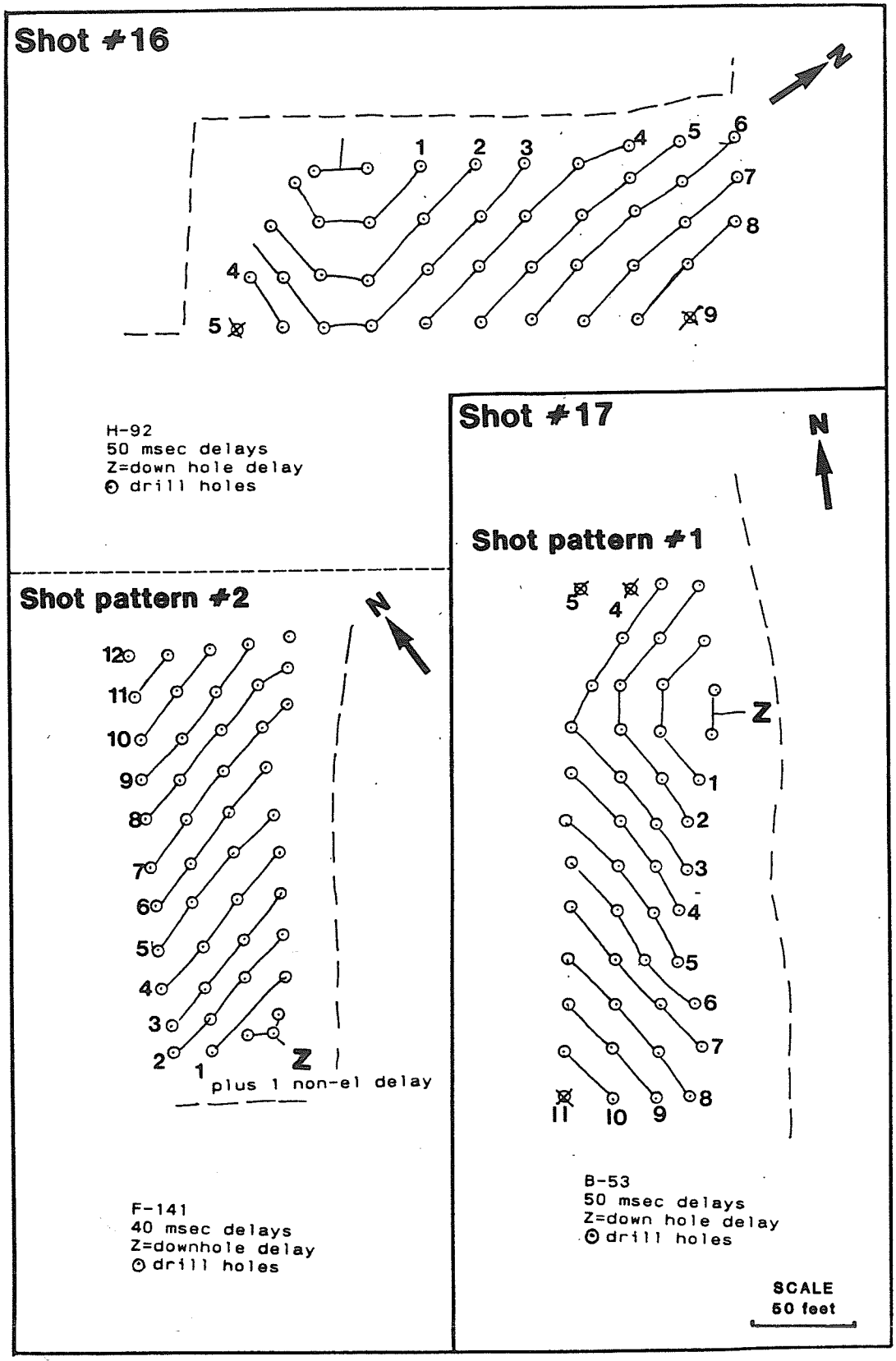

Figure F.10: Shot patterns used for shots #16 and #17.

Appendix G

PROGRAMS

Program SPLOT first reads each shot signal from tape then filters the record to a bandpass of 6-40 Hz using a Butterworth bandpass filter. The program then plots the signal.

```
C//BOBCAT JOB '1359,,,R=256,T=2M,I=200,L=09','SAM'
C/*D6250 SAM006 BIN 1616
C/*TAPE VPLOT
C/*TSO
C// EXEC FORTHCLG,USERLIB='SYS3.VPLOTLIB',SIZE=400K,OPT=2
C//FORT.SYSIN DD *
      INTEGER CT1,CT2,CT3,CT4,CT5,CT6,CT7,CT8,CT9,CT10,CT11,
     *        NBLK,ULIMIT
      REAL SHOT(10),RMAX,DATA1
      DIMENSION D(8),DATA(30000),TIME(30000)
      CALL BNDPAS(6.0,40.0,1.,D,G)
      READ(5,*) NPLOT,(SHOT(CT1),CT1=1,NPLOT)
      WRITE(6,*) NPLOT,(SHOT(CT1),CT1=1,NPLOT)
      DO 600 CT10=1,NPLOT
      READ(5,*) NWTRAC,NWHDER,SI,ULIMIT,ISTART
      NBLK=NWTRAC/5000+1
      RMAX=0.0
      TIME(2)=0.0
      WRITE(6,*) NWTRAC,NWHDER,SI,NBLK,ULIMIT,ISTART
      CT11=0
  700 CONTINUE
      CT1=-4999
      CT11=CT11+1
      WRITE(6,*) CT11
      IF(CT11.GE.500) GO TO 800
      DO 100 CT2=1,NBLK
      CT1=CT1+5000
      CT5=CT1+4999
      READ(8)  (DATA(CT4),CT4=CT1,CT5)
  100 CONTINUE
      IF(DATA(1).NE.SHOT(CT10)) GO TO 700
      CALL FILTER(DATA,NWTRAC,D,G,1)
      DO 200 CT3=3,NWTRAC
      DATA1=ABS(DATA(CT3))
      IF(DATA1.GT.RMAX) RMAX=ABS(DATA(CT3))
      CT8=CT3-1
      TIME(CT3)=TIME(CT8)+SI
  200 CONTINUE
      DO 300 CT6=3,NWTRAC
      CT7=CT6-2
      DATA(CT7)=DATA(CT6+ISTART)/RMAX
      IF(CT7.GT.ULIMIT) DATA(CT7)=0.0
      TIME(CT7)=TIME(CT6)
  300 CONTINUE
      DO 400 CT1=1,250
      WRITE(6,*) DATA(CT1),TIME(CT1),CT1
  400 CONTINUE
      CALL GRAPH(TIME,DATA,ULIMIT)
  600 CONTINUE
      GO TO 900
```

```
 800 CONTINUE
     WRITE(6,10)
 900 CONTINUE
     CALL PLOT(4.0,0.0,9999)
  10 FORMAT(' ','SHOT CANNOT BE FOUND')
     STOP
     END
C
C
C
C
     SUBROUTINE GRAPH(TAU,GTAU,ULIMIT)
     INTEGER ULIMIT,UL1,UL2,IBUF(6000)
     REAL TAU(30000),GTAU(30000)
     UL1=ULIMIT+1
     UL2=ULIMIT+2
     CALL PLOTS(IBUF,6000)
     CALL NEWPEN(2)
     CALL PLOT(0.0,-10.0,-3)
     CALL PLOT(0.0,0.5,-3)
     CALL FACTOR(.75)
     CALL SCALE(TAU,4.0,ULIMIT,1)
     CALL SCALE(GTAU,2.0,ULIMIT,1)
     CALL AXIS(0.0,0.0,'TIME',-4,4.0,0.0,TAU(UL1),TAU(UL2))
     CALL AXIS(0.0,0.0,'AMPLITUDE',9,2.0,90.0,GTAU(UL1),
    *         GTAU(UL2))
     CALL LINE(TAU,GTAU,ULIMIT,1,0,4)
     CALL PLOT(4.0,0.0,999)
     RETURN
     END
C
     SUBROUTINE BNDPAS(F1,F2,DELT,D,G)
     COMPLEX P(4),S(8),Z1,Z2
     DIMENSION D(8),XC(3),XD(3),XE(3)
     TWOPI=6.2831853
     WRITE (6,1) F1,F2,DELT
   1 FORMAT ('1 BANDPASS FILTER DESIGN FOR A BAND FROM ',F8.3,
    .'TO',F8.3,' HERTZ.',//' SAMPLE INTERVAL IS ',F5.2,
    .'MILLISECONDS.')
     DT=DELT/1000.0
     TDT=2.0/DT
     FDT=4.0/DT
     P(1)=CMPLX(-.3826834,.9238795)
     P(2)=CMPLX(-.3826834,-.9238795)
     P(3)=CMPLX(-.9238795,.3826834)
     P(4)=CMPLX(-.9238795,-.3826834)
     W1=TWOPI*F1
     W2=TWOPI*F2
     W1=TDT*TAN(W1/TDT)
     W2=TDT*TAN(W2/TDT)
     HWID=(W2-W1)/2.0
     WW=W1*W2
     DO 19 I=1,4
     Z1=P(I)*HWID
     Z2=Z1*Z1-WW
```

```
      Z2=CSQRT(Z2)
      S(I)=Z1+Z2
   19 S(I+4)=Z1-Z2
C     WRITE (6,2) S
    2 FORMAT ('-S PLANE POLES ARE AT:',/' ',8(/' ',E12.6,' + I '
     .,E12.6))
      G=.5/HWID
      G=G*G
      G=G*G
      DO 29 I=1,7,2
      B=-2.0*REAL(S(I))
      Z1=S(I)*S(I+1)
      C=REAL(Z1)
      A=TDT+B+C/TDT
      G=G*A
      D(I)=(C*DT-FDT)/A
   29 D(I+1)=(A-2.0*B)/A
      G=G*G
C     WRITE (6,3)
    3 FORMAT ('-FILTER IS (1-Z** 2)**4 / B1*B2*B3*B4')
C     WRITE (6,4) D
    4 FORMAT (4(/' B(I) = 1 + ',E12.6,' Z + ',E12.6,' Z**2'))
C     WRITE (6,5) G
    5 FORMAT ('-FILTER GAIN IS ',E12.6)
      RETURN
      END
C
C
C
C
C
      SUBROUTINE FILTER(X,N,D,G,IG)
      COMPLEX P(4),S(8),Z1,Z2
      DIMENSION D(8),X(30000),XC(3),XD(3),XE(3)
C
C      X = DATA VECTOR OF LENGTH N CONTAINING DATA TO BE FILTERED
C      D = FILTER COEFFICIENTS CALCULATED BY BNDPAS
C      G = FILTER GAIN
C      IG = 1 MEANS TO REMOVE THE FILTER GAIN SO THAT THE GAIN
C           IS UNITY
C
C      APPLY FILTER IN FORWARD DIRECTION
C
   31 XM2=X(1)
      XM1=X(2)
      XM=X(3)
      XC(1)=XM2
      XC(2)=XM1-D(1)*XC(1)
      XC(3)=XM-XM2-D(1)*XC(2)-D(2)*XC(1)
      XD(1)=XC(1)
      XD(2)=XC(2)-D(3)*XD(1)
      XD(3)=XC(3)-XC(1)-D(3)*XD(2)-D(4)*XD(1)
      XE(1)=XD(1)
      XE(2)=XD(2)-D(5)*XE(1)
      XE(3)=XD(3)-XD(1)-D(5)*XE(2)-D(6)*XE(1)
```

```
      X(1)=XE(1)
      X(2)=XE(2)-D(7)*X(1)
      X(3)=XE(3)-XE(1)-D(7)*X(2)-D(8)*X(1)
      DO 39 I=4,N
      XM2=XM1
      XM1=XM
      XM=X(I)
      K=I-((I-1)/3)*3
      GO TO (34,35,36),K
   34 M=1
      M1=3
      M2=2
      GO TO 37
   35 M=2
      M1=1
      M2=3
      GO TO 37
   36 M=3
      M1=2
      M2=1
   37 XC(M)=XM-XM2-D(1)*XC(M1)-D(2)*XC(M2)
      XD(M)=XC(M)-XC(M2)-D(3)*XD(M1)-D(4)*XD(M2)
      XE(M)=XD(M)-XD(M2)-D(5)*XE(M1)-D(6)*XE(M2)
   39 X(I)=XE(M)-XE(M2)-D(7)*X(I-1)-D(8)*X(I-2)
C
C     FILTER IN REVERSE DIRECTION
C
      XM2=X(N)
      XM1=X(N-1)
      XM=X(N-2)
      XC(1)=XM2
      XC(2)=XM1-D(1)*XC(1)
      XC(3)=XM-XM2-D(1)*XC(2)-D(2)*XC(1)
      XD(1)=XC(1)
      XD(2)=XC(2)-D(3)*XD(1)
      XD(3)=XC(3)-XC(1)-D(3)*XD(2)-D(4)*XD(1)
      XE(1)=XD(1)
      XE(2)=XD(2)-D(5)*XE(1)
      XE(3)=XD(3)-XD(1)-D(5)*XE(2)-D(6)*XE(1)
      X(N)=XE(1)
      X(N-1)=XE(2)-D(7)*X(1)
      X(N-2)=XE(3)-XE(1)-D(7)*X(2)-D(8)*X(1)
      DO 49 I=4,N
      XM2=XM1
      XM1=XM
      J=N-I+1
      XM=X(J)
      K=I-((I-1)/3)*3
      GO TO (44,45,46),K
   44 M=1
      M1=3
      M2=2
      GO TO 47
   45 M=2
      M1=1
```

```
      M2=3
      GO TO 47
   46 M=3
      M1=2
      M2=1
   47 XC(M)=XM-XM2-D(1)*XC(M1)-D(2)*XC(M2)
      XD(M)=XC(M)-XC(M2)-D(3)*XD(M1)-D(4)*XD(M2)
      XE(M)=XD(M)-XD(M2)-D(5)*XE(M1)-D(6)*XE(M2)
   49 X(J)=XE(M)-XE(M2)-D(7)*X(J+1)-D(8)*X(J+2)
      IF (IG.NE.1) RETURN
      DO 59 I=1,N
   59 X(I)=X(I)/G
      RETURN
      END
C//GO.FT08F001 DD UNIT=D6250,DISP=(OLD,PASS),VOL=SER=SAM006,
C// DSN=S01,LABEL=(01,,,IN),DCB=(RECFM=VBS,BLKSIZE=20008,
C// LRECL=20004)
C// DD UNIT=D6250,DISP=(OLD,PASS),VOL=SER=SAM006,DSN=S02,
C// LABEL=(02,,,IN),DCB=(RECFM=VBS,BLKSIZE=20008,LRECL=20004)
C//GO.VWORK DD DSN=&&VWORK,UNIT=SYSDA,DISP=(NEW,PASS),
C// SPACE=(CYL,(2,2))
C//GO.FT01F001 DD DSN=&&FT01F001,UNIT=SYSDA,DISP=(NEW,PASS),
C// SPACE=(18,(100,60))
C//GO.FT04F001 DD SYSOUT=A
C//GO.SYSIN DD *
2 1.0 2.0
27003 2 .001 2000 0
27003 2 .001 2000 600
C/*
C// EXEC VPLOT
C/*
```

```
      Program RICKER generates far field Ricker wavelets
      and stores them in a data set to be later read into
      the source generating program (SOURCE).
-----------------------------------------------------------
C
C//BOBCAT JOB '0117,,,R=50,T=30,I=50,L=9','SAM'
C/*TSO
C// EXEC FORTHCLG,USERLIB='SYS3.VPLOTLIB'
C//FORT.SYSIN DD *
      INTEGER LENGTH,N,M,NPLOT,OPTION,STDAT,ENDDAT,ZERO
      REAL DATA(5000),DATA1(5000),DATA2(5000),T(5000)
      REAL SI,VS,VP,A,B,R,K1,FREQO,START
      REAL START
      READ(5,*) NPLOT
      DO 2 I=1,NPLOT
      ITIME=0
      NTIME=0
      RMAX=0.0
      DO 6 N=1,5000
      DATA(N)=0.0
      DATA1(N)=0.0
      DATA2(N)=0.0
    6 CONTINUE
      READ(5,*) LENGTH,SI,START,OPTION
      READ(5,*) VS,VP,R,A,B,FREQO,K1
      T(1)=START
      DO 1 N=1,LENGTH
      CALL RICKER(DATA,T,VP,R,A,B,FREQO,K1,N,LENGTH)
      CALL SIGNAL(DATA,DATA1,DATA2,R,OPTION,N)
      M=N+1
      T(M)=T(N)+SI
      IF(ABS(DATA1(N)).GT.RMAX) ZERO=N
      IF(ABS(DATA2(N)).GT.RMAX) ZERO=N
      IF(ABS(DATA1(N)).GT.RMAX) RMAX=ABS(DATA1(N))
      IF(ABS(DATA2(N)).GT.RMAX) RMAX=ABS(DATA2(N))
    1 CONTINUE
    2 CONTINUE
      DO 3 N=1,LENGTH
      DATA1(N)=DATA1(N)/RMAX
      IF(OPTION.EQ.3) DATA2(N)=DATA2(N)/RMAX
      IF(ITIME.NE.0) GO TO 5
      IF(DATA1(N).GT.0.0000001) STDAT=N
      IF(DATA1(N).GT.0.0000001) ITIME=1
      IF(DATA2(N).GT.0.0000001) STDAT=N
      IF(DATA2(N).GT.0.0000001) ITIME=1
      WRITE(6,*) DATA1(N),DATA2(N),STDAT,N
    5 CONTINUE
      IF(NTIME.NE.0) GO TO 4
      M=LENGTH-N+1
      IF(DATA1(M).GT.0.0000001) ENDDAT=M
      IF(DATA1(M).GT.0.0000001) NTIME=1
      IF(DATA2(M).GT.0.0000001) ENDDAT=M
      IF(DATA2(M).GT.0.0000001) NTIME=1
      WRITE(6,*) DATA1(M),DATA2(M),ENDDAT,N,M
```

```
  4   CONTINUE
  3   CONTINUE
      ZERO=ZERO-STDAT+1
      LENGTH=ENDDAT-STDAT+1
      WRITE(9,10)  ZERO,LENGTH
      WRITE(9,20)  (DATA1(N),N=STDAT,ENDDAT)
      IF(OPTION.EQ.3)  WRITE(9,10)  ZERO,LENGTH
      IF(OPTION.EQ.3)  WRITE(9,20)  (DATA2(N),N=STDAT,ENDDAT)
  10  FORMAT(I5,I5)
  20  FORMAT(5F10.7)
      STOP
      END
C
C     SUBROUTINE TO GENERATE FAR FIELD RICKER WAVELET
C
      SUBROUTINE RICKER(DF,T,V,R,A,B,FREQO,K1,N,LENGTH)
      INTEGER N,I,LENGTH
      REAL T(5000),SI,A,B,R,K,K1,M,GAMMA1,GAMMA2,GAMMA3,GAMMA4,V,
     1     DF(5000),U,USQ,USQSQ,FREQO,HQ,DHQ,NUO,PI,F(5000)
      PI=3.141592654
      M=2.0*PI*FREQO/(V*SQRT(K1))
      K=4.0*PI*(A**2)*B*(FREQO**2)/((V**2)*K1*R)
      NUO=2.0*PI*FREQO/V
      GAMMA1=SQRT(PI)/2.0
      GAMMA2=3.0*SQRT(PI)/4.0
      GAMMA3=15.0*SQRT(PI)/8.0
      GAMMA4=105.0*SQRT(PI)/64.0
      U=NUO*(R-V*T(N))/(SQRT(K1)*SQRT(R))
      USQ=U**2
      USQSQ=USQ**2
      RNUM=-USQ/4
      IF(RNUM.LE.-75.0)  RNUM=-75.0
      IF(RNUM.GT.75.0)  RNUM=75.0
      HQ=SQRT(PI)*U*EXP(RNUM)/4
      DHQ=HQ*(1-USQ/2)/U
      DF(N)=-(K*M*V*DHQ)/(R*SQRT(R))
      F(N)=-(K*M*V*HQ)/(R*SQRT(R))
      RETURN
      END
C
C
C
      SUBROUTINE SIGNAL(DATA,DATA1,DATA2,DIST,OPTION,M)
      INTEGER OPTION
      REAL DATA1(15000),DATA(15000),DATA2(15000),DIST
      PHI=ATAN(DIST/130.0)
      IF(OPTION.NE.2)  DATA1(M)=DATA(M)*COS(PHI)
      IF(OPTION.EQ.2)  DATA1(M)=DATA(M)*SIN(PHI)
      IF(OPTION.EQ.3)  DATA2(M)=DATA(M)*SIN(PHI)
      RETURN
      END
C//GO.FT01F001 DD DSN=&&FT01F001,UNIT=SYSDA,DISP=(NEW,PASS),
C// SPACE=(CYL,(2,2))
C//GO.VWORK DD DSN=&&VWORK,UNIT=SYSDA,DISP=(NEW,PASS),
C// SPACE=(CYL,(2,2))
```

```
C//FT09F001 DD DSN=MAXWELL.IN.DATA,DISP=(OLD,KEEP),UNIT=DISK
C//GO.SYSIN DD *
```

Program CYLSOURCE generates cylindrical source wavelets and put them in a data set to be later read by the source generating program (SOURCE). Note that there are many options to this program listed under the sub-routine called SIGNAL.

```
C//BOBCAT JOB '0117,,,R=50,T=30,I=50,L=9','SAM'
C/*TSO
C// EXEC FORTHCLG,USERLIB='SYS3.VPLOTLIB',SIZE=500K
C//FORT.SYSIN DD *
      INTEGER NPLOT,LENGTH,OPTN1,OPTN2,STDAT,ENDDAT,ZERO
      REAL VS,VP,SMOD,R1,Z,A,DEPTH,PHI,TO,PO,RO,RELAMP,SI
      REAL GT(10000),T(10000)
      READ(5,*) NPLOT,OPTN2
      DO 3 I=1,NPLOT
      RMAX=0.0
      NMAX=0
      ITIME=0
      NTIME=0
      MMAX=0
      K=1
      READ(5,*) LENGTH,SI,START,OPTN1
      READ(5,*) VS,VP,R1,Z,A,DEPTH,TO,PO,RO,RELAMP
      SMOD=RO*(VS**2)
      T(1)=START
      DO 9 N=1,LENGTH
      GT(N)=0.0
      T(N)=0.0
   9  CONTINUE
      DO 2 J=1,LENGTH
      CALL SIGNAL(GT,T,VS,VP,SMOD,R1,Z,A,DEPTH,PHI,TO,PO,J,K,
     *            RELAMP,OPTN1)
      M=J+1
      T(M)=T(J)+SI
      IF(ABS(GT(J)).GT.RMAX) RMAX=ABS(GT(J))
   2  CONTINUE
      DO 5 N=1,LENGTH
      GT(N)=GT(N)/RMAX
      IF(ITIME.NE.0) GO TO 4
      IF(ABS(GT(N)).GT.0.0000001) STDAT=N
      IF(ABS(GT(N)).GT.0.0000001) ITIME=1
   4  CONTINUE
      IF(NTIME.NE.0) GO TO 6
      M=LENGTH-N+1
      IF(ABS(GT(M)).GT.0.0000001) ENDDAT=M
      IF(ABS(GT(M)).GT.0.0000001) NTIME=1
   6  CONTINUE
   5  CONTINUE
      RZERO=SQRT(Z**2+R1**2)/VP
      WRITE(6,*) RZERO
      RZERO=RZERO/SI+0.5
      ZERO=RZERO
      ZERO=ZERO-STDAT+1
```

```
      LENGTH=ENDDAT-STDAT+1
      WRITE(9,10)  STDAT,ZERO,LENGTH
      WRITE(9,20)  (GT(N),N=STDAT,ENDDAT)
   10 FORMAT(I5,I5,I5)
   20 FORMAT(5F10.7)
    3 CONTINUE
      STOP
      END
C
C ============================================================
C
C      SUBROUTINE SIGNAL GENERATES A FAR FIELD CYLINDRICAL
C      SOURCE WAVELET. THERE ARE SEVERAL OPTNIS OF THE
C      SUBROUTINE. THESE OPTION'S ARE:
C            1-VELOCITY OF DISPLACEMENT IN Z-DIRECTION (TOTAL)
C            2-DISPLACEMENT IN Z-DIRECTION (TOTAL)
C            3-VELOCITY OF DISPLACEMENT IN R-DIRECTION (TOTAL)
C            4-DISPLACEMENT IN R-DIRECTION (TOTAL)
C            5-VELOCITY OF DISPLACEMENT IN PHI-DIRECTION (TOTAL)
C            6-DISPLACEMENT IN PHI-DIRECTION (TOTAL)
C            7-VELOCITY OF DISPLACEMENT IN Z-DIRECTION (P-WAVE)
C            8-DISPLACEMENT IN Z-DIRECTION (P-WAVE)
C            9-VELOCITY OF DISPLACEMENT IN R-DIRECTION (P-WAVE)
C            10-DISPLACEMENT IN R-DIRECTION (P-WAVE)
C            11-VELOCITY OF DISPLACEMENT IN Z-DIRECTION (SV-WAVE)
C            12-DISPLACEMENT IN Z-DIRECTION (SV-WAVE)
C            13-VELOCITY OF DISPLACEMENT IN R-DIRECTION (SV-WAVE)
C            14-DISPLACEMENT IN R-DIRECTION (SV-WAVE)
C            15-SOURCE FUNCTION
C ============================================================
C
      SUBROUTINE SIGNAL(U,T,VS,VP,SMOD,R1,Z,A,DEPTH,PHI,TO,PO,CT1,
     *                  CT2,RELAMP,OPTN1)
      INTEGER CT1,CT2,OPTN1
      REAL T(10000),TAU1,TAU2,SI,VS,VP,VOL,AREA,DEPTH,A,R,R1,Z,PI,
     *     SMOD,PH11,PHI2,PHI3,PHI4,VALUE,COSQ,LEN
      REAL U(10000),UP,WP,USV,WSV,DUP,DWP,DUSV,DWSV,UTP,UTSV,UTSH,
     *     DUPT,DUTSV,DUTSH,UT,WT,DUT,DWT
      REAL PPT,QPT,PST,QSP,SST,DPPT,DPST,DQPT,DQST,DSST,DDPPT,DDPST
      REAL F1,F2,G1,G2
      PI=3.141592654
      PHI=ATAN(Z/R1)
      PHI2=PHI+PI/2
      R=SQRT(R1**2+Z**2)
      PHI3=2*PHI2
      COSQ=COS(PHI2)**2
      TAU1=T(CT1)-R/VP
      TAU2=T(CT1)-R/VS
      VOL=2*PI*DEPTH*(A**2)
      AREA=4*PI*A*DEPTH
      VALUE=4*PI*SMOD
      CALL IMPULS(PPT,DPPT,DDPPT,TAU1,TO,PO,PI)
      CALL IMPULS(PST,DPST,DDPST,TAU2,TO,PO,PI)
      QPT=PPT
      QST=PST
```

```
      SST=PST
      DQPT=DPPT
      DQST=DPST
      DSST=DPST
      F1=VOL*(1-2*(VS**2)*COSQ/(VP**2))/(VALUE*VP)
      G1=-AREA*(VS**2)*COS(PHI2)/(VALUE*VP*VP)
      F2=VOL*SIN(PHI3)/(VALUE*VS)
      G2=AREA*SIN(PHI2)/VALUE
      K=VOL*SIN(PHI2)/(VALUE*VS)
      UP=((F1*DPPT/R)+(G1*QPT/R))*SIN(PHI2)
      WP=-((F1*DPPT/R)+(G1*QPT/R))*COS(PHI2)
      USV=((F2*DPST/R)+(G2*QST/R))*COS(PHI2)
      WSV=((F2*DPST/R)+(G2*QST/R))*SIN(PHI2)
      VSH=K*SST/R
      DUP=((F1*DDPPT/R)+(G1*DQPT/R))*SIN(PHI2)
      DWP=-((F1*DDPPT/R)+(G1*DQPT/R))*COS(PHI2)
      DUSV=((F2*DDPST/R)+(G2*DQST/R))*COS(PHI2)
      DWSV=((F2*DDPST/R)+(G2*DQST/R))*SIN(PHI2)
      DVSH=K*DSST/R
      UT=UP+USV
      WT=WP+WSV
      VT=VSH
      DUT=DUP+DUSV
      DWT=DWP+DWSV
      DVT=DVSH
      IF(OPTN1.GT.15) GO TO 10
      IF(OPTN1.LE.0) GO TO 10
      IF(OPTN1.LE.1) U(CT1)=DWT
      IF(OPTN1.EQ.2) U(CT1)=WT
      IF(OPTN1.EQ.3) U(CT1)=DUT
      IF(OPTN1.EQ.4) U(CT1)=UT
      IF(OPTN1.EQ.5) U(CT1)=DVT
      IF(OPTN1.EQ.6) U(CT1)=VT
      IF(OPTN1.EQ.7) U(CT1)=DWP
      IF(OPTN1.EQ.8) U(CT1)=WP
      IF(OPTN1.EQ.9) U(CT1)=DUP
      IF(OPTN1.EQ.10) U(CT1)=UP
      IF(OPTN1.EQ.11) U(CT1)=DWSV
      IF(OPTN1.EQ.12) U(CT1)=WSV
      IF(OPTN1.EQ.13) U(CT1)=DUSV
      IF(OPTN1.EQ.14) U(CT1)=USV
      IF(OPTN1.EQ.15) U(CT1)=DVSH
      IF(OPTN1.EQ.16) U(CT1)=PPT
      GO TO 20
   10 CONTINUE
      CT2=CT2+1
      IF(CT2.EQ.1) WRITE(6,100)
  100 FORMAT(' ','ERROR IN SELECTING OPTN1 NUMBER')
      U(CT1)=0.0
   20 CONTINUE
      RETURN
      END
C
C  SUBROUTINE TO GENERATE SOURCE FUNCTION
C
```

```
      SUBROUTINE IMPULS(PT,DPT,DDPT,T,TO,PO,PI)
      REAL PT,DPT,T,TO,PO,PI,VAL
      VAL=(T**2)*PI/(TO**2)
      IF(VAL.GT.75.0) VAL=75.0
      IF(VAL.LT.-75.0) VAL=-75.0
      PT=PO/EXP(VAL)
      DPT=PT*(-2)*PI*T/(TO**2)
      DDPT=2*PI*PT*((2*(T**2)*PI/(TO**2))-1)/(TO**2)
      RETURN
      END
C//GO.FT01F001 DD DSN=&&FT01F001,UNIT=SYSDA,DISP=(NEW,PASS),
C// SPACE=(CYL,(2,2))
C//GO.VWORK DD DSN=&&VWORK,UNIT=SYSDA,DISP=(NEW,PASS),
C// SPACE=(CYL,(2,2))
C//FT09F001 DD DSN=MAXWELL.IN.DATA,DISP=(OLD,KEEP),UNIT=DISK
C//GO.SYSIN DD *
```

Program WREAD reads any wavelet and converts the dominant frequency (period) of that wavelet to any required frequency. The data is then stored in a data set to be input into the source generating program (SOURCE).

```
C//BOBCAT JOB '0117,,,R=50,T=1M,I=60,L=9','SAM'
C/*TSO
C// EXEC FORTHCLG,USERLIB='SYS3.VPLOTLIB',SIZE=500K
C//FORT.SYSIN DD *
      INTEGER OPTION,CT1,CT2,NPLOT
      INTEGER LENGTH
      REAL DATA(15000),PDATA(15000),SDATA(15000),DIST,PRD,RPRD,SI
      REAL T(15000)
      READ(5,*) NPLOT
      DO 3 CT1=1,NPLOT
      RMAX=0.0
      READ(5,*) LENGTH,SI,PRD,RPRD,DIST,ZPT,OPTION
      READ(5,10)  (DATA(CT2),CT2=1,LENGTH)
      CALL INTR(DATA,PDATA,LDATA,LENGTH,IZPT,ZPT,PRD,200.0,ZCONST)
      CALL INTR(PDATA,DATA,LENGTH,LDATA,IZPT,ZPT,200.0,RPRD,ZCONST)
      CALL SIGNAL(DATA,PDATA,SDATA,LENGTH,SI,DIST,RMAX,OPTION,T)
      CALL GRAPH(T,GT,CT2,LENGTH)
      WRITE(9,20)  IZPT,LENGTH
      WRITE(9,30)  (PDATA(CT2),CT2=1,LENGTH)
      IF(OPTION.EQ.3) WRITE(9,20)  IZPT,LENGTH
      IF(OPTION.EQ.3) WRITE(9,30)  (SDATA(CT2),CT2=1,LENGTH)
   10 FORMAT(5F10.7)
   20 FORMAT(I5,I5)
   30 FORMAT(5F10.7)
    3 CONTINUE
      CALL PLOT(4.0,0.0,9999)
      STOP
      END
C
C  SUBROUTINE TO INTERPOLATE DATA
C
      SUBROUTINE INTR(DATA,IDATA,LDATA,LDATA1,IZPT,ZPT,PRD,RPRD,Z)
      INTEGER ML,MB,CT1,LDATA,LTDATA
      REAL DATA(15000),IDATA(15000),R,Z,B,PRD,RPRD,SI
      Z=PRD/RPRD
      LDATA=LDATA1/Z
      ZPT=ZPT/Z+.5
      IZPT=ZPT
      R=0.0
      ML=0
      MB=0
      B=0.0
      DO 20 CT1=1,LDATA
      R=R+Z
      ML=R
      MB=R+1.0
      B=ML
      IDATA(CT1)=DATA(ML)+(DATA(MB)-DATA(ML))*(R-B)
```

```
  20 CONTINUE
     WRITE(6,100)
 100 FORMAT(' ','INTERPOLATION SUCCESSFULLY COMPLETED')
     RETURN
     END
C
C  GENERATES P AND S-WAVE SIGNALS
C
     SUBROUTINE SIGNAL(DATA,DATA1,DATA2,LDATA,SI,DIST,RMAX,
    *                  OPTION,T)
     INTEGER CT1,OPTION,LDATA
     REAL DATA1(15000),DATA(15000),DATA2(15000),SI,DIST,T(15000)
     PHI=ATAN(DIST/130.0)
     DO 1 CT1=1,LDATA
     IF(OPTION.NE.2) DATA1(CT1)=DATA(CT1)*COS(PHI)
     IF(OPTION.EQ.2) DATA1(CT1)=DATA(CT1)*SIN(PHI)
     IF(OPTION.EQ.3) DATA2(CT1)=DATA(CT1)*SIN(PHI)
     IF(ABS(DATA1(CT1)).GT.RMAX) RMAX=ABS(DATA1(CT1))
     IF(ABS(DATA2(CT1)).GT.RMAX) RMAX=ABS(DATA2(CT1))
   1 CONTINUE
     T(1)=0.000
     DO 2 CT1=1,LDATA
     DATA1(CT1)=DATA1(CT1)/RMAX
     DATA2(CT1)=DATA2(CT1)/RMAX
     N=CT1+1
     T(N)=T(CT1)+0.001
   2 CONTINUE
     RETURN
     END
C//GO.FT01F001 DD DSN=&&FT01F001,UNIT=SYSDA,DISP=(NEW,PASS),
C// SPACE=(CYL,(2,2))
C//GO.VWORK DD DSN=&&VWORK,UNIT=SYSDA,DISP=(NEW,PASS),
C// SPACE=(CYL,(2,2))
C//FT09F001 DD DSN=MAXWELL.IN.DATA,DISP=(OLD,KEEP),UNIT=DISK
C//GO.SYSIN DD *
```

Program SOURCE generates a source signal from a spike series and convolves with a wavelet(s) input into the program. The spike series are representations of the shot patterns used in the experiment. See the program listing for the options of the program.

```
C//BOBCAT JOB '0117,,,R=50,T=3M,I=500,L=9','SAM',CLASS=F
C/*TAPE   VPLOT
C/*TSO
C// EXEC FORTHCLG,USERLIB='SYS3.VPLOTLIB',SIZE=500K
C//FORT.SYSIN DD *
      INTEGER CT1,CT2,CT3,CT4,CT5,CT7,NPLOT,OPTN1,OPTN2,OPTN3
      INTEGER LENGTH,LTH,BLTH,EVTLTH,NSEG,NRFLN,NSHOTS(10),ZERO
      INTEGER DELAY(10),DELAY2(10),RFTIME(10),DELAY3(5),SLTH,PLTH
      INTEGER BPLTH,BSLTH
      REAL VS,VP,SMOD,R1,Z,A,DEPTH,PHI1,PHI2,TO,PO,RO,RCOEF
      REAL GT(20001),GPT(20001),GST(20001),T(20001),WPT(500),
     *     WST(500)
      REAL SP,START,SI,BLAST(20001),AMP(10,50),VAR1(5),VAR2(5),R(5)
      REAL GSPT(20001),GSST(20001),EVENTS(20001)
C
C ---------------------------------------------------
C                NUMBER OF DATA SETS TO BE GENERATED
C
      READ(5,*) NPLOT
      WRITE(6,*) NPLOT
      DO 3 CT1=1,NPLOT
C
C ---------------------------------------------------
C              READ AND WRITE PRELIMINARY INPUT DATA
C
      NTIME=1
      CALL READO(SP,OPTN2,OPTN3,OPTN1,LENGTH,VS,VP,R1,R,Z,
     *           NSPAT,SI,VAR1,VAR2,START)
C
C ---------------------------------------------------
C                                          ZERO ARRAYS
C
      DO 15 N=1,10000
      GT(N)=0.0
      GST(N)=0.0
      GPT(N)=0.0
      GSPT(N)=0.0
      GSST(N)=0.0
      BLAST(N)=0.0
      T(N)=1000/SI
   15 CONTINUE
C
C  ---------------------------------------------------
C                  READ SHOT PATTERN PARAMETERS AND
C           DERIVES THE DELAY BETWEEN SHOT PATTERNS
C
      DO 7 CT7=1,NSPAT
```

```
      CALL READ4(NSEG,NSHOTS,DELAY,DELAY2,DELAY3,AMP,CT7,VP,Z,
     *           R1,VAR1)
      IF(NSPAT.EQ.1) DELAY3(1)=0
C
C  ------------------------------------------------
C  GENERATES SERIES OF SPIKES FOR EACH SHOT PATTERN
C
      CALL OPER(AMP,BLAST,BLTH,NSHOTS,SI,DELAY,DELAY2,NSEG,
     *          DELAY3,CT7)
   99 FORMAT('NSEG=',7X,I2,'BLTH=',7X,I4)
   98 FORMAT(10F4.2)
    7 CONTINUE
C
C  ------------------------------------------------
C                                    READ WAVELET(S)
C
      IF(OPTN2.EQ.2) GO TO 8
      READ(5,10) ZERO,PLTH
      READ(5,20) (WPT(N),N=1,PLTH)
      IF(OPTN2.NE.3) GO TO 9
    8 READ(5,10) ZERO,SLTH
      READ(5,20) (WST(N),N=1,SLTH)
    9 CONTINUE
C
C  ------------------------------------------------
C               GENERATE SPIKE SERIES TO REPRESENT
C               DIFFERENT ARRIVALS
C
      VS2=VAR1(1)
      VP2=VAR2(1)
      DEPTH=VAR1(2)
      NTIMED=0
      VEL=VP
      VEL2=VP2
      IF(OPTN2.EQ.2) VEL=VS
      IF(OPTN2.EQ.2) VEL2=VS2
    5 IF(OPTN2.EQ.3.AND.NTIMED.EQ.1) VEL=VS
      IF(OPTN2.EQ.3.AND.NTIMED.EQ.1) VEL2=VS2
      DO 19 N5=1,10000
      EVENTS(N5)=0.0
   19 CONTINUE
      IF(OPTN1.EQ.1) CALL DRAY(EVENTS,R,Z,VEL,SI,NTIMED,EVTLTH,
     *                         OPTN2,OPTN3)
      IF(OPTN1.EQ.2) READ(5,*) EVTLTH
      IF(OPTN1.EQ.2) READ(5,20) (EVENTS(N),N=1,EVTLTH)
C    6 CONTINUE
C
C  ------------------------------------------------
C                            GENERATE SOURCE SIGNAL
C
      IF(NTIMED.EQ.2) GO TO 17
      BPLTH=BLTH
      BSLTH=BLTH
      IF(OPTN2.EQ.2) GO TO 16
      CALL CONV(START,T,GPT,BLAST,BPLTH,WPT,PLTH,SI)
```

```
  16 IF(OPTN2.GT.1) CALL CONV(START,T,GST,BLAST,BSLTH,WST,SLTH,SI)
     LENGTH=BLTH
     DIST=R(1)
     IF(OPTN2.EQ.2) GO TO 17
     CALL CONV(START,T,GSPT,EVENTS,EVTLTH,GPT,BPLTH,SI)
     CALL TIME(GSPT,T,EVTLTH,SI,START,ZERO)
     IF(OPTN2.EQ.3.AND.NTIMED.EQ.1) GO TO 5
  17 IF(OPTN2.GT.1) CALL CONV(START,T,GSST,EVENTS,EVTLTH,GST,
    *                          BSLTH,SI)
     IF(OPTN2.GT.1) CALL TIME(GSST,T,EVTLTH,SI,START,ZERO)
     LENGTH=EVTLTH
     CALL AD(GT,GSPT,GSST,LENGTH)
C
C  ------------------------------------------------
C                   NORMALIZE AND PLOT SOURCE SIGNAL
C
     CALL NORMLZ(GT,LENGTH)
     CT111=CT1
     CALL GRAPH(T,GT,N,LENGTH,SP)
C
C  ------------------------------------------------
C                    SIGNIFY END OF CURRENT DATA SET
C
     WRITE(6,50) CT1
  10 FORMAT(I5,I5)
  20 FORMAT(5F10.7)
  21 FORMAT(5F12.7)
  50 FORMAT(//' ','----------------',,'PLOT ',I1,' COMPLETED',
    *       '----------------')
   3 CONTINUE
     CALL PLOT(8.0,0.0,9999)
  11 FORMAT(' ',2X,'SHOT=',I2,2X,'OPTN1=',I2,2X,'OPTN2=',I1,
    *       2X,'OPTN3=',I1)
     STOP
     END
C
C ========================================================
C      SUBROUTINE READO READS AND WRITES PRELIMINARY
C      INPUT DATA.
C           OPTN1 REPRESENTS THE TYPE OF ARRIVALS TO INPUT
C                 1-ONLY DIRECT RAYS
C                 2-INPUT SPIKE SERIES FROM OTHER PROGRAM
C                   REPRESENTING DIFFERENT ARRIVALS
C           OPTN2 REPRESENTS TYPE OF WAVES
C                 1-P-WAVE ONLY
C                 2-S-WAVE ONLY
C                 3-BOTH P AND S-WAVE
C           OPTN3 REPRESENTS TYPE OF WAVELET
C                 1-CYLINDRICAL SOURCE WAVELET
C                 2-RICKER OR SPHERICAL SOURCE WAVELET
C ========================================================
C
     SUBROUTINE READO(SP,OPTN2,OPTN3,OPTN1,LENGTH,VS,VP,R1,R,Z,
    *                 NSPAT,SI,VAR1,VAR2,START)
      INTEGER OPTN2,OPTN3,OPTN1,CT1,LENGTH,NSPAT
```

```
      REAL VS,VP,R1,R(5),Z,SI,VAR1(5),VAR2(5),SP,START
      READ(5,10) SP,OPTN1,OPTN2,OPTN3
      WRITE(6,70) SP,OPTN1,OPTN2,OPTN3
      READ(5,20) LENGTH,SI,NSPAT,START
      WRITE(6,80) LENGTH,SI,NSPAT,START
      READ(5,30) VS,VP,Z,GRAD,(R(CT1),CT1=1,NSPAT)
      R1=R(1)
      WRITE(6,90) VS,VP,R1,Z
      READ(5,*) (VAR1(CT1),VAR2(CT1),CT1=1,4)
      WRITE(6,120) (VAR1(CT1),VAR2(CT1),CT1=1,4)
   10 FORMAT(//5X,F4.1,10X,I1,10X,I1,10X,I1)
   20 FORMAT(6X,I5,5X,F5.3,21X,I2,8X,F6.3)
   30 FORMAT(5X,F6.1,7X,F6.1,8X,F6.2,8X,F5.3,8X,5F8.2)
   40 FORMAT(9X,F4.1,7X,F5.1,4X,F6.4,4X,F4.1,9X,F4.2)
   50 FORMAT(6X,F4.1,15X,I1,4X,5F5.2)
   60 FORMAT(9X,8F5.1)
   70 FORMAT(' ','SHOT #',F3.1,', OPTN1=',I2,', OPTN2=',I2,
     *       ', OPTN3=',I2)
   80 FORMAT(' ','LDATA=',I5,', SI=',F5.3,', NSPAT=',I1,
     *      ', START='F5.3)
   90 FORMAT(' ','SVEL=',F6.1,', PVEL=',F6.1,', HDIST=',F6.1,
     *       ', VDIST=',F5.1)
  100 FORMAT(' ','DIAMETER=',F4.1,', DEPTH=',F5.1,', TO=',F6.4,
     *       ', PO=',F4.1,', DENSITY=',F4.2)
  110 FORMAT(' ','RCOEF=',F4.1,', # OF RFLECTNS=',I1,4X,10F5.2)
  120 FORMAT(' ','VARIABLES',8F7.1)
      RETURN
      END
C
C ========================================================
C     SUBROUTINE READ4 READS INPUT PARAMETERS FOR
C     SHOT PATTERN BEING CONSIDERED.
C ========================================================
C
      SUBROUTINE READ4(NSEG,NSHOTS,DELAY,DELAY2,DELAY3,AMP,CT4,
     *                 VP,Z,R,VAR1)
      INTEGER CT1,CT2,CT3,CT4,CT5,NSEG,NSHOTS(10),NSHOT,DELAY(10),
     *        DELAY2(10),DELAY3(5)
      REAL AMP(10,50),R(5),R1,R2,R3,Z,DIST,GRAD,VAR1(5),D,D1,D2,
     *     PHI1,PHI2,VP
      DELAY3(1)=0
      READ(5,10) NSEG
      WRITE(6,70) NSEG
      READ(5,20) (NSHOTS(CT1),CT1=1,NSEG)
      WRITE(6,80) (NSHOTS(CT2),CT2=1,NSEG)
      READ(5,30) (DELAY(CT1),CT1=1,NSEG)
      WRITE(6,90) (DELAY(CT2),CT2=1,NSEG)
      READ(5,40) (DELAY2(CT1),CT1=1,NSEG)
      WRITE(6,100) (DELAY2(CT2),CT2=1,NSEG)
      DO 1 CT1=1,NSEG
      NSHOT=NSHOTS(CT1)
      READ(5,50) (AMP(CT1,CT2),CT2=1,NSHOT)
      WRITE(6,110) CT1,(AMP(CT1,CT2),CT2=1,NSHOT)
    1 CONTINUE
      READ(5,*) R3,DLAY
```

```
      WRITE(6,*) R3,DLAY
      R1=R(1)
      R2=R(CT4)
      DHT=0.230
      IF(CT4.EQ.1) DHT=0.0
      D=R1**2+Z**2
      D1=SQRT(D)
      D=R2**2+Z**2
      D2=SQRT(D)
      CT5=CT4+1
      DELAY3(CT4)=(DLAY+DHT+(R3/6.56)+((D2-D1)/VP))*1000.0
    7 CONTINUE
      WRITE(6,99) DELAY3(CT4),DLAY,DHT,R3,D2,D1
   99 FORMAT(' ','DELAY3=',I4,5X,5F6.1)
   10 FORMAT(30X,I2)
   20 FORMAT(36X,15I2)
   30 FORMAT(27X,15I4)
   40 FORMAT(24X,15I4)
   50 FORMAT(20X,15F4.2)
   70 FORMAT(' ','# OF SEGMENTS IN SHOT PATTERN',I2)
   80 FORMAT(' ','# OF SHOTS IN EACH SEGMENT=',15I2)
   90 FORMAT(' ','DELAYS WITHIN EACH SEGMENT=',15I4)
  100 FORMAT(' ','DELAYS BETWEEN EACH SEGMENT=',15I4)
  110 FORMAT(' ','SPIKES OF SEGMENT #',I2,15F4.1)
      RETURN
      END
C
C ========================================================
C     SUBROUTINE TIME ALLOCATES TIMES TO THE DATA SUCH
C     THAT THE REQUIRED FIRST ARRIVALS ARRIVE AT THE PROPER
C     TIME.
C ========================================================
C
      SUBROUTINE TIME(DATA,T,LDATA,SI,START,ZERO)
      INTEGER N1,N2,N3,LDATA,LDATA1,ZERO
      REAL DATA(20001),DATA1(20001),T(20001)
      REAL SI,START
      N2=ZERO
      DO 1 N1=1,LDATA
      DATA1(N1)=DATA(N2)
      N2=N2+1
    1 CONTINUE
      N2=START/SI+0.5
      LDATA=LDATA-ZERO+1
      DO 2 N1=1,LDATA
      N2=N2+1
      IF(N2.GT.0) DATA(N1)=DATA1(N2)
      IF(N2.LE.0) DATA(N1)=0.0
      T(N1)=START+N1*SI
    2 CONTINUE
  100 FORMAT(' ','TIME SUCCESSFULLY COMPLETED')
      RETURN
      END
C
C
```

```
C ========================================================
C     SUBROUTINE DRAY DERIVES A SPIKE SERIES TO
C     REPRESENT THE ARRIVAL OF A DIRECT RAY.
C ========================================================
C
      SUBROUTINE DRAY(EVENTS,R,Z,VEL,SI,NTIMED,MAXTIM,OPTN2,OPTN3)
      INTEGER OPTN2,OPTN3
      REAL PHI1,PHI2,R,Z,DIST,ARRVAL,EVENTS(20001)
      PI=3.141592654
      PHI1=ATAN(Z/R)+PI/2
      PHI2=ATAN(R/Z)
      DIST=SQRT(R**2+Z**2)
      TIME=DIST/VEL
      IF(OPTN2.EQ.2) GO TO 2
      IF(OPTN2.EQ.3.AND.NTIMED.GT.0) GO TO 2
      ARRVAL=COS(PHI2)/SQRT(R*R*R*R*R)
      IF(OPTN3.EQ.1) ARRVAL=-COS(PHI1)*COS(PHI2)
      GO TO 3
    2 ARRVAL=SIN(PHI2)/SQRT(R*R*R*R*R)
      IF(OPTN3.EQ.1) ARRVAL=SIN(PHI1)*SIN(PHI2)
    3 CONTINUE
      ITIME=TIME/SI+0.5
      ITIME=ITIME+1
      DO 4 N=1,ITIME
      EVENTS(N)=0.0
      IF(N.EQ.ITIME) EVENTS(N)=ARRVAL
    4 CONTINUE
      MAXTIM=ITIME
      NTIMED=NTIMED+1
      RETURN
      END
C
C ========================================================
C     SUBROUTINE AD ADDS THE DIFERENT TYPES OF
C     WAVES TOGETHER
C ========================================================
C
      SUBROUTINE AD(DATA,DATA1,DATA2,LDATA)
      INTEGER CT1,LDATA
      REAL DATA1(20001),DATA(20001),DATA2(20001)
      DO 1 CT1=1,LDATA
      DATA(CT1)=DATA1(CT1)+DATA2(CT1)
    1 CONTINUE
      RETURN
      END
C
C ========================================================
C     SUBROUTINE CONV IS A SIMPLE CONVOLUTION ROUTINE
C     WHICH TAKES AN OPERATOR (WAVELET) AND CONVOLVES
C     IT WITH A DATA SET (DATA). SINCE THE OPERATOR IS
C     IS OFTEN AS LONG OR LONGER THAN THE LENGTH OF THE
C     DATA SET, ZEROES ARE ADDED TO THE FRONT OF THE
C     DATA SET. THE NUMBER OF ZEROES IS EQUAL TO THE
C     LENGTH OF THE OPERATOR. THIS IS VALID SINCE THE
C     DATA AT THE BEGINNING OF THE DATA SET IS ESSENT-
```

```
C      IALLY ZERO.
C ========================================================
C
      SUBROUTINE CONV(START,TIME,DATA2,DATA,LDATA,OPTOR,OPLTH,SI)
      INTEGER CT1,CT2,CT3,CT4,LDATA1,LDATA2,LDATA,OPLTH,
     *        DELAY(10),DELAY2(10)
      REAL START,DATA(20001),DATA1(20001),OPTOR(500),TIME(20001),
     *     DATA2(20001)
      DO 1 CT1=1,10000
      DATA2(CT1)=0.0
    1 CONTINUE
      LDATA1=LDATA+OPLTH-1
      LDATA2=LDATA1+OPLTH-1
      TIME(1)=START
      DO 10 CT1=1,LDATA2
      CT2=CT1-(OPLTH-1)
      IF(CT2.LE.0) DATA1(CT1)=0.0
      IF(CT2.GT.0.AND.CT1.LE.LDATA1) DATA1(CT1)=DATA(CT2)
      IF(CT1.GT.LDATA1) DATA1(CT1)=0.0
   10 CONTINUE
      DO 200 CT1=1,LDATA1
      DATA2(CT1)=0.0
      CT2=CT1
      DO 100 CT3=1,OPLTH
      CT4=OPLTH-CT3+1
      DATA2(CT1)=DATA1(CT2)*OPTOR(CT4)+DATA2(CT1)
      CT2=CT2+1
  100 CONTINUE
  200 CONTINUE
      LDATA=LDATA1
   20 FORMAT(5F10.7)
      RETURN
      END
C
C ========================================================
C     SUBROUTINE OPER GENERATES A SERIES OF SPIKES
C     TO REPRESENT EACH SHOT IN A BLAST. THE AMPLITUDE
C     OF EACH SPIKE DEPENDS ON THE NUMBER OF SHOTS
C     EXPLODING AT ANY PARTICULAR TIME. THE SERIES OF
C     SPIKES WILL THEN BE CONVOLVED WITH A WAVELET TO
C     GENERATE THE SOURCE SIGNAL.
C ========================================================
C
      SUBROUTINE OPER(AMP,OPR1,LTH1,NSHOTS,SI,DELAY,DELAY2,
     *                NSEG,DELAY3,CT4)
      INTEGER CT1,CT2,CT3,DELAY(10),DELAY2(10),NSHOTS(10),NSEG,
     *        LTH,BLTH,LTH1,DELAY3(5),CT4
      REAL AMP(10,50),OPR(20001),OPR1(20001),SI,BLAST(20001)
      DO 1 CT1=1,20001
      OPR(CT1)=0.0
    1 CONTINUE
      DO 3 CT1=1,NSEG
      CALL OP(AMP,BLAST,BLTH,NSHOTS,SI,DELAY,CT1)
      LTH=BLTH+DELAY2(CT1)
      DO 2 CT2=1,LTH
```

```
      CT3=CT2-DELAY2(CT1)
      IF(CT3.LE.0)  BLAST(CT3)=0.0
      OPR(CT2)=OPR(CT2)+BLAST(CT3)
    2 CONTINUE
    3 CONTINUE
      LTH1=LTH+DELAY3(CT4)
      DO 4 CT1=1,LTH1
      CT2=CT1-DELAY3(CT4)
      IF(CT2.LE.0)  CT2=2
      OPR1(CT1)=OPR1(CT1)+OPR(CT2)
    4 CONTINUE
      RETURN
      END
C
C ========================================================
C     SUBROUTINE OP GENERATES A SERIES OF SPIKES
C     WHICH REPRESENTS PART OF THE OPERATOR REPRESENT-
C     THE BLAST. THE OPERATORS GENERATED IN THIS SUB-
C     ROUTINE ARE ADDED TOGETHER IN OPER TO GENERATE
C     A COMPLETE OPERATOR TO REPRESENT THE BLAST.
C ========================================================
C
      SUBROUTINE OP(AMP,BLAST,BLTH,NSHOTS,SI,DELAY,CT2)
      INTEGER CT1,CT2,CT3,NSHOTS(10),DELAY(10),LENGTH,BLTH,
     *        MOD1,IDSAMP
      REAL BLAST(20001),AMP(10,50),OPR(20001),SI,RDSAMP,RDELAY
      CT1=2
      RDELAY=DELAY(CT2)
      RDSAMP=RDELAY/(SI*1000)+0.1
      IDSAMP=RDSAMP
      BLTH=NSHOTS(CT2)*IDSAMP-IDSAMP+1
      BLAST(1)=AMP(CT2,1)
      IF(DELAY(CT2).EQ.0)  RETURN
      DO 30 CT3=2,BLTH
      MOD1=MOD(CT3,IDSAMP)
      IF(MOD1.EQ.1)  GO TO 10
      BLAST(CT3)=0
      GO TO 20
   10 BLAST(CT3)=AMP(CT2,CT1)
      CT1=CT1+1
   20 CONTINUE
   30 CONTINUE
      RETURN
      END
C
C ============================================================
C     SUBROUTINE NORMLZ NORMALIZES THE SOURCE SIGNAL
C     DATA TO 'ONE'.
C ============================================================
C
      SUBROUTINE NORMLZ(GT,LENGTH)
      REAL GMAX,GT(20001),GTAU
      INTEGER CT1,CT2,LENGTH
      GMAX=0.0
      DO 1 CT1=1,LENGTH
```

```
      GTAU=GT(CT1)
      IF(ABS(GTAU).GT.GMAX)  GMAX=ABS(GTAU)
    1 CONTINUE
      WRITE(6,10)  GMAX
      DO 2 CT2=1,LENGTH
      GT(CT2)=GT(CT2)/GMAX
    2 CONTINUE
   10 FORMAT(' ','GMAX=',F15.10)
      RETURN
      END
C
C ================================================================
C     SUBROUTINE GRAPH PLOTS THE FINAL SOURCE SIGNAL
C ================================================================
C
      SUBROUTINE GRAPH(TAU,GTAU,N,LENGTH,SHOT)
      INTEGER IBUF,LENGTH,LENTH1,LENTH2
      REAL TAU(20001),GTAU(20001)
      DO 11 NN=LENGTH,4000
      GTAU(NN)=0.0
      NN2=NN-1
      TAU(NN)=TAU(NN2)+0.001
   11 CONTINUE
      LENGTH=8000
      LENTH1=LENGTH+1
      LENTH2=LENGTH+2
C     CALL SIZE(12.0)
      CALL PLOTS(IBUF,8000)
      CALL PLOT(0.0,-11.0,-3)
      CALL PLOT(0.0,0.5,-3)
C     CALL FACTOR(2.0)
      CALL NEWPEN(2)
      CALL FACTOR(0.75)
      CALL SCALE(TAU,8.0,LENGTH,1)
      CALL SCALE(GTAU,2.0,LENGTH,1)
      CALL AXIS(0.0,0.0,'TIME',-4,8.0,0.0,TAU(LENTH1),TAU(LENTH2))
      CALL AXIS(0.0,0.0,'AMPLITUDE',9,2.0,90.0,GTAU(LENTH1),
     *          GTAU(LENTH2))
      CALL LINE(TAU,GTAU,LENGTH,1,0,4)
      CALL NUMBER(0.96,2.4,0.07,SHOT,0.,1)
      CALL PLOT(8.0,0.0,999)
      RETURN
      END
C//GO.FT01F001 DD DSN=&&FT01F001,UNIT=SYSDA,DISP=(NEW,PASS),
C// SPACE=(CYL,(2,2))
C//GO.VWORK DD DSN=&&VWORK,UNIT=SYSDA,DISP=(NEW,PASS),
C// SPACE=(CYL,(2,2))
C//GO.SYSIN DD *
2 ---------------EXAMPLE DATA SET-------------------
-----------------SHOT #1 ( H-84) -------------------
-------------------------------------------------
SHOT= 1.0, OPTION1=1, OPTION2=3, OPTION3= 1
LDATA= 1000, SI=0.001, # OF SHOT PATTERNS= 1, START= 0.0
SVEL=3000.0, PVEL=4700.0, VDIST=102.00, VGRAD=0.000, HDIST=  441.96
4000.0 5700.0 100.0 1.0 1.0 1.0 1.0 1.0
```

```
 # OF SEGMENTS IN SHOT PATTERN= 1
 # OF SHOTS WITHIN EACH SHOT PATTERN=12
 DELAYS WITHIN EACH SEGMENT=  50
 DELAYS BETWEEN SEGMENTS=   0
 SPIKES OF SEGMENT  #1 1.0 2.0 3.0 4.0  4.0 5.0 4.0 4.0  4.0 3.0 2.0
1.0
 0.0 0.0
 -------------SHOT #2 (H-86 AND I-36)----------------
 ------------------------------------------------
 SHOT= 2.0, OPTION1=1, OPTION2=3, OPTION3= 1
 LDATA= 1000, SI=0.001, # OF SHOT PATTERNS= 2, START= 0.0
 SVEL=3500.0, PVEL=5700.0, VDIST=102.00, VGRAD=0.000, HDIST=  219.46
405.38
 4000.0 6000.0 120.0 1.0 1.0 1.0 1.0 1.0
 # OF SEGMENTS IN SHOT PATTERN= 4
 # OF SHOTS WITHIN EACH SHOT PATTERN=24242424
 DELAYS WITHIN EACH SEGMENT=  50  50  50  50
 DELAYS BETWEEN SEGMENTS=   0  65  65  65  65
 SPIKES OF SEGMENT  #1 1.0 1.0 1.0 1.0  1.0 1.0 1.0 1.0  1.0 1.0 1.0
1.0 1.0 1.0 1
 SPIKES OF SEGMENT #1 1.0 1.0 1.0 1.0 1.0 1.0 1.0 1.0 1.0
 SPIKES OF SEGMENT  #2 1.0 1.0 1.0 1.0  1.0 1.0 1.0 1.0  1.0 1.0 1.0
1.0 1.0 1.0 1
 SPIKES OF SEGMENT #2 1.0 1.0 1.0 1.0 1.0 1.0 1.0 1.0 1.0
 SPIKES OF SEGMENT  #3 1.0 1.0 1.0 1.0  1.0 1.0 1.0 1.0  1.0 1.0 1.0
1.0 1.0 1.0 1
 SPIKES OF SEGMENT #3 1.0 1.0 1.0 1.0 1.0 1.0 1.0 1.0 1.0
 SPIKES OF SEGMENT  #4 1.0 1.0 1.0 1.0  1.0 1.0 1.0 1.0  1.0 1.0 1.0
1.0 1.0 1.0 1.
 SPIKES OF SEGMENT #4 1.0 1.0 1.0 1.0 1.0 1.0 1.0 1.0 1.0
 0.0 0.0
 # OF SEGMENTS IN SHOT PATTERN= 1
 # OF SHOTS WITHIN EACH SHOT PATTERN= 7
 DELAYS WITHIN EACH SEGMENT=  50
 DELAYS BETWEEN SEGMENTS=   0
 SPIKES OF SEGMENT #1 2.0 3.0 4.0 5.0 4.0 2.0 1.0
 0.073 0.68
```

LIST OF REFERENCES

Anderson, N.L., 1979. An expanding spread seismic reflection survey across the Snake bay-Kakagi Lake greenstone belt, northwest Ontario. MSc. thesis, University of Manitoba.

Ayres, L.D., 1978. Metamorphism in the Superior Province of Northwestern Ontario and its relationship to crustal developement; in Metamorphism in the Canadian Shield, Geological Survey of Canada, Paper 78-10, pp.25-36.

Beakhouse, G.P., 1977. A subdivision of the western English River Subprovince. Canadian Journal of Earth Sciences, 14, pp.1481-1489.

Berry, M.J. and Fuchs, K., 1973. Crustal structure of the Superior and Grenville provinces of the northeastern Canadiand Shield. Bulletin of the Seismological Society of America, 63, pp.1393-1432.

Breaks, F.W., Bond, W.D., Harris, N. and Westerman, C., 1976. Operation Kenora-Ear Falls, District of Kenora; in Summary of Field Work, 1975, by the Geological Branch, edited by V.G.Milne, D.F.Hewlitt, K.D.Card, and J.A.Robertson. Ontario Division of Mines, Miscellaneous Paper 63, pp.19-33.

Breaks, F.W., Bond, W.D., McWilliams, G.H. and Grower, C., 1974. Operation Kenora-Sydney Lake, District of Kenora; in Summary of Field Work, 1974, by the Geological Branch, edited by V.G.Milne, D.F.Hewlitt and K.D.Card, Ontario Division of Mines, Miscellaneous Paper 59, pp.17-36.

Breaks, F.W., Bond, W.D. and Stone, D., 1978. Preliminary geological synthesis of the English River Subprovince, Northwestern Ontario and its bearing upon mineral exploration. Ontario Geological Survey, Miscellaneous Paper 72.

Brown, R.J., Friesen, G.H., Hall, D.H. and Stephenson, O.G., 1977. Weighted vertical stacking in crustal seismic reflection studies on the Canadian Shield. Geophysical Prospecting, 25, pp.251-268.

Bruce, E.L., 1924. Geology of the basin of Red Lake, District of Patricia; Ontario Department of Mines, Volume 33, part 4, pp.12-39.

Butterworth, S., 1930. On the theory of filter amplifiers. Wireless Engr 1.

Bruce, E.L., 1934. Geology of the Red Lake Area; Canadian Mining Journal, Volume 55, pp.438-441.

Chapman, C.H., 1978. A new method of computing synthetic seismograms. Geophysical Journal (RaS), 58, pp.490-503.

DeLandro, W.I., 1981. Deep seismic sounding in southern Manitoba and Saskathewan. Msc. thesis, University of Manitoba.

Dorn, T.F., 1974. The development and testing of a portable single-trace seismic recording system for crustal studies. M.Sc. thesis, University of Manitoba.

Dowling, D.B., 1894. Report on the country in the vicinity of Red Lake and part of the Berens River, Keewatin; Geological Survey of Canada, Volume 7, part F (published 1896).

Dwibedi, K., 1966. Petrography of the English River Gneiss Belt, northwestern Ontario and southeastern Manitoba. Ph.D. thesis, University of Manitoba.

Ferguson, S.A., 1965. Geology of the Eastern Part of Baird Township, District of Kenora; Ontario Department of Mines, Geological Report 39 (accompanied by Map 2071).

Ferguson, S.A., 1966. Geology of Dome Township, District of Kenora; Ontario Departmant of Mines, Geological Report 45 (accompanied by Map 2074).

Ferguson, S.A., 1968. Geology of the Northern Part of Heyson Township, District of Kenora; Ontario Department of Mines, Geological Report 56 (accompanied by Map 2125).

Ferguson, S.A., Brown, D., Davies, J.C. and Pryslak, A.P., 1970. Red Lake-Birch Lake Sheet; Ontario Department of Mines, Geological Compilation Series, Map 2175.

Green, A.G., Hall, D.H. and Stephenson, O.G., 1978. A sub-critical seismic crustal reflection survey over the Aulneau batholith, Kenora region, Ontario. Canadian Journal of Earth Sciences, 15, pp.301-315.

Green, A.g., Anderson, N.L. and Stephenson, O.G., 1979. An expanding spread seismic reflection survey across the Snake Bay-Kakagi Lake greenstone belt, northwestern Ontario. Canadian Journal of Earth Sciences, 16, pp.1599-1612.

Gupta, V.G. and Barlow, R.B., 1984. Interpretation of a detailed gravity profile across the English River Subprovince, northwestern Ontario. Canadian Journal of Earth Sciences, 21, pp.145-151.

Hall, D.H., 1971. Geophysical determination of deep crustal structure in Manitoba. The Geological Association of Canada, Special Paper 91, pp.83-88.

Hall, D.H. and Hajnal, Z., 1969. Crustal structure in northwestern Ontario: refraction seismology. Canadian Journal of Earth Sciences, 6, pp.81-89.

Hall, D.H. and Hajnal, Z., 1973. Deep seismic crustal studies in Manitoba. Bulletin of the Seismological Society of America, 63, pp.885-910.

Heelan, P.A., 1953. Radiation from a cylindrical source of finite length. Geophysics, 15, pp.685-694.

Horwood, H.C., 1940. Geology and mineral deposits of the Red Lake area; Ontario Department of Mines, Volume 49, Part 2 (published 1945).

Jones, R.D., 1973. Metamorphism across the English River Gneissic Belt, along the Red Lake road. M.Sc. thesis, University of Manitoba.

Kanasewich, E.R., 1975. Time sequence analysis in geophysics. University of Alberta Press.

Morris, G., 1950. Some considerations of the mechanism of the generation of seismic waves by explosives. Geophysics, 15, pp.61-69.

Pirie, J., 1978a. Byshe, Ranger and Willans Townships area, District of Kenora, Patricia Portion; in Summary of Field Work, 1978, by the Ontario Geological Survey, edited by V.G.Milne, O.L.White, R.B.Barlow and J.A.Robertson, Ontario Geological Survey, Miscellaneous Paper 82, pp.16-19.

Pirie, J., 1978b. Geology of the Red Lake Area, District of Kenora; in Summary of Field Work, 1978, by the Ontario Geological Survey, edited by V.G.Milne, O.L.White, R.B.Barlow and J.A.Robertson, Ontario Geological Survey, Miscellaneous Paper 82, pp.20-21.

Pirie, J., 1979a. Heyson township area district of Kenora, Patricia; in Summary of Field Work, 1979, by the Ontario Geological Survey, edited by V.G.Milne, O.L.White, R.B.Barlow and C.R.Kustra, Ontario Geological Survey, Miscellaneous Paper 90, pp.8-11.

Pirie, J., 1979b. Red Lake Synoptic Project, District of Kenora; in Summary of Field Work, 1979, by the Ontario Geological Survey, edited by V.G.Milne, O.L.White, R.B.Barlow and C.R.Kustra, Ontario Geological Survey, Miscellaneous Paper 90, pp.12-15.

Ricker, N.H., 1940. The form and nature of seismic waves and the structure of seismograms. Geophysics, 5, pp.348-366.

Ricker, N.H., 1944. Wavelet functions and their polynomials. Geophysics, 9, pp.314-323.

Ricker, N.H., 1953a. The form and laws of propagation of seismic wavelets. Geophysics, 18, pp.10-40.

Ricker, N.H., 1953b. Wavelet contraction, wavelet expansion and the control of seismic resolution. Geophysics, 18, pp.769-792.

Ricker, N.H., 1977. Transient waves in visco-elastic media. Developments in solid earth geophysics, 10. Elsevier Scientific Publishing Company.

Sharpe, J.A., 1942. The production of elastic waves by explosion pressures: 1. Theory and emperical field observations. Geophysics, 7, pp. 144-154.

Sheriff, R.E., 1976. Encyclopedic Dictionary of Exploration Geophysics. The Society of Exploration Geophysics.

Shklanka, R., 1970. Geology of the Bruce Lake Area, District of Kenora; Ontario Department of Mines, Geological Report 82 (accompanied by Map 2195).

Stacy, F.D., 1977. Physics of the Earth. John Wiley and sons, Inc.

Telford, W.M., Geldart, L.P., Sheriff, R.E and Keys, P.A., 1976. Applied Geophysics. Cambridge University press.

Thurston, P.C., 1981. Western Uchi Subprovince Synoptic Project; in Summary of Field Work, 1981, by the Ontario Geological Survey, edited by J.Wood, O.L.White, R.B.Barlow and A.C.Colvine, Ontario Geological Survey, Miscellaneous Paper 100, pp.8-11.

Thurston, P.C. and Breaks, F.W., 1978. Metamorphic and evolution of the Uchi-English River Subprovince; in Metamorphism in the Canadian Shield, Geological Survey of Canada, Paper 78-10, pp.49-62.

Wallace, H., 1980. Red Lake Synoptic Project, District of Kenora; in Summary of Field Work, 1980, by the Ontario Geological Survey, edited by V.G.Milne, O.L.White, R.B.Barlow, J.A.Robertson and A.C.Colvine, Ontario Geological Survey, Miscellaneous Paper 96, pp.10-12.

Wallace, H., 1981. Red Lake Synoptic Project, District of Kenora; in Summary of Field Work, 1981, by the Ontario Geological Survey, edited by J.Wood, O.L.White, R.B.Barlow and A.C.Colvine, Ontario Geological Survey, Miscellaneous Paper 100, pp.12-14.

Wallace, H., 1982. Red Lake Synoptic Project, District of Kenora; in Summary of Field Work, 1982, by the Ontario Geological Survey, edited by J.Wood, O.L.White, R.B.Barlow and A.C.Colvine, Ontario Geological Survey, Miscellaneous Paper 106, pp.5-7.

Whittal, K.R. and Clowes, R.M., 1979. A simple efficient method for calculation of traveltimes and ray paths in laterally inhomogeneous media. C.S.E.G Journal, 15, pp.21.

Wilson, H.D.B., 1971. The Superior Province in the Precambrian of Manitoba. Geological Association of Canada, Special Paper No.9, pp.41-49.